Universitat Autònoma de Barcelona

Mononuclear Ruthenium Complexes and their Application in Homogeneous and Heterogeneous Catalysis.

PhD Thesis presented by

LYDIA VAQUER MALIA

Supervised by

Prof. Antoni Llobet Dalmases and Dr. Xavier Sala Román

Programa de doctorado de "Catálisis Homogénea"

Departamento de Química

Facultad de Ciencias

2011

ICIQ
Institut
Català
d'Investigació
Química

Memòria presentada per aspirar al Grau de Doctor per Lydia Vaquer Malia.

Lydia Vaquer Malia

Vist i plau

Prof. Antoni Llobet Dalmases	Dr. Xavier Sala Román
Institut Català d'Investigació Química (ICIQ), Tarragona Universitat Autònoma de Barcelona, Bellaterra, Barcelona	Dept. Química Facultat de Ciències Universitat Autònoma de Barcelona

Bellaterra, 26 d'Abril de 2011

A mis padres, a mis hermanas
y al hombrecillo que crece en su interior,

Acknowledgements

El trabajo aquí presentado refleja la culminación de una etapa, una etapa en la que ha intervenido mucha gente y cada uno de los cuales ha puesto su granito de arena. Por ello me gustaría aprovechar esta sección para agradecerles su apoyo y compañía a lo largo de estos años y por formar parte de mis recuerdos del futuro.

En primer lugar, me gustaría agradecer a Toni el haberme dado la oportunidad de trabajar en su grupo, por sus conocimientos, amabilidad y disponibilidad.

A Xavi, mil gracias, porque, aun sin saberlo, tus palabras hicieron que continuara adelante. Gracias por haberme dirigido durante estos últimos años, por tu proximidad, dedicación y por ser alguien a quien valoro tanto como químico como persona.

Gracias a todos los compañeros y amigos del laboratorio, a los actuales y a los que han abandonado el barco. A Stephan por tu compañía y tranquilidad desde los inicios hasta ahora, a Carlo, por tu ayuda incondicional y amistad, a Isidoro por los buenos momentos dentro y fuera del laboratorio; a Nora por tu comprensión, Somnath and Tomasz for your good mood, Sukanta for your help in supra's project, Takashi for your disponibility, Laura por tu proximidad y Pau por tu empeño en ser un grupo. A Matías, por toda tu ayuda al llegar a Tarragona, a Fernando y Elena, por vuestra ayuda en la época carbénica, a Chiara por tu risa y alegría, a Sophie, a Markus, a Sebastian, a Ilaria y a Sven, por todos los momentos compartidos. A los compañeros y amigos de los otros laboratorios, a Rocío, por estar siempre allí, y a los del zulo, por compartir esos grandes momentos de tensión.

A los miembros de soporte del ICIQ, gracias por vuestra ayuda y disponibilidad.

Gracias a todos aquellos que han participado en los proyectos en colaboración, a Miquel Pericàs, Pau Ballester, Paola, Susana, Mª Angeles, Eddy y Sarabindu, por haber ayudado a que los proyectos siguieran adelante y por haber mantenido una comunicación directa que han hecho de las colaboraciones algo muy enriquecedor.

Prof. Gade, Ihnen danke ich vielmals für die freundliche Aufnahme in Ihren Arbeitskreis und für das Vertrauen, das Sie mir entgegengebracht haben. Thanks to all the members of the group for making my stay in Germany really pleasant, specially to my lab mates Desi and Christoph for all the laughing moments, y al grupillo de los españoles, Julio, Jose y Lara, porque sabéis acoger a la gente como nadie y por haberme hecho sentir como en casa.

Y no me olvido de mis inicios en la uni. Muchas gracias a toda la planta de inorgánica por hacer que guarde un gran recuerdo de ese primer año. Gracias a Lluis por haberme ayudado tanto en el laboratorio y a Laia, porque, aunque nos separásemos, seguimos unidas.

A mis amigas de toda la vida, Cris, Blanca y Laura porque siempre habeis estado a mi lado y porque es un privilegio teneros como amigas.

Y por último, a toda mi familia, porque sois los que más me habéis apoyado siempre, muchas gracias.

Lydia

The work performed in the present doctoral thesis has been possible thanks to the funding of:

- Institut Català d'Investigació Química (ICIQ).
- Grups de Recerca reconeguts de la Generalitat de Catalunya, SGR2009-69.
- Ministerio de Ciencia e Inovacion (MICINN) through Projects: CTQ2007-67918, CTQ2010-21497 .
- MICNN through Consolider Ingenio 2010 (CSD2006-0003) within the framework of "Diseño de Catalizadores para una Química Sostenible: Una Aproximación Integrada" (INTECAT).
- Comission of the European Union throgh project SOLAR-H2 (EU 212508).
- American Chemical Society through the Petroleun Research Fund, 48619-AC3.

Finally I would also like to thank AGAUR for the pre-doctoral FI grant.

Graphical Abstracts

Chapter 1. General Introduction (pages 1 – 16)

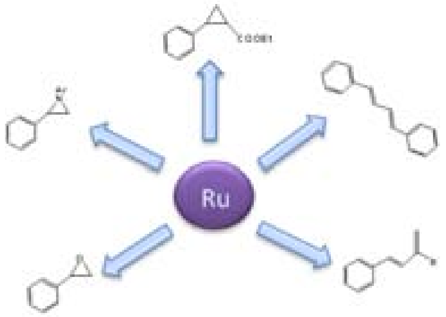

Introduction to the field of study based on ruthenium chemistry with special interest in Ru-OH_2 complexes. An overview of their coordination chemistry, redox properties and reactivity is presented; paying special attention to their electrochemical properties that makes them especially relevant for oxidative transformations.

Chapter 2. Objectives (pages 17 – 20)

Chapter 3. Redox Properties of Ru-OH_2 Complexes and their Reactivity in Homogeneous Oxidations (pages 21 – 73)

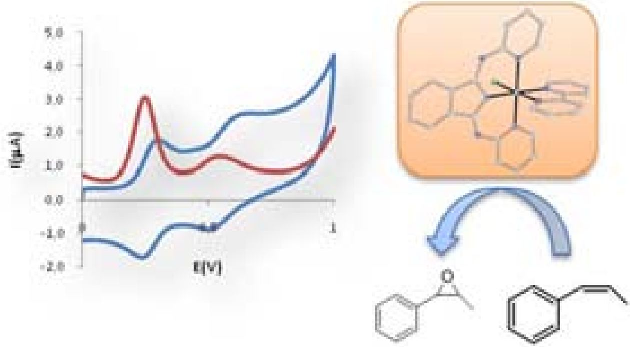

A family of Ru-OH_2 complexes has been synthesized with the aim of obtaining a collection of complexes with different redox properties. For this purpose σ-donor and π-acceptor ligands have been selected. The influence of the electronic properties of the ligands on the redox potentials of the complexes has been studied, together with their reactivity towards C-H bond oxidation and alkene epoxidation.

Chapter 4. Heterogenization of Stereoselective Ru Complexes on Magnetic Nanoparticles (pages 75 –136)

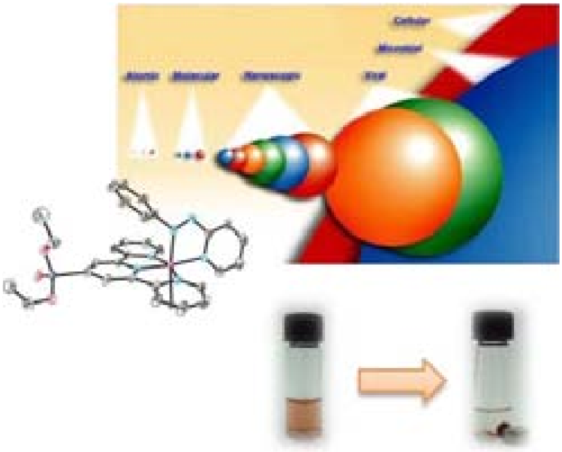

Two ruthenium complexes, properly functionalized with a phosphonate group, were immobilized on the surface of magnetic nanoparticles (NPs) without modifying the intrinsic coordination and electronic properties of the original complex. The behavior of this heterogeneous system in epoxidation catalysis has been studied and compared with the analogous homogeneous system. The use of magnetic NPs offered the opportunity of easily removing and recycling the catalyst by the application of an external magnetic field.

Chapter 5. Cavitand-based Ruthenium Complexes: towards Selective Supramolecular Oxidation Catalysis (pages 137 - 162)

Ruthenium complexes have also been functionalized with a bulky resorcinarene-based group. These complexes have been designed and synthesized, and their activity in epoxidation catalysis has been studied. The resorcinarene cavity shape offers the possibility of being used for supramolecular recognition and, therefore, in regio-selective oxidation catalysis.

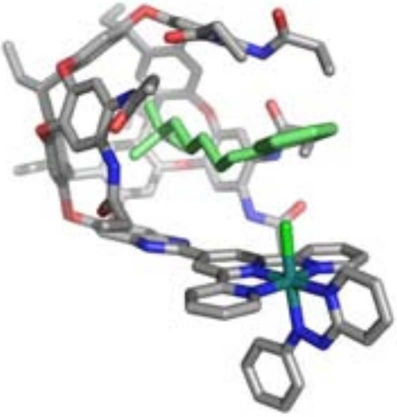

Chapter 6. New Ruthenium Complexes with Enantiomerically pure Bis(pinene)fused Tridentate Ligands. (pages 163-222)

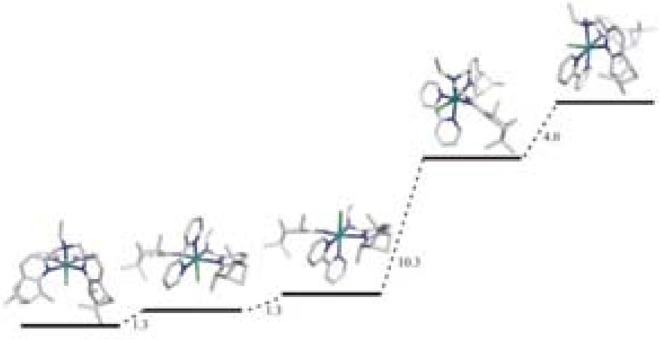

Chirality was introduced into the catalytic system through the coordination of a new pineno-fused bpea ligand. This ligand was synthesized and characterized and its coordination chemistry to ruthenium studied, paying special attention to the influence of the steric hindrance promoted by the ligand in the degree of the resulting isomeric mixture. A light-driven isomerization reaction together with DFT calculations and catalytic results are presented.

Chapter 7. Summary and Conclusions (pages 223 –228)

TABLE OF CONTENTS

Graphical Abstracts I

Table of Contents V

Glossary of Terms and Abbreviations IX

CHAPTER 1. General Introduction 1

1.1. Ruthenium chemistry 5

1.2. Polypyridyl Ru aqua complexes 7

1.3. $Ru^{IV}=O$ as oxidation catalyst 10

1.4. References 14

CHAPTER 2. Objectives 19

CHATER 3. Redox Properties of Ru-OH_2 Complexes and their Reactivity in Homogeneous Oxidations 21

3.1. Introduction 25

3.1.1. Modulation of the electronic properties of $Ru^{IV}=O$ complexes 25

3.1.2. Reactivity of $Ru^{IV}=O$ complexes as oxidants of C-H bonds 32

3.1.3. Epoxidation of alkenes catalyzed by $Ru^{IV}=O$ complexes 37

3.2. Results and Discussion 42

3.2.1. Synthesis of the complexes 42

3.2.2. Characterization of C9-Cl, C10-Cl and C11-Cl. 43

3.2.3. Electrochemical properties of C9, C10 and C11. 46

3.2.4. Oxidation of C-H bonds 50

3.2.5. Epoxidation of alkenes 53

3.2.6. Experimental section 61

3.3. References 66

3.4. Supporting Information 69

CHAPTER 4. Heterogenization of Stereoselective Ru Complexes on Magnetic Nanoparticles 75

4.1. Introduction 79

4.1.1. Heterogenized catalysts for oxidation reactions 79

4.1.2. Immobilization methods 80

4.1.3. Supports 81

4.1.4. Nanoparticles 82

4.2. Results and Discussion 91

4.2.1. Strategies for the immobilization of Ru complexes 91

4.2.2. Synthesis and structural, spectroscopic and electrochemical characterization of $[Ru(L1)Cl_3]$ (C3), $[Ru(L1)(azpy)Cl]^+$ (C4) and $[Ru(L1)(bpm)Cl]^+$ (C5). 96

4.2.3. Catalytic activity of C5. 101

4.2.4. Hydrolysis of the phosphonate group. Synthesis of C6 and C7. 103

4.2.5. Preparation of magnetic nanoparticles of Fe_3O_4 (NPs). 103

4.2.6. Immobilization of Ru complexes C6 and C7 on NPs. 104

4.2.7. Catalytic activity of NP-C6 and NP-C7. Comparison with the homogeneous system. 106

4.2.8. Experimental section 111

4.3. References 118

4.4. Supporting Information 122

CHAPTER 5. Cavitand-based Ruthenium Complexes: towards Selective Supramolecular Oxidation Catalysis 137

5.1. Introduction 141

5.1.1. Resorcin-[4]-arene cavitand-based molecular switches 141

5.1.2. Supramolecular catalysis 142

5.2. Results and Discussion 146

5.2.1. Synthesis and characterization of the ligand L1 146

5.2.2. Synthesis and characterization of complexes C3, C4 and C5 149

5.2.3. Catalytic epoxidation of alquenes 152

5.2.4. Experimental section 153

5.3 References 157

5.4. Supporting Information 159

CHAPTER 6. New Ru Complexes with Enantiomerically Pure bis(pinene)-fused Tridentate Ligands 163

6.1. Introduction 167

6.1.1. Chiral ligands 167

6.1.2. Ru-catalyzed asymmetric epoxidation 169

6.1.3. Ru bpea-based chiral complexes 173

6.2. Results and Discussion 177

6.2.1. Synthesis of and characterization of (-)-L3. 177

6.2.2. Synthesis of [Ru((-)-L3)(bpy)Cl]$^+$ (C3). 180

6.2.3. Spectroscopic and Electrochemical Characterization of [Ru((-)-L3)(bpy)Cl]$^+$ (C3). 182

6.2.4. DFT calculations. 184

6.2.5. Isomerization of C3c to C3a. 188

6.2.6. Catalytic epoxidation of alkenes 192

6.2.7. Experimental section 193

6.3. References 202

6.4. Supporting Information 206

CHAPTER 7. Summary and Conclusions 223

Glossary of Terms and Abbreviations

bpy	2,2’-bipyridine
bpea	bis(2-pyridyl)ethylamine
azpy	2-(phenylazo)pyridine
bpm	2,2’-bipyrimidine
pic	picolinate
Hbid	1,3-bis(2-pyridylimino)isoindoline
trpy	2,2’:6’,2’’-terpyridine
NHE	Normal Hydrogen Electrode
Ep,a	Anodic peak
Ep,c	Cathodic peak
COSY	Correlation Spectroscopy
J	Coupling Constant
CV	Cyclic Voltammetry
DFT	Density Functional Theory
DCM	Dichloromethane
DPV	Differential Pulse Voltammetry
d	doublet
ET	Electron Transfer
GC	Gas Chromatography
$E_{1/2}$	Half wave potential
IR	Infra Red
MS	Mass Spectroscopy
m/z	Mass-to-charge ratio
MALDI	Matrix assisted lased desorption/ionization

MLCT	Metal to Ligand Charge Transfer
MNPs	Magnetic Nanoparticles
NMR	Nuclear Magnetic Resonance
NOESY	Nuclear Overhouser Spectroscopy
NPs	Nanoparticles
E	Potential
PCET	Proton Coupled Electron Transfer
py	pyridine
RT	Room Temperature
s	singlet
SPS	Solvent Purification System
E^0	Standard potential
SSCE	Sodium Saturated Calomel Electrode
TBAH	Tetrea(n-butyl)ammonium hexafluorophosphate
TEM	Transmission Electron Microscopy
t	triplet
TON	Turn Over Number
UV-vis	Ultraviolet-visible spectroscopy
λ	wavelength

Chapter 1

General Introduction

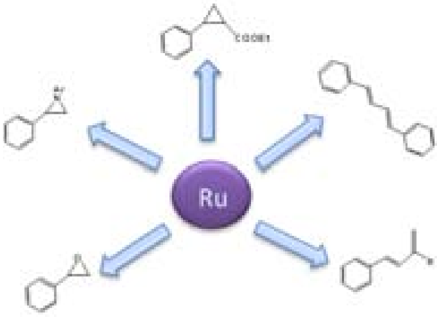

Introduction to the field of study based on ruthenium chemistry with special interest in Ru-OH_2 complexes. An overview of their coordination chemistry, redox properties and reactivity is presented; paying special attention to their electrochemical properties that makes them especially relevant for oxidative transformations.

TABLE OF CONTENTS

CHAPTER 1. General Introduction 1

1.1. Ruthenium chemistry 5

1.2. Polypyridyl Ru aqua complexes 7

1.3. $Ru^{IV}=O$ as oxidation catalyst 10

1.4. References 14

Chapter 1

General Introduction

1.1. Ruthenium chemistry

The electronic configuration of ruthenium, $4d^7$ s^1, makes this metal, together with osmium, unique among all the elements of the periodic table, presenting the widest range of accessible oxidation states (from -2 in $[Ru(CO)_2]^{2-}$ to +8 in RuO_4), covering the complete range of 11 oxidation states theoretically possible for a transition metal (from d^0 to d^{10}).[1]

The kinetic stability of ruthenium complexes in different oxidation states and the often reversible nature of the redox pairs make these complexes particularly interesting. The application of ruthenium complexes is wide, being clearly correlated with the nature of the ligands coordinated to the metal center. Ruthenium complexes with π-conjugate ligands or systems that enable electronic delocalization have shown specific properties in nonlinear optics,[2-4] magnetism,[5,6] molecular sensors[7] and liquid crystals.[8] Ruthenium sulfoxide complexes have been extensively studied due to their relevant usefulness in chemotherapy.[9,10] Ruthenium complexes with heterocyclic N-donor ligands, definitely the most employed ones, have received great attention owing to their spectroscopic, photophysical and electrochemical properties, which lead to potential uses in diverse areas such as photosensitizers for photochemical conversion of solar energy,[11-13] molecular electronic devices[14-16] and photoactive DNA cleavage agents for therapeutic purposes.[17-19]

Synthetic versatility, easily available high oxidation states and a robust first coordination sphere make ruthenium complexes particularly useful for catalytic transformations, such as cyclopropanation, isomerization, metal-promoted radical reactivity, oxidation, hydrogenation, C-H and C-Halogen bond activation and olefin metathesis.

The effect of the ligand is crucial in determining the type of the catalytic reaction, in such a way that, by modification of the ligands coordinated to the metal center, the properties of the metal catalyst can be tuned. Therefore, the same metal can transform the same substrate in different products by changing the ligands around it. As an example, in Figure 1 is shown how styrene can be transformed into multiple products using different ruthenium complexes.[20]

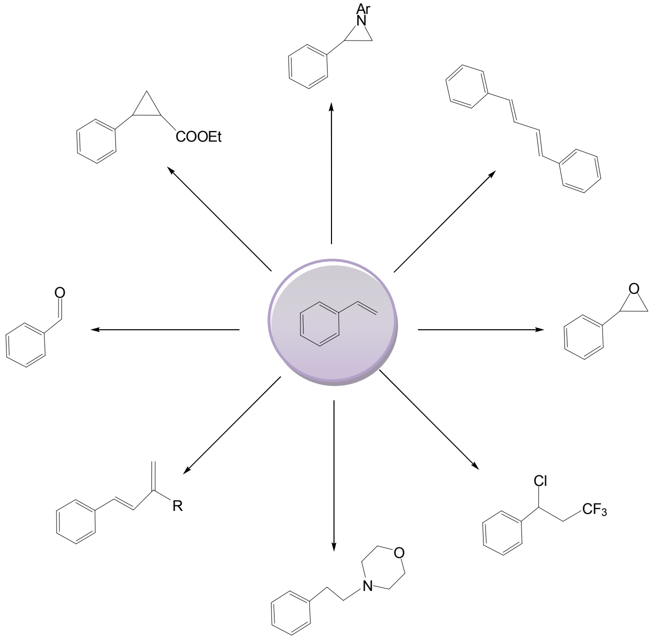

Figure 1. Styrene transformations catalyzed by different Ru complexes.

Due to the importance of the ligand environment, numerous studies have been focused on the understanding of their electronic and geometric properties and how these properties influence on the metal reactivity.

1.2. Polypyridyl Ru aqua complexes

The contributions of Frances P. Dwyer and co-workers in the 1940s, 1950s and 1960s can be considered as the beginning of the synthetic chemistry of polypyridyl complexes of ruthenium and osmium.[21] Afterwards, Thomas J. Meyer and collaborators began a systematic investigation of their redox reactivity.[22-26] Based on the procedures described by Dwyer, it was possible to create families of related complexes in which their properties could be varied by changing the ligands. The reactivity properties of these complexes turned out to be quite extraordinary based on the accessibility of long-lived excited states and oxidation states varying from M(II) to M(VI).

Polypyridyl ligands are stable against oxidation and present a great coordinative capacity, increased by their quelating effect, conferring great stability to the formed complex (Figure 2).

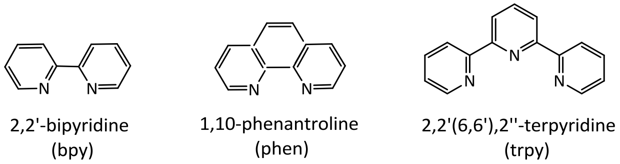
2,2'-bipyridine (bpy)
1,10-phenantroline (phen)
2,2'(6,6'),2''-terpyridine (trpy)

Figure 2. Examples of polypyridyl ligands used in ruthenium coordination chemistry.

The redox properties of these complexes become specially interesting when an aqua ligand is coordinated to the metal center. In this case, a proton-coupled-electron transfer (PCET) is possible; becoming high oxidation states fairly accessible.[27] In this procedure the successive oxidations from Ru(II) to Ru(IV) are accompanied by a sequential loss of protons favored by the enhanced acidity of the bonded aqua ligand. Therefore, the initial Ru^{II}-OH_2 is oxidized to Ru^{IV}=O, passing through a Ru^{III}-OH species. (Figure 3)

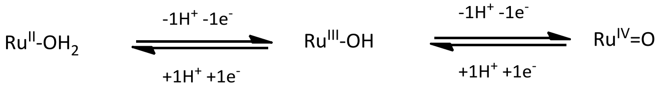

$$Ru^{II}\text{-}OH_2 \underset{+1H^+\ +1e^-}{\overset{-1H^+\ -1e^-}{\rightleftharpoons}} Ru^{III}\text{-}OH \underset{+1H^+\ +1e^-}{\overset{-1H^+\ -1e^-}{\rightleftharpoons}} Ru^{IV}{=}O$$

Figure 3. PCET oxidation process characteristic of Ru-aqua complexes.

As a consequence of this behavior, the redox potentials of the aqua complexes are directly correlated with the pH of the medium in such a way that, if pH increases, the Ru(III/II) and Ru(IV/III) couples are shifted to lower potentials. This dependence of redox potentials and pH is reflected in the Nernst equation, in which, for a monoprotic and monoelectronic transfer, the redox couple half wave potential ($E_{1/2)}$ diminishes in 59 mV by every pH unit increased (Equation 1).

$$E_{1/2} = E^0{}_{1/2} - 0.059(m/n)\ pH$$

Equation 1. Relation between potential and pH in the Nernst equation.

In order to illustrate the importance of a PCET, in Figure 4 the Latimer diagrams of two Ru-polypyridyl complexes are shown. In eq 1 of the same figure, the oxidation of *cis*-$[Ru(bpy)_2(Cl)_2]$ is represented and in eq 2, the oxidation of *cis*-$[Ru(bpy)_2(py)(H_2O)]^{2+}$ is shown. In the latter case, two anionic chloro ligands of *cis*-$[Ru(bpy)_2(Cl)_2]$ are replaced by a neutral pyridine and aquo ligand. The electronic configuration of all the species is also shown, being the electrons gained and lost from dπ levels.

$$\underset{(d\pi^4)}{cis\text{-}[Ru^{IV}(bpy)_2(Cl)_2]^{2+}} \overset{1.7\text{ V}}{\rule[0.5ex]{3em}{0.4pt}} \underset{(d\pi^5)}{cis\text{-}[Ru^{III}(bpy)_2(Cl)_2]^{+}} \overset{0.0\text{ V}}{\rule[0.5ex]{3em}{0.4pt}} \underset{(d\pi^6)}{cis\text{-}[Ru^{II}(bpy)_2(Cl)_2]^{o}} \qquad (1)$$

$$\underset{(d\pi^4)}{cis\text{-}[Ru^{IV}(bpy)_2(py)(O)]^{2+}} \overset{0.78\text{ V}}{\rule[0.5ex]{3em}{0.4pt}} \underset{(d\pi^5)}{cis\text{-}[Ru^{III}(bpy)_2(py)(OH)]^{2+}} \overset{0.67\text{ V}}{\rule[0.5ex]{3em}{0.4pt}} \underset{(d\pi^6)}{cis\text{-}[Ru^{II}(bpy)_2(py)(H_2O)]^{2+}} \qquad (2)$$

(V versus NHE, $\mu = 0.1$ at pH = 7)

Figure 4. Latimer diagrams of Ru polypyridyl complexes not containing (1) and containing (2) and aqua ligand.

The example shown in eq 1 of Figure 4 is typical for Ru polypyridyl couples with oxidation of Ru(II) to Ru(III) taking place at easily accessible potentials. The 1.7 V increase in potential for the Ru(IV/III) couple is due to the increase in charge and oxidation state compared to the Ru(III/II) couple.[28] In the couples shown in eq 2, where an aqua ligand is coordinated to the metal center, the increase in charge and changes in bonding increase the potential for oxidation of Ru^{II}-OH_2 to Ru^{III}-OH by over 0.6 V compared to the analogous couple in eq 1.[29-31] When comparing both equations it’s surprising to observe a much smaller difference between the Ru(IV/III) and Ru(III/II) couples in eq. 2. These data point to a dramatic stabilization of Ru(IV) in the aqua-containing complex.

This stabilization is promoted by the proton loss; *i.e.* by the loss of a positive charge, maintaining the total charge of the complex, and by a σ and π donation of the oxo group to the electron deficient metal center. Stabilization of Ru(IV) as the oxo complex causes the near overlap of Ru(IV/III) and Ru (III/II) potentials. There is an important implication in reactivity in this closeness of the redox potentials, being Ru(IV), thermodynamically, nearly as good two-electron oxidant as one-electron oxidant.

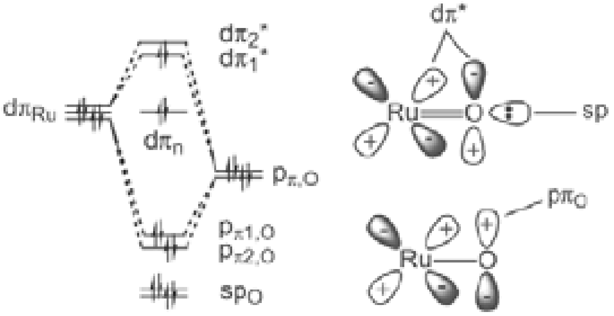

Figure 5. Ru^{IV}=O schematic energy orbital diagram

The observation of the energy orbital diagram of $d\pi_{Ru}$-$2p_{\pi,O}$ multiple bond interaction provides an electronic clue to the extensive reactivity of Ru=O complexes (Figure 5). The LUMO is dπ* and provides a site for initial orbital interaction with electron donors and is available for electron pair donation and initial coordination expansion. The sp^2 and $p\pi_O$ electron pairs are available for electron donation and orbital interactions with electron acceptors.

1.3. Ru^{IV}=O as oxidation catalyst

The Ru^{IV}=O complexes are able to act as efficient oxidants for a wide range of substrates. This behavior can be attributed to the accessibility of high oxidation states, their ability to accept two electrons avoiding radicalary reaction pathways of high energy and reactivity,[32-34] and to the robust character of the first coordination sphere.

Among the oxidation reactions promoted by Ru^{IV}=O complexes, the oxidation of alkanes, the epoxidation of alkenes, the cleavage of double bonds, the oxidation of alcohols and ethers, and the oxidation of amines and amides can be pointed out.

The orbital and energetic properties of Ru^{IV}=O promote different mechanistic pathways, including outer-sphere electron transfer, proton-coupled electron transfer, electrophilic ring attack, oxo transfer, hydride transfer and C-H insertion. In Table 1 a summary of different oxidative pathways for *cis*-$[Ru^{IV}(bpy)_2(py)O]^{2+}$, probably the most paradigmatic and studied complex inside this family, is shown.[29-31,35-44] The mechanisms mentioned in this table are the result of a lengthy and exhaustive series of mechanistic studies through UV-Visible and Infrared spectroscopy data, isotopic labeling, observation of intermediates and kinetic isotope effect. This table lists the reductant, the oxidized product, the mechanistic pathway, rate constant informations and comments about the mechanism.

Table 1. Mechanistic summary for *cis*-$[Ru(bpy)_2(py)(O)]^{2+\,a}$

Reduced Form	Oxidized Form	Pathway	k (25ºC)^a M^{-1} S^{-1}	Comment
$[Os^{II}(bpy)_3]^{2+}$	$[Os^{III}(bpy)_3]^{3+}$	Outer-sphere e^- transfer	< 1 x $10^{3\,b}$	Slowed by intitial formation of *cis*-$Ru^{III}(bpy)_2(py)(O)^{2+}$
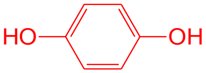 Hydroquinone	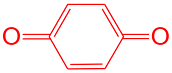 Benzoquinone	Proton-coupled e^- transfer	9.6 x $10^{5\ b}$	$^kH_2O/^kD_2O = 30$
H_2O_2	O_2	Proton-coupled e^- transfer	1.7 ^{b}	$^kH_2O/^kD_2O = 22$
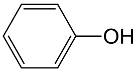 Phenol	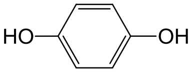 Hydroquinone ^{c}	Electrophilic ring attak	1.9 x 10^{-2}	$^kH/^kD = 5.5$ (C_5D_5OH)
$(CH_3)_2SO$	$(CH_3)S_2O$	O transfer	17	Bound Sulfoxide observed
$(CH_3)_2SO$	$(CH_3)SO_2$	O transfer	0.14	-
PPh_3	$O{=}PPh_3$	O transfer	1.8 x 10^5	Bound Ru(II) and $O{=}PPh_3$ observed
Cis-, trans estilbè PhHC=CHPh	Cis-, trans- 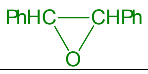	O transfer	0.28 *trans* 2.5 x 10^{-3}, *cis.*	Bound Ru(II) epoxide observed
$PhCH_2OH$	PhCHO	H^- transfer	2.4	$^kH/^kD = 50$
HCO_2^-	CO_2	H^- transfer	4.2	$^kH/^kD = 19$
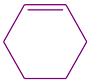	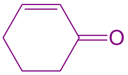	C-H insertion	0.6	$^kH/^kD = 18$ Bound Ru(II) ketone observed
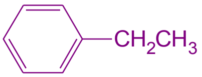	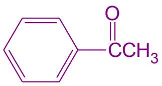	C-H insertion	6.6 x 10^{-2}	Bound Ru(III) ketone observed

^{a} In CH_3CN except where indicated. ^{b} H_2O (μ = 0.1). ^{c} Followed by rapid oxidation to the quinone. ^{d} Through an intermediate, bound alcohol complex that undergoes further oxidation.

The catalytically active Ru=O species act as excellent catalysts for the oxidation of different organic substrates following the catalytic cycle shown in Figure 6. In this cycle the active species is generated and regenerated chemically or electrochemically by oxidation of the corresponding Ru^{II}-OH_2 species. Different oxidants have been used for this purpose, such as PhIO, $PhI(OAc)_2$ and pyridine N-oxides (NMO, Cl_2PyNO), gathering special attention the atom-economic and environmentally friendly H_2O_2 and O_2.[45-49]

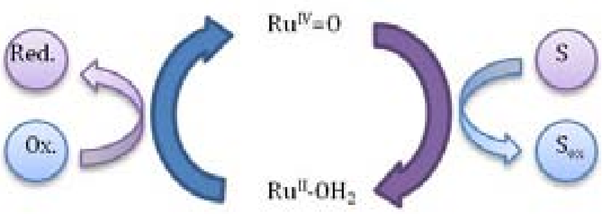

Figure 6. Scheme of a catalytic cycle of oxidation of a substrate (S) with Ru^{IV}=O species.

With regard to substrates, alkenes are useful raw materials for both commodities and fine chemicals because of the high reactivity of the double bond.[50] However, an inherent difficulty in the oxidation of olefins is caused by different competing modes of oxidation, for example, epoxidation, allylic oxidation and double-bond cleavage. An overview of the different oxidation reactions of alkenes catalyzed by ruthenium is shown in Figure 7. The selectivity of the epoxidation reaction *vs.* allylic oxidation, for example, depends heavily on the nature of the alkene studied. For instance, in the case of the oxidation of cyclohexene, the allylic C-H bond is more easily oxidized than the C=C bond and, thus, the allylic C-H bond, exhibits enhanced reactivity.[50] On the other hand, in the case of cyclooctene or norbornene, the allylic C-H bonds are much less reactive and epoxidation is highly favored. In the case of the oxidation of styrene or stilbene, both epoxidation and C=C bond cleavage reactions are observed as well as isomerization around the double bond.

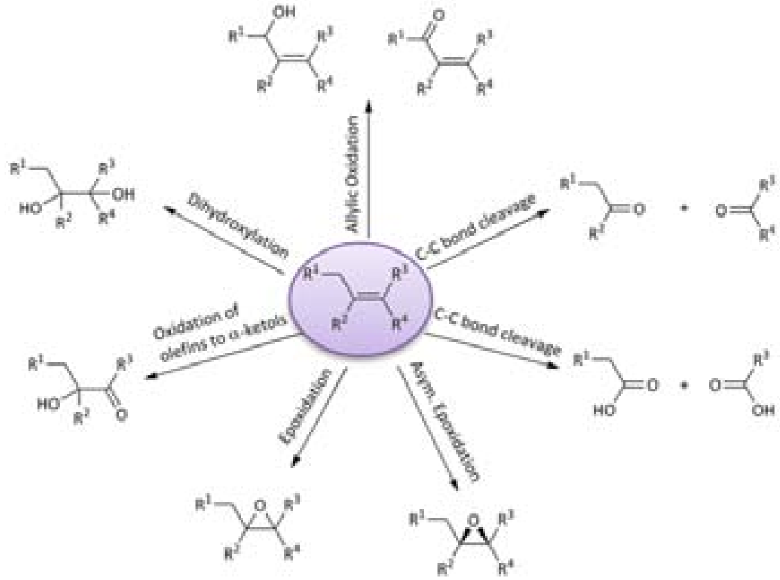
Allylic Oxidation
C-C bond cleavage
C-C bond cleavage
Asym. Epoxidation
Epoxidation
Oxidation of olefins to α-ketols
Dihydroxylation

Figure 7. Possible transformations of alkenes with ruthenium catalysts.

1.4. References

(1) Griffith, W. P. *Chem. Soc. Rev.* **1992**, *21*, 179-185.

(2) Whittall, I. R.; McDonagh, A. M.; Humphrey, M. G.; Samoc, M. In *Advances in Organometallic Chemistry, Vol 43*; Academic Press Inc: San Diego, 1999; Vol. 43, p 349-405.

(3) Whittall, I. R.; McDonagh, A. M.; Humphrey, M. G.; Samoc, M. In *Advances in Organometallic Chemistry, Vol 42*; Academic Press Inc: San Diego, 1998; Vol. 42, p 291-362.

(4) Verbiest, T.; Houbrechts, S.; Kauranen, M.; Clays, K.; Persoons, A. *Journal of Materials Chemistry* **1997**, *7*, 2175-2189.

(5) Larionova, J.; Mombelli, B.; Sanchiz, J. n.; Kahn, O. *Inorganic Chemistry* **1998**, *37*, 679-684.

(6) Hmyene, M.; Yassar, A.; Escorne, M.; Percheron-Guegan, A.; Garnier, F. *Advanced Materials* **1994**, *6*, 564-568.

(7) Constable, E. C. *Angewandte Chemie International Edition in English* **1991**, *30*, 407-408.

(8) Dembek, A. A.; Burch, R. R.; Feiring, A. E. *Journal of the American Chemical Society* **1993**, *115*, 2087-2089.

(9) Galanski, M.; Arion, V. B.; Jakupec, M. A.; Keppler, B. K. *Curr. Pharm. Des.* **2003**, *9*, 2078-2089.

(10) Keppler, B. K.; VCH: 1993, p 1-8.

(11) Balzani, V.; Barigelletti, F.; Belser, P.; Bernhard, S.; De, C. L.; Flamigni, L. *J. Phys. Chem.* **1996**, *100*, 16786-16788.

(12) Juris, A.; Balzani, V.; Barigelletti, F.; Campagna, S.; Belser, P.; Von, Z. A. *Coord. Chem. Rev.* **1988**, *84*, 85-277.

(13) Xie, P.-H.; Hou, Y.-J.; Wei, T.-X.; Zhang, B.-W.; Cao, Y.; Huang, C.-H. *Inorg. Chim. Acta* **2000**, *308*, 73-79.

(14) Newkome, G. R.; Cho, T. J.; Moorefield, C. N.; Mohapatra, P. P.; Godinez, L. A. *Chem.--Eur. J.* **2004**, *10*, 1493-1500.

(15) Mishra, L.; Yadaw, A. K.; Govil, G. *Indian J. Chem., Sect. A: Inorg., Bio-inorg., Phys., Theor. Anal. Chem.* **2003**, *42A*, 1797-1814.

(16) Barigelletti, F.; Flamigni, L. *Chem. Soc. Rev.* **2000**, *29*, 1-12.

(17) Hotze, A. C. G.; Velders, A. H.; Ugozzoli, F.; Biagini-Cingi, M.; Manotti-Lanfredi, A. M.; Haasnoot, J. G.; Reedijk, J. *Inorg. Chem.* **2000**, *39*, 3838-3844.

(18) Hotze, A. C. G.; Broekhuisen, M. E. T.; Velders, A. H.; Van, d. S. K.; Haasnoot, J. G.; Reedijk, J. *Eur. J. Inorg. Chem.* **2002**, 369-376.

(19) Delaney, S.; Pascaly, M.; Bhattacharya, P. K.; Han, K.; Barton, J. K. *Inorg. Chem.* **2002**, *41*, 1966-1974.

(20) van, L. P. W. N. M. *Homogeneous Catalysis: Understanding the Art*; Springer, 2004.

(21) Dwyer, F. P.; Mellor, D. P.; Editors *Chelating Agents and Metal Chelates*; Academic Press, 1964.

(22) Meyer, T. J.; Huynh, M. H. V. *Inorganic Chemistry* **2003**, *42*, 8140-8160.

(23) Durham, B.; Caspar, J. V.; Nagle, J. K.; Meyer, T. J. *J. Am. Chem. Soc.* **1982**, *104*, 4803-10.

(24) Pugh, J. R.; Bruce, M. R. M.; Sullivan, B. P.; Meyer, T. J. *Inorg. Chem.* **1991**, *30*, 86-91.

(25) Gersten, S. W.; Samuels, G. J.; Meyer, T. J. *J. Am. Chem. Soc.* **1982**, *104*, 4029-30.

(26) Murphy, W. R., Jr.; Takeuchi, K. J.; Meyer, T. J. *J. Am. Chem. Soc.* **1982**, *104*, 5817-19.

(27) Costentin, C.; Robert, M.; Savel̀�ant, J.-M. *Chemical Reviews* **2010**, *110*, PR1-PR40.

(28) Eggleston, D. S.; Goldsby, K. A.; Hodgson, D. J.; Meyer, T. J. *Inorg. Chem.* **1985**, *24*, 4573-80.

(29) Moyer, B. A.; Meyer, T. J. *Inorg. Chem.* **1981**, *20*, 436-44.

(30) Moyer, B. A.; Meyer, T. J. *J. Am. Chem. Soc.* **1978**, *100*, 3601-3.

(31) Binstead, R. A.; Moyer, B. A.; Samuels, G. J.; Meyer, T. J. *J. Am. Chem. Soc.* **1981**, *103*, 2897-9.

(32) Masllorens, E.; Rodriguez, M.; Romero, I.; Roglans, A.; Parella, T.; Benet-Buchholz, J.; Poyatos, M.; Llobet, A. *Journal of the American Chemical Society* **2006**, *128*, 5306-5307.

(33) Meyer, T. J. *J. Electrochem. Soc.* **1984**, *131*, 221C-228C.

(34) Keene, F. R. *Coord. Chem. Rev.* **1999**, *187*, 121-149.

(35) Binstead, R. A.; McGuire, M. E.; Dovletoglou, A.; Seok, W. K.; Roecker, L. E.; Meyer, T. J. *J. Am. Chem. Soc.* **1992**, *114*, 173-86.

(36) Lebeau, E. L.; Binstead, R. A.; Meyer, T. J. *J. Am. Chem. Soc.* **2001**, *123*, 10535-10544.

(37) Gilbert, J. A.; Gersten, S. W.; Meyer, T. J. *J. Am. Chem. Soc.* **1982**, *104*, 6872-3.

(38) Gilbert, J.; Roecker, L.; Meyer, T. J. *Inorg. Chem.* **1987**, *26*, 1126-32.

(39) Seok, W. K.; Dobson, J. C.; Meyer, T. J. *Inorg. Chem.* **1988**, *27*, 3-5.

(40) Roecker, L.; Dobson, J. C.; Vining, W. J.; Meyer, T. J. *Inorg. Chem.* **1987**, *26*, 779-81.

(41) Moyer, B. A.; Sipe, B. K.; Meyer, T. J. *Inorg. Chem.* **1981**, *20*, 1475-80.

(42) Stultz, L. K.; Binstead, R. A.; Reynolds, M. S.; Meyer, T. J. *J. Am. Chem. Soc.* **1995**, *117*, 2520-32.

(43) Roecker, L.; Meyer, T. J. *J. Am. Chem. Soc.* **1987**, *109*, 746-54.

(44) Roecker, L.; Meyer, T. J. *J. Am. Chem. Soc.* **1986**, *108*, 4066-73.

(45) Armor, J. N. *Appl. Catal., A* **1999**, *189*, 153-162.

(46) Beckman, E. J. *Green Chem.* **2003**, *5*, 332-336.

(47) Srinivas, K. A.; Kumar, A.; Chauhan, S. M. S. *Chem. Commun. (Cambridge, U. K.)* **2002**, 2456-2457.

(48) Liang, J.; Tang, Q.; Meng, G.; Wu, H.; Zhang, Q.; Wang, Y. *Chem. Lett.* **2004**, *33*, 1140-1141.

(49) Anastas, P. T.; Kirchhoff, M. M. *Acc. Chem. Res.* **2002**, *35*, 686-694.

(50) Bruneau, C.; Dixneuf, P. H.; Arends, I. W. C. E.; Kodama, T.; Sheldon, R. A. In *Ruthenium Catalysts and Fine Chemistry*; Springer Berlin / Heidelberg: 2004; Vol. 11, p 277-320.

Chapter 2

Objectives

Chapter 2.

Objectives

The interesting features of $Ru^{IV}=O$ complexes as catalysts for oxidative transformations presented in Chapter 1, together with the key influence of the electronic and steric properties of their ligand surrounding on the final output of the catalytic oxidation, were the basic ideas that directed the goals of this PhD thesis. Therefore, we envisaged a systematic study to better understand the relation between ligand properties, catalyst redox potentials and final catalytic results. This thorough investigation should allow us the design of improved selective oxidation catalysts. For this purpose, a family of $Ru-OH_2$ complexes bearing ligands with different electronic and steric properties will be synthesized, their redox properties will be studied and their catalytic activity towards the oxidation of organic substrates will be evaluated.

Once we have a wide set of well studied and characterized $Ru-OH_2$ catalysts on hand, we propose the selection of the most efficient ones to develop more complex systems to be used in (a) heterogeneous catalysis (gathering this way easily recyclable catalytic systems) and (b) supramolecular catalysis (in order to pursue the regio-selective oxidation of organic substrates).

In order to undergo heterogeneous catalysis we envisage the immobilization of selected catalysts on the surface of magnetic nanoparticles (MNPs) in collaboration with Prof. Pericàs group (ICIQ). The dispersion properties and easy catalyst separation of MNPs makes them suitable for the development of *quasi-homogeneous* systems combining both the advantages of homogeneous and heterogeneous processes.

In order to undergo supramolecular catalysis, and accounting with the wide expertise of Prof. Ballesters's group (ICIQ) in this field, we envisage the use of a cavitand-based ligand capable to interact with selected organic substrates and develop their regioselective oxidation.

The final goal of this PhD is the introduction of chirality into our catalytic systems. Therefore, the annulation of a pinene moiety in a polypyridyl bpea ligand is proposed. Previous work developed in our research group studying the coordination chemistry of a pinene-based bpea ligand to ruthenium was recently reported. In this work, the influence of the steric hindrance promoted by a chiral ligand (Figure 1 (a)) in the resulting isomeric complex mixtures was discussed. Herein, we propose an increase in the ligand steric hindrance (by means of the preparation of an stereoselectively alkylated derivative of [5,6]-pinene-bpea (Figure 2.1 (b)) in order to reduce the obtained isomeric mixture of Ru complexes upon coordination and study the asymmetric performance of the new ruthenium catalysts gathered towards oxidation reactions.

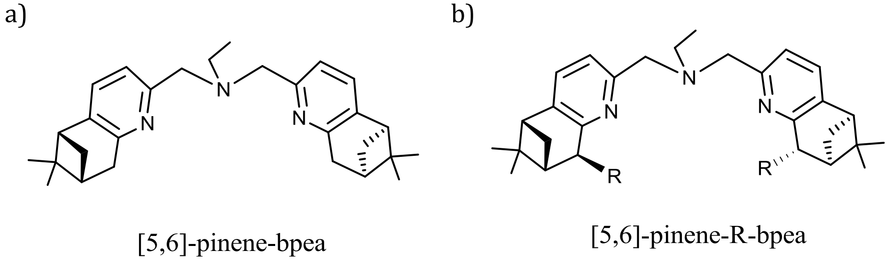

Figure 1. (a) chiral pineno-fused bpea ligand previously reported (b) envisaged alkylated chiral pineno-fused bpea ligand.

Chapter 3

Redox Properties of Ru-OH$_2$ Complexes and their reactiviy in Homogeneous Oxidations

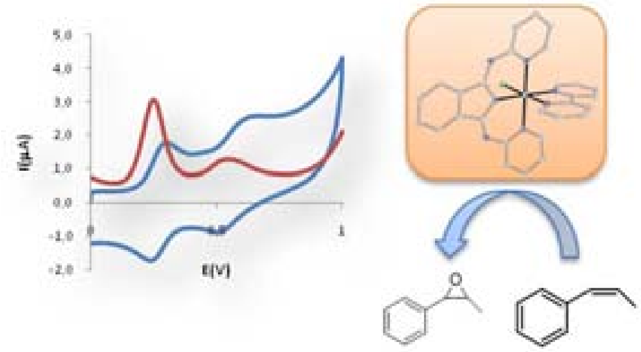

A family of Ru-OH$_2$ complexes has been synthesized with the aim of obtaining a collection of complexes with different redox properties. For this purpose σ-donor and π-acceptor ligands have been selected. The influence of the electronic properties of the ligands on the redox potentials of the complexes has been studied, together with their reactivity towards C-H bond oxidation and alkene epoxidation.

TABLE OF CONTENTS

CHATER 3. Redox Properties of Ru-OH$_2$ Complexes and their Reactivity in Homogeneous Oxidations 21

3.1. Introduction 25

3.1.1. Modulation of the electronic properties of Ru^{IV}=O complexes 25

3.1.2. Reactivity of Ru=O complexes as oxidants of C-H bonds 32

3.1.3. Epoxidation of alkenes catalyzed by Ru=O complexes 37

3.2. Results and Discussion 42

3.2.1. Synthesis of the complexes 42

3.2.2. Characterization of C9-Cl, C10-Cl and C11-Cl. 43

3.2.3. Electrochemical properties of C9, C10 and C11. 46

3.2.4. Oxidation of C-H bonds 50

3.2.5. Epoxidation of alkenes 53

3.2.6. Experimental section 61

3.3. References 66

3.4. Supporting Information 69

Chapter 3

Redox Properties of Ru-OH_2 Complexes and their Reactivity in Homogeneous Oxidations

3.1. Introduction

3.1.1. Modulation of the electronic properties of Ru^{IV}=O complexes

The reactivity of Ru^{IV}=O complexes can be modulated by tuning the electronic properties of the ligands. Through the modification of the ligands the redox properties of these complexes and, hence, their reactivity, is altered. This fact, together with the growing interest of the fine chemical industry to obtain selective catalysts for oxidation reactions, have promoted a huge number of systematic studies focused on the redox properties of these catalysts containing ligands of different nature.[1-4]

The desired modulation of the redox properties can be either by using different ligands or by introducing to the same ligand substituents of different electronic nature (electro-withdrawers or electron-acceptors). As an example, in Table 1 the redox potentials of three ruthenium complexes, $[Ru(tpm)(bpy)(OH_2)]^{2+}$, $[Ru(tpm)(bpy\text{-}NO_2)(OH_2)]^{2+}$, and $[Ru(tpm)(bpy\text{-}NH_2)(OH_2)]^{2+}$ (tpm = tris(1-pyrazolyl)methane, bpy = 2,2'-bipyridine, bpy-NO_2 = 4,4'-dinitro-2,2'-bipyridine, bpy-NH_2 = 4,4'-diamino-2,2'-bipyridine), are shown. In all cases the tridentate tpm ligand is unaltered and the bidentate bpy is modified in the 4 and 4' positions with nitro and amino groups. The complex with the non-substituted bpy is also added for comparison.

Table 1. Electrochemical parameters of Ru-OH$_2$ complexes.[a]

Entry	Complex	$E_{1/2}$ (V)			
		$Ru^{III/II}$	$Ru^{IV/III}$	$Ru^{IV/II}$ [b]	$\Delta E_{1/2}$[c]
1	$[Ru(tpm)(bpy\text{-}NO_2)(OH_2)]^{2+}$	0.57	0.75	0.66	0.18
2	$[Ru(tpm)(bpy)(OH_2)]^{2+}$	0.40	0.71	0.55	0.31
3	$[Ru(tpm)(bpy\text{-}NH_2)(OH_2)]^{2+}$	0.21	0.59	0.40	0.38

[a] In H$_2$O at pH 7.0, T = 22 ºC, I = 0,1 M, E vs SSCE. [b] $E_{1/2}$ values for the Ru^{III}-OH/Ru^{II}-OH$_2$, Ru^{IV}=O/Ru^{III}-OH, and Ru^{IV}=O/Ru^{II}-OH$_2$ couples. [c] $\Delta E_{1/2} = E_{1/2}(Ru(IV/III) - E_{1/2}(Ru(III/II)$.

As a graphical representation of the influence of the electronic properties of the ligands on the redox parameters of the complex, the Pourbaix diagrams of $[Ru(tpm)(bpy\text{-}NO_2)(OH_2)]^{2+}$ and $[Ru(tpm)(bpy\text{-}NH_2)(OH_2)]^{2+}$, compared with the non-substituted $[Ru(tpm)(bpy)(OH_2)]^{2+}$, are presented in Figure 1. In these diagrams the half-wave redox potentials of the Ru-OH$_2$ complexes are plotted *vs.* pH and the thermodynamic stability areas of the different oxidation states are represented.

There is a clear effect promoted by the substituents in the redox properties of the complex. In general, in the presence of electron-donor substituents (bpy-NH$_2$) high oxidation states are stabilized and, hence, the redox potentials decrease. On the contrary, with electron-withdrawing substituents (bpy-NO$_2$) low oxidation states are stabilized and, hence, the redox potentials increase.

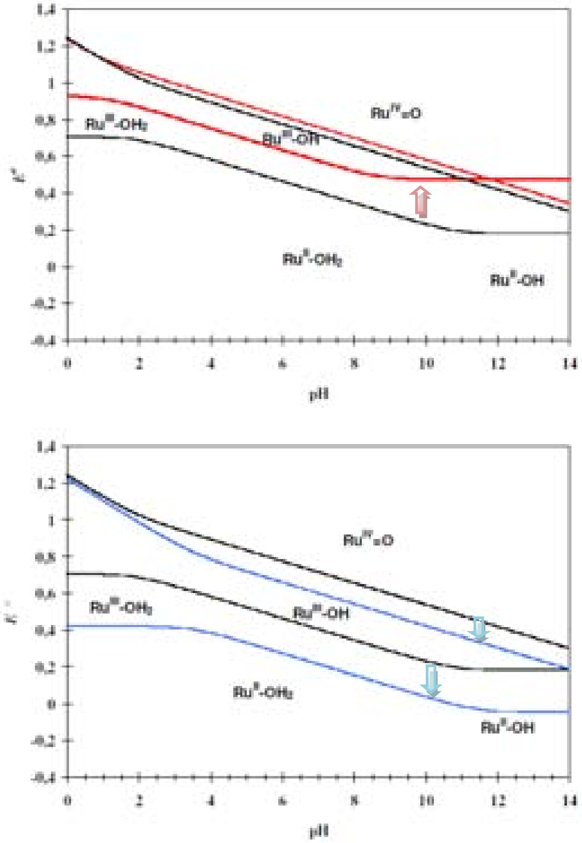

Figure 1. Simulated Pourbaix diagrams: (a)$[Ru(tpm)(bpy)(OH_2)]^{2+}$ (black) and $[Ru(tpm)(bpy\text{-}NO_2)(OH_2)]^{2+}$ (red). (b) $[Ru(tpm)(bpy)(OH_2)]^{2+}$ (black) and $[Ru(tpm)(bpy\text{-}NH_2)(OH_2)]^{2+}$ (blue).

A stronger effect can be obtained when the ligand is not modified but replaced by another one. In Table 2 a selection of the electrochemical information of different Ru-OH_2 complexes is shown.

Table 2. Electrochemical parameters of selected Ru-OH$_2$ complexes.

Entry	Complex	***E$_{1/2}$*** **(V)**			
		Ru$^{III/II}$	**Ru$^{IV/III}$**	**Ru$^{IV/II\ b}$**	***ΔE$_{1/2}$***^{c}
1	$[Ru(NH_3)_5(OH_2)]^{2+}$	-0.33	0.35	0.01	0.68
2	$[Ru(tpy)(acac)(OH_2)]^{+}$	0.19	0.56	0.38	0.37
3	$[Ru(tpy)(C_2O_4)(OH_2)]^{+}$	0.16	0.45	0.31	0.29
4	$[Ru(tpy)(OH_2)_3]^{2+\ c}$	0.35	0.64	0.50	0.29
5	*trans*-$[Ru(tpy)(pic)(OH_2)]^{+}$	0.21	0.45	0.33	0.24
6	*cis*-$[Ru(tpy)(pic)(OH_2)]^{+}$	0.38	0.56	0.47	0.22
7	*cis*-$[Ru(6,6'\text{-}Me_2\text{-}bpy)_2(OH_2)_2]^{2+\ d}$	0.57	0.73	0.65	0.16
8	$[Ru(tpy)(tmen)(OH_2)]^{2+}$	0.36	0.59	0.48	0.13
9	$[Ru(tpy)(phen)(OH_2)]^{2+}$	0.50	0.60	0.55	0.10
10	*cis* -$[Ru(bpy)_2(py)(OH_2)]^{2+}$	0.43	0.53	0.48	0.11
11	$[Ru(tpy)(bpy)(OH_2)]^{2+}$	0.49	0.62	0.56	0.13
12	*cis* -$[Ru(tpy)(4,4'\text{-}((CO_2Et)_2bpy)(OH_2)]^{2+}$	0.66	0.80	0.73	0.13
13	*cis* -$[Ru(tpy)(4,4'\text{-}Me_2\text{-}bpy)_2(OH_2)]^{2+}$	0.47	0.61	0.54	0.14
14	*cis* -$[Ru(bpy)_2(AsPh_3)(OH_2)]^{2+}$	0.50	0.67	0.59	0.17
15	*cis* -$[Ru(bpy)(biq)(PEt_3)(OH_2)]^{2+}$	0.45	0.63	0.54	0.18
16	$[Ru(tpm)(4,4'\text{-}(NO_2)_2\text{-}bpy)(OH_2)]^{2+}$	0.56	0.75	0.66	0.19
17	*cis* -$[Ru(bpy)_2(PEt_3)(OH_2)]^{2+}$	0.46	0.67	0.57	0.21
18	*cis* -$[Ru(bpy)(biq)(PPh_3)(OH_2)]^{2+}$	0.48	0.70	0.59	0.22
19	*cis* -$[Ru(bpy)_2(PPh_3)(OH_2)]^{2+}$	0.50	0.76	0.63	0.36
20	*cis* -$[Ru(bpy)_2(P(i\text{-}Pr)_3(OH_2)]^{2+}$	0.45	0.68	0.57	0.23
21	*cis* -$[Ru(bpy)_2(SbPh_3)(OH_2)]^{2+}$	0.52	0.80	0.66	0.28
22	$[Ru(tpy)(dppene)(OH_2)]^{2+\ e}$	1.17	1.53	1.35	0.36

[a] In H$_2$O at pH 7.0, T = 22 ± 2 ºC, I = 0,1 M vs SSCE. [b] E$_{1/2}$ values for the Ru^{III}-OH/Ru^{II}-OH$_2$, Ru^{IV}=O/Ru^{III}-OH, and Ru^{IV}=O/Ru^{II}-OH$_2$ couples. [c] ΔE$_{1/2}$ = *E$_{1/2}$*(Ru(IV/III) – *E$_{1/2}$*(Ru(III/II). [d] pH 4.0. [e] In CH$_2$Cl$_2$/H$_2$O (3:1). Abbreviations: biq = 1,1'-biquinoline; tmen = N,N,N,N-tetramethylethylenediamine; dppene = *cis*-1,2-bis(diphenylphosphino)ethylene; pic: picolinate anion. Acac = acethyl acetonate anion.

As previously stated, the Ru(III/II) couple is clearly influenced by the electronic properties of the ligand. The Ru(II) oxidation state is stabilized by $d\pi$-π^* back-bonding in the presence of ligands with low-lying acceptor levels, such as PPh_3. On the contrary, Ru(III) oxidation state is stabilized in the presence of electron donating ligands, such as the anionic acac or C_2O_4. In consequence, if we compare the redox potentials of $[Ru(tpy)(bpy)(OH_2)]^{2+}$ (entry 10 of Table 2) with $[Ru(tpy)(acac)(OH_2)]^{+}$ (entry 1 of Table 2) we observe a decrease in $E_{1/2}$ (III/II); and if we compare the values for *cis* -$[Ru(bpy)_2(py)(OH_2)]^{2+}$ (entry 9) with *cis* -$[Ru(bpy)_2(PPh_3)(OH_2)]^{2+}$ (entry 18) an increase in $E_{1/2}$ (III/II) is observed.

In general, the Ru(IV/III) couples are far less sensitive to ligand variations than the Ru(III/II) couples. For example, when changing a neutral bpy ligand (entry 10) for an anionic acac one (entry 1) the $E_{1/2}$(III/II) decreases 300 mV, while $E_{1/2}$(IV/III) just diminish 6 mV. This fact can be understood taking into account the important effect of the oxo group in the $Ru^{IV}=O$ species, where the stabilization promoted by this group is predominant over any other ligand effect.

Because of the different responses of the Ru(IV/III) and Ru(III/II) couples to ligand variations, the difference between both redox potentials ($\Delta E_{1/2}$) have a significant ligand dependence which mainly follows the ligand dependencies of the Ru(III/II) couple. A number of factors determine the magnitude of $\Delta E_{1/2}$. However, in general, variations in $\Delta E_{1/2}$ can be understood by taking into account that (1) the Ru(III/II) couple is most strongly affected and (2) the net effect represents a balance between stabilization of Ru(II) by back-bonding and of Ru(III) by electron donation.

$\Delta E_{1/2}$ is a quantitative value for the stability of Ru(III) against disproportionation and has an important influence in the reactivity of the corresponding aquo complexes. In general, $\Delta E_{1/2}$ is a positive value; *i.e.* a sequential oxidation of Ru(II) to Ru(III) and from Ru(III) to Ru(IV) takes place. As discussed before, the value of $\Delta E_{1/2}$ can be reduced by modification of the ligands reaching, in special cases, an overlap between $E_{1/2}$(III/II) and $E_{1/2}$(IV/III). In this situation the oxidation state III is unstable and a direct 2-electron transfer is favored, avoiding the radicalary reaction pathways of high energy and reactivity usually generated by mono-electronic transfers.[5-7]

With the aim of graphically representing the effect of the electronic properties of the ligands in $\Delta E_{1/2}$, Meyer and collaborators represented $\Delta E_{1/2}$ *vs* $\sum E_L$ (Figure 2).[3] E_L is an empiric ligand parameter introduced by Lever based on reduction potential measurements of Ru(III/II) couples.[8] The ligand parameters are determined by assuming that electrochemical potentials are additive with substitution of one ligand for another; *i.e.* each ligand has a specific effect on the metal center and the global effect derives from the sum of the effects of all ligands coordinated.

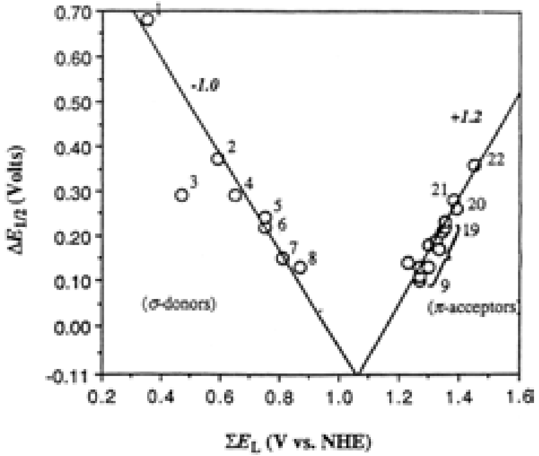

Figure 2. Meyer-Lever plot representing $\Delta E_{1/2}$ *vs* $\sum E_L$

Based on over 200 ligands, reasonable linear correlations are found between $E_{1/2}$(Ru(III/II)) and the E_L parameters by means of the following equation:

$$E_{1/2}(\mathrm{Ru(III/II)}) = S_M[\sum a_i E_L(L_i)] + I_M$$

In this equation $E_L(L_i)$ is the characteristic parameter for ligand L_i and a_i the number of such ligands. The quantities S_M and I_M are constants that depend on coordination number, stereochemistry and spin state. For Ru(III/II) couples in H_2O, $E_{1/2}(Ru(III/II)) = 1.14[\sum E_L(L_i)] - 0.35$.

In Figure 2 $\sum E_L$ is the sum of Lever parameters for the five ancillary ligands in the Ru-OH_2 complexes. This representation is consistent with the data of Table 2, where the complexes are ordered by increasing value of $\sum E_L$. As suggested by the labels in Figure 2, both the increase of effective back-bonding and electron-dononation enlarge $\Delta E_{1/2}$.

The lines drawn through the data points are best-fit lines of slopes -1.0 and 1.2. By extrapolation, the separate parts of the correleation intersect at $\sum E_L = 1.06$ V, at which point $\Delta E_{1/2} = -0.11$. This leads to the interesting suggestion that in complexes with $\sum E_L$ close to 1.06 V, Ru(III) should be unstable with respect to disproportionation. In consequence, Ru(IV) would become a more powerful two-electron oxidant than a one-electron oxidant.

The value of $\sum E_L = 1.06$ V could be achieved previously in our group by using pyridyl carbenic ligands to form the Ru-OH_2 complex $[Ru(CNC)(CN)(OH_2)]^{2+}$ (Figure 3) and, corroborating the hypothesis of Meyer *et al*, oxidation state III became unstable.[5]

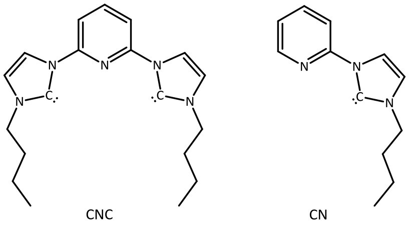

Figure 3. Pyridyl carbenic ligands of $[Ru(CNC)(CN)(OH_2)]^{2+}$.

In Figure 4 the Pourbaix diagram of this complex is shown, where the direct reduction of Ru(IV) to Ru(II) is illustrated.

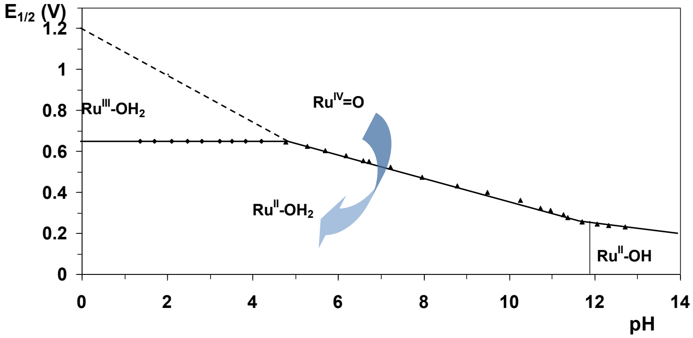

Figure 4. Pourbaix diagram of $[Ru(CNC)(CN)(OH_2)]^{2+}$

Though being this complex the only one described in the literature with a calculated Lever parameter of 1.06 V, there are a few more examples of complexes that undergo a direct 2-electron reduction. To the best of our knowledge, these complexes are the following ones: $[Ru(trpy)(azpy)(OH_2)]^{2+}$,[9] $[Ru(trpy)(bpm)(OH_2)]^{2+}$,[10] $[Ru(trpy)(bpz)(OH_2)]^{2+}$,[11] $[Ru(trpy)(Me\text{-}CN)(OH_2)]^{2+}$,[12] $[Ru(S,S\text{-}Pr^ipybox)(py)_2(OH_2)]^{2+}$,[13] and $[Ru(S,S\text{-}Pr^ipybox)(bpy)_2(OH_2)]^{2+}$.[13] The two electron nature of these complexes has been established by spectrophotometric redox titration with Ce(IV) or peak current comparisons with $[Fe(CN)_6]^{4-/3-}$ or $[Ru(bpy)_3]^{3+/2+}$.

3.1.2. Reactivity of Ru=O complexes as oxidants of C-H bonds

The selective oxidation of C-H bonds in alkanes and alkylaromatic compounds is of great technological and fundamental interest.[14-16] Ru-oxo compounds, being powerful and versatile oxidants, have received special attention in this area.[17-20]

Different mechanisms can be followed in C-H bond oxidation reactions, being hydrogen atom transfer (HAT) the predominant one. In Figure 5 the most common mechanistic pathways using toluene as a typical substrate are presented. Electron transfer oxidation of alkanes is considered a quite difficult process because of the high ionization energies of these substrates. However, electron transfer from aromatic compounds is frequently observed, forming radical cations that often lead to biaryl compounds. Through a HAT mechanism carbon radicals are formed. The formation of this species is sometimes indicated by radical coupling or rearrangement products. Hydride transfer gives carbocations which can be trapped by nucleophiles, including the aromatic initial substrate. Radical cations, carbon radicals and carbocations are somehow related; carbon radicals can be formed by deprotonation of radical cations and carbocations can be formed by oxidation of carbon radicals.

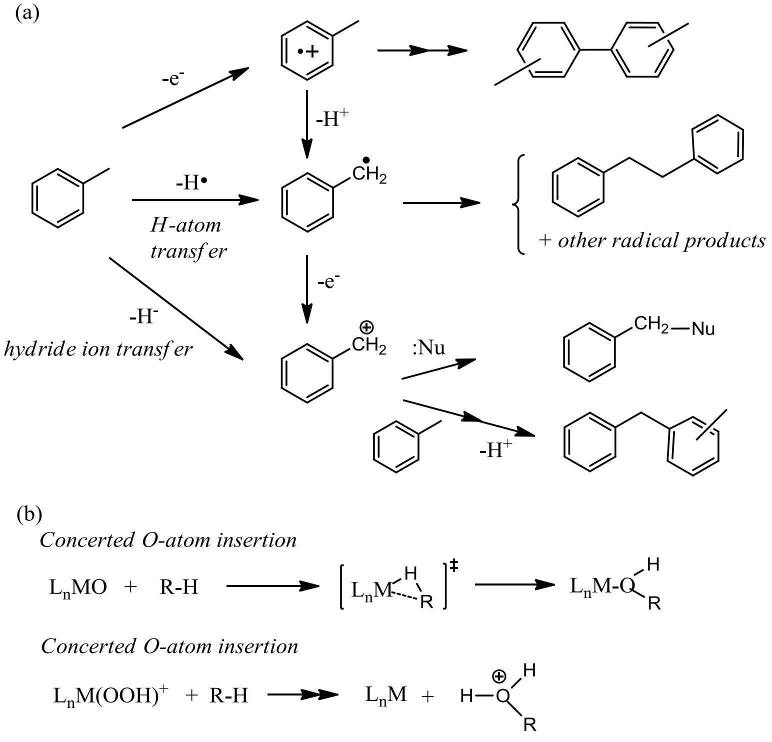
(a)
-e⁻
•+
-H⁺
-H•
H-atom transfer
CH2
+ other radical products
-e⁻
-H⁻
hydride ion transfer
CH2
:Nu
CH2—Nu
-H⁺
(b)
Concerted O-atom insertion
LnMO + R-H
LnM
H
R
‡
LnM-O
H
R
Concerted O-atom insertion
LnM(OOH)⁺ + R-H
LnM +
H—O
H
R

Figure 5. Possible mechanisms of C-H bond oxidation.

Two concerted mechanisms, oxygen atom insertion (for oxocomplexes of Ru and Fe)[21] and OH^+ insertion (in cytochrome P450 and methane monooxygenase enzymes)[20], have also been described (Figure 5, b). Concertness is usually indicated by the formation of the products of direct insertion, without any rearrangement, racemization or inversion of an intermediate radical or carbocation.

From the previous mechanisms, HAT (Figure 5) has been most widely proposed, being the nature of the products and the selectivity of oxidation often determined by the trapping of the radical species formed. Typically, three types of radical trapping reactions can take place: transfer of a second hydrogen atom to give an alkene (Figure 6, a), transfer of a ligand such as an halogen (Figure 6, b), and addition to a metal oxo group (Figure 6, c). These trapping reactions compete with dimerization reactions of the radical species.

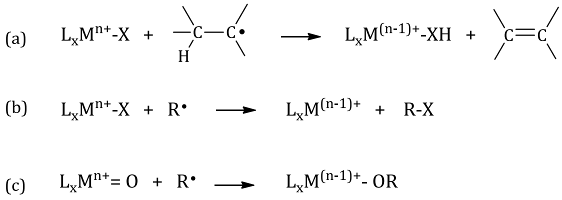
(a) L_xM^{n+}-X + H–C–C• → $L_xM^{(n-1)+}$-XH + C=C
(b) L_xM^{n+}-X + R• → $L_xM^{(n-1)+}$ + R-X
(c) L_xM^{n+}= O + R• → $L_xM^{(n-1)+}$- OR

Figure 6. Possible radical trapping reactions.

The C-H oxidation operating mechanism of the Ru^{IV}=O complex $[Ru(O)(bpy)_2(py)]^{2+}$ was studied in detail by the groups of Meyer[22] and Mayer.[18-20] This complex reacts with a range of alkylaromatic compounds following a HAT mechanism, as indicated by the product distribution and kinetic studies.[19]

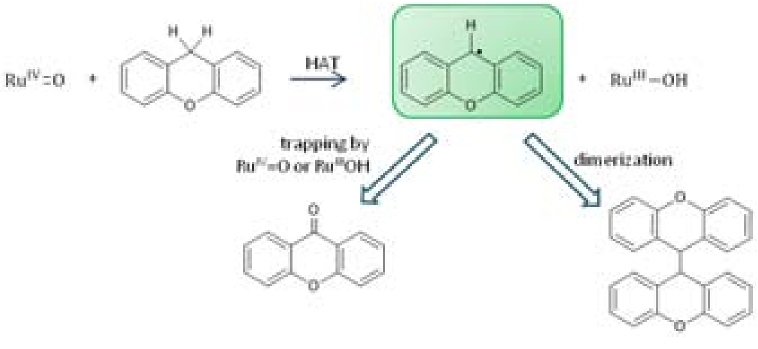

Figure 7. HAT mechanism proposed for different alkylaromatic compounds. Xanthene is used as example.

The product distributions for the oxidation reactions of dihydroanthracene (DHA), xanthene and fluorene were studied and all of them were consistent with the formation of radical species. In the case of DHA, a mixture of anthracene, anthrone and anthraquinone was observed (Figure 8, a). Anthracene was the major product as a consequence of the weakness of the C-H bond of the radical species. The product distribution was dependent on the initial concentration of oxidant and substrate ([Ru^{IV}=O] = 1-4 mM; [DHA] = 1-10 mM).

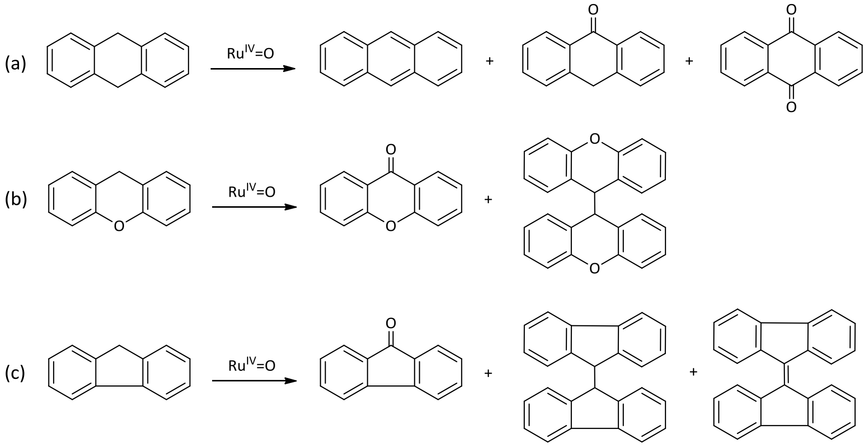

Figure 8. Oxidation of a) DHA to anthracene, anthrone and anthraquinone; b) xanthenes to xanthone and 9,9'-bixanthene; c) fluorene to fluorenone, bifluorene and bifluorenylidene with $[Ru(O)(bpy)_2(py)]^{2+}$.

In the oxidation of xanthene there is no hydrogen α or γ to the radical center, in consequence, the radical is either trapped to give xanthone or dimerizes to form 9,9'-bixanthene (Figure 8, b). The formation of this dimer is indicative of a HAT mechanism were radical species are formed. When using $[Ru(O)(bpy)_2(py)]^{2+}$ both products were observed, being xanthone the major species. It should be noted that xanthone was the only product observed when using MnO_4^- as oxidant and bixanthene the sole product observed with Fe^{III} (Hbim).[20] The different product distribution indicates that these different oxidants trap the xanthenyl radical at very different rates.[23]

The oxidation of fluorene proceeded in a similar way compared with xanthene. In this case, the reaction products were fluorenone as the major one, bifluorene and very small amounts of bifluorenylidene (Figure 8, c). Both for xanthenes and fluorene, the products correspond to a 64-80% of the ruthenium equivalents consumed. The remaining $Ru^{IV}=O$ may be consumed by further oxidation of bixanthene or bifluorene, whose tertiary benzylic C-H bonds should be still quite reactive. The dimeric products, bixanhtene and bifluorene, are formed in low yields (1-3 %). These yields are larger with lower ruthenium and higher substrate concentrations. A larger amount of dimeric products was observed when using 1mM of $Ru^{IV}=O$ and 10 mM of substrate (3.6 % for xanthene and 2.3 % for fluorene).

Another indication for a HAT mechanism was the good correlation between rate constants for the initial hydrogen atom transfer and the strength of the C-H bond being activated. In Figure 9 the rate constants *vs.* C-H bond dissociation energies (BDEs) is shown. These rate constants did not correlate so well with ionization energies (IEs); for instance, $Ru^{IV}=O$ abstracts hydrogen from cyclohexene 28 times faster than from cumene, even though cumene has a 0.22 eV lower IE. This fact suggests a HAT instead of an electron transfer.

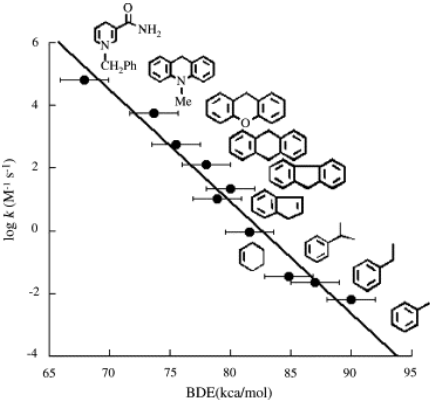

Figure 9. Hydrogen atom transfer rate constants *vs*. strength of the activated C-H bond.

3.1.3. Epoxidation of alkenes catalyzed by Ru=O complexes

The catalytic epoxidation of alkenes is both an important industrial technology and a useful synthetic method.[24,25] Ru^{IV}=O complexes have proven to act as efficient catalysts for this organic transformation.

It's believed that the oxygen atom transfer involves a side-on approach of the olefin to the Ru^{IV}=O active site. This kind of approach explains the lower enantioselectivities generally observed for trans-olefins than for *cis*-olefins, both with porphyrin-based complexes and Jacobsen type manganese salen ligands, since the approach of *trans*-olefins is clearly more hindered.

Different mechanisms, both concerted and non-concerted, have been proposed as possible pathways for oxygen atom transfers. In Figure 10 these pathways are presented. An oxygen atom can be transferred directly through a concerted oxene insertion (pathway a); through the formation of a 4 membered ring where both Ru and O atoms are respectively bonded to the Cα and Cβ of the olefin (pathway b); through a single electron transfer with the formation of a radical cation (pathway c); or through the formation of a benzylic radical intermediate (pathway d).

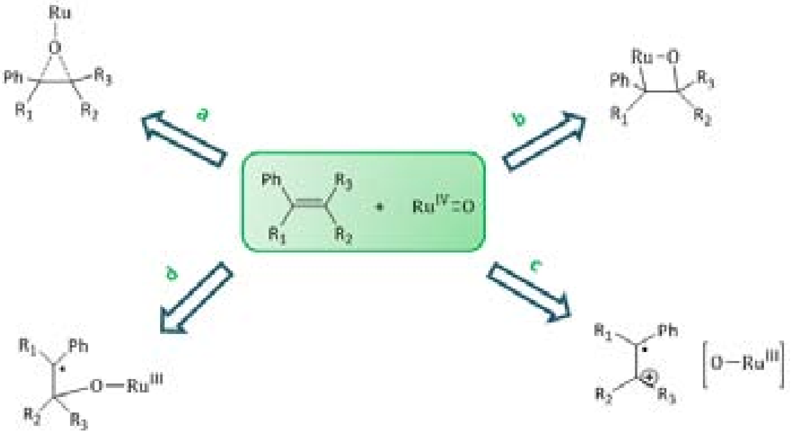

Figure 10. Proposed mechanistic pathways for oxygen atom transfer process

A thorough mechanistic investigation was developed by Che and co-workers for the epoxidation of alkenes with the following oxoruthenium complexes: [Ru(trpy)(6,6'-Cl$_2$-bpy)O](ClO$_4$)$_2$ (**1a**: trpy = 2,2':6',2''-terpyridine; 6,6'-Cl$_2$-bpy = 6,6'-dichloro-2,2'-bipyiridine), [Ru(trpy)(tmeda)O](ClO$_4$)$_2$ (**1b**: tmeda = N,N,N',N'-tetramethylethylenediamine), [Ru(Cn)(bpy)O](ClO$_4$)$_2$ (**1c**: Cn = 1,4,7-trimethyl-1,4,7-triazacyclononane), [Ru(PPz*)(bpy)O](ClO$_4$)$_2$ (**1d**: PPz* = 2,6-bis[(4S,7R)-7,8,8-trimethyl-4,5,6,7-tetrahydro-4,7-methanoindazol-2-yl]pyridine) and [Ru(PPz*)(6,6'-Cl$_2$-bpy)O](ClO$_4$)$_2$ (**1e**).[26]

Clean second-order kinetics for the oxidation of styrene and *cis*-β-methylstyrene was observed, being in concordance with a simple bimolecular kinetic scheme. For the oxidation of *cis* and *trans*-stilbene more complicated kinetics were observed and a direct oxygen atom insertion was proposed.[27]

The second-order rate constants for the stoichiometric styrene oxidation did not correlate linearly with the redox potentials of the ruthenium complexes used ($E_{1/2}(Ru^{IV/III})$ values). Therefore, the rate-limiting formation of an alkene-derived cation radical intermediate (pathway c) could not be plausible. Moreover, a one-electron reduction of $Ru^{IV}=O$ to Ru(III) would disrupt the dπ-pπ metal-oxo bond and is energetically highly demanding without a coupled proton transfer.

The use of *cis*-alkenes, such as *cis*-β-methylstyrene, is known to be useful for determining whether a concerted or non-concerted pathway takes place.[28-31] If the epoxidation of the *cis*-alkene involves a breakage of the C=C π bond resulting in the formation of an acyclic intermediate (paths c and d, Figure 11), isomerization by rotation of the C-C bond can take place, leading to the corresponding *trans*-epoxide. In consequence, the formation of mixtures of *cis* and *trans*-epoxides in the oxidation of *cis*-alkenes, can be considered as an indication of a non-concerted pathway.

Stereoselectivities for *cis*-alkene epoxidations varied with both *cis*-alkenes and ruthenium oxidants. In the epoxidation of *cis*-β-mehtylsytene mixtures of *cis* and *trans*-epoxides were observed (*cis*: *trans* ratios varying from 2:1 to 5:1). This loss of stereospecificity could not be explained with a concerted insertion of $Ru^{IV}=O$ into the C=C bond (path a, Figure 11) and, hence, a non-concerted pathway was proposed.

For the epoxidation of *cis*-β-deuteriostyrene with Che's catalysts **1a-1d**, mixtures of *cis* and *trans* epoxides were observed, discarding again the possibility of a concerted pathway. When using $1e^-$-oxidants a >90% proportion of *cis*-epoxide was observed. However, this high stereoretention cannot possibly be due to a concerted oxene insertion reaction taking into account that an inverse secondary kinetic isotope effect (KIE) was only observed for the β-d_2-styrene oxidation but not for the α-deuteriostyrene, indicating a change in hybridation of Cβ from sp^2 to sp^3 while Cα remains as sp^2.

Both product distribution analysis and kinetic experiments were in concordance with the formation of a benzylic radical intermediate in the rate-determining step (path d, Figure 11). In consequence, this mechanism was proposed for the epoxidation of aromatic alkenes with $Ru^{IV}=O$ complexes. The carboradical intermediate formed would undergo ring closure to produce the corresponding epoxide. Prior to this closure, the sigma C-C bond could rotate, leading to the formation of the isomerized epoxide. The formed radical species could also lead to the formation of byproducts, such as aldehydes, etc. (Figure 11).

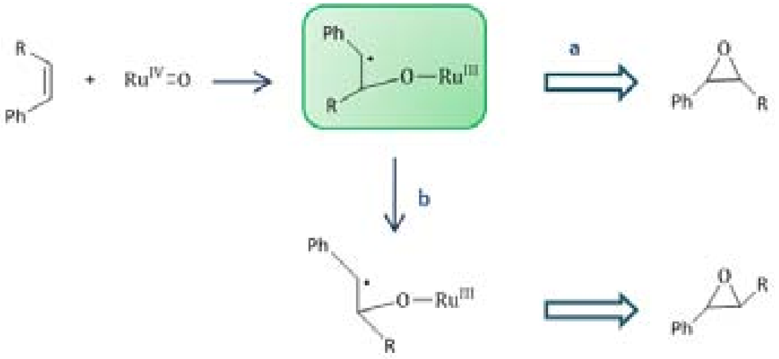
R
Ph
+
Ru^{IV}=O
Ph
R
O—Ru^{III}
a
O
Ph
R
b
Ph
O—Ru^{III}
R
O
R
Ph

Figure 11. Ring closure of the benzylic radical intermediate (a) to form the *cis*-epoxide and rotation of the C-C bond (b) prior to ring closure to form the *trans*-epoxide.

Abstract.

In this chapter we present the synthesis of a family of Ru-OH_2 complexes where the electrochemical properties are varied systematically by changing the electronic properties of the ligands. The studied complexes are shown in Figure 12. Taking into account their electrochemical properties and choosing as reference $[Ru(trpy)(bpy)(OH_2)]^{2+}$ (**C7**), they can be divided into 3 different groups: in Group I bpy has been substituted by strongly π-acceptor ligands (azpy and bpm); in Group II the pyridyl ligands have been substituted by more σ-donor ligands (pic and bid); and in Group III both π-acceptor and σ-donor ligands were combined (bid with azpy and bpm). Moreover, the reactivity of these complexes towards the oxidation of C-H bonds and epoxidation of alkenes has been studied. The influence of the electronic properties of the complexes in their reactivity has also been discussed.

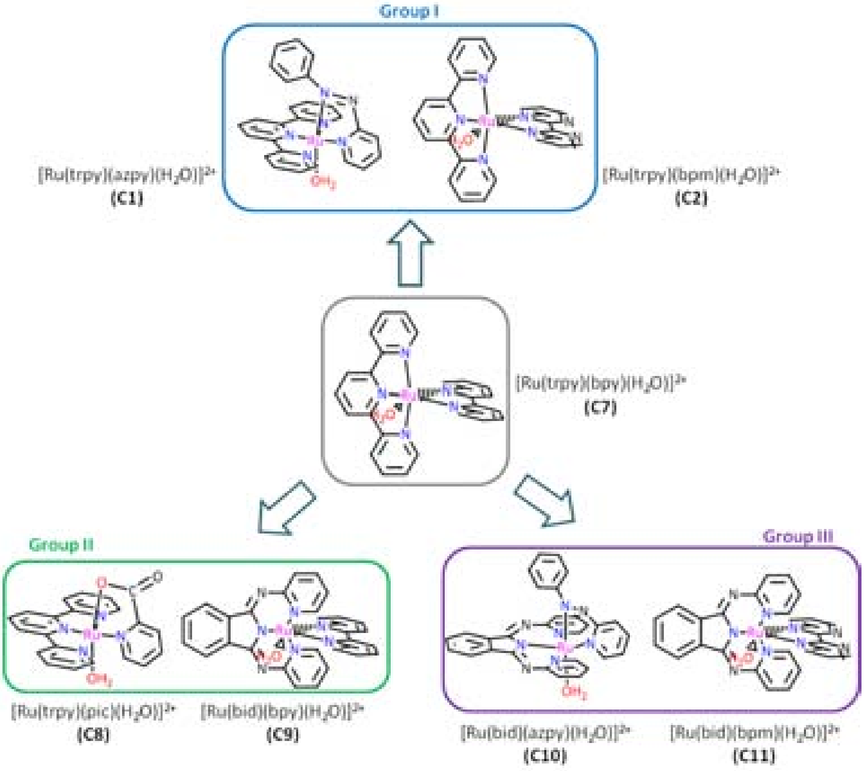
Group I
[Ru(trpy)(azpy)(H2O)]2+
(C1)
[Ru(trpy)(bpm)(H2O)]2+
(C2)
[Ru(trpy)(bpy)(H2O)]2+
(C7)
Group II
[Ru(trpy)(pic)(H2O)]2+
(C8)
[Ru(bid)(bpy)(H2O)]2+
(C9)
Group III
[Ru(bid)(azpy)(H2O)]2+
(C10)
[Ru(bid)(bpm)(H2O)]2+
(C11)

Figure 12. Family of Ru-OH_2 complexes studied in this work

3.2. Results and Discussion

3.2.1. Synthesis of the complexes

The synthetic procedure followed for the obtention of $[Ru(trpy)(bpy)(OH_2)]^{2+}$(**C7**), $[Ru(trpy)(azpy)(OH_2)]^{2+}$ (**C1**),[9] $[Ru(trpy)(bpm)(OH_2)]^{2+}$ (**C2**) and $[Ru(trpy)(pic)(OH_2)]^{+}$ (**C8**) was based on the reports described in the literature (Scheme 1). In complexes **C1** and **C8** the pyridyl ring of the bidentate ligand was placed in *cis* to the aqua ligand. For all of them $RuCl_3$ was used as metal precursor and, in a first step, the tridentate trpy ligand was coordinated to the metal center. The resulting Ru(III) species were then reduced with triethylamine and the corresponding bidentate ligands were coordinated. Finally, the chloro ligand was removed by precipitation with Ag^+ in an aqueous solution and the corresponding aquo-complexes were formed.

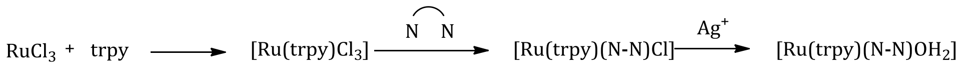

Scheme 1. Synthetic procedure for the formation of $[Ru(trpy)(N\text{-}N)OH_2]$, where N-N corresponds to a generic bidentate ligand

In order to complete the family of aquo complexes $[Ru(bid)(bpy)(OH_2)]^{+}$ (**C9**), $[Ru(bid)(azpy)(OH_2)]^{+}$ (**C10**) and $[Ru(bid)(bpm)(OH_2)]^{+}$ (**C11**) were designed, synthesized and characterized.

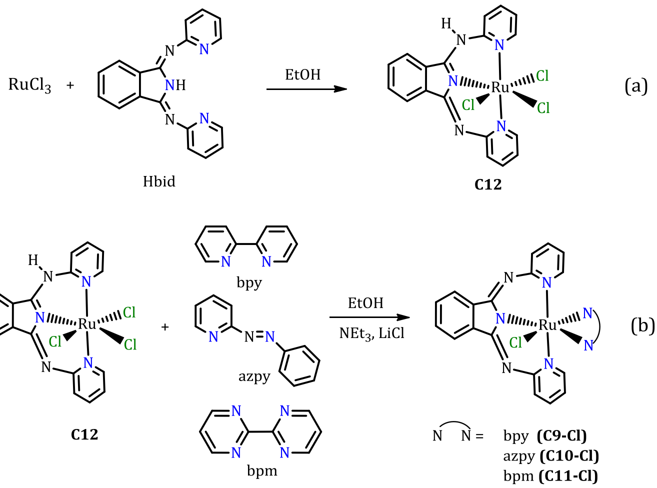

Figure 13. Synthetic pathways followed for bid-containing complexes

The synthetic strategy followed (Figure 13) was similar to the one of the other complexes. In a first step the tridentate Hbid ligand was coordinated to ruthenium by reaction with $RuCl_3$ refluxing in ethanol during 4 h to obtain **C12** as a brown solid with high yields.[37] This compound was used in the second step and, by reaction with the different bidentate ligands (bpy, azpy and bpm) in refluxing ethanol, complexes **C9-Cl**, **C10-Cl** and **C11-Cl** were obtained. In this reaction, triethylamine acts both as reducing agent and base in order to reduce Ru(III) to Ru(II) and deprotonate the Hbid ligand. All three complexes were obtained by precipitation with diethyl ether. **C9-Cl** was purified by recrystalization with dichloromethane/diethyl ether, obtaining a green solid, and **C10-Cl** and **C11-Cl** were purified by column chromatography of alumina, obtaining red and green solids, respectively.

3.2.2. Characterization of C9-Cl, C10-Cl and C11-Cl.

C9-Cl, **C10-Cl** and **C11-Cl** were characterized by the usual structural, spectroscopic and electrochemical techniques. Suitable crystals for X-Ray diffraction analysis were obtained by diffusion of diethyl ether over a solution of complex in dichloromethane. In Figure 14 the obtained structures are shown. All three complexes present a distorted octahedral geometry around the metal center. In complex **C10-Cl** the pyridyl ring of the non-symmetric azpy ligand is disposed in *cis* to the chloro ligand. This *cis* isomer was the only one observed in the synthesis of **C10-Cl**.

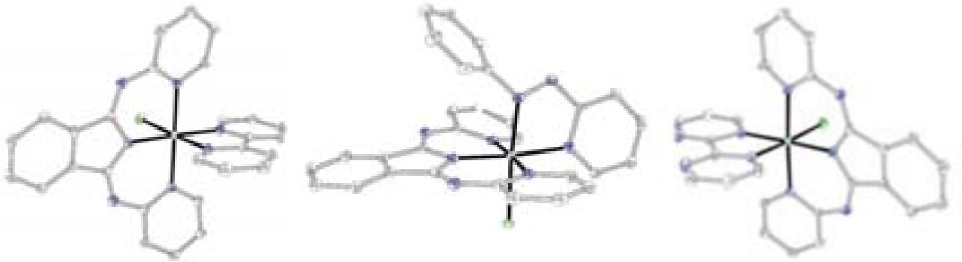

Figure 14. X-Ray structure of the cationic moieties of **C9-Cl** (left), **C10-Cl** (center) and **C11-Cl** (right)

These complexes were completely characterized by ^{1}H and ^{13}C-NMR, being all signals unambiguously assigned, as shown in Figure 15.

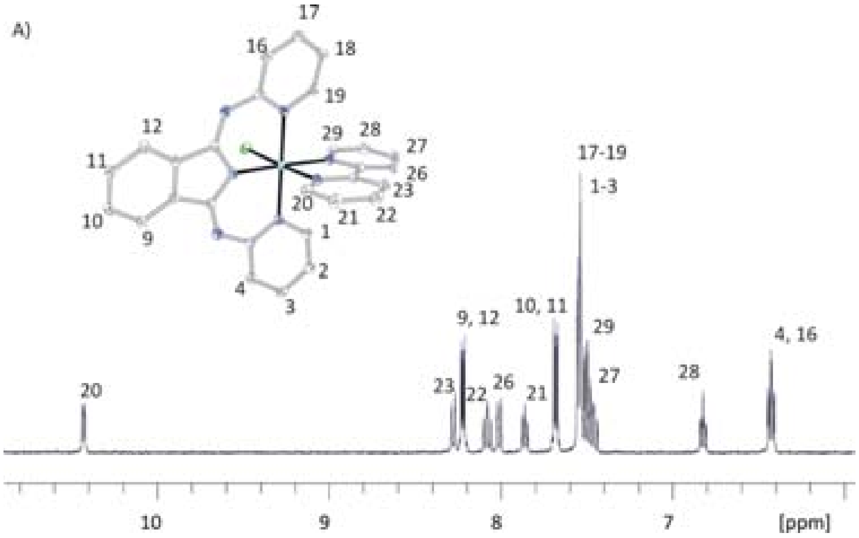

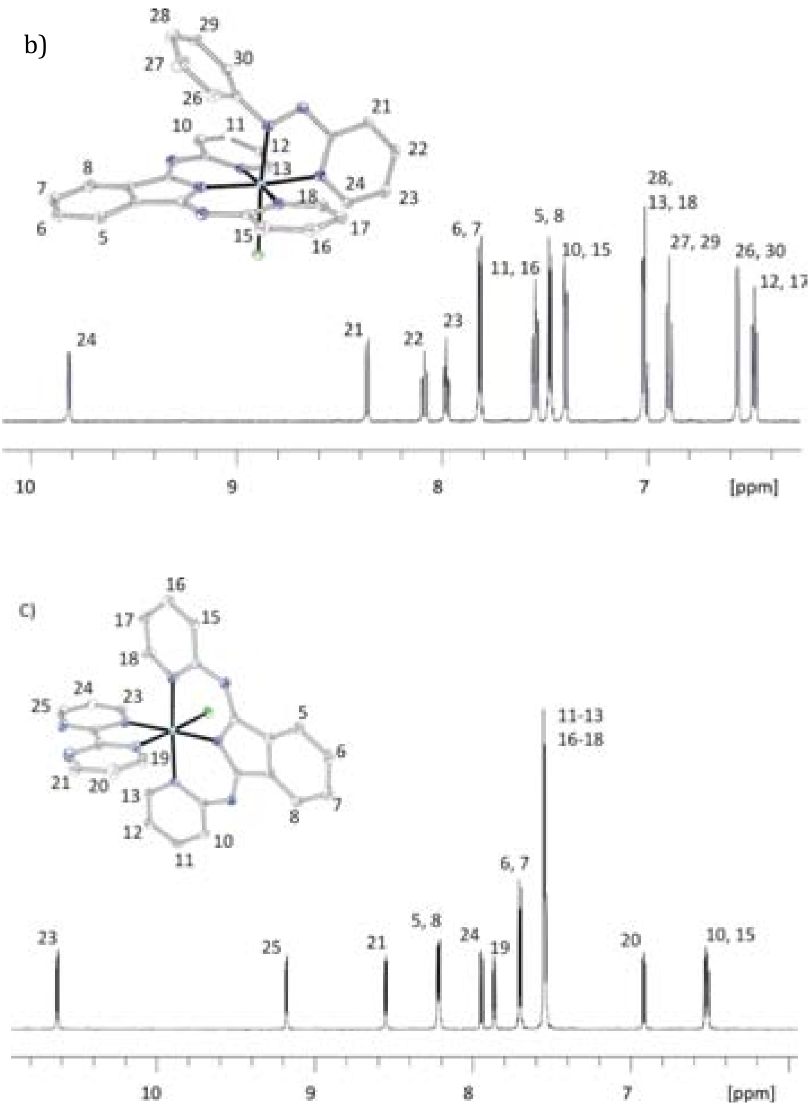

Figure 15. ^1H-NMR spectra in CD_2Cl_2 and resonance assignment of a) **C9-Cl**, b) **C10-Cl** and c) **C11-Cl**

With regard to their electrochemical properties, **C9-Cl**, **C10-Cl** and **C11-Cl** presented a reversible wave at a half wave potential ($E_{1/2}$) of 290 mv, 700 mV and 430 mV, respectively. If we compare these potential with the analoguous $[Ru(trpy)(bpy)Cl]^+$ (880 mV), $[Ru(trpy)(azpy)Cl]^+$ (133 mV) and $[Ru(trpy)(bpm)Cl]^+$ (113 mV) we can observe the effect of the negatively charged bid ligand compared with the neutral trpy ligand. As expected, this negative charge stabilizes oxidation state (III) of Ru and, in consequence, the potentials decrease. Moreover, it's also interesting to point out the effect of the π-accpetor ligands, azpy and bpm, which promote an increase in the half wave potentials, especially with azpy.

3.2.3. Electrochemical properties of C9, C10 and C11.

The Ru-OH$_2$ complexes **C9**, **C10** and **C11** were generated in situ in a mixture of H_2O (pH 7) and acetone (3:1). Acetone was added to increase the solubility of **C9-Cl**, **C10-Cl** and **C11-Cl.** In aquous solution the chloro ligands of these compounds were replaced by an aquo ligand. This substitution can be clearly observed by cyclic voltammetry, where the Ru(III/II) wave of the chloro complexes disappear and two new waves, corresponding to the oxidation of Ru^{II} to Ru^{III} and from Ru^{III} to Ru^{IV} of the aqua complexes, appeared. A change of color was also observed when substituting the chloro with an aqua ligand, what can be considered as a qualitative observation of an in situ formation of a new complex (**C9-Cl** changed from green to purple, **C10-Cl** from red to pink and **C11-Cl** from green to blue).

In Figure 16 the cyclic voltammograms of the aqua complexes are presented. The half wave potentials appear at $E_{1/2}$(III/II) = 176 mV, $E_{1/2}$(IV/III) = 508 mV ($\Delta E_{1/2}$ = 332 mV) for **C9**; $E_{1/2}$(III/II) = 512 mV, $E_{1/2}$(IV/III) = 643 mV ($\Delta E_{1/2}$ = 131 mV) for **C10**; and $E_{1/2}$(III/II) = 252 mV, $E_{1/2}$(IV/III) = 544 mV ($\Delta E_{1/2}$ = 292 mV) for **C11**.

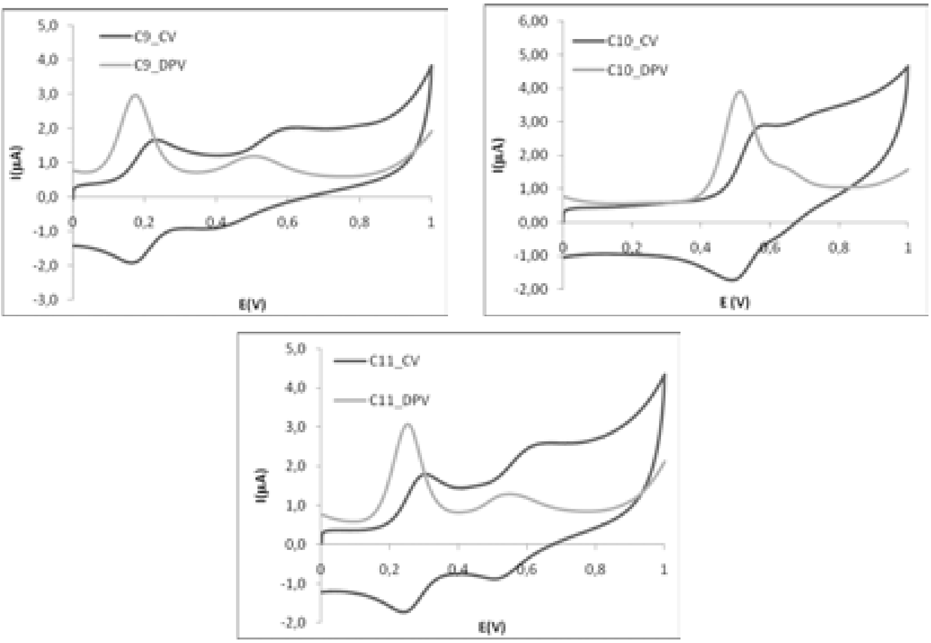

Figure 16. Cyclic Voltammetry and Differential Pulse Voltammetry of **C9**, **C10** and **C11**.

A great influence of the electronic properties of the ligands was observed in the redox potentials of the complexes. Both azpy and bpm are π-acceptor ligands, having azpy a stronger influence in the electrochemical properties of the complex. This π-acceptor character destabilized the orbitals of the electron poor ruthenium in high oxidation states, increasing the Ru(II/III) potential in more than 300 mV in the case of **C10** compared with **C9.** Moreover, a strong influence in $\Delta E_{1/2}$ was also observed, being specially decreased in **C10** ($\Delta E_{1/2}$ (**C9**) **-** $\Delta E_{1/2}$(**C10**) = 200 mV).

3.2.4. Electrochemical properties of the Ru-OH$_2$ complexes.

In order to have an overall view of the electrochemical properties of the synthesized family of Ru-OH$_2$ complexes, their redox potentials were compared. In Table 3 $E_{1/2}$(IV/III), $E_{1/2}$(III/II), $E_{1/2}$(IV/II) and $\Delta E_{1/2}$ of the different Ru-OH$_2$ complexes are shown.

Table 3. Electrochemical data for the whole family of complexes discussed in this work[a]

Ru-OH_2	$E_{1/2}$(III/II)	$E_{1/2}$(IV/III)	$E_{1/2}$(IV/II)	$\Delta E_{1/2}$
$[Ru(trpy)(bpy)(OH_2)]^{2+}$ (**C7**)	0.57	0.74	0.65	0.17
$[Ru(trpy)(azpy)(OH_2)]^{2+}$ (**C1**)	-	-	0.78	0.0
$[Ru(trpy)(bpm)(OH_2)]^{2+}$ (**C2**)	-	-	0.66	0.0
$[Ru(trpy)(pic)(OH_2)]^{2+}$ (**C8**)	0.21	0.45	0.33	0.24
$[Ru(bid)(bpy)(OH_2)]^{2+}$ (**C9**)[b]	0.18	0.51	0.34	0.33
$[Ru(bid)(azpy)(OH_2)]^{2+}$ (**C10**)[b]	0.51	0.64	0.58	0.13
$[Ru(bid)(bpm)(OH_2)]^{2+}$ (**C11**)[b]	0.25	0.54	0.40	0.29

[a] In H_2O at pH 7.0, I = 0.1 M vs SSCE. [b] In $H_2O/(CH_3)_2CO$ (3:1). $E_{1/2} = (E_{p,a} + E_{p,c})/2$. $\Delta E_{1/2} = E_{1/2}(IV/III) - E_{1/2}(III/II)$.

$[Ru(trpy)(bpy)(OH_2)]^{2+}$ (**C7**), with polypyridyl ligands that was taken as reference. The other complexes can be classified into 3 different groups: Group I would include the complexes **C1** and **C2**, where bpy was substituted by strongly π-acceptor ligands (apzy and bpm); Group II comprises the complexes **C8** and **C9** with σ-donor anionic ligands (pic and bid); and, finally, Group III includes complexes **C10** and **C11** where σ-donor and π-acceptor ligands were combined.

The electrochemical properties of these complexes have been graphically represented in Figure 17, where $E_{1/2}$(IV/III) and $E_{1/2}$(III/II) of each group are plotted in comparison with **C7**.

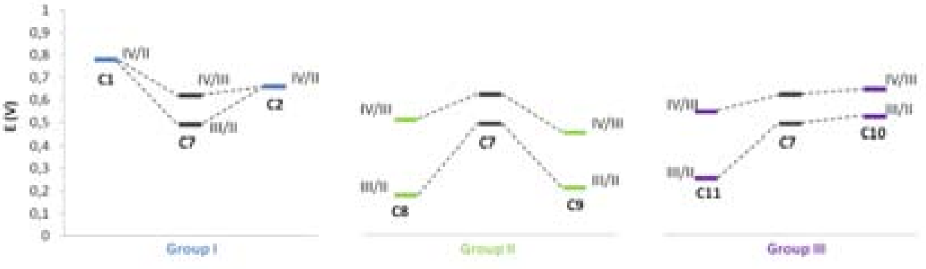

Figure 17. Representation of the electrochemical properties of **C9**, **C10** and **C11** in terms of $E_{1/2}$ and classified in Group I, II and III. $E_{1/2}$ of the complexes of each group are represented together with **C7** to facilitate the discussion.

It can be observed how different and clear trends are followed by each group. The substitution of bpy by azpy or bpm (Group I) leads to an increase in the redox potentials, as a result of the destabilization of high oxidation states. On the contrary, in Group II the potentials are decreased, being high oxidation states stabilized by the electron rich anionic ligands pic and bid. Finally, in Group III a combination of both effects is induced to the metal center, being in **C10** these effects nearly completely compensated and predominating in **C11** the effect of the σ-donor bid over the π-acceptor bpm.

The influence of the ligands in $\Delta E_{1/2}$ can also be observed in Figure 17. In all cases, E(III/II) is more strongly influenced than E(IV/III) and, in consequence, $\Delta E_{1/2}$ for Group I decreases and for Group II increases. In complexes **C1** and **C2** $\Delta E_{1/2}$ decreases up to the point of collapsing both E(IV/III) and E(III/II), leading to a direct 2-electron process instead of to two sequential 1-electron processes. This interesting property can potentially lead to an improvement in the catalytic selectivity for the oxidation of organic substrates, avoiding the formation of radicalary species (see above, section 3.1.3).

3.2.4. Oxidation of C-H bonds

Once the electronic properties of the family of Ru-OH$_2$ complexes were discussed we envisaged a study of their reactivity for the oxidation of C-H bonds and epoxidation of alkenes, paying special attention to the relation between their activity and their electronic properties. In this section, the oxidation of C-H bonds of xanthene and fluorene is presented.

The oxidation of both substrates was developed catalytically with complexes **C1**, **C2**, **C7** and **C8**, belonging **C1** and **C2** to Group I and **C8** to group II. **C7** was used as reference. The Ru^{IV}=O species were generated by addition of iodobenzene diacetate.

In the oxidation of xanthene, xanthone was observed as product and no dimer was detected (Figure 18). In Table 4 the concentration of xanthone obtained after 24 h of reaction and the initial rate for the formation of this product are presented.

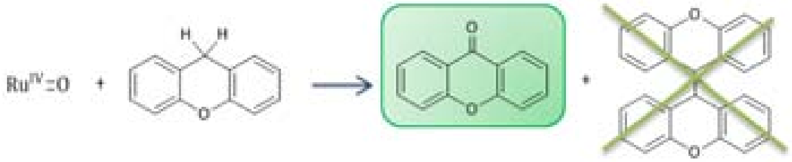

Figure 18. Product distribution for the oxidation of xanthene with complexes **C1**, **C2**, **C7** and **C8**.

Table 4. Catalytic oxidation of xanthene[a]

Complex	[xanthene][b]	[xanthone][b]	[dimer][b]	υ_i [c]
$[Ru(trpy)(bpy)(OH_2)]^{2+}$ (**C7**)	58.0	18.9	-	1.0
$[Ru(trpy)(azpy)(OH_2)]^{2+}$ (**C1**)	54.9	19.0	-	2.5
$[Ru(trpy)(bpm)(OH_2)]^{2+}$ (**C2**)	43.4	44.4	-	2.7
$[Ru(trpy)(pic)(OH_2)]^{2+}$ (**C8**)	72.5	< 5	-	-
blank	72.8	< 5	-	-

[a] [Ru] = 1.0 mM, $[xanthene]_0$ = 98.2 mM, [ox] = 99.8 mM, 1 mL dichloroethane; values obtained after 24 h of reaction. [b] (mM). [c] (10^{-6} mol·h^{-1}).

In Figure 19 a graphical representation of the yield of xanthone vs. time is shown. It can be observed that the initial rate of the reaction was enhanced by the presence of electron withdrawing ligands; i.e. by complexes **C1** and **C2** (2-electron oxidants with the highest redox potentials).

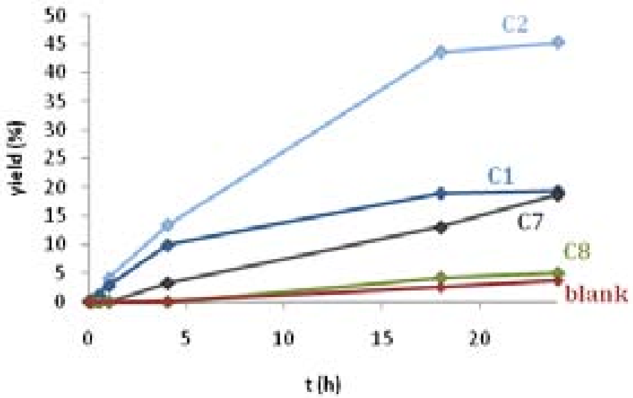

Figure 19. Evolution of the formation of xanthone with **C1**, **C2**, **C7** and **C8**. The results obtained for a blank experiment, in which no catalyst was used are added. Yield = $([xanthone]/[xanthene]_0)\cdot 100$.

Complexes **C1** and **C2**, with electron withdrawing ligands, present higher activity than **C8**, bearing electron donor ligands.

In the case of fluorene, fluorenone was observed as major product and just traces of dimer were observed (Figure 20). **C1**, with π-acceptor ligands, was the most active catalysts, being **C7** and **C8** practically non-reactive (Table 5).

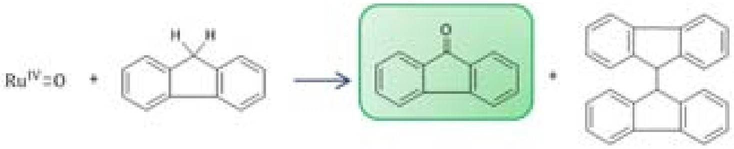

Figure 20. Oxidation of fluorene with **C1**, **C2**, **C7** and **C8**.

Table 5. Catalytic oxidation of fluorene[a]

Complex	[fluorene][b]	[fluorenone][b]	[dimer][b]	υ_i[c]
$[Ru(trpy)(bpy)(OH_2)]^{2+}$ (**C7**)	99.8	-	-	-
$[Ru(trpy)(azpy)(OH_2)]^{2+}$ (**C1**)	54.8	26.5	traces	3.3
$[Ru(trpy)(bpm)(OH_2)]^{2+}$ (**C2**)	85.8	2.5	traces	-
$[Ru(trpy)(pic)(OH_2)]^{2+}$ (**C8**)	99.5	traces	-	-
blank	99.4	-	-	-

[a] [Ru] = 1.0 mM, $[fluorene]_0$ = 97.1 mM, [ox] = 98.5 mM, 1 mL dichloroethane; values obtained after 24 h of reaction. [b] (mM). [c] (10^{-6} mol·h^{-1}).

A graphical representation of the evolution of the formation of fluorenone within time is shown in Figure 21. It can be observed that both initial rate and reactivity are significantly higher in the presence of the azpy ligand.

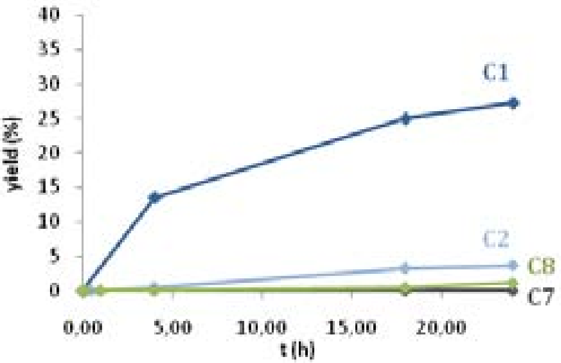

Figure 21. Evolution of the formation of fluorenone with **C1**, **C2**, **C7** and **C8**. Yield = ([xanthone]/[xanthene]$_0$)·100.

Thus, an enhancement in the reactivity and reaction rate for the oxidation of xanthene and fluorene is promoted by catalysts presenting a 2-electron nature (direct oxidation of Ru^{II} to Ru^{IV}) and high redox potentials. The formation of dimeric species was not observed for the oxidation of xanthene and, in the case of fluorene, just traces of these species were detected. This fact would be in concordance with a) a faster radical trapping by $Ru^{IV}=O$ in comparison with the rate of reaction between two radical species; or b) a direct oxene insertion favored by the overlap of the Ru(IV/III) and Ru(III/II) redox potentials.

3.2.5. Epoxidation of alkenes

The reactivity of the Ru-OH_2 complexes towards epoxidation was studied for the epoxidation of *cis*-β-metylstyrene, being this substrate useful for extracting information about the mechanistic pathways, as discussed previously (Section 3.1.3).

The reaction was performed in dichloromethane, under Ar and using iodobenzene diacetate as oxidant. A concentration of catalyst of 2.5 mM and a relation of cat:sust:ox of 1:100:200 was used (Eq. 1). 3.6 μl of H_2O were added in order to enhance the reactivity.

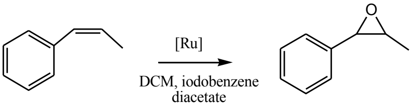

(Eq. 1)

The corresponding *cis*-epoxide (1-phenyl-propyleneoxide) was detected as the major product, with no formation of the *trans*-epoxide or just traces. In Table 6 the catalytic results obtained using the whole family of Ru-OH$_2$ complexes are summarized in terms of conversion of substrate, yield in *cis*-epoxide, benzaldehyde, and ketone, selectivity cis/trans (% of *cis*-epoxide respect to the *trans*-epoxide) and selectivity in epoxide (percentage of formed *cis*-epoxide with regard to converted substrate).

Table 6. Catalytic epoxidation of *cis*-β-methylstyrene with of all the catalysts studied in this chapter (Conditions: [Ru] = 2.5 mM, [substrate] = 250 mM, [PhI(OAc)$_2$] = 500 mM, [D$_2$O] = 500 mM, CD$_2$Cl$_2$ (0.4 mL). Conversions and yields are evaluated by ^{1}H-NMR analysis with dodecane as internal standard.[a]

Cat.	Conv. (%)	Yield (%)			Sel. (%)		υ_i
		epox$_{cis}$	Ald	ketone	*cis/trans* [c]	epox[d]	(10^{-6} mol/h)
(**C7**)	46	23	7.5	8.7	94	52	3.7
(**C1**)	88/100[b]	59/52[b]	4.4	15	97	67	8.9
(**C2**)	100	68	19	2.8	100	68	5.2
(**C8**)	100	65	14	1.8	97	65	31
(**C9**)	100	69	1.8	2.2	100	69	5.5
(**C10**)	100	38	29	13	99	38	6.2
(**C11**)	100	29	12	0.8	100	29	4.4

[a] Results obtained after 20 h of reaction; [b] Results obtained after 24 h. [c] Sel. *cis/trans* = epox$_{cis}$/(epox$_{cis}$ + epox$_{trans}$)x100. [d]Sel. epox = (Yield epox$_{cis}$/conv. subst.)x100.

It can be observed that, in presence of electron donor and/or electron acceptor ligands, the activity of the catalyst was increased, reaching all of them complete conversion after 24 h except with the complex used as reference, **C7**.

Both yield and selectivity were increased when using either electron donor (**C1** and **C2**) or electron acceptor ligands (**C8** and **C9**), being comprised between 65 % and 69 %. When both types of ligands were combined in **C10** and **C11**, the selectivity dropped down to 38 % and 29%.

The family of Ru-OH$_2$ complexes used was stereoselective, obtaining in all cases >94 % of *cis*-epoxide.

The byproducts detected in the oxidation reaction were benzaldehyde and 2-phenylketone.

In Figure 22 three graphs plotting the evolution of the formation of *cis*-epoxide are presented. The results obtained for the different Ru-OH$_2$ complexes have been classified in three different plots, being grouped depending on their electronic properties. Thus, in the first graph the results obtained with complexes with electron acceptor ligands azpy and bpm (Group I) are shown; in the second graph the results with complexes **C8** and **C9**, containing electron donating ligands pic and bid (Group II) are presented; and in the third graph the catalytic results obtained for the complexes with both σ-donating and π-acceptor ligands (**C10** and **C11** of Group III) are shown.

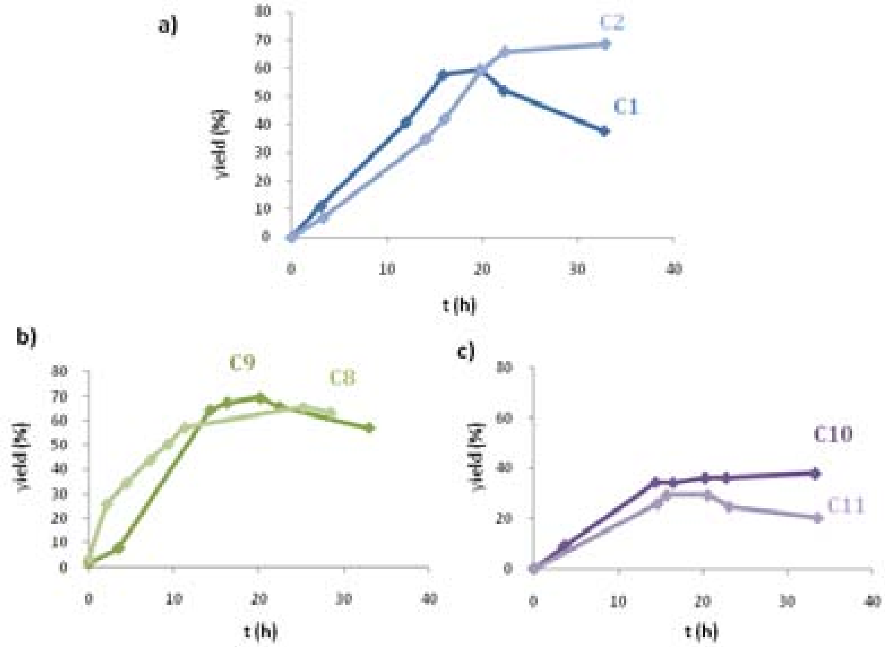

Figure 22. Evolution of the formation of *cis*-epoxide with catalysts bearing: a) electron acceptor ligands (Group I), b) electron donor ligands (Group II) and c) combined electron donor and electron acceptors ligands (Group III). Conditions: [Ru] = 2.5 mM, [substrate] = 250 mM, [PhI(OAc)$_2$] = 500 mM, [D$_2$O] = 500 mM, CD$_2$Cl$_2$ (0.4 mL). The results presented with **C8** were obtained by addition of D$_2$O after 18 h of reaction.

It can be observed that the complexes that belong to the same group follow similar trends, reaching complexes of Group I and Group II higher yields (around 70 %) compared to complexes of Group III (around 40 %).

These graphs provide also information about the stability of the formed epoxide upon further oxidation, being, in general, most of them quite stable. However, when **C1** was used as catalyst and the reaction reached 100 % conversion, the formed epoxide reacted to form the ketone phenylacetone. This ketone could be detected either by ^{1}H-NMR (singlet at 3.7 ppm) or GC-MS.

The family of Ru-OH$_2$ complexes synthesized was able to undergo a stereoselective oxidation of *cis*-β-methylstyrene. This stereoselectivity would be in concordance with a direct oxene insertion or with a fast ring closure reaction of a radical intermediate (Figure 23).

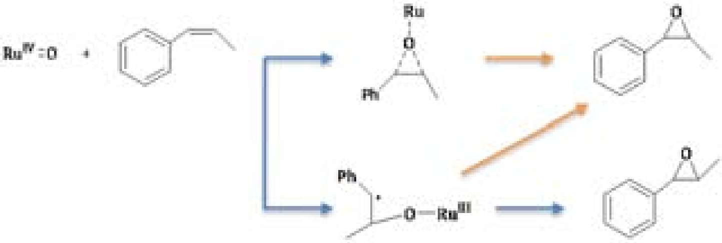

Figure 23. Proposed stereroselective reaction pathways (orange) for the epoxidation of *cis*-β-methylstyrene by Ru^{IV}=O catalysts.

Taking into account the extremely different redox properties of these complexes, it would be reasonable to expect that with **C1** and **C2**, complexes that undergo a direct 2-electron process from Ru(IV) to Ru(II), a direct concerted mechanism would be favoured. On the contrary, with complexes **C8** and **C9**, with a higher $\Delta E_{1/2}$, two sequential 1-electron processes would be favored.

In these experiments 200 eq. of H_2O were added in order to enhance the reaction rate (cat:sust:ox:H_2O 1:100:200:200). The effect promoted by the addition of H_2O can be observed in Figure 24, in which the ^{1}H-NMR spectra obtained by following the epoxidation reaction along time using **C9** as catalyst are shown. The evolution of the reaction could be easily followed, presenting both substrate and product characteristic signals of the non-aromatic C-H groups at 6.4 ppm and 5.8 ppm for *cis*-β-methylstyrene, and 4.0 ppm and 3.3 ppm for the *cis*-epoxide. It can be observed that after 48 h of reaction just a small amount of epoxide was formed and, after the addition of H_2O, 2 h were enough to observe a significant increase in the concentration of this product. After 17 h complete conversion of the substrate was achieved.

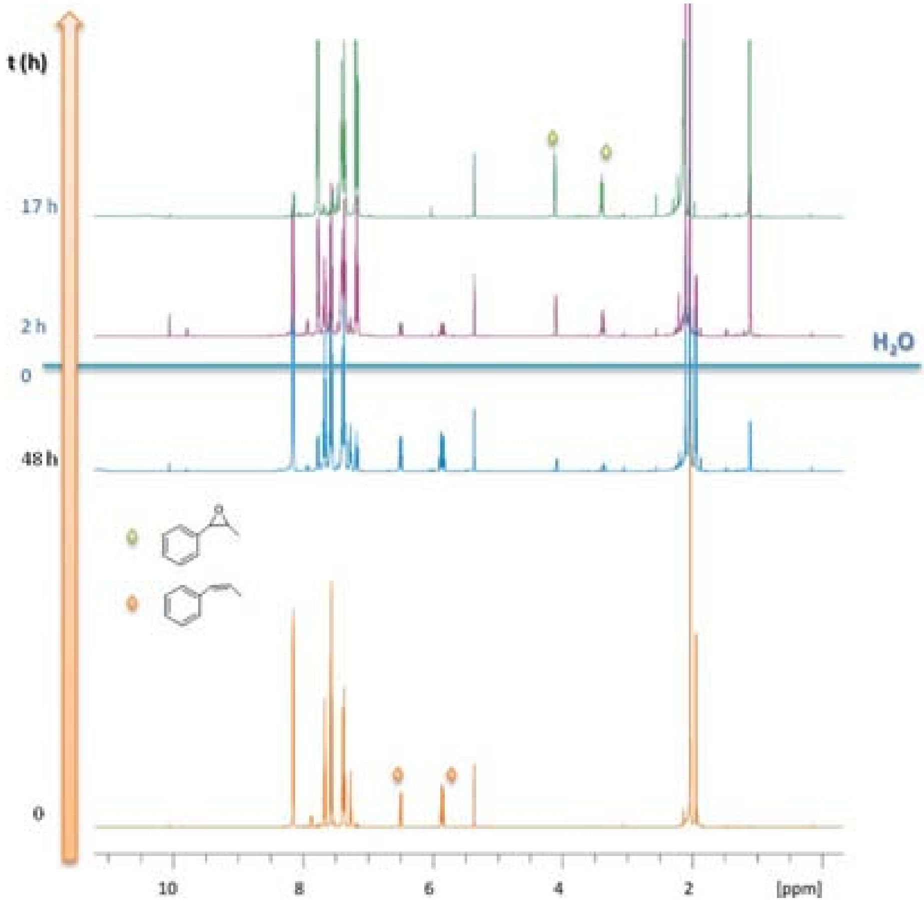

Figure 24.^{1}H-NMR monitoring of the **C9** catalyzed epoxidation of *cis*-β-methylstyrene. Effect of water addition.

The effect of H_2O in the epoxidation reaction was studied for all the Ru-OH$_2$ complexes synthesized and it was confirmed that the activity was increased for all catalysts.

On one hand, this water can be used to generate the aqua complex when using **C9-Cl** and **C10-Cl** or to regenerate the aqua complex after each catalytic cycle (Figure 25).

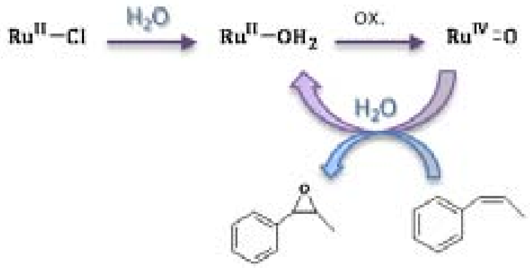

Figure 25. Formation of Ru^{II}-OH$_2$ species by substitution of a chloro ligand or regeneration from Ru^{IV}=O

Moreover, it has been observed that water reacts with iodobenzene diacetate, oxidant of the catalytic reaction. In Figure 26 the effect of water in a solution of oxidant is shown. This compound resulted quite stable for 30 h in dry d_2-dcm and when water was added iodosylbenzene was formed. It is commonly accepted that the use of iodobenzene diacetate for oxidation reactions leads to iodosylbenzene, which is capable of undergoing oxidation reactions.[32] Thus, the formation of this compound, accelerated in the presence of water, is proposed. At the same time, this reaction could also explain the enhancement of reactivity observed with the addition of water to the catalytic epoxidation reaction.

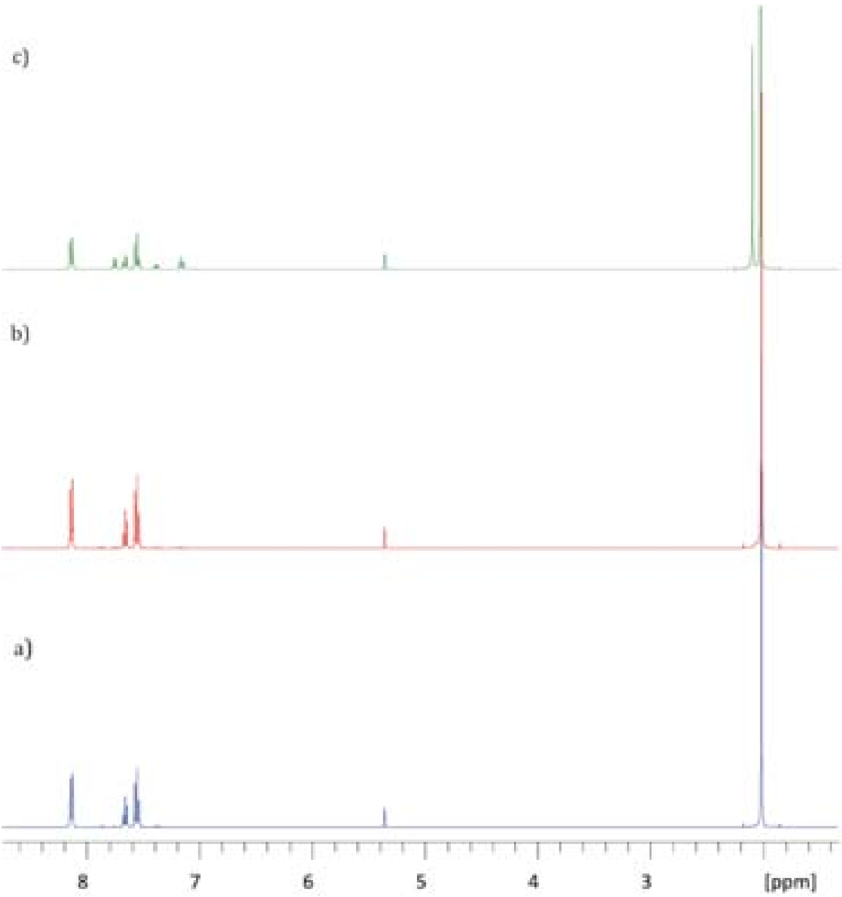

Figure 26. Reactivity of iodobenzene diacetate with H_2O. a) iodobenzene diacetate in *d*$_2$-dcm, b) after 30 h, c) after 16 h of addition of H_2O.

In conclusion, different reactions involved in the catalytic epoxidation of *cis*-β-methylstyrene with Ru-OH$_2$ complexes and iodobenzene diacetate can be influenced by the addition of water.

In order to summarize and better understand the catalytic system in study, the different reactions that take place during the catalytic epoxidation of *cis*-β-methylstyrene starting from a Ru^{II}-OH$_2$ species and PhI(OAc)$_2$ have been gathered (Figure 27).

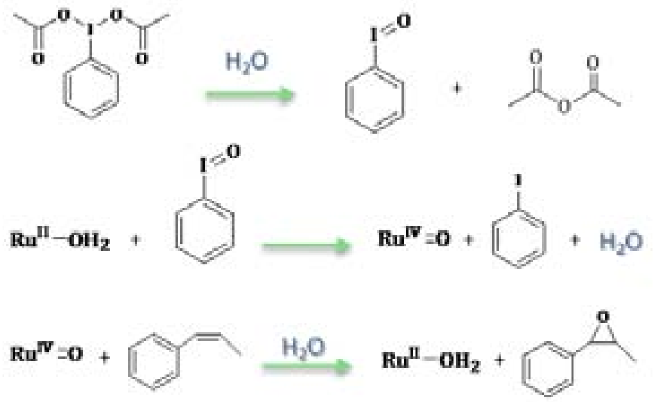

Figure 27. Summary of the reactions taking place in the catalytic epoxidation of *cis*-β-methylstyrene starting with Ru^{II}-OH_2 species and $Ph(IOAc)_2$.

As previously proposed, iodosylbenzene is formed in situ and promotes the oxidation of Ru^{II}-OH_2 to Ru^{IV}=O. This Ru species is catalytically active and capable to undergo the epoxidation of *cis*-β-methylstyrene, regenerating the initial Ru^{II}-OH_2 species and closing the catalytic cycle.

3.2.6. Experimental section

Materials. All commercial reagents from Sigma-Aldrich and TCI were directly used without any purification.

Preparations. The azpy,[33] bpm[34] and Hbid[35] ligands, the starting complexes $[Ru(trpy)Cl_3]$[36] and $[Ru(Hbid)Cl_3]$[37] and the complexes $[Ru(trpy)(azpy)Cl](ClO_4)$ (**C1-Cl**), [9] $[Ru(trpy)(azpy)(OH_2)](ClO_4)_2$ (**C1**), [9] $[Ru(trpy)(bpm)Cl](PF_6)$ (**C2-Cl**),[38] $[Ru(trpy)(bpm)(OH_2)](PF_6)_2$ (**C2**),[38] $[Ru(trpy)(bpy)Cl](ClO_4)$ (**C7-Cl**),[2] $[Ru(trpy)(bpy)(OH_2)](ClO_4)_2$ (**C7**),[2] $[Ru(trpy)(pic)Cl]$ (**C8-Cl**)[39] and $[Ru(trpy)(pic)(OH_2)](ClO_4)$ (**C8**)[39] were prepared as described in the literature. Complexes **C9-Cl**, **C10-Cl** and **C11-Cl** were synthesized and characterized in the group of Prof. L. Gade (University of Heidelberg, Germany) during a PhD short stay.

Instrumentation and Measurements. The NMR spectroscopy experiments were performed on a BrukerAvance 500 and 600 Ultrashield NMR spectrometer. Samples were run in CD_2Cl_2 and d_4-MeOD. Cyclic Voltammetry (CV) experiments were performed on an IJ-Cambria HI-660 potentiostat using a three-electrode cell. Typical CV experiments were carried out at a scan rate of 100 mV/s. A glassy carbon electrode (2 mm diameter) was used as working electrode, platinum wire as auxiliary electrode, and a SSCE as a reference electrode. Working electrodes were polished with 0.05 micron Alumina paste and washed with distilled water and acetone before each measurement. The complexes were dissolved in CH_2Cl_2 containing the necessary amount of n-Bu_4NPF_6 (TBAH) as supporting electrolyte to yield a 0.1 M ionic strength solution. $E_{1/2}$ values reported in this work were estimated from CV experiments as the average of the oxidative and reductive peak potentials $(E_{p,a} + E_{p,c})/2$. Mass spectrometry analysis were performed in a mass spectrometer with matrix assisted laser desorption ionization (MALDI-TOF, Bruker Autoflex).

X-Ray Structure Determination. Suitable crystals of **C9-Cl**, **C10-Cl** and **C11-Cl** were grown up by slow diffusion of diethyl ether into a solution of complex in dichloromethane. Data collection was performed on a Bruker Nonius FR 591 system equipped with a multilayer Montel 200 mirror monochromator Mo Kα (λ = 0.71073 Å) radiation and an Apex II CCD detector. The molecular structure was resolved by direct methods and refined of F^2 by full matrix least squares techniques using SHELX TL package with anisotropic thermal parameters.

Final R indices [$F_o > 4s(F_o)$] $R(F)$, $wR(F^2)$	**C9-Cl**: R1 = 0.0310, wR2 = 0.0864
	C10-Cl: R1 = 0.0471, wR2 = 0.0899
	C11-Cl: R1 = 0.0401, wR2 = 0.0725
Final R indices (all data) $R(F)$, $wR(F^2)$	**C9-Cl**: R1 = 0.0392, wR2 = 0.0971
	C10-Cl: R1 = 0.0714, wR2 = 0.0966
	C11-Cl: R1 =0.0694, wR2 = 0.0813

Synthesis of Ru(bid)(bpy)Cl (C9-Cl).

100 mg (0.197 mmol) of Ru(Hbid)Cl_3 (**C12**) were solved in 50 mL of ethanol. 37 mg (0.237 mmol) of 2,2'-bipyridine were added. The mixture was heated to reflux for 1h. 42 mg (0.986 mmol) of LiCl and 0.1 mL (0.790 mmol) of triethylamine were added. The mixture was heated to reflux for 4h. Complex **2** was separated by filtration and cleaned with diehtylether Yield: 42.9 % (50.0 mg, 0.0846 mmol). **^{1}H NMR** (500 MHz, DMF) δ 10.31 (d, *J* = 5.1 Hz, 1H, H29), 8.84 (d, *J* = 8.2 Hz, 1H, H26), 8.55 (d, *J* = 8.1 Hz, 1H, H23), 8.31 (td, *J* = 7.9, 1.5 Hz, 1H, H27), 8.18 (m, 1H, H9), 8.06 (m, 1H, H28), 7.72 (m, 2H, H10, H11), 7.65 (m, 1H, H27), 7.61-7.56 (m, 4H, H1, H3, H17, H19), 7.55 – 7.49 (m, 3H, H4, H16, H20), 7.06 (ddd, *J* = 7.3, 5.9, 1.3 Hz, 1H, H21), 6.55 (td, *J* = 6.6, 1.7 Hz, 2H, H2, H18). **^{13}C NMR** (125 MHz, DMF-d_7): δ 160.5 (C24), 160.2 (C25), 158.2 (C15), 154.5 (C29), 153.0 (C1, C19), 152.4 (C7, C14), 150.9 (C20), 142.1 (C8, C13), 136.4 (C27), 135.0 (C22), 134.6 (C3, C17), 130.0 (C10, C11), 128.4 (C28), 128.2 (C4, C16), 126.2 (C21), 124.5 (C26), 124.2 (C23), 121.1 (C9, C12), 117.1 (C2, C18). **CV**: $E_{1/2}$ **=** 260 mV vs. SSCE; $E_{p,a}$ = 400 mV; $E_{p,c}$ = 190 mV. **MALDI$^+$ HRMS**: [M-Cl]$^+$, Calc. for C28H20N7Ru$^+$: 556.08182; Found: 556.0758.

Synthesis of Ru(bid)(azpy)Cl (C10-Cl).

70 mg (0.14 mmol) of Ru(bid)Cl_3 (**C12**)were solved in 50 mL of dry ethanol. 0.2 mL (1.43 mmol) of triethylamine, 28 mg (0.15 mmol) of 2-phenylazopyridine and 30 mg (0.7 mmol) of LiCl were added. The mixture was heated to reflux for 1h. In the thin layer using dichloromethane/acetone 1:1 a small band of a green product (Ru(azpy)$_2Cl_2$) and complex **C10-Cl** as the major product were eluted. The solvent was evaporated and the solid was purified by column chromatography of alumina. **^{1}H NMR** (600 MHz, CD_2Cl_2) δ 9.81 (d, *J* = 5.7 Hz, 1H, H24), 8.36 (d, *J* = 8.1 Hz, 1H, H21)), 8.12 – 8.05 (m, 1H, H22), 7.98 (ddd, *J* = 7.3, 5.7, 1.3 Hz, 1H, H23), 7.82 (dd, *J* = 5.4, 3.0 Hz, 2H, H6, H7), 7.54 (ddd, *J* = 8.6, 7.0, 1.8 Hz, 2H, H11, H16), 7.47 (dd, *J* = 5.4, 3.0 Hz, 2H, H5, H8), 7.40 (dd, *J* = 8.2, 1.4 Hz, 2H, H10, H15), 7.04 – 6.98 (m, 3H, H 13, H18, H28), 6.89 (t, *J* = 7.9 Hz, 2H, H27, H29), 6.59 – 6.53 (m, 2H, H26, H30), 6.51 – 6.45 (m, 2H, H12, H17). **^{13}C NMR** (CD_2Cl_2) δ 168.8 (Cq), 156.9 (Cq), 156.5

(2Cq), 152.1 (C13, C18), 150.7 (C24), 140.1 (C20), 137.5 (C22), 137.3 (C11, C16), 129.9 (C5, C8), 128.4 (C28), 127.8 (C27, C29), 126.9 (C10, C15), 124.8 (C23), 122.8 (C21), 121.6 (C26, C30), 120.9 (C6, C7), 118.0 (C12, C17). **CV**: $E_{1/2}$ **=** 700 mV vs. SSCE; $E_{p,a}$ = 750 mV; $E_{p,c}$ = 650 mV. **MALDI⁺ HRMS**: $[M\text{-}Cl]^+$, Calc. for $C29H21ClN8Ru^+$: 618.0616; Found: 618.0663.

Synthesis of Ru(bid)(bpm)Cl (C11-Cl).

100 mg (0.197 mmol) of Ru(bpi)Cl_3 (**C12**) were solved in 100 mL of dry ethanol. 31.2 mg (0.197 mmol) of 2,2'-bipyrimidine were added. The mixture was heated to reflux for 1h. 40 mg (0.943 mmol) of LiCl and 0.2 mL (1.4 mmol) of triethylamine were added. The mixture was heated to reflux for 2h. The solvent was evaporated, dichloromethane was added. The solution was filtered and hexane was added until the precipitation of a green solid. The solid was purified by column chromatography of alumina. With a mixture of dichloromethane/acetone 6:4 complex **C11-Cl** is eluted. Yield: 30 % (35 mg, 0.059 mmol)). **^{1}H NMR** (500 MHz, CD_2Cl_2) δ 10.63 (dd, *J* = 5.7, 2.2 Hz, 1H, H23), 9.18 (dd, *J* = 4.7, 2.1 Hz, 1H, H25), 8.55 (dd, *J* = 4.5, 2.0 Hz, 1H, H21), 8.21 (dd, *J* = 5.4, 3.0 Hz, 2H, H5, H8), 7.94 (dd, *J* = 5.7, 4.7 Hz, 1H, H24), 7.86 (dd, *J* = 6.0, 2.0 Hz, 1H, H19), 7.70 (dd, *J* = 5.4, 3.0 Hz, 2H, H6, H7), 7.55 (m, 6H, H11-H13, H16-H18), 6.92 (dd, *J* = 5.9, 4.5 Hz, 1H, H20), 6.52 (m, 2H, H10, H15). **^{13}C NMR** (CD_2Cl_2) δ 166.7 (Cq), 162.2 (C23), 158.0 (C19), 157.6 (Cq), 155.2 (C25), 153.6 (C21), 153.5 (Cq), 152.2 (CH), 141.1 (Cq), 134.8 (CH), 129.8 (C6, C7), 127.7 (CH), 124.1 (C24), 121.5 (C20), 121.0 (C5, C8), 117.1 (C10, C15).). **CV**: $E_{1/2}$ **=** 430 mV vs. SSCE; $E_{p,a}$ = 490 mV; $E_{p,c}$ = 380 mV. **MALDI⁺ HRMS**: $[M\text{-}Cl]^+$, Calc. for $C26H18ClN9Ru^+$: 593.0412; Found: 593.0476.

Catalytic C-H bond oxidation.

Substrate/internal standard solution (A) and oxidant solution (B) were prepared in standard flasks. Blank samples were taken from A and 1,5 mL of A were introduced to test tubes containing proper amounts of catalyst (for 0 mM or 1 mM final concentration) and magnetic stir bar, then 1 mL of B was introduced to each test tube. Reactions were preceded in Metler-Toledo Mini Block in 25°C under argon. Aliquots were taken usually after 1 min, 30 min, 60 min, 4 h, 18 h, 24 h, 48 h. After removal of ruthenium complexes using alumina (or Celite) columns, samples were analyzed by GC/FID and GC/MS.

Catalytic epoxidation.

General procedure for the epoxidation of cis-β-methylstyrene using a relation of cat:subst:ox:H_2O of 1:100:200:200. All the experiments were developed under Ar atmosphere.

a) Followed by ^{1}H-NMR: 64.4 mg (200 μmol) of Iodobenzene diacetate were placed in and NMR tube. 0.4 mL of CD2Cl2, 13 μl (100 μmol) of cis-β-methylstyrene, 10 μl of dodecane (43.6 μmol) and 1 μmol of the Ru catalyst were added. After making a ^{1}H-NMR in order to register the product distribution at t_0, 3.6 μl (200 μmol) of D_2O were added. The data were colleted by either manual integration of the signals or with the "multi_integ3" macro of TOPSPIN.

b) Followed by GC-FID/GC-MS: To a solution of 2.5 μmol of Ru catalyst in 0.4 mL of dichloromethane in a glass tube, 33 μl (250 μmol) of cis-β-methylstyrene, 20 μl of dodecane, 165 mg (500 μmol) of iodobenzene diacetate and 0.6 mL more of dichloromethane were added. Aliquot for analysis of t_0 was taken and 9 μl (500 μmol) of H_2O were added. Aliquots taken for the analysis by GC-FID and/or GC-MS were filtered through a Pasteur pipette filled with celite and diethyl ether was added in order to elute the organic compounds.

Acknowledgements:

The experiments of the catalytic oxidation of C-H bonds presented in section 3.2.5 were developed by Dr. Tomasz Paczesniak in our research group.

3.3. References

(1) Roecker, L.; Kutner, W.; Gilbert, J. A.; Simmons, M.; Murray, R. W.; Meyer, T. J. *Inorganic Chemistry* **1985**, *24*, 3784-3791.

(2) Takeuchi, K. J.; Thompson, M. S.; Pipes, D. W.; Meyer, T. J. *Inorganic Chemistry* **1984**, *23*, 1845-1851.

(3) Dovletoglou, A.; Adeyemi, S. A.; Meyer, T. J. *Inorganic Chemistry* **1996**, *35*, 4120-4127.

(4) Suen, H. F.; Wilson, S. W.; Pomerantz, M.; Walsh, J. L. *Inorganic Chemistry* **1989**, *28*, 786-791.

(5) Masllorens, E.; Rodriguez, M.; Romero, I.; Roglans, A.; Parella, T.; Benet-Buchholz, J.; Poyatos, M.; Llobet, A. *Journal of the American Chemical Society* **2006**, *128*, 5306-5307.

(6) Richard Keene, F. *Coordination Chemistry Reviews* **1999**, *187*, 121-149.

(7) Meyer, T. J. *J. Electrochem. Soc.* **1984**, *131*, 221C-228C.

(8) Lever, A. B. P. *Inorganic Chemistry* **1990**, *29*, 1271-1285.

(9) Pramanik, N. C.; Bhattacharya, S. *Transition Metal Chemistry* **1997**, *22*, 524-526.

(10) Concepcion, J. J.; Jurss, J. W.; Templeton, J. L.; Meyer, T. J. *Journal of the American Chemical Society* **2008**, *130*, 16462-16463.

(11) Gerli, A.; Reedijk, J.; Lakin, M. T.; Spek, A. L. *Inorganic Chemistry* **1995**, *34*, 1836-1843.

(12) Dakkach, M.; Fontrodona, X.; Parella, T.; Atlamsani, A.; Romero, I.; Rodríguez, M. *Advanced Synthesis & Catalysis* **2011**, *353*, 231-238.

(13) Hua, X.; Shang, M.; Lappin, A. G. *Inorganic Chemistry* **1997**, *36*, 3735-3740.

(14) Kung, H. H. *Appl. Catal., A* **2001**, *211*, 131-132.

(15) Livingston, K. *Science (Washington, D. C.)* **1995**, *268*, 1779.

(16) Meunier, B.; Editor *Biomimetic Oxidations Catalyzed by Transition Metal Complexes*; Imperial College Press, 2000.

(17) Gunay, A.; Theopold, K. H. *Chem. Rev. (Washington, DC, U. S.)* **2010**, *110*, 1060-1081.

(18) Goldberg, K. I.; Goldman, A. S.; Editors *Activation and Functionalization of C-H Bonds. (Proceedings of the American Chemical Society Symposium held 7-9 April 2002 in Orlando, Florida.) [In: ACS Symp. Ser.; 2004, 885]*; American Chemical Society, 2004.

(19) Bryant, J. R.; Mayer, J. M. *Journal of the American Chemical Society* **2003**, *125*, 10351-10361.

(20) Mayer, J. M.; Mader, E. A.; Roth, J. P.; Bryant, J. R.; Matsuo, T.; Dehestani, A.; Bales, B. C.; Watson, E. J.; Osako, T.; Valliant-Saunders, K.; Lam, W. H.; Hrovat, D. A.; Borden, W. T.; Davidson, E. R. *Journal of Molecular Catalysis A: Chemical* **2006**, *251*, 24-33.

(21) Stultz, L. K.; Huynh, M. H. V.; Binstead, R. A.; Curry, M.; Meyer, T. J. *Journal of the American Chemical Society* **2000**, *122*, 5984-5996.

(22) Meyer, T. J.; Huynh, M. H. V. *Inorg. Chem.* **2003**, *42*, 8140-8160.

(23) Larsen, A. S.; Wang, K.; Lockwood, M. A.; Rice, G. L.; Won, T.-J.; Lovell, S.; Sadilek, M.; Turecek, F.; Mayer, J. M. *J. Am. Chem. Soc.* **2002**, *124*, 10112-10123.

(24) Sheldon, R. A. *J. Mol. Catal.* **1980**, *7*, 107-26.

(25) Joergensen, K. A. *Chem. Rev.* **1989**, *89*, 431-58.

(26) Fung, W.-H.; Yu, W.-Y.; Che, C.-M. *J. Org. Chem.* **1998**, *63*, 7715-7726.

(27) Stultz, L. K.; Binstead, R. A.; Reynolds, M. S.; Meyer, T. J. *J. Am. Chem. Soc.* **1995**, *117*, 2520-32.

(28) Castellino, A. J.; Bruice, T. C. *J. Am. Chem. Soc.* **1988**, *110*, 158-62.

(29) Castellino, A. J.; Bruice, T. C. *J. Am. Chem. Soc.* **1988**, *110*, 7512-19.

(30) Groves, J. T.; Stern, M. K. *J. Am. Chem. Soc.* **1987**, *109*, 3812-14.

(31) Groves, J. T.; Stern, M. K. *J. Am. Chem. Soc.* **1988**, *110*, 8628-38.

(32) Benet-Buchholz, J.; Comba, P.; Llobet, A.; Roeser, S.; Vadivelu, P.; Wiesner, S. *Dalton Trans.* **2010**, *39*, 3315-3320.

(33) Krause, R. A.; Krause, K. *Inorganic Chemistry* **1980**, *19*, 2600-2603.

(34) Vaid, G. b.; Horvath, I. n. T. *The Journal of Organic Chemistry* **2002**, *67*, 6550-6552.

(35) Siegl, W. O. *J. Organomet. Chem.* **1976**, *107*, C27-C30.

(36) Stoessel, S. J.; Elliott, C. M.; Stille, J. K. *Chem. Mater.* **1989**, *1*, 259-68.

(37) Marks, D. N.; Siegl, W. O.; Gagne, R. R. *Inorganic Chemistry* **1982**, *21*, 3140-3147.

(38) Swavey, S.; Fang, Z.; Brewer, K. J. *Inorganic Chemistry* **2002**, *41*, 2598-2607.

(39) Llobet, A.; Doppelt, P.; Meyer, T. J. *Inorganic Chemistry* **1988**, *27*, 514-520.

3.4. Supporting Information

- **[Ru(bid)(bpy)Cl] (C9-Cl)**

NMR: Figure S 1- Figure S 2

Cyclic Voltammetry: Figure S 5

- **[Ru(bid)(azpy)Cl] (C10-Cl)**

NMR: Figure S 3

Cyclic Voltammetry: Figure S 6

- **[Ru(bid)(azpy)Cl] (C10-Cl)**

NMR: Figure S 4

Cyclic Voltammetry: Figure S 7

NMR characterization

- **[Ru(bid)(bpy)Cl] (C9-Cl)**

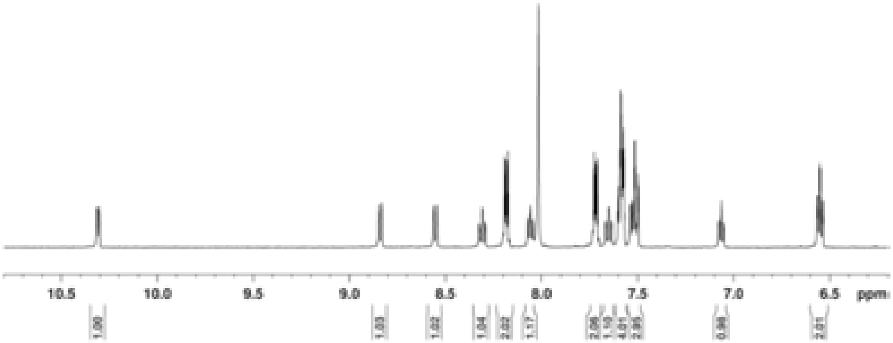

Figure S 1. ^{1}H-NMR of **C9-Cl**

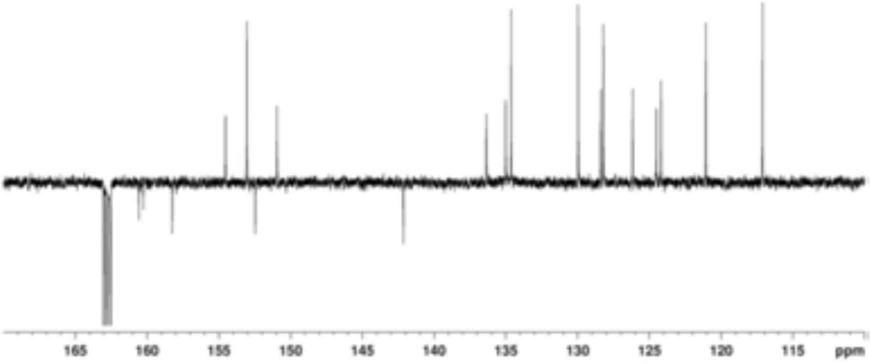

Figure S 2. DEPT135 of **C9-Cl**

- **[Ru(bid)(azpy)Cl] (C10-Cl)**

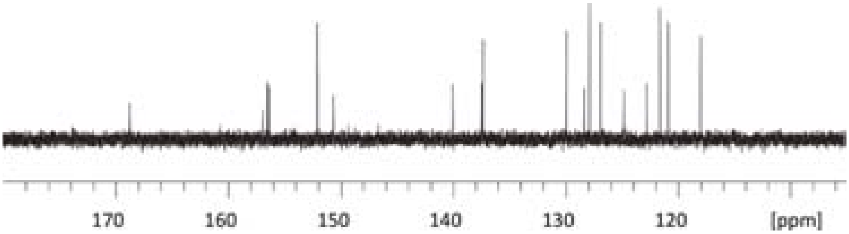

Figure S 3. ^{13}C-NMR of **C10-Cl**

- **[Ru(bid)(bpm)Cl] (C11-Cl)**

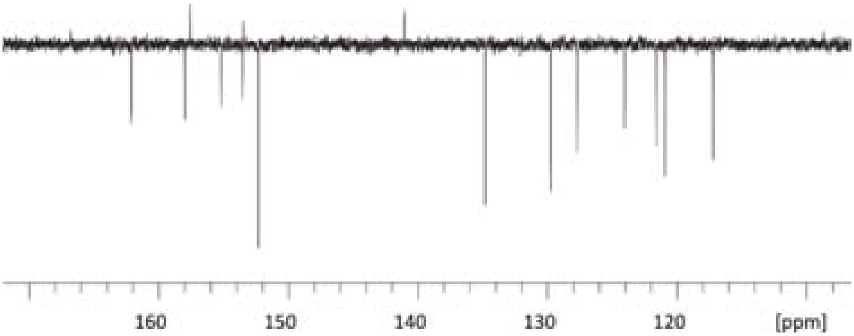

Figure S 4. DEPT135 of **C11-Cl**

Cyclic Voltammetry

- **[Ru(bid)(bpy)Cl] (C9-Cl)**

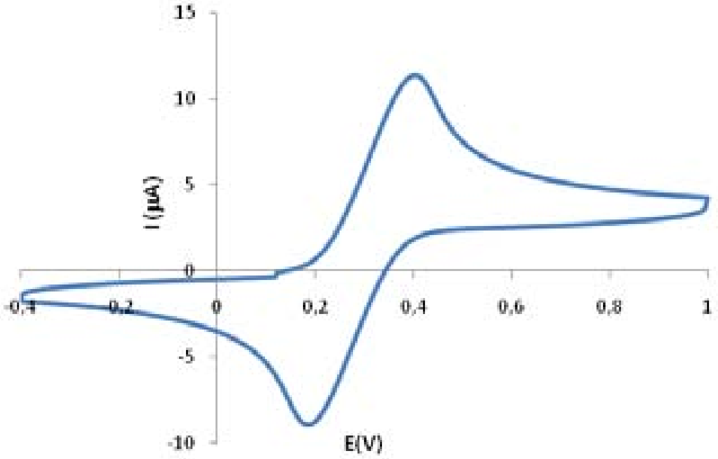

Figure S 5. Cyclic Voltammetry of **C9-Cl**

- **[Ru(bid)(azpy)Cl] (C10-Cl)**

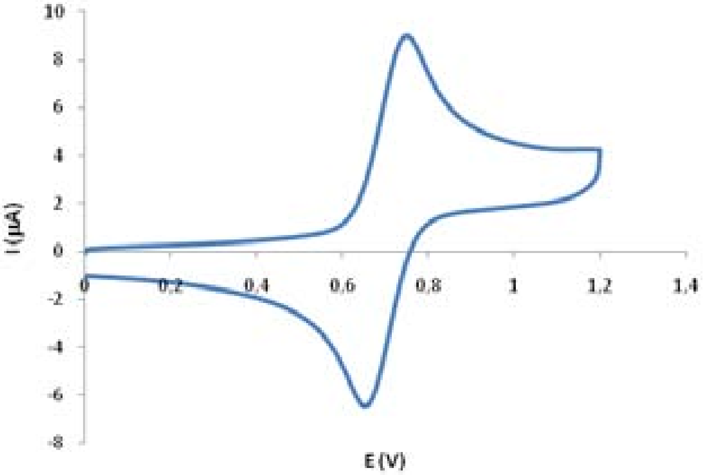

Figure S 6. Cyclic Voltammetry of **C10-Cl**

- **[Ru(bid)(bpm)Cl] (C11-Cl)**

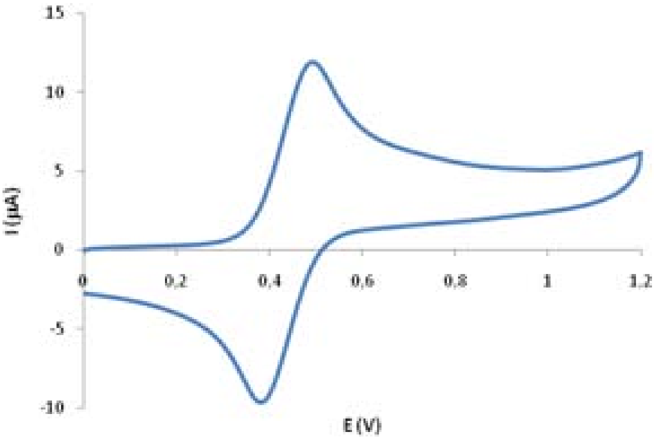

Figure S 7. Cyclic Voltammetry of **C11-Cl**

Chapter 4

Heterogenization of Stereoselective Ru complexes on Magnetic Nanoparticles

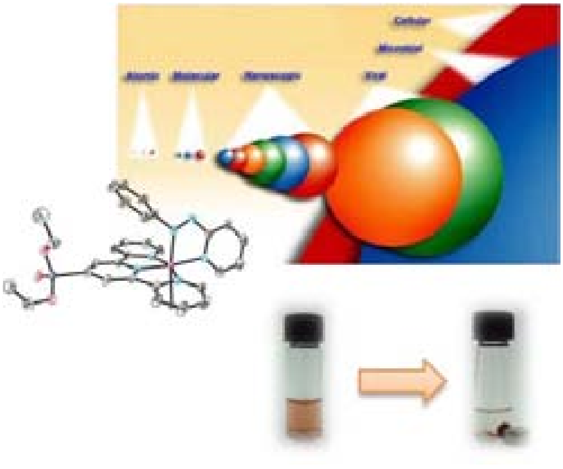

In this chapter we present the immobilization of two stereoselective ruthenium complexes on the surface of magnetic nanoparticles (NPs). For this purpose a collaboration with Prof. Miquel Pericàs (ICIQ) was developed. The behavior of the heterogeneous system in epoxidation catalysis will be studied and compared with the analogous homogeneous system.

TABLE OF CONTENTS

CHAPTER 4. Heterogenization of Stereoselective Ru Complexes on Magnetic Nanoparticles 75

4.1. Introduction 79

4.1.1. Heterogenized catalysts for oxidation reactions 79

4.1.2. Immobilization methods 80

4.1.3. Supports 81

4.1.4. Nanoparticles 82

4.2. Results and Discussion 91

4.2.1. Strategies for the immobilization of Ru complexes 91

4.2.2. Synthesis and structural, spectroscopic and electrochemical characterization of [Ru(L1)Cl_3] (C3), $[Ru(L1)(azpy)Cl]^+$ (C4) and $[Ru(L1)(bpm)Cl]^+$ (C5). 96

4.2.3. Catalytic activity of C5. 101

4.2.4. Hydrolysis of the phosphonate group. Synthesis of C6 and C7. 103

4.2.5. Preparation of magnetic nanoparticles of Fe_3O_4 (NPs). 103

4.2.6. Immobilization of Ru complexes C6 and C7 on NPs. 104

4.2.7. Catalytic activity of NP-C6 and NP-C7. Comparison with the homogeneous system. 106

4.2.8. Experimental section 111

4.3. References 118

4.4. Supporting Information 122

Chapter 4

Heterogenization of Stereoselective Ru Complexes on Magnetic Nanoparticles

4.1. Introduction

4.1.1. Heterogenized catalysts for oxidation reactions

The immobilization of homogeneous catalysts is nowadays one of the most endeavouring areas of heterogeneous catalysis.[1,2] Following this methodology, the structure of the homogeneous catalyst is retained (achieving a control and understanding of the active sites similar to in the homogeneous system), the stability of the catalyst is increased and its recycling is simple (both characteristic advantages of an heterogeneous system). The overall objective in this area is to achieve an optimal separation, recovery and recyclability of the often toxic and expensive catalyst through the heterogenization, while preferably enhancing their activity.

When dealing with oxidation catalysis, which usually involves the use or formation of oxometal complexes and other metal-oxygen bonds, the inhibition of undesired interactions between catalyst molecules will lead to the enhancement of their stability. In consequence, the heterogenization of the catalyst prevents its deactivation, either by ligand oxidative degradation or by formation of μ-oxo-bridged dimers or other oligonuclear species.

The range of immobilized catalysts used to perform the epoxidation of olefins is broad. Among the metals used we can find manganese,[3-5] iron,[4,6-8] titanium,[9] cobalt,[10] molybdenum,[11,12] tungsten[13-16] and ruthenium.[17-20]

4.1.2. Immobilization methods [1]

The most common methods used for the immobilization of catalysts on the surface of solid supports are: adsorption, electrostatic immobilization, physical entrapment and covalent binding.

a) Adsorption [21]

The adsorption is usually established by van der Waals interactions between groups such as aromatic systems and by hydrogen bonds. This method is one of the most time- and cost-effective procedures. However, the scope of this technique is quite limited taking into account that the surface of most supports is polar (limiting the application to the immobilization of polar catalysts) and that the adsorptive interactions are rather weak and can be disrupted by solvent effects or competition from oxidation products or polar oxidants. The range of supports that are used with this methodology is broad, including both amorphous and crystalline materials, such as silica and zeolites.

b) Electrostatic immobilization [22,23]

The immobilization by electrostatic interactions is a simple and fast approach to the fabrication of heterogenized catalytic systems. However, an obvious limitation is that only charged catalyst can be immobilized in this manner. When using this method, possible interactions between the support and ionic substrates or oxidants that could compete with the catalyst must be considered. The charged supports used are ion-exchange resins, zeolites, clays, layered double-hydroxides, etc.

c) Physical entrapment

This technique is based on the encapsulation of the catalyst inside the pores of the support. Encapsulation presents the advantage that the homogeneous catalyst does not suffer any change in its structure and chemical properties when being immobilized. Another advantage, is the impossibility of deactivation by oligomerization, since each molecule, and just one, is encased in a well-defined cage, without being possible the interaction with neighbouring molecules. The range of applications of this method is limited to complexes with a well-defined size and possible diffusion limitations of the substrate through the pores should be considered. This technique is very useful for the immobilization of complexes with bulky ligands such as porphyrins, phtalocyanines,[24] bipyridines,[25-27] tetradentate Schiff bases, etc. The supports used are often crystalline and contain cages, such as zeolites, mesoporous silica and coordination polymers.

d) Covalent binding [28-30]

This type of immobilization is the one that gives a stronger interaction between catalyst and support and, in consequence, yields the most stable systems. Following this methodology the catalyst must be modified by adding a linking group that attaches to the solid support. The most common linking groups used are organosilanes, of general formula R_nSiX_{3-n} (X = Cl, alkoxy), and organophosphorus acids resulting in the formation of a M-O-Si or M-O-P bond between the inorganic support (M) and the linker. In the case of a phosphonic acid up to three M-O-P bonds can be formed with the metal oxide surface, as represented in Figure 1.

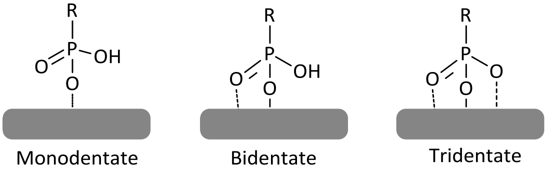

Figure 1. Possible binding modes of a phosphonate unit to a metal oxide surface.[30]

4.1.3. Supports

When choosing a support for the immobilization of a catalyst, two main aspects must be taken into account. First, the metal complex must be well dispersed through the surface of the support in order to achieve proper activities and good diffusion conditions. For this reason, parameters such as surface charge, polarity and particle and pore size must be considered. Secondly, the system must be chemically and physically stable in the catalytic reaction conditions.

The supports can be *organic*[31,32] (such as polymers with a polystyrene or polyacrylate backbone), *inorganic*[33] (silica, alumina, titania, zeolites, metallic nanoparticles, etc.) or *metal-organic frameworks*. Inorganic supports, compared with the organic ones, are chemically and thermally more stable, being able to endure the high temperatures usually used in the industry and resisting oxidative conditions.

4.1.4. Nanoparticles

Nanoparticles (NPs) can be defined as microscopic particles with a diameter of 1-100 nm. They are considered as a bridge between molecular structures and bulk materials or, in catalytic terms, a bridge between homogeneous and heterogeneous catalysis – these systems are often referred to as "quasihomogenous" (or soluble heterogeneous) systems.[34-36]

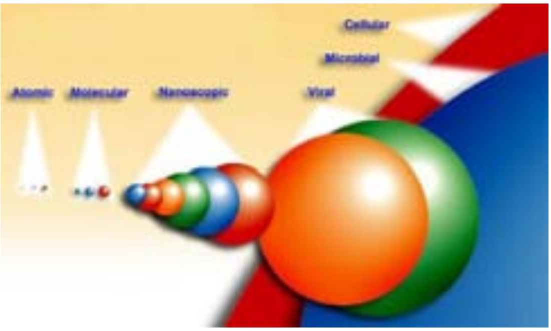

Figure 2. Size of NPs compared with other chemical and biological entities.

The first studies focused on the catalytic applications of metal nanoparticles were developed by Nord[37-39] in 1941 and were based on the reduction of nitrobenzene.

i) Properties of nanoparticles

Two great advantages of NPs can be pointed out. First, they are characteristic for presenting a large surface-to-volume ratio, what derives in large amount of active sites and increase the catalytic activity in comparison with the analogous bulk solid. An interesting example is the reactivity observed with gold nanoparticles. Gold in oxidation state zero is known to be one of the less reactive metals. However, when the size of gold particles is in a nanometer scale (3-5 nm) they become highly reactive and they are, for instance, capable to oxidize CO even at 200 K.[40]

A second advantage of the use of NPs is the possibility of separation and recycling, making them highly desirable from an environmental point of view. Different methods of separation have been developed among which we can find centrifugation, precipitation, flocculation, nanofiltration and magnetic decantation (in the case of magnetic nanoparticles).

ii) Stabilization of metal nanoparticles in solution

NPs present a large surface-to-volume ratio and, as a consequence, are thermodynamically unstable with respect to agglomeration. For this reason, the stabilization of NPs is a crucial aspect that must be taken into account. At short interparticle distances, two particles will be attracted to each other by van der Waals forces and, in absence of repulsive forces that counteract, these particles will coagulate. This counteraction can be achieved by two methods: electrostatic stabilization and steric stabilization.

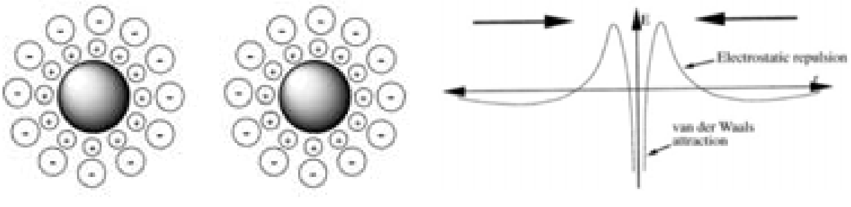

Figure 3. Electrostatic stabilization of MNPs. Attractive van del Waal forces are outweighed by repulsive electrostatic forces between adsorbed ions and associated counterions at moderate interparticle separation.

The **electrostatic stabilization** is based on the formation of a double layer of cations and anaions over the NPs' surface (Figure 3). If the electric potential associated with the double layer is sufficiently high, the electrostatic repulsion prevents the agglomeration of the particles. A classical example is the stabilization of gold nanoparticles with sodium citrate. The resulting NPs are then surrounded by an electrical double layer formed by adsorbed citrate and chloride anions and sodium cations, preventing in this way the agglomeration. If this charge is reduced by addition of a more strongly binding neutral ligand, such as pyridine, the van der Waals forces will promote the aggregation of the particles as shown in Figure 4.[41]

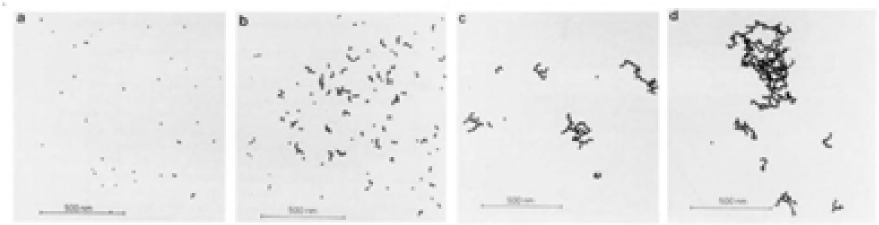

Figure 4. Aggregation of an electrostatically stabilized Au NP by the addition of pyridine.[41]

Another method used to avoid aggregation is **steric stabilization**. This method is based on the adsorption of large molecules such as polymers, surfactants or ligands at the surface of the particles, thus providing a protective layer. The most useful stabilizing ligands are considered to be vinyl polymers with polar side groups such as poly(vinylpyrrolidone) (PVP) and poly(vinylalcohol).

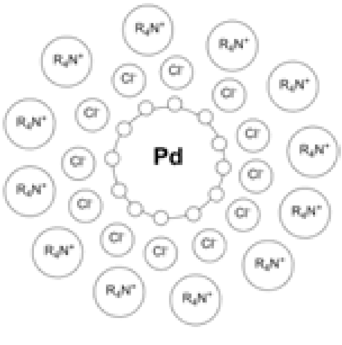

Figure 5. Electrostatic and steric stabilization of Pd NPs with tetra-*n*-octilammonium chloride.

Both electrostatic and steric stabilization can be combined by using ionic surfactants. For instance, NPs of palladium have been stabilized with tetra-*n*-octilammonium chloride (Figure 5).[42,43] In this system the chloride ions interact with the metallic surface, attracting at the same time the ammonium cations, which are disposed with the alkylic chains outwards forming a protective shield.

iii) Magnetic iron oxide nanoparticles [34]

Iron oxide nanoparticles have attracted extensive interest due to their superparamagnetic properties and their potential applications in many fields, such as multi-tera bit storage devices, catalysis, sensors and medical diagnosis.[34] There are three common iron oxides: iron (II) oxide (FeO), iron (III) oxide (Fe_2O_3) and iron (II,III) oxide (Fe_3O_4). Among these, γ-Fe_2O_3 (maghemite) and Fe_3O_4 (magnetite) have received more attention in catalysis than FeO since small FeO NP are quite sensitive towards oxygen. In the present work magnetite is used as support for the immobilization of ruthenium catalysts.

In magnetite ($Fe^{2+}Fe_2^{3+}O_4$) the iron ions are distributed in the octahedral (O_h) and tetrahedral (T_d) sites of a spinel structure. Magnetite is an inverse spinel, being the smaller tetrahedral sites occupied by the smaller Fe(III) and the remaining Fe(III) and Fe(II) occupying the octahedral sites (Figure 6).[44]

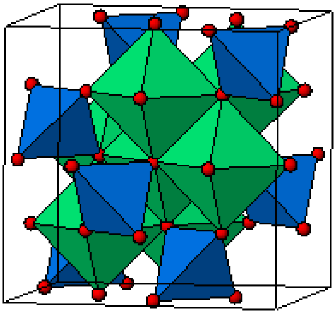

Figure 6. Polyhedra network (blue for T_d and green for O_h) of magnetite inverse spinel unit cell.

Both magnetite and maghemite are ferromagnetic materials that become superparamagnetic when the particle size is in the nano-scale. Superparamagnetic nanoparticles can be manipulated by external magnetic field gradients. When this field is removed (in contrast to ferromagnetic materials) thermal energy allows reorientation of the spins of the particles in such a way that no external energy is required to demagnetize the system.

Synthesis of superparamagentic iron oxide nanoparticles

Numerous methods have been used to synthesize magnetic iron oxide nanoparticles. Among these co-precipitation and thermal decomposition are the most commonly employed.[45,46]

a) Co-precipitation

Co-precipitation is considered the simplest way to generate iron oxides. It is typically carried out with an aqueous solution of Fe(II)/Fe(III) salts in the presence of base under inert conditions and at room temperature (Eq. 1). The resulting nanoparticles are stabilized by surfactants or ions. The major drawback of this method is the difficulty of controlling the size of the particles and, in consequence, polydisperse products are obtained.

$$Fe^{3+} + 2Fe^{2+} + 8OH^{-} \rightarrow Fe_3O_4 + 4H_2O \qquad \text{(Eq.1)}$$

b) Thermal decomposition

The thermal decomposition of iron precursors generally results in a high degree of stability and accurate control over the particle size. Monodisperse MNPs can be easily obtained through this approach by using (organo)metallic precursors (mainly metal-cupferron complexes, metal acetylacetonates, or metal carbonyls) in high-boiling solvents in the presence of surfactants as stabilizers. Hyeon *et al*. and Sun *et al*. developed very successful methods to produce monodisperse Fe_3O_4-NPs based on the presence of oleic acid and oleylamine as stabilizers.[47-49] When a Fe(III) complex is used as starting material, such as $[Fe(acac)_3]$, the formation of magnetite Fe_3O_4 nanoparticles is only possible through a partial reduction of the iron center to Fe(II). For this reason a reducing agent, such as benzylalcohol, must be added.

iv) *Magnetic nanoparticles (MNPs) and their application in catalysis*

Magnetic nanoparticles are considered as ideal supports for the heterogenization of homogeneous catalysts since they efficiently disperse catalytic active sites in the reaction medium. Furthermore, magnetic separation is a green process since it avoids the complications of filtration (such as loss of catalyst, oxidation of sensitive metal complexes, and usage of additional solvents for additional steps). Thus, waste and costs can be greatly reduced.

MNPs have been used for the oxidation of alcohols, olefins and amines as well as for the epoxidation of alkenes.[50-53] Herein we present four examples of catalyst immobilization on MNP for oxidation reactions, reflecting the last two examples the work of Lin *et.al*[56] and Peng *et.*al[57] with Ru complexes.

a) Mizuno and co-workers investigated the aerobic oxidation of alcohols and amines by using ruthenium hydroxide supported on magnetite ($Ru(OH)_x/Fe_3O_4$).[54] Primary and secondary benzylic alcohols were converted into the corresponding aldehydes and ketones in high yields. Primary alcohols reacted significantly faster, which was attributed to the formation of ruthenium alkoxides. The catalysts were also active in the oxidation of sulphur-containing alcohols and of primary benzylic, aliphatic, and heterocyclic amines. The reactions with amines resulted in the formation of the corresponding nitriles in high yields (Scheme 1).

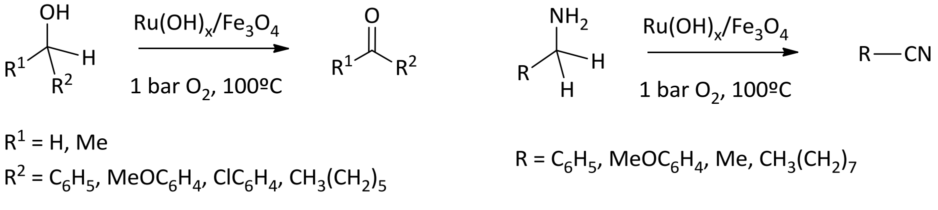

Scheme 1. Aerobic oxidation of alcohols and amines catalyzed by $Ru(OH)_x/Fe_3O_4$.[54]

b) Organic-inorganic hybrid nanocatalysts obtained by covalently anchoring [(L-L)$MoO(O_2)_2$] (L-L = (3-triethoxy-silylpropyl)[3-(2-pyridyl)-1-pyrazolyl]acetamide) on silica-coated MNPs were reported by Thiel and co-workers to be robust magnetically separable epoxidation catalysts (Scheme 2).[55] This system was active in the epoxidation of a variety of substrates, such as cyclooctene, cycloheptene, cyclohexene, styrene and 1-octene. The relatively strong interaction between the chelating ligand and the molybdenum centre as well as the covalent binding between the organic ligand and the magnetic silica support prevent leaching of the active sites. In this way, the catalyst could be recycled up to 6 times.

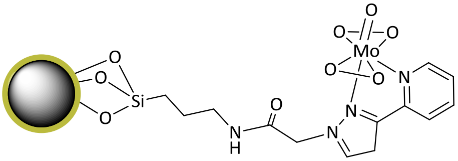

Scheme 2. Heterogenized molybdenumperoxo catalyst for olefin epoxidation on silica-coated MNPs.[34]

c) Magnetite nanoparticles were used to immobilize the ruthenium (II) complex with phosphonic acid-substituted BINAP [Ru(BINAP-PO_3H_2)(DPEN)Cl_2] (Scheme 3).[56] MNPs were prepared in two different ways; NP1 was synthesized by thermal decomposition and NP2 by co-precipitation. The Ru(II) complex was immobilized in NP1 and NP2 and was used for the hydrogenation of aromatic ketones presenting high reactivity and enantioselectivity. A wide range of aromatic ketones were hydrogenated to their corresponding secondary alcohols with complete conversion. Ru-NP1 and Ru-NP2 were successfully reused for the asymmetric hydrogenation of 1-acetonaphtone without decrease of the enantioselectivity. When using Ru-NP1 the activity did not decrease for the first 4 runs and with Ru-NP2 the catalyst could be reused up to 14 times with no conversion decrease.

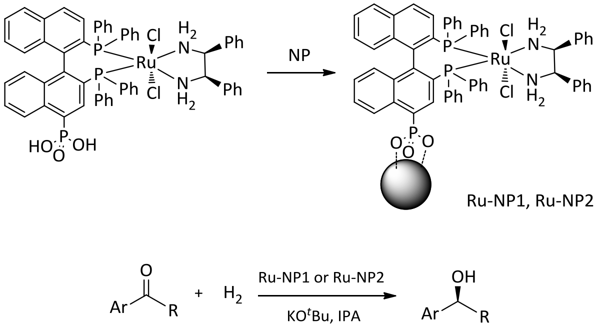
NP
Ru-NP1, Ru-NP2
Ru-NP1 or Ru-NP2
KO^{t}Bu, IPA
+ H$_2$

Scheme 3. Immobilization of [Ru(BINAP-PO_3H_2)(DPEN)Cl_2] on MNP for the hydrogenation of aromatic ketones.

d) The second generation Hoveyda-Grubbs catalyst was immobilized on the surface of commercially available MNPs (diameter 100 nm) with a loading amount of 0.28 mmol Ru/g NP (Scheme 4). The supported catalyst was active for the self- and cross-metathesis of methyl oleate in quantitative conversions. The immobilized catalyst could be recovered and reused up to 5 times with sustained activity.

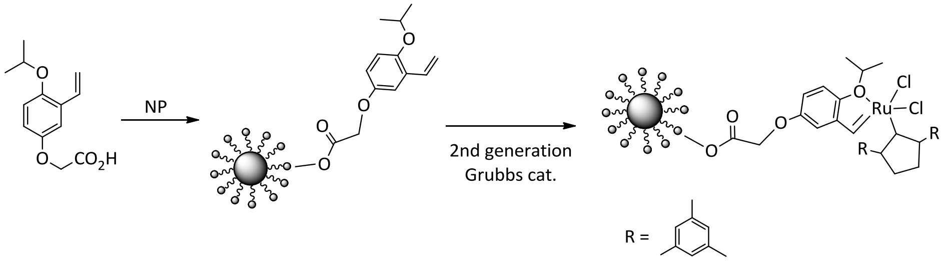
NP
2nd generation
Grubbs cat.
R =

Scheme 4. Immobilization of the 2nd generation Hoveyda-Grubbs catalyst on MNP.

Abstract

In this chapter we present the immobilization of two ruthenium complexes on the surface of magnetite nanoparticles. These nanoparticles were prepared by thermal decomposition of [Fe(acac)$_3$]. The complexes [Ru(trpy)(azpy)OH$_2$]$^{2+}$ (**C1**) and [Ru(trpy)(bpm)OH$_2$]$^{2+}$ (**C2**) (Figure 7) were selected for the heterogenization, belonging both of them to the family of the so-called 2-electron-complexes introduced in Chapter 1 and catalytically evaluated in Chapter 3. The use of these complexes allowed us to develop a stereoselective and heterogeneous catalytic oxidation of organic substrates.

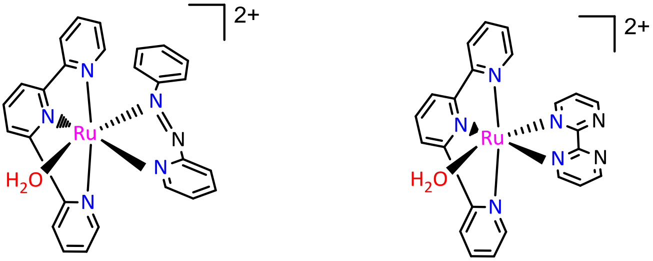

C1 **C2**

Figure 7. Representation of [Ru(trpy)(azpy)OH$_2$]$^{2+}$ **(C1)** and [Ru(trpy)(bpm)OH$_2$]$^{2+}$ **(C2)**

4.2. Results and Discussion

4.2.1. Strategies for the immobilization of Ru complexes

The immobilization method used for the heterogenization of $[Ru(trpy)(azpy)OH_2]^{2+}$ and $[Ru(trpy)(bpm)OH_2]^{2+}$ presented here was based on a covalent binding, thus achieving a strong interaction between the catalyst and the solid support.

In order to create this covalent bond a linking group that joined complex and solid support was added without modifying the intrinsic properties of the homologous complex. Two different linking groups have been used: phosphonate and trialkoxysilane (Scheme 5).

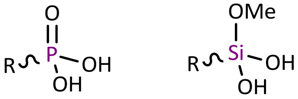

Scheme 5. Phosphonate and trialkoxysilane linking groups.

This linker can be a functional group of the ruthenium complex or a modification of the support's surface. In the latter case the linker of the NP and the complex must have functional groups able to react with each other. Taking this into account, different strategies were followed for the immobilization of complexes $[Ru(trpy)(azpy)OH_2]^{2+}$ and $[Ru(trpy)(bpm)OH_2]^{2+}$:

i) Using ligands modified with a linker.

Different terpyridines were used; **L1** and **L2** were functionalized with a phosphonate group and **L3** with a trialkoxysilane group (Scheme 6). **L2** consists of two terpyridines bonded by a nitrogen atom and with a linkers' chain longer than in **L1**.

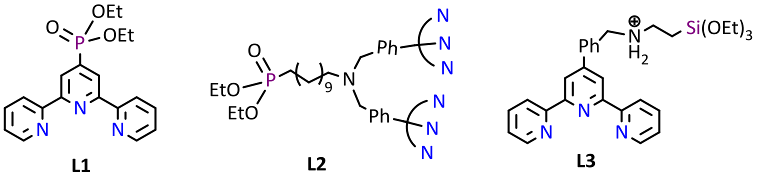

Scheme 6. Representation of **L1**, **L2** and **L3**.

L1 was commercially available. **L2** was synthesized by a nucleophilic attack of an amino-phosphonate (**1**) to a bromo-derivative of terpyridine (**L4**) using DIPEA as a base. The synthesis of **L3** was based on the attack of an amino-silane (**2**) to the bromo derivative of terpyridine, in this case, in absence of base (Scheme 7).

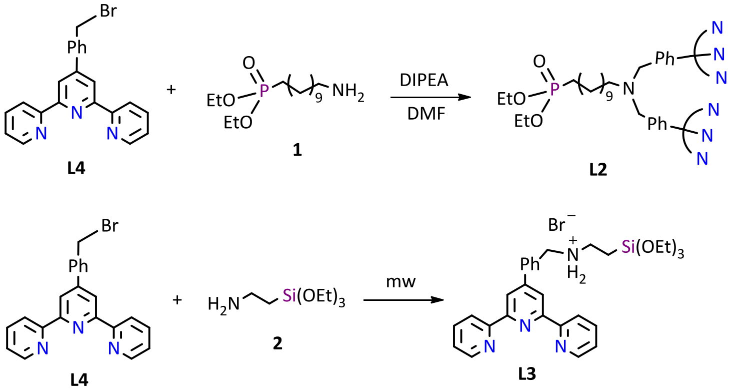

Scheme 7. Procedure followed for the synthesis of **L2** and **L3**.

The experimental procedure used for the synthesis of the ruthenium complexes with the modified terpyridines **L1**, **L2** and **L3** was based on the methods shown in Scheme 8. In a first step **L1**, **L2** and **L3** were coordinated to ruthenium using $RuCl_3$ as metal precursor, thus obtaining the neutral complexes [Ru(**L1**)Cl_3], [Ru(**L2**) Cl_3] and [Ru_2(**L3**)Cl_6] in almost quantitative yields. In a second step two chloride atoms were replaced by the bidentate ligands (azpy or bpm).

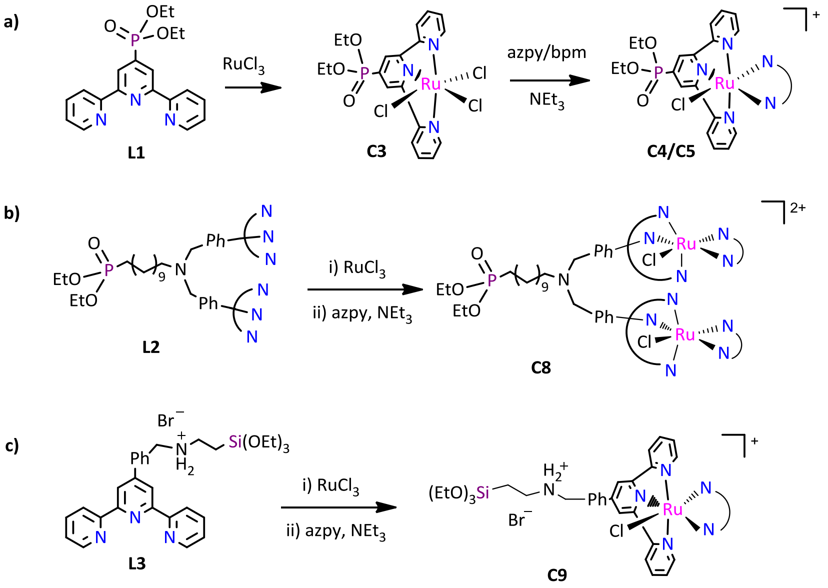

Scheme 8. Synthetic procedure of (a) Ru(**L1**), **C4** and **C5** (b) Ru(**L2**), **C8** and (c) Ru(**L3**), **C9** complexes.

Complexes with **L1**, [Ru(**L1**)(azpy)Cl]$^+$ (**C4**) and [Ru(**L1**)(bpm)Cl]$^+$ (**C5**), were isolated by precipitation with diethyl ether with moderate to good yields (**C4**: 78 %, **C5**: 50 %).

In the case of **L2**, the first reaction proceeded with good yield. However, in the subsequent coordination of the bidentate ligand mixtures of products were obtained, including different isomers (*cis* and *trans* disposition of the non-symmetric azpy ligand) and complexes in which **L2** was broken having just one terpyridine and one phosphonate group. By employing a semi-preparative HPLC with reverse phase column (C18) these compounds could be separated and purely obtained with low yields.

When using a terpyridine with a trialkoxysilane group (**L3**) a mixture of complexes was obtained. The final complex **C9** could be isolated by column chromatography of alumina with low yields.

ii) Using NPs with the linker anchored on the surface.

Another approach for the formation of the final NP-Ru with the ruthenium complex anchored through a trialkoxysilane linker (as in the case of **L3**) was tested. In this approach the trialkoxysilane was anchored on the nanoparticle, in contrast to the case of **L3** where the trialkoxysilane was part of the trpy ligand (Scheme 9).

NPs modified with an aliphatic chain anchored through a trialkoxysilane group and with a terminal amine (**NP-NH$_2$** of Scheme 9) were used. This terminal group could easily react with the functionalized terpyridine **L4**.

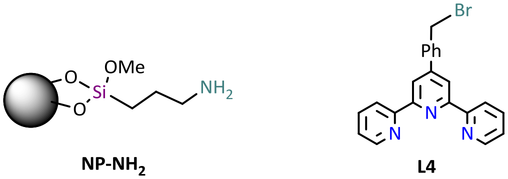

Scheme 9. Representation of the functionalized nanoparticle **NP-NH$_2$** and terpyridine **L4**.

The synthetic strategy consisted on the formation of complex [Ru(**L4**)(azpy)Cl]$^+$ and its subsequent heterogenization on MNPs (Scheme 10). A first drawback of this strategy was found in the synthesis of the complex. The functionalized terpyridine was not stable in the reaction conditions and, even after purification by column chromatography of alumina, a mixture of two complexes, with and without the bromo group in the trpy ligand, were obtained. These two complexes were unambiguously identified by ^{1}H-NMR and, taking into account that just the bromo-derivative complex would react with the amine of **NP-NH$_2$**, the next step of heterogenization was attempted, obtaining the final desired heterogenized complex. However, the trialkoxysilane linkage didn't seem very stable when using ultrasound to disperse the sample.

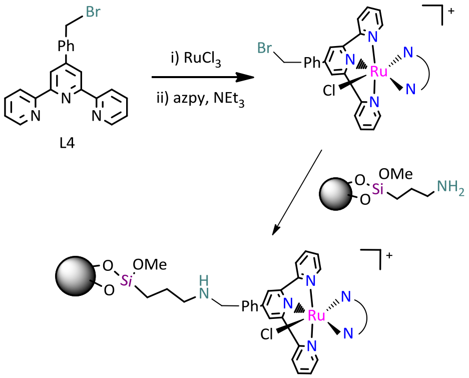
Br
Ph
L4
i) RuCl$_3$
ii) azpy, NEt$_3$
Br
Ph
N
N
Ru
N
N
Cl
N
+
O
OMe
Si
O
NH$_2$
O
OMe
Si
O
H
N
Ph
N
N
Ru
N
N
Cl
N
+

Scheme 10. Immobilization of a Ru catalyst from **L4** and trialkoxysilane-functionalized MNPs.

From the different approaches presented here, the use of **L1** was chosen as the best strategy. The corresponding complexes, with azpy and bpm, could be easily obtained with good yields, and the phosphonate linkage resulted in a very stable interaction. Herein we present the synthesis and characterization of the complexes, their heterogenization process and the final catalytic studies in detail.

4.2.2. Synthesis and structural, spectroscopic and electrochemical characterization of [Ru(L1)Cl$_3$] (C3), [Ru(L1)(azpy)Cl]$^+$ (C4) and [Ru(L1)(bpm)Cl]$^+$ (C5).

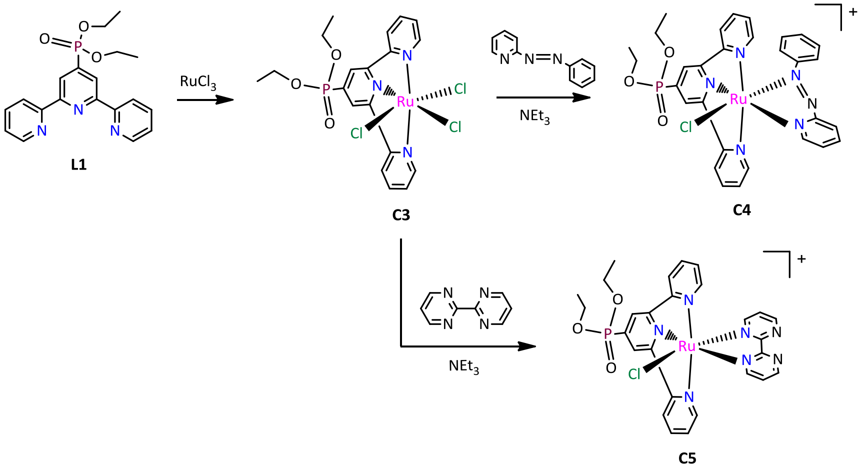

Scheme 11. Synthetic scheme for the coordination of **L1** and formation of complexes **C4** and **C5**.

In a first step, **L1** was coordinated to ruthenium using RuCl$_3$ as metal precursor in refluxing ethanol during 4 h (Scheme 11). **C3** precipitated in the reaction solution as a brown solid. After leaving the solution to stand at 4ºC for 1 h, the product was filtrated, washed with cold ethanol and diethyl ether and dried under vacuum. The yield of this reaction was nearly quantitative (93%). The resulting compound showed a higher solubility in organic solvents, such as dichloromethane, compared to the analogous [Ru(trpy)Cl$_3$], making evident a solubility effect of the phosphonate group. **C3** was analyzed by electrochemical and spectrometric techniques. This Ru(III) complex showed a reversible wave at a half wave potential of 0.26 V (Figure 8). In mass spectrometry the species M-Cl was detected (Figure S20, S21, Supporting Information).

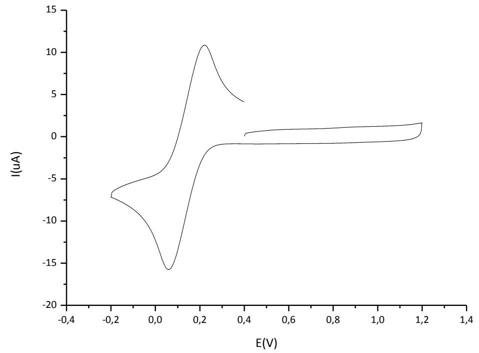

Figure 8. Cyclic voltammogram of **C3** in dichloromethane (0.1 M TBAH).

In a second step, the bidentate ligand, azpy or bpm, reacted with **C3** in the presence of triethylamine in order to reduce Ru(III) to Ru(II). In the case of **C5** the bidentate bpm ligand was added slowly in order to avoid the formation of dimeric species where bpm acted as a bridge between two metal centres.

Both complexes were isolated by precipitation with diethyl ether and purified by recrystallization with dichloromethane/diethyl ether.

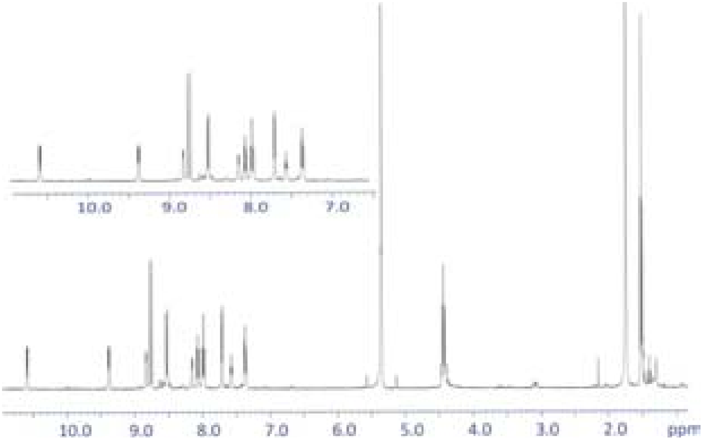

Figure 9. ^{1}H-NMR of **C5**.

Due to the non-symmetric nature of azpy, two isomers of **C4** were obtained, being the species with the pyridine in *cis* to the chloro ligand the major isomer (Figure

9). With a first addition of dichloromethane to the obtained solid both isomers were solved and separated from the remaining solid. Further addition of dichloromethane to this remaining solid and precipitation with diethyl ether allowed the isolation of the *cis*-**C4** isomer with 97 % purity. The ^{1}H-NMR spectrum of this complex is shown in Figure 10.

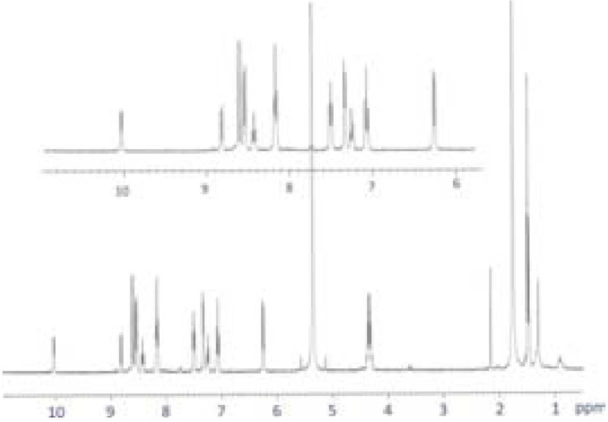

Figure 10. ^{1}H-NMR of *cis*-**C4**.

Suitable crystals for X-Ray diffraction analysis of the PF_6 salts of both *cis*- and *trans*-**C4** isomers could be obtained by slow diffusion of diethyl ether over a solution of complex in dichloromethane (Figure 11). Both complexes present a distorted octahedral geometry with a Cl-Ru-$N_{pyr,azpy}$ and Cl-Ru-$N_{azo,azpy}$ bond angles of 169.88º and 173.44º for the *cis* and *trans* isomers respectively. The Ru-Cl bond distances, 2.4049 Å and 2.3983 Å respectively, are comparable, thus revealing a similar *trans* effect induced by the azo N and pyridylic N of the azpy ligand. In the synthesis of the analogous [Ru(trpy)(azpy)Cl]$^+$ just the *cis* isomer (the most stable one) is formed (See Chapter 1). When adding a phosphonate group in the terpyridine ligand the steric hindrance between the azpy phenyl group and the phosphonate ethyl chains leads to an energy equilibration of the *cis* and *trans* isomers. In consequence, both are formed, though remaining the *cis* isomer as the major product.

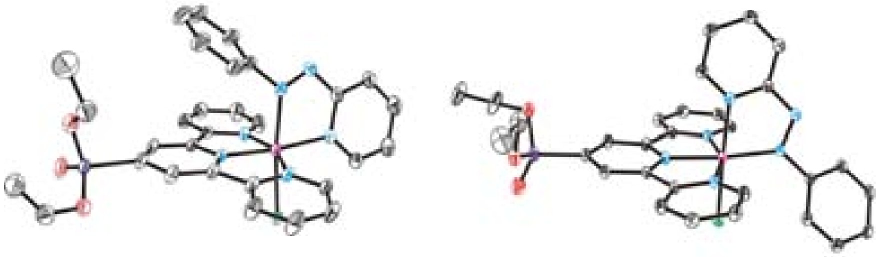

Figure 11. X-Ray structures of the cationic moieties of *cis*-**C4** and *trans*-**C4**.

In addition to NMR and X-Ray diffraction, *cis*-**C4** and **C5** were also characterized by High Resolution Mass Spectrometry (HRMS) and the species M-Cl were detected for both complexes (see Figures S22-S24 in Supporting Information section).

The electrochemical properties of complexes *cis*-**C4** and **C5** were studied by cyclic voltammetry. The different electronic characteristics of the bidentate ligands makes them differ in 0.27 V, appearing *cis*-**C4** at higher potential ($E_{1/2}$ (II/III) = 1.37 V vs SSCE) compared with **C5** ($E_{1/2}$ (II/III) = 1.10 V vs SSCE) due to the stronger π-accepting character of azpy (Figure 12).

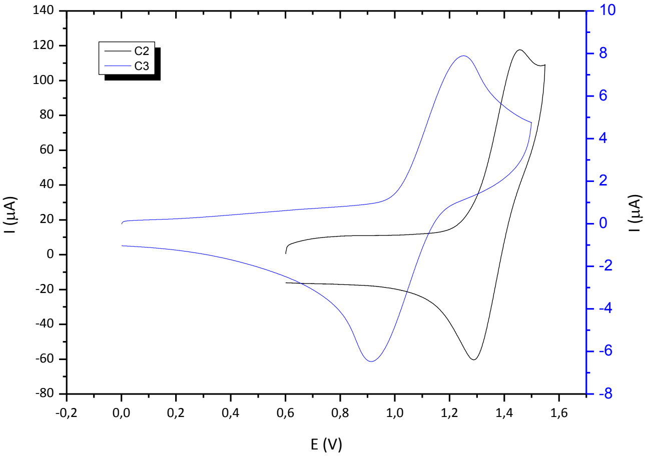

Figure 12. Cyclic voltammograms of *cis*-**C4** and **C5** in DCM (0.1 M TBAH), scan rate of 0.1 $V{\cdot}s^{-1}$.

The chloro ligand of these complexes is considered quite labile, being possible the *in-situ* formation of the corresponding aqua complexes. The cyclic voltammetry of **C5** was registered in H_2O (pH 7) and one wave at 0.60 V was observed. This wave corresponds to the 2-electron transition of Ru(IV/II) and is in concordance with the electrochemical properties observed for the analogous $[Ru(trpy)(bpm)(OH_2)]^{2+}$.[58] Moreover, the solution of **C5** in H_2O had a brown color while in dichloromethane was red. This difference could be observed by UV-Vis, being the MLCT dπ-π* band of the chloro complex red shifted with regard to the aqua complex (

Figure **13**). This shift can be explained by the increase in energy of the dπ orbitals promoted by the chloro ligand. In the presence of anionic ligands the ionization energy decreases; i.e. the energy of the dπ orbitals increases, decreasing at the same time the energy gap between dπ and π* orbitals.

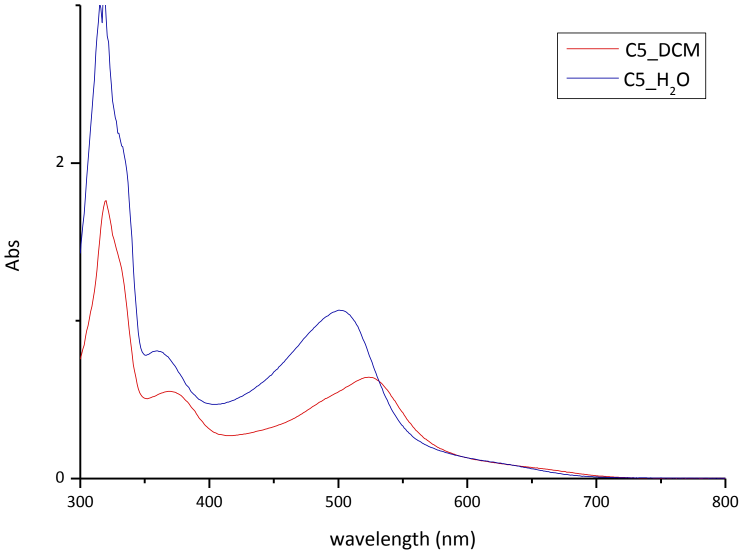

Figure 13. UV-Vis spectra of a solution 0.1 mM of **C5** in dichloromethane (black) and in H_2O (red).

4.2.3. Catalytic activity of C5.

The catalytic activity of **C5** was tested for the epoxidation of *cis*-β-methylstyrene, obtaining complete conversion and a TN_{epox} of 69 after 25 h. In Figure 14 the evolution of the reaction is shown in terms of epoxide yield and remaining substrate. The *cis* configuration of the substrate was maintained; *i.e.* a stereoselective process takes place. The activity of **C5** is fairly similar to the activity of the analogous $[Ru(trpy)(bpm)OH_2]^{2+}$ complex (see Chapter 3, section 3.2.4), confirming that the active site of the catalyst is not significantly affected by the added phosphonate group.

The reaction was followed by ^1H-NMR and the mass balance could be rationalized, accounting the detected products for 90% of the initial substrate. Benzaldehyde and acetaldehyde as products of a C=C bond cleavage (21%) and small amounts of the ketone 1-phenylpropan-2-one (1.4 %), probably product from the epoxide's opening, were detected.

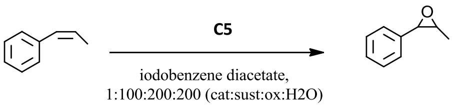

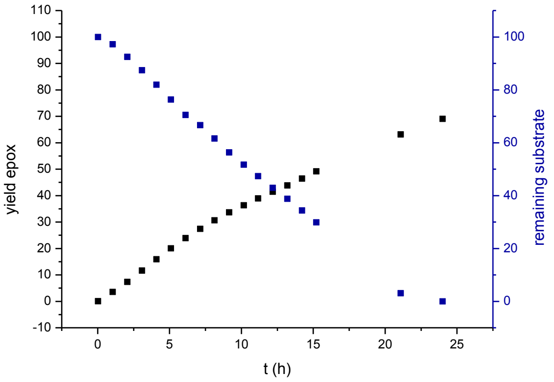

Figure 14. Epoxide yield and remaining substrate for the catalytic epoxidation of *cis*-β-methylstyrene with **C5** (cat:subst:ox:H_2O 1:100:200:200).

In Figure 15 the ^1H-NMR spectra after 15 h of reaction is shown. In this figure, representative signals for the substrate, *cis*-epoxide, benzaldehyde, acetaldehyde and dodecane (internal standard) are highlighted. Between 7 and 8.5 ppm appear the signals of the aromatic rings of the substrate, epoxide, benzaldehyde, Iodobenzene diacetate, Iodosobencene and Iodobencene. At 2.0 and 2.1 ppm the singlets for the methyl groups of Iodo bencene diacetate and, probably, acetic acid are respectively observed. Iodosobenzene is formed by reaction of Iodobenzene diacetate with water and, after oxidizing the Ru(II) complex, iodobenzene is formed.

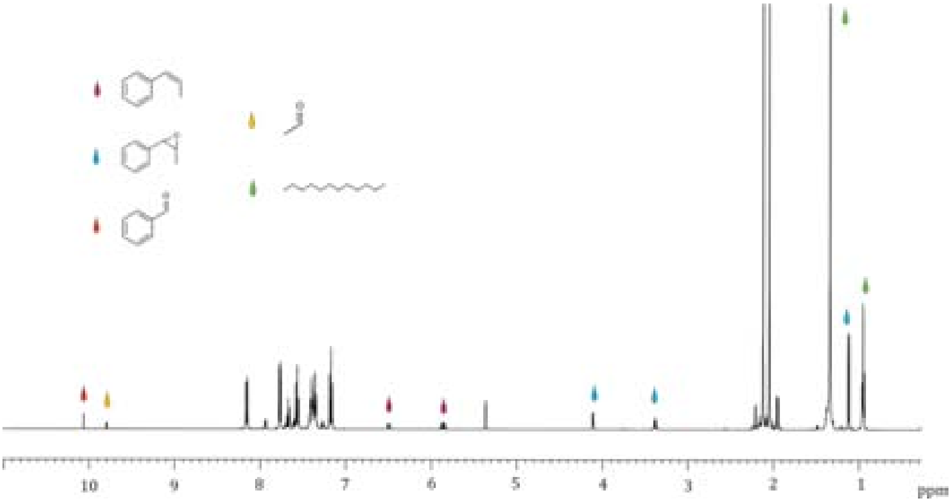

Figure 15. ^{1}H-NMR spectra after 15h of catalytic oxidation of *cis*-β-mehtylstyrene with **C5** (cat: subst:ox:H2O 1:100:200:200).

The addition of water was also needed here to promote the catalytic reaction, as expected taking into account the already commented behaviour of the analogous $[Ru(trpy)(bpm)OH_2]^{2+}$ complex (Chapter 3, section 3.2.5). Moreover, in this case the aqua complex is generated in situ, being water also needed for this reason. An excess of Iodobenzene diacetate was also needed to reach complete conversions; when just a small excess of oxidant (1.2 eq. respect to substrate) was used the reaction stopped after reaching 80% conversion.

4.2.4. Hydrolysis of the phosphonate group. Synthesis of C6 and C7.

The deprotection of the phosphonate group of *cis*-**C4** and **C5** was carried out using an excess of trimethylbromosilane (TMBS) in dry CH_2Cl_2. After evaporation of the solvent the resulting silane derivative could be easily hydrolyzed in methanol at room temperature (Scheme 12). The final complexes, *cis*-**C6** and **C7**, were isolated by precipitation with diethyl ether with high yields.

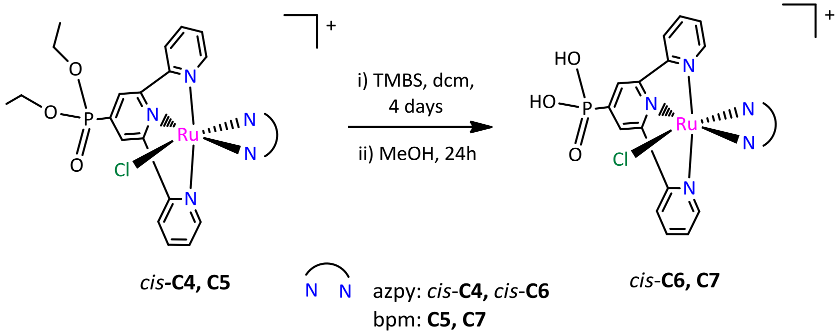

Scheme 12. Hydrolysis of the phosphonate groups of *cis*-**C4** and **C5**.

The resulting complexes were completely hydrolized as confirmed by ^{1}H-NMR spectroscopy, where no ethyl groups in the aliphatic region were observed (Figure S16 – S17, Supporting Information).

4.2.5. Preparation of magnetic nanoparticles of Fe_3O_4 (NPs).

Magnetite NPs were prepared by thermal decomposition of $[Fe(acac)_3]$ following the method described by Sun *et.al.*[48,49] in the presence of 1,2-dodecanediol as reducing agent and oleic acid and oleylamine as surfactants together with benzyl ether as solvent (Scheme 13). The temperature of the mixture was increased to 260 ºC and after 3 h the formed MNPs were isolated by application of an external magnetic field.

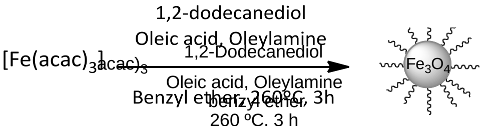
[Fe(acac)3]
acac)3
1,2-dodecanediol
Oleic acid, Oleylamine
Benzyl ether, 260ºC, 3h
1,2-Dodecanediol
Oleic acid, Oleylamine
benzyl ether
260 ºC. 3 h
Fe3O4

Scheme 13. Procedure for the preparation of Fe_3O_4 NPs.

The spherical NPs were analyzed by Transmission Electron Microscopy (TEM), where no aggregation was observed. The size distribution was homogenous, being the average size of 5.63 ± 1.32 nm (Figure 16).

4.2.6. Immobilization of Ru complexes C6 and C7 on NPs.

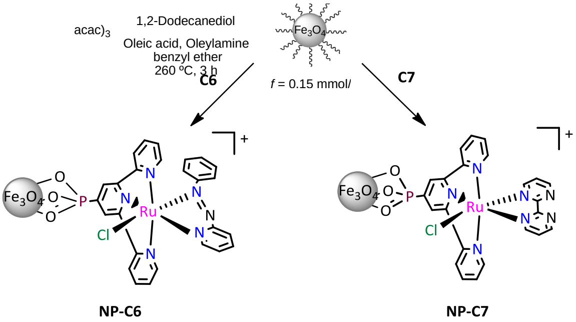
acac)3
1,2-Dodecanediol
Oleic acid, Oleylamine
benzyl ether
260 ºC, 3 h
C6
Fe3O4
f = 0.15 mmol/
C7
+
+
Fe3O4
O
O
O
P
N
N
Ru
N
N
N
Cl
N
Ru
Cl
NP-C6
NP-C7

Scheme 14. Immobilization of **C6** and **C7** in MNPs.

Complexes **C6** and **C7** were immobilized on the surface of the prepared magnetite NPs by mechanic stirring of a mixture of Ru complex and NPs in methanol at room temperature for 4 days (Scheme 14). The final NPs were isolated by application of an external magnetic field together with the addition of diethyl ether to accelerate the magnetic decantation. Following this procedure **NP-C6** and **NP-C7**, with a functionalization of 0.23 and 0.61 mmol Ru/g NP, respectively, were obtained. The low functionalization of **NP-C6** can be attributed to the close disposition of the phenyl group of the azpy ligand with respect to the anchoring phosphonate group. The functionalization of the resulting NPs was calculated by elemental analysis of N, considering negligible the initial amount of this element.

The immobilized Ru complexes avoided the aggregation of NPs as observed by TEM. The type of stabilization promoted by these complexes can be considered as both steric and electrostatic. No significant change in the size and size distribution of the resulting NPs upon catalyst anchoring was observed (Figure 16).

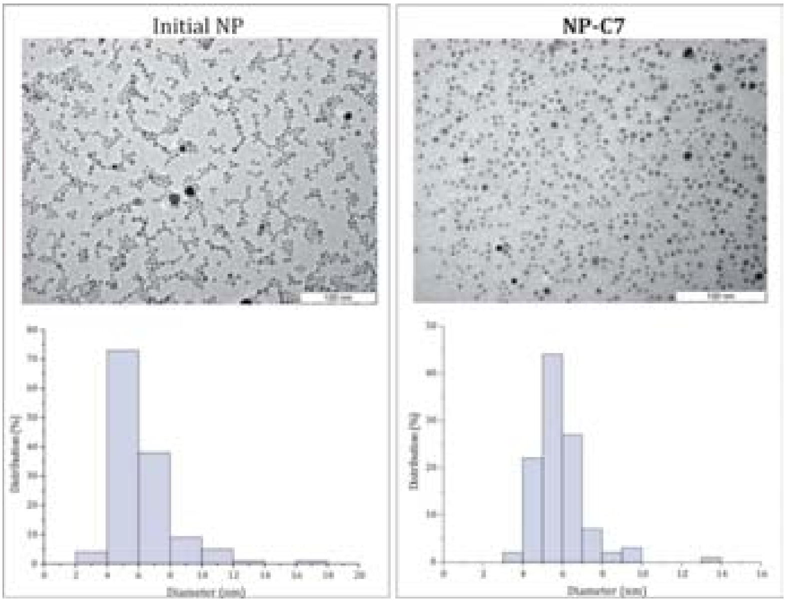

Figure 16. TEM micrographs and size distribution diagrams of the initial NPs and **NP-C7**.

The immobilization of Ru complexes on NPs had an important effect on their dispersion properties. While the initial NPs were highly dispersible in hexane due to the presence of surfactants, **NP-C6** and **NP-C5** were highly dispersible in methanol, making evident the role of the NPs' coating in the solubility properties. Taking advantage of this high solubility in methanol, **NP-C5** was analyzed by UV-Vis spectroscopy, where the characteristic metal-to-ligand charge transfer (MLCT) band at around 500 nm was observed. The UV-Vis spectra of the homogeneous and heterogeneous system were compared, confirming the effective immobilization of **C5** on the NPs' surface (Figure 17). Moreover, the solution of **NP-C5** was filtered through celite to separate the NPs and the colorless resulting solution presented no absortion bands in the UV-Vis region. This experiment also confirms that the bands observed for **NP-C5** are in fact from a heterogeneous system.

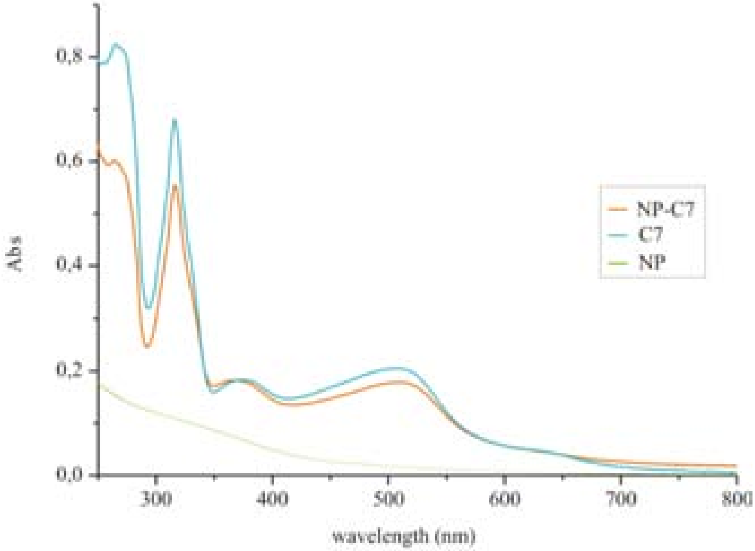

Figure 17. UV-Vis of **NP-C7** and **C7** in methanol and of the initial **NPs** in hexane.

4.2.7. Catalytic activity of NP-C6 and NP-C7. Comparison with the homogeneous system.

The heterogeneous systems **NP-C6** and **NP-C7** were active in the epoxidation of *cis*-β-methylstyrene showing comparable activities to the analogous homogeneous systems and maintaining the stereoselectivity promoted by the Ru metal center. In Table 1 the results obtained for both homogeneous and heterogeneous systems are presented.

Table 1. Catalytic epoxidation of *cis*-β-methylstyrene with the heterogeneous (**NP-C4** and **NP-C5**) and homogenous ($[Ru(trpy)(azpy)(OH_2)]^{2+}$ (**C1**), $[Ru(trpy)(bpm)(OH_2)]^{2+}$ (**C2**), and **C5**) systems.[a]

Het.[b]	**yield$_{epox}$ (%)**	**Conv. (%)**	Hom.[c]	**yield$_{epox}$ (%)**	**Conv. (%)**
NP-C6	52	100	**C1**	52	100
NP-C7	71	100	**C2**	68	100
			C5	69	100

[a] In 1 mL of DCM; oxidant: Iodobenzene diacetate; cat:subst:ox:H_2O 1:100:200:200; [b] Aliquots analyzed by GC after filtration through celite, 48 h reaction; [c] Aliquots analyzed by ^{1}H-NMR, 24 h reaction.

The activity of **NP-C7** was also tested for the epoxidation of different organic substrates. The results obtained, in terms of TN_{epox}, conversion and selectivity, are shown in Table 2. The relation of catalyst:substrate used was 1:100, hence, the number of catalytic cycles to form the epoxide (TN_{epox}) is also indicative of the epoxide yield.

Table 2. Catalytic epoxidation of alkenes with **NP-C7.**[a]

Entry	Substrate	TN_{epox}	Conv. (%)	Select. (%)
1	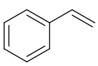	49	90	54
2	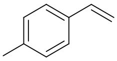	20	89	22
3	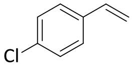	28	70	40
4	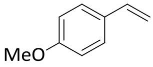	-	100	-
5	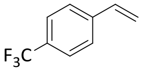	32	71	45
6	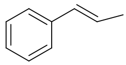	75	100	75
7	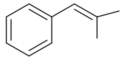	79	100	79
8	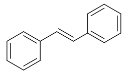	40	100	40
9	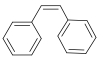	42	100	42
10	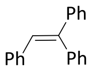	21	49	43
11	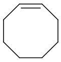	88	100	88

[a] In 1 mL of DCM; oxidant: Iodobenzene diacetate; cat:subst:ox:H_2O 1:100:200:200; Aliquots analyzed by GC after filtration through celite, 48 h reaction.

Different activated alkenes with aromatic substituents have been used. In general, styrene and its derivatives were quite reactive, reaching high conversions but poor selectivities (entries 1-5 in Table 2). With Styrenes bearing electron-withdrawing groups, such as CF_3 and Cl, the reaction was slowed down (entries 3 and 5). Therefore, for instance, the CF_3-substituted styrene derivative didn't reach complete conversion (86%) and gave low epoxyde yield (32%) despite employing longer reaction times (72 h instead of 48 h). On the other hand, with electron donating groups, such as methyl and methoxide substituents, the selectivity decreased dramatically (entries 2 and 4), even up to the point of converting all the substrate and not detecting any epoxide (entry 4). This fact suggests that, with higher electron rich alkenes, other reaction pathways are favored, either leading to the formation of other oxidized products or to the decomposition of the formed epoxide.

When 1 or 2 methyl groups were added as substituents, the best results among aromatic alkenes were obtained (75 % and 79 % yield and complete conversions; entries 6 and 7 in Table 2). With three phenyl substituents in the alkene, the reaction was slowed down in comparison with *cis* and *trans*-stilbene, probably due to the increased steric hindrance (entries 8, 9 and 10). When lower temperatures were used for the epoxidation of *cis*-stilbene the conversion and selectivity decreased (T = 0 ºC, 39 % conversion, 28 % selectivity).

When the cyclic alkene cyclooctene was used, the best results in terms of conversion (100%), yield (88%) and selectivity (88%) were obtained (entry 11).

In all cases the aliquots were filtered through celite in order to separate the NPs and were analyzed by GC and GC-MS. The solution after filtration was colorless, suggesting that there was no leaching of the catalyst.

The evolution of the catalytic oxidation of *cis*-β-methylstyrene was followed, reaching complete conversion and an epoxide yield of 71 % after 30 h (Figure 18). The catalytic performance of the heterogeneous system is comparable with that of the homogenous one, in which 69 % of epoxide yield was obtained. It can be observed that some more time is needed to reach complete conversion for the heterogeneous system, which can be attributed to the incomplete solubility of **NP-C5** in the catalytic reaction conditions.

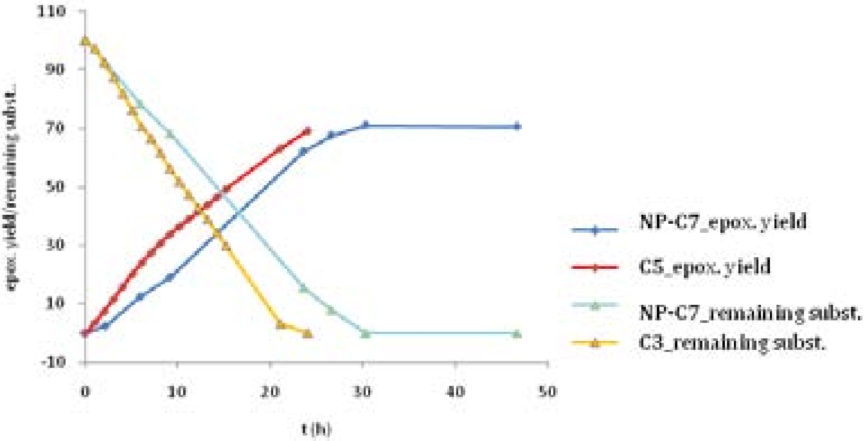

Figure 18. Plot of epoxide yield and remaining substrate for the catalytic epoxidation of *cis*-β-mehtylstyrene with **C5** and **NP-C7** (cat:subst:ox:H_2O 1:100:200:200).

NP-C7 could be separated by application of an external magnetic field and reused for further catalytic cycles. In Table 3 the results obtained for 5 recycling cycles are shown. The activity, in terms of conversion, is maintained along the recycling experiments and the selectivity is slightly decreased.

Table 3. Recycling experiments with **NP-C7**.[a]

cycle	TN_{epox}	Conv. (%)	Select. (%)
1	68	100	68
2	63	100	63
3	55	100	55
4	51	93	55
5	55	100	55

[a] Oxidation of *cis*-β-methylstyrene in 1 mL of DCM; oxidant: Iodobenzene diacetate; cat:subst:ox:H_2O 1:100:200:200; Aliquots analyzed by GC after filtration through celite, 48 h reaction.

The resulting **NP-C7** after the recycling experiments were analyzed by TEM and aggregated NPs were observed (Figure 19).

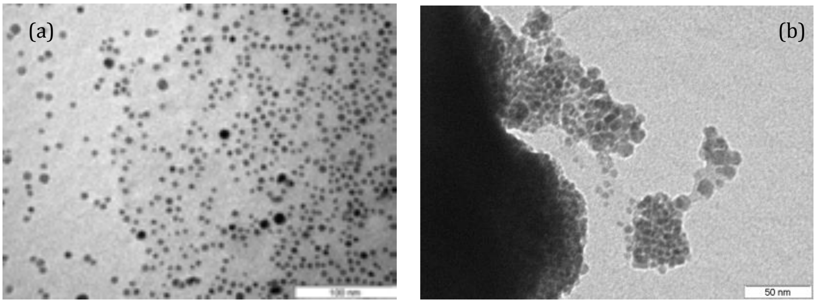

Figure 19. TEM images of (a) **NP-C7** and (b) **NP-C7** after 5 catalytic cycles.

When the equivalents of substrate with respect to catalyst were increased from 1:100 to 1:1000, the heterogeneous system **NP-C7** was able to make up to 770 cycles and reach complete conversion of the substrate after 27 h. In Table 4 the results obtained for the homogenous and heterogeneous systems are compared. After 24 h complete conversion with **C5** and nearly complete conversion with **NP-C7** was obtained. The corresponding epoxide was obtained with comparable yields (77 % for **NP-C7** and 78 % for **C5**), demonstrating that the developed heterogeneous system behaves as the analogous homogenous one in terms of activity and selectivity.

Table 4. Epoxidation of *cis*-β-methylstyrene with 0.1 mol% cat.[a]

Catalyst	t (h)	conv (%)	yield ep. (%)	TN
NP-C7[b]	24	97	76	760
	27	100	77	770
C5	24	100	78	780
	27	100	77	770

[a] In 1 mL of DCM; oxidant: iodobenzene diacetate; cat:subst:ox:H_2O 1:1000:1500:1500; aliquots analyzed by GC after filtration through celite.

Moreover, when 0.1 mol% of catalyst was used (cat:substr 1:1000), the rate of the reaction in the homogeneous and heterogeneous system was pretty similar. This can be graphically observed in Figure 20, where the TN_{epox} *vs.* time is plotted. The relevance of this observation must be pointed out, being this behaviour a paradigm in the area of catalyst immobilization. The use of NPs as immobilization support allowed the obtention of a heterogeneous system presenting the same behaviour as the homogeneous counterpart in terms of rate and activity.

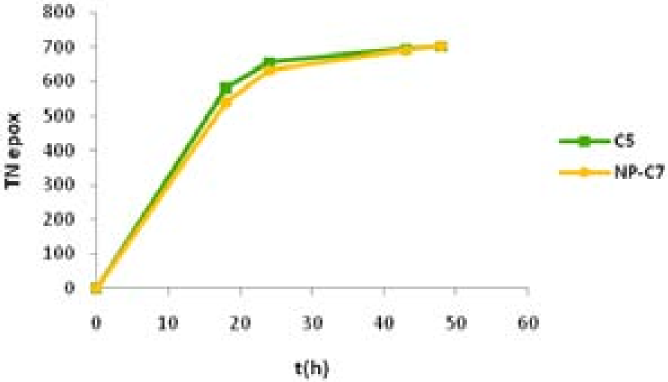

Figure 20. TN_{epox} *vs*. time for the epoxidation of *cis*-β-methylstyrene; cat:subst:ox:H_2O 1:1000:1100:1000 with **C5** and NP-**C7**; aliquots analyzed by GC after filtration through celite.

4.2.8. Experimental section.

Materials. All commercial reagents from Sigma-Aldrich and TCI were directly used without any purification. Diethyl 2,2'-6,2''-terpyridine-4'-phosphonate (**L1**) supplied by HetCat was purified by flash chromatography of alumina with ethyl acetate.

Instrumentation and Measurements. The NMR spectroscopy experiments were performed on a BrukerAvance 500 Ultrashield NMR spectrometer. Samples were run in CD_2Cl_2 and d_3-MeOH. Cyclic Voltammetry (CV) experiments were performed on an IJ-Cambria HI-660 potentiostat using a three-electrode cell. Typical CV experiments were carried out at a scan rate of 100 mV/s. A glassy carbon electrode (2 mm diameter) was used as working electrode, platinum wire as auxiliary electrode, and a SSCE as a reference electrode. Working electrodes were polished with 0.05 micron Alumina paste and washed with distilled water and acetone before each measurement. The complexes were dissolved in CH_2Cl_2 containing the necessary amount of n-Bu_4NPF_6 (TBAH) as supporting electrolyte to yield a 0.1 M ionic strength solution. $E_{1/2}$ values reported in this work were estimated from CV experiments as the average of the oxidative and reductive peak potentials ($(E_{p,a} + E_{p,c})/2$). UV-Vis spectroscopy was performed on a Cary 50 (Varian) UV-Vis spectrophotometer in 1 cm quartz cuvettes. Mass spectrometry analysis were performed in a mass spectrometer with matrix assisted laser desorption ionization (MALDI-TOF, Bruker Autoflex). Elemental analysis was performed in EA-1108, CHNS-O elemental analyzer from Fisons Instruments (Universidad de Santiago) and in LECO CHNS-model 932 by C.A.I. microanálisis elemental (Departamento de Química Orgánica y Farmacéutica, Universidad Complutense de Madrid, Madrid, Spain). IR spectra were recorded on a Thermo Nicolet 5700 FTIR spectrometer, using KBr pellets. Potassium bromide used in the preparation of the pellets was kept in an oven at 50 ^{o}C. TEM images were recorded using JEOL JEM 1011 microscope equipped with lanthanum hexaboride filament, operated at an acceleration voltage of 100 kV, at Microscopy Units, Universitat Rovira i Virgili, Tarragona, Spain. A drop of the MNPs suspension was added to a holey-carbon coated 200 mesh copper grid allowing the solvent to evaporate before being introduced into the microscope. Catalytic experiments were analyzed in an Agilent 6890N gas chromatograph coupled to a mass selective detector with ionization by electronic impact and in an Agilent 6890N with a FID detector.

X-Ray Structure Determination. Suitable crystals of *cis*-**C4** and *trans*-**C4** were grown up by slow diffusion of diethyl ether into a solution of a mixture of *cis*-**C4** and *trans*-**C4** in dichloromethane. Data collection was performed on a Bruker Nonius FR 591 system equipped with a multilayer Montel 200 mirror monochromator Mo $K\alpha$ (λ = 0.71073 Å) radiation and an Apex II CCD detector. The molecular structure was resolved by direct methods and refined of F^2 by full matrix least squares techniques using SHELX TL package with anisotropic thermal parameters.

Synthesis of [Ru(L1)Cl$_3$] (C3).

A solution of 250 mg of RuCl$_3$ (0.96 mmol) in 40 ml of degassed ethanol was heated to reflux during 1 h. A solution of 350 mg (0.95 mmol) of L1 in 10 mL of degassed ethanol was added and the reaction mixture was mantained at reflux during 4 h. The solution stood in the fridge for 1 h and the brown precipitate was filtered, washed with cold ethanol and diethyl ether and dried under vacuum. Yield: 93 % (508 mg, 0.88 mmol). **CV**: $E_{1/2}$ **=** 260 mV vs. SSCE; $E_{p,a}$ = 460 mV; $E_{p,c}$ = 60 mV. **MALDI$^+$ MS**: [M-Cl]$^+$ 541.1.

Synthesis of [Ru(L1)(azpy)Cl]Cl (C4).

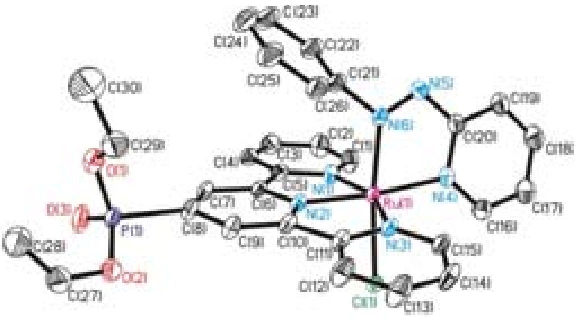

To a solution of 200 mg (0.35 mmol) of **C3**, 95.3 mg (0.52 mmol) of 2-phenyl-azopyridine, 74 mg (1.75 mmol) of LiCl in 15 mL of a mixture of ethanol/water (3:1) under Ar atmosphere 54 µl (0.38 mmol) of NEt$_3$ were added and the reaction mixture was heated to reflux for 1h. Diethyl ether was added until the precipitation of a dark solid. After filtration 20 mL of dichloromethane were added to dissolve partially this solid. Solution and solid were separated. Diethyl ether was added to the solution and 138 mg of **C4** as a mixture of isomers *cis*/*trans* (1:0.24) was obtained (Yield: 52%). With further reprecipitation of the remaining dark solid with dichloromethane/diethyl ether 68 mg of the pure *cis* isomer were obtained (Yield: 26 %). Global yield : 78 %. **^{1}H-NMR** (CD$_2$Cl$_2$): δ = 10.0 (d, J = 6.0 Hz, 1H, H16), 8.82 (d, J = 7.7 Hz, 1H, H19), 8.63 (d, J = 13 Hz, 2H, H7, H9), 8.58 (d, J = 7.9 Hz, 2H, H4, H11), 8.44 (dt, J1 = 7.7 Hz, J2 = 1.4 Hz, 1H, H18), 8.18 (m, 3H, H3, H13, H17), 7.52 (t, J = 6.6 Hz, 2H, H2, H14), 7.33 (d, J = 5.5 Hz, 2H, H1, H15), 7.25 (d, J = 7.2 Hz, 1H, H24), 7.07 (t, J = 8.0 Hz, 2H, H23, H25), 6.26 (d, J = 8.7 Hz, 2H, H22, H26), 4.35 (m, 4H, H27, H29), 1.45 (t, J = 6.6 Hz, 6H, H28, H30). **^{13}C-NMR** (CD$_2$Cl$_2$): δ = 165.9 (C20), 157.1 (C5, C11), 155.8 (C6, C8, C10), 155.0 (C21), 152.2 (C1), 150.3 (C16), 139.6 (C3, C13), 139.0 (C18), 129.9 (C24), 128.9 (C23, C25), 128.5 (C2, C14), 126.6 (C17), 125.8 (C19), 124.8 (C4, C12), 124.5 (C7, C9), 120.4 (C22, C26), 63.9 (C27, C29), 16.3 (C28, C30). **^{31}P {1H}31-NMR** (CD_2Cl_2): δ = 14.5 **CV**: 1.37 V vs. SSCE. **MALDI$^+$ HRMS**: [M-Cl]$^+$, Calc. for C30H29ClN6O3PRu: 689.0771; Found: 689.0789. **EA**: Calc. for C30H31ClF6N6O4P2Ru: C 42.29, H 3.67, N 9.86. Found: C 42.41, H 3.56, N 9.89.

Synthesis of [Ru(L1)(bpm)Cl]Cl (C5).

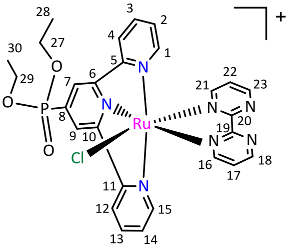

A solution of 124 mg (0.78 mmol) of 2,2'-bipyrimidine and 80.1 µl (0.55 mmol) of triethylamine in 30 mL of a mixture ethanol/water (3:1) under Ar atmosphere was heated to reflux. A dispersion of 300 mg (0.52 mmol) of **C1** in 15 mL of ethanol was added slowly during a period of 45 min. The resulting solution is heated to reflux for 30 min more. Diethyl ether is added to the red solution until precipitation of a solid. This solid was filtered and purified by reprecipitation with dichloromethane/diethyl ether. Yield: 50% (180 mg, 0.26 mmol). **^{1}H-NMR** (CD_2Cl_2): δ = 10.6 (dd, J1 = 5.6 Hz, J2 = 2.0 Hz, 1H, H16), 9.39 (dd, J1 = 5.1 Hz, J2 = 2.2 Hz, 1H, H18), 8.82 (dd, J1 = 4.6 Hz, J2 = 2.1 Hz, 1H, H21), 8.70 (d, J = 13 Hz, 2H, H7, H9), 8.44 (d, J = 8.1 Hz, 2H, H4, H12), 8.06 (t, J = 5.3 Hz, 1H, H17), 7.99 (t, J = 7.7 Hz, 2H, H3, H13), 7.74 (dd, J1 = 6.0 Hz, J = 2.1 Hz, 1H, H23), 7.69 (d, J = 4.9 Hz, 2H, H1, H15), 7.38 (t, J = 6.7 Hz, 2H, H2, H14), 7.24 (t, J = 5.3 Hz, 1H, H22), 4.41 (m, 4H, H27, H29), 1.52 (t, J = 7.1 Hz, 6H, H28, H30). **^{13}C-NMR** (CD_2Cl_2): δ = 160 (C23), 159 (C16), 158 (C6, C10), 157 (C18), 156 (C21), 152 (C1, C15), 137 (C3, C13), 128 (C2, C14), 124.2 (C4, C12), 124.0 (C7, C9), 127.7 (C17), 123.3 (C22), 63.7 (C27, C29), 16.2 (C28, C30). **^{31}P {^{1}H}-NMR** (CD_2Cl_2): δ = 15.7. **CV**: 1.1 V vs. SSCE, ΔE = 320 mV. **MALDI$^+$ HRMS**: [M-Cl]$^+$, Calc for C27H26ClN7O3PRu: 664.0561; Found: 664.0677

Synthesis of [Ru(L1-POOH)(azpy)Cl]Cl (C6) and [Ru(L1-POOH)(bpm)Cl]Cl (C7).

The same procedure was followed for **C6** and **C7**. The methodology for **C6** is presented here as representative from both.

To a suspension of 75 mg of **C4** (0.107 mmol) in 20 mL of dry CH_2Cl_2 at 0 ºC under argon atmosphere, 291 μl of bromo trimethyl silane (2.14 mmol) were added. The reaction was stirred at r.t during 4 days. After evaporation of the solvent, 20 mL of MeOH were added and the mixture was stirred for 24 hours. Afterwards, Et_2O was added to obtain **C6** as a purple solid. Yield: 83 % (59 mg, 0.09 mmol).

[Ru(L1-POOH)(azpy)Cl]Cl (C6). The same numeration as for **C5** is used.
^{1}H NMR (400 MHz, MeOD): δ = 10.02 (d, *J* = 5.7 Hz, 1H), 8.94 (d, *J* = 8.5 Hz, 1H), 8.76 (d, *J* = 12.8 Hz, 2H), 8.69 – 8.41 (m, 3H), 8.24 (t, *J* = 18.2 Hz, 3H), 7.58 (d, *J* = 7.1 Hz, 2H), 7.48 (d, *J* = 5.0 Hz, 2H), 7.33 (s, 1H), 7.14 (t, *J* = 8.0 Hz, 2H), 6.39 (d, *J* = 7.5 Hz, 2H).

[Ru(L1-POOH)(bpm)Cl]Cl (C7).

The same numeration as for **C5** is used. **^{1}H-NMR** (MeOD): δ = 10.5 (dd, 1H, H16), 9.46 (dd, 1H, H18), 8.94 (d, 2H, H7, H9), 8.89 (dd, 1H, H21), 8.71(d, 2H, H4, H12), 8.266 (t, 1H, H17), 8.09 (t, 2H, H3, H13), 7.93 (m, 3H, H1, H15, H23), 7.49 (t, 2H, H2, H14), 7.29 (t, 1H, H22). **^{31}P {^{1}H}-NMR** (MeOD): δ = 13.0. **EA**: Calc. For C23H20Br2N7O4PRu: C 36.82, H 2.69, N 13.07. Found: C 36.50, H 2.98, N 13.44.

Preparation of Magnetic Nanoparticles of Fe_3O_4 (NPs) by thermal decomposition.[48,49]

1.8 g (5 mmol) of iron(III) acetylacetonate, 5.6 g (25 mmol) of 1,2-dodecanediol, 5.3 mL (15 mmol) of oleic acid, 7 mL (15 mmol) of oleylamine and 20 mL of benzyl ether were mixed at room temperature under argon. The reaction mixture was warmed at 265 ºC during 3 h and was cooled down at room temperature. The NPs were removed using an external magnetic field, washed several times with MeOH, acetone and dried under vacuum. **EA (NP)**: C 13.20; H 2.08; N 0.16.

Immobilization of Ru complexes C6 and C7 on magnetic nanoparticles of Fe_3O_4 (NPs).

The same procedure was used for the immobilization of both complexes. Herein the procedure for **C7** is presented.

To a suspension of 41.25 mg of NPs of Fe_3O_4 in 4 mL of MeOH, 49.5 mg (0.07 mmol) of **C7** were added. The reaction was stirred in a shaker during 4 days. The resulting **NP-C7** was removed using an external magnetic field, washed several times with Et_2O and dried under vaccum.

EA (NP-C6): C 10.33; H 1.35; N 1.94; *f* = 0.23 mmol Ru/g NP

EA (NP-C7): C 20.87; H 2.21; N 5.99; *f* = 0.61 mmol Ru/g NP

The functionalization of the NP was calculated from the data of the EA of N as shown in the next equation, taking as example the calculation for **NP-C7**:

$$f = \frac{5.99\ \mathrm{g\ N}}{100\ \mathrm{g\ NP}} \cdot \frac{1\ \mathrm{mol\ N}}{14\ \mathrm{g\ N}} \cdot \frac{1\ \mathrm{mol\ Ru}}{7\ \mathrm{mol\ N}} \cdot \frac{10^3\ \mathrm{mmol\ Ru}}{1\ \mathrm{mol\ Ru}} = 0.61\ \mathrm{mmol\ Ru/g}\ NP$$

Catalytic epoxidation.

General procedure for the epoxidation of cis-β-methylstyrene using a relation of cat:subst:ox:H_2O of 1:100:200:200. All the experiments were developed under Ar atmosphere.

a) Followed by ^{1}H-NMR: 64.4 mg (200 μmol) of Iodobenzene diacetate were placed in and NMR tube. 0.4 mL of CD_2Cl_2, 13 μl (100 μmol) of cis-β-methylstyrene, 10 μl of dodecane (43.6 μmol) and 1 μmol of the Ru catalyst were added. After making a ^{1}H-NMR in order to register the product distribution at t_0, 3.6 μl (200 μmol) of D_2O were added. The data were colleted by either manual integration of the signals or with the “multi_integ3” macro of TOPSPIN.

b) Followed by GC-FID/GC-MS: To a solution of 2.5 μmol of Ru catalyst in 0.4 mL of dichloromethane in a glass tube, 33 μl (250 μmol) of cis-β-methylstyrene, 20 μl of dodecane, 165 mg (500 μmol) of iodobenzene diacetate and 0.6 mL more of dichloromethane were added. Aliquot for analysis of t_0 was taken and 9 μl (500 μmol) of H_2O were added. Aliquots taken for the analysis by GC-FID and/or GC-MS were filtered through a Pasteur pipette filled with celite and diethyl ether was added in order to elute the organic compounds.

For the heterogeneous system, the amount of NP-Ru was calculated taking into account the functionalization of NP-Ru (mmol Ru/g NP-Ru) and the reaction tube was placed in a shaker instrument.

For the recycling experiments; after 48 h of reaction of the first catalytic run an aliquot to taken to be analyzed. Then, diethyl ether was added to the solution mixture to allow a faster separation with a magnet. When all the NP was trapped aside with the magnet the solution was removed and the NP was washed twice with dichloromethane.

Acknowledgements:
The preparation of MNPs, hydrolysis of the phosphonate group and anchoring of the Ru complexes presented in sections 4.2.4, 4.2.5 and 4.2.6 were performed by Dr. Paola Riente of Prof. Pericàs group. The synthesis of **L2** and the immobilization of Ru complexes presented in section 4.2.1 were performed by Dr. Susana Jansat and Dr. Sarabindu Roy of Prof. Pericàs group.

4.3. References

(1) *Heterogenized homogeneous catalysts for fine chemicals production*; Pierluigi Barbaro, F. L., Ed.; Springer, 2010.

(2) Dioos, B. M. L.; Vankelecom, I. F. J.; Jacobs, P. A. *Adv. Synth.Catal.* **2006**, *348*, 1413-1446.

(3) Alkordi, M. H.; Liu, Y.; Larsen, R. W.; Eubank, J. F.; Eddaoudi, M. J. Am. Chem. Soc. **2008**, *130*, 12639-12641.

(4) Faria, A. L.; Mac Leod, T. O. C.; Barros, V. r. P.; Assis, M. D. *Journal of the Brazilian Chemical Society* **2009**, *20*, 895-906.

(5) Lou, L.-L.; Yu, K.; Ding, F.; Zhou, W.; Peng, X.; Liu, S. *Tetrahedron Letters* **2006**, *47*, 6513-6516.

(6) Parton, R. F.; Neys, P. E.; Jacobs, P. A.; Sosa, R. C.; Rouxhet, P. G. *J. Catal.* **1996**, *164*, 341-346.

(7) Zucca, P.; Sollai, F.; Garau, A.; Rescigno, A.; Sanjust, E. *J. Mol. Catal. A: Chemical* **2009**, *306*, 89-96.

(8) Halma, M.; Castro, K. A. D. d. F.; Prévot, V.; Forano, C.; Wypych, F.; Nakagaki, S. *J. Mol. Catal. A: Chemical* **2009**, *310*, 42-50.

(9) Ballesteros, R.; Pérez, Y.; Fajardo, M.; Sierra, I.; del Hierro, I. *Microporous and Mesoporous Materials* **2008**, *116*, 452-460.

(10) Luque, R.; Badamali, S. K.; Clark, J. H.; Fleming, M.; Macquarrie, D. J. *Applied Catalysis A: General* **2008**, *341*, 154-159.

(11) Deubel, D. V.; Sundermeyer, J. r.; Frenking, G. J. Am. Chem. Soc. **2000**, *122*, 10101-10108.

(12) Haas, G. R.; Kolis, J. W. *Organometallics* **1998**, *17*, 4454-4460.

(13) Le, Y.; Yang, X.; Dai, W.-L.; Gao, R.; Fan, K. *Catal. Commun.* **2008**, *9*, 1838-1841.

(14) Liu, P.; Wang, C.; Li, C. *J. Catal.* **2009**, *262*, 159-168.

(15) Sofia, L. T. A.; Krishnan, A.; Sankar, M.; Kala Raj, N. K.; Manikandan, P.; Rajamohanan, P. R.; Ajithkumar, T. G. *The J.Phys. Chem. C* **2009**, *113*, 21114-21122.

(16) Sels, B. F.; De Vos, D. E.; Buntinx, M.; Jacobs, P. A. *J. Catal.*, *216*, 288-297.

(17) Li, Y.; Li, Z.; Li, F.; Wang, Q.; Tao, F. *Org.Biomol. Chem.* **2005**, *3*, 2513-2518.

(18) Che, C.-M.; Huang, J.-S. *Chem. Commun.* **2009**, 3996-4015.

(19) Nestler, O.; Severin, K. *Org. Lett.* **2001**, *3*, 3907-3909.

(20) Zhang, J.-L.; Che, C.-M. *Org. Lett.s* **2002**, *4*, 1911-1914.

(21) Kobayashi, S.; Sugiura, M. *Adv. Synth. Catal.* **2006**, *348*, 1496-1504.

(22) Barbaro, P.; Liguori, F. *Chem. Rev.* **2008**, *109*, 515-529.

(23) Shaughnessy, K. H. *Chem. Rev.* **2009**, *109*, 643-710.

(24) Parton, R. F.; Vankelecom, I. F. J.; Casselman, M. J. A.; Bezoukhanova, C. P.; Uytterhoeven, J. B.; Jacobs, P. A. *Nature* **1994**, *370*, 541-544.

(25) Lee, C.-H.; Lin, H.-C.; Cheng, S.-H.; Lin, T.-S.; Mou, C.-Y. *J. Phys. Chem. C* **2009**, *113*, 16058-16069.

(26) Mori, K.; Kagohara, K.; Yamashita, H. *The J.Phys. Chem. C* **2008**, *112*, 2593-2600.

(27) Knops-Gerrits, P.-P.; De Vos, D.; Thibault-Starzyk, F.; Jacobs, P. A. *Nature* **1994**, *369*, 543-546.

(28) Masteri-Farahani, M. *J. Mol. Catal. A: Chemical* **2010**, *316*, 45-51.

(29) Stamatis, A.; Giasafaki, D.; Christoforidis, K. C.; Deligiannakis, Y.; Louloudi, M. *J. Mol.r Catal. A: Chemical* **2010**, *319*, 58-65.

(30) Mutin, P. H.; Guerrero, G.; Vioux, A. *J. Mater. Chem.* **2005**, *15*, 3761-3768.

(31) Bergbreiter, D. E. *Chem. Rev.* **2002**, *102*, 3345-3384.

(32) Mandoli, A.; Lessi, M.; Pini, D.; Evangelisti, C.; Salvadori, P. *Adv. Synth.Catal.* **2008**, *350*, 375-379.

(33) Sels, B. F.; De Vos, D. E.; Jacobs, P. A. *Catalysis Reviews: Science and Engineering* **2001**, *43*, 443 - 488.

(34) Shylesh, S.; Schünemann, V.; Thiel, W. R. Angew. Chem. Int. Ed. **2010**, *49*, 3428-3459.

(35) Bradley, J. S.; Schmid, G.; Talapin, D. V.; Shevchenko, E. V.; Weller, H. *Syntheses and Characterizations: 3.2 Synthesis of Metal Nanoparticles*; Wiley-VCH Verlag GmbH & Co. KGaA, 2005.

(36) Schmid, G. *Nanoparticles: From Theory to Application*; John Wiley & Sons, Incorporated, 2010.

(37) Rampino, L. D.; Nord, F. F. J. Am. Chem. Soc. **1941**, *63*, 2745-2749.

(38) Rampino, L. D.; Nord, F. F. *J. Am. Chem. Soc.* **1941**, *63*, 3268-3268.

(39) Kavanagh, K. E.; Nord, F. F. J. Am. Chem. Soc. **1943**, *65*, 2121-2125.

(40) Zanella, R.; Delannoy, L.; Louis, C. *Applied Catalysis A: General* **2005**, *291*, 62-72.

(41) Labib, M. E. *Colloids Surf.* **1988**, *29*, 293-304.

(42) Bönnemann, H.; Brijoux, W.; Brinkmann, R.; Joußen, T.; Korall, B.; Dinjus, E. *Angew. Chem. Int. Ed.* **1991**, *30*, 1312-1314.

(43) Bucher, S.; Hormes, J.; Modrow, H.; Brinkmann, R.; Waldöfner, N.; Bönnemann, H.; Beuermann, L.; Krischok, S.; Maus-Friedrichs, W.; Kempter, V. *Surface Science* **2002**, *497*, 321-332.

(44) Ranganath, K. V. S.; Glorius, F. *Catal. Sci. Technol.* **2011**, *1*, 13-22.

(45) Lu, A.-H.; Salabas, E. L.; Schüth, F. Angew. Chem. Int. Ed. **2007**, *46*, 1222-1244.

(46) *Metal oxide nanoparticles in organic solvents*; Niederberger, M. P., N., Ed., 2009.

(47) Hyeon, T.; Lee, S. S.; Park, J.; Chung, Y.; Na, H. B. J. Am. Chem. Soc. **2001**, *123*, 12798-12801.

(48) Sun, S.; Zeng, H.; Robinson, D. B.; Raoux, S.; Rice, P. M.; Wang, S. X.; Li, G. *J. Am. Chem. Soc.* **2003**, *126*, 273-279.

(49) Sun, S.; Zeng, H. *J. Am. Chem. Soc.* **2002**, *124*, 8204-8205.

(50) Guin, D.; Baruwati, B.; Manorama, S. V. *Org. Lett.* **2007**, *9*, 1419-1421.

(51) Jacinto, M. J.; Santos, O. H. C. F.; Jardim, R. F.; Landers, R.; Rossi, L. M. *Applied Catalysis A: General* **2009**, *360*, 177-182.

(52) Abu-Reziq, R.; Wang, D.; Post, M.; Alper, H. *Adv. Synth.Catal.* **2007**, *349*, 2145-2150.

(53) Tsang, S. C.; Caps, V.; Paraskevas, I.; Chadwick, D.; Thompsett, D. *Angew. Chem. Int. Ed.* **2004**, *43*, 5645-5649.

(54) Kotani, M.; Koike, T.; Yamaguchi, K.; Mizuno, N. *Green Chemistry* **2006**, *8*, 735-741.

(55) Shylesh, S.; Schweizer, J.; Demeshko, S.; Schünemann, V.; Ernst, S.; Thiel, W. R. *Adv. Synth. Catal.* **2009**, *351*, 1789-1795.

(56) Hu, A.; Yee, G. T.; Lin, W. *J. Am. Chem. Soc.* **2005**, *127*, 12486-12487.

(57) Yinghuai, Z.; Kuijin, L.; Huimin, N.; Chuanzhao, L.; Stubbs, L. P.; Siong, C. F.; Muihua, T.; Peng, S. C. *Adv. Synth. Catal.* **2009**, *351*, 2650-2656.

(58) Concepcion, J. J.; Jurss, J. W.; Templeton, J. L.; Meyer, T. J. J. Am. Chem. Soc. **2008**, *130*, 16462-16463.

4.5. Supporting Information

- **[Ru(L1)Cl$_3$] (C1)**

Cyclic Voltammetry: Figure S 18

Mass spectrometry: Figure S 20-Figure S 21

- ***cis*-[Ru(L1)(azpy)Cl]Cl$_2$ (*cis*-C2)**

NMR: Figure S1-Figure S7

CV: Figure S 19

Mass spectrometry: Figure S 22-Figure S 23

- **[Ru(L1)(azpy)Cl]Cl (C2)_mixture of isomers**

NMR: Figure S8

- **[Ru(L1)(bpm)Cl](PF$_6$) (C3)**

NMR:

Figure S9-

Figure S15

CV: Figure S 19

Mass spectrometry: Figure S 24

- **[Ru(L1-POOH)(azpy)Cl]Cl (C4)**

NMR:

Figure S 16

- **[Ru(L1-POOH)(bpm)Cl]Cl (C5).**

NMR:

Figure S 17

IR: Figure S 25

- **NP**

IR: Figure S 25

- **NP-C5**

IR: Figure S 25

NMR characterization

- ***cis*-[Ru(L1)azpyCl]Cl₂ (*cis*-C2)**

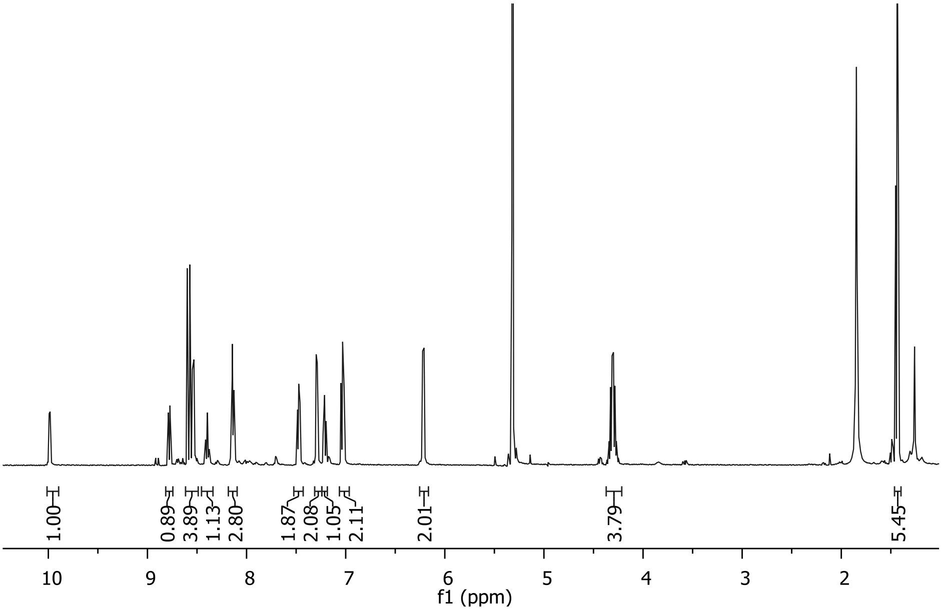

Figure S1. ^{1}H-NMR of *cis*-**C2**

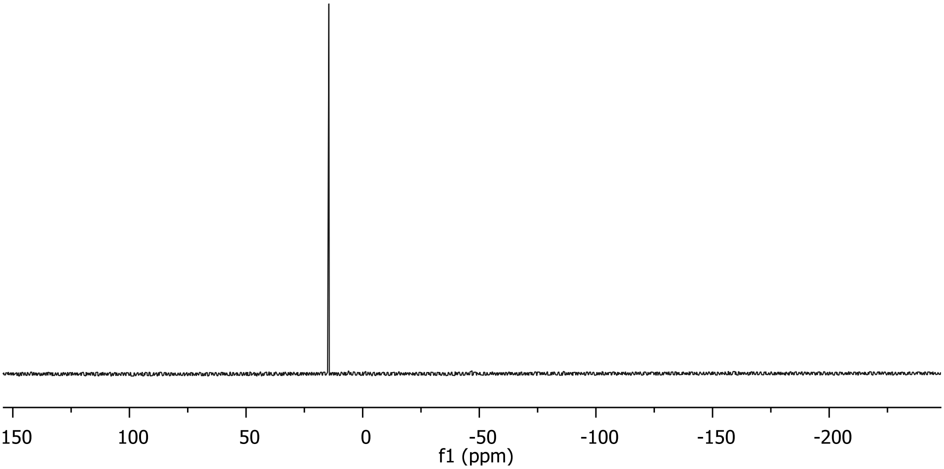

Figure S2. ^{31}P-NMR of *cis*-**C2**

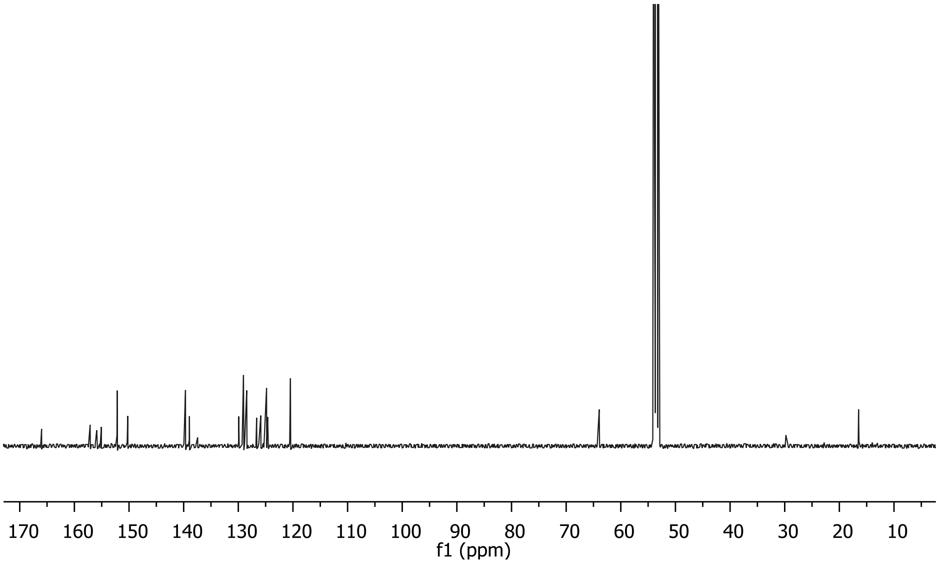

Figure S3. ^{13}C-NMR of *cis*-**C2**

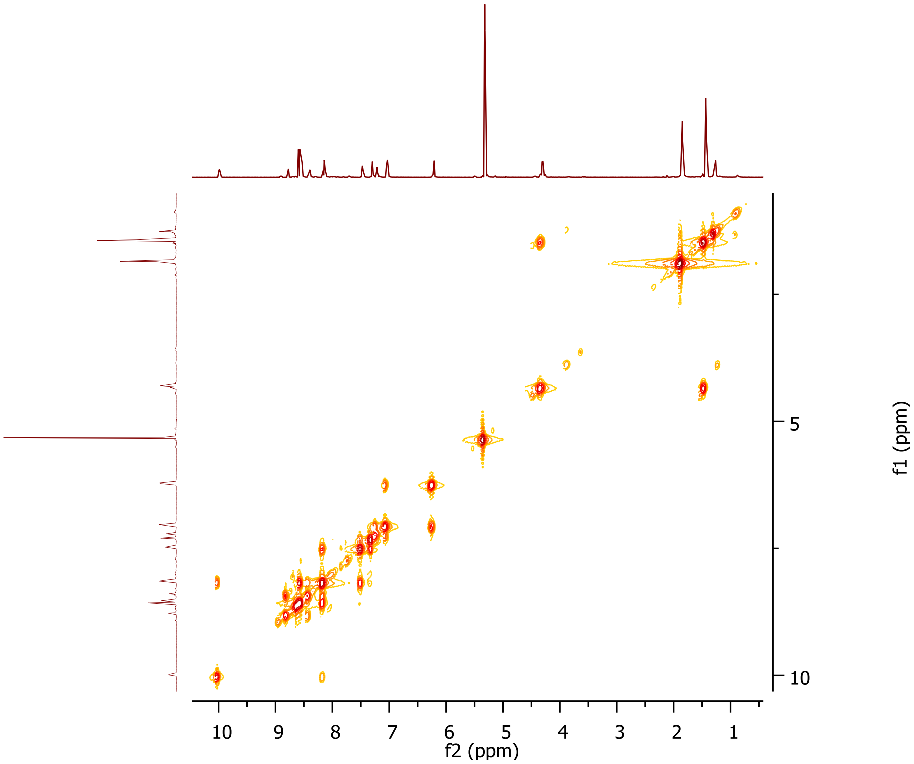

Figure S4. COSY of *cis*-**C2**

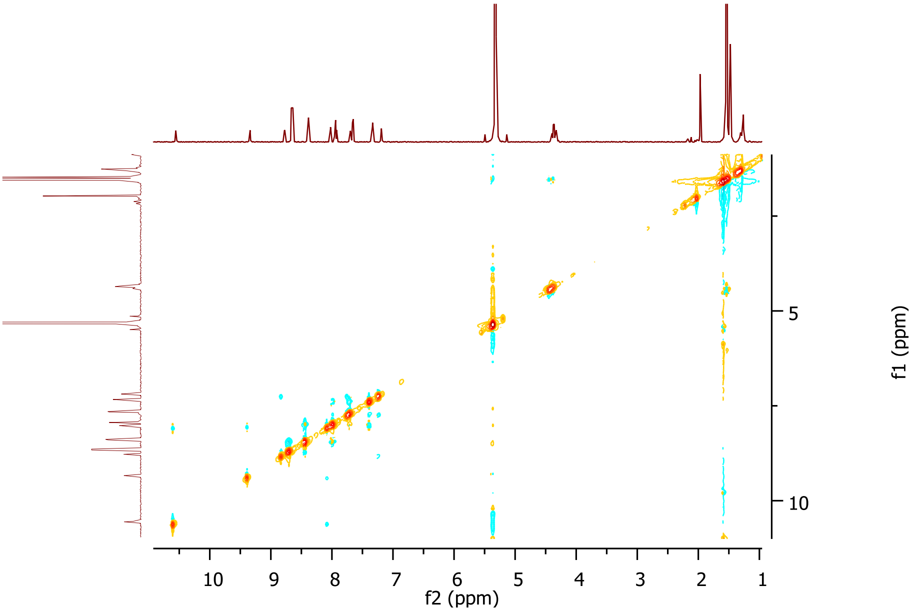

Figure S5. NOESY of *cis*-**C2**

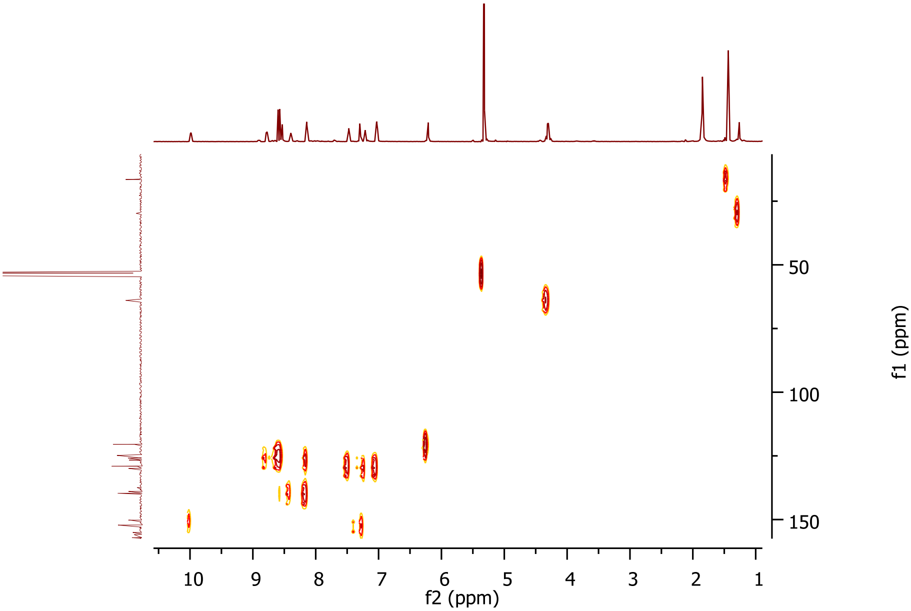

Figure S6. HMQC of *cis*-**C2**

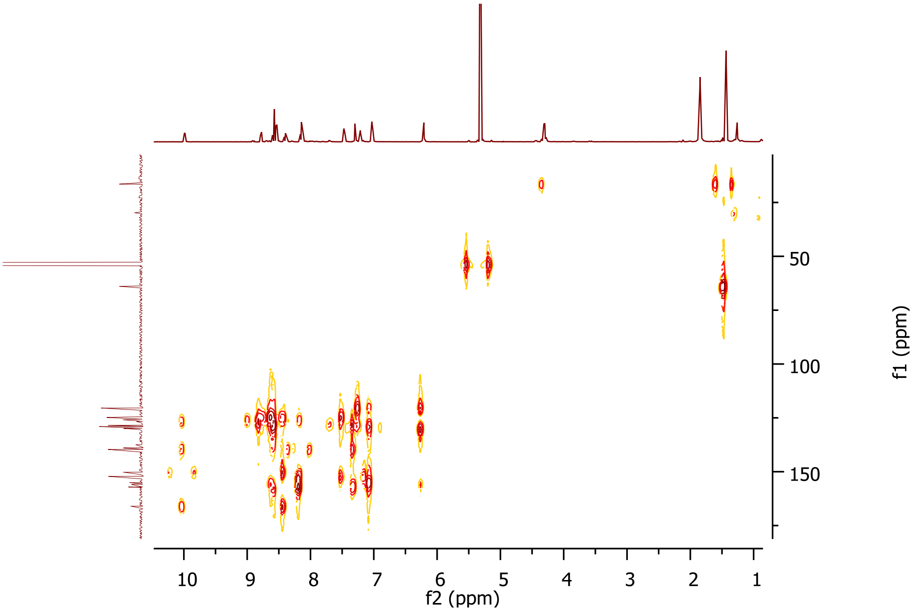

Figure S7. HMBC of *cis*-**C2**

- **[Ru(L1)(azpy)Cl]Cl (C2)_mixture of isomers**

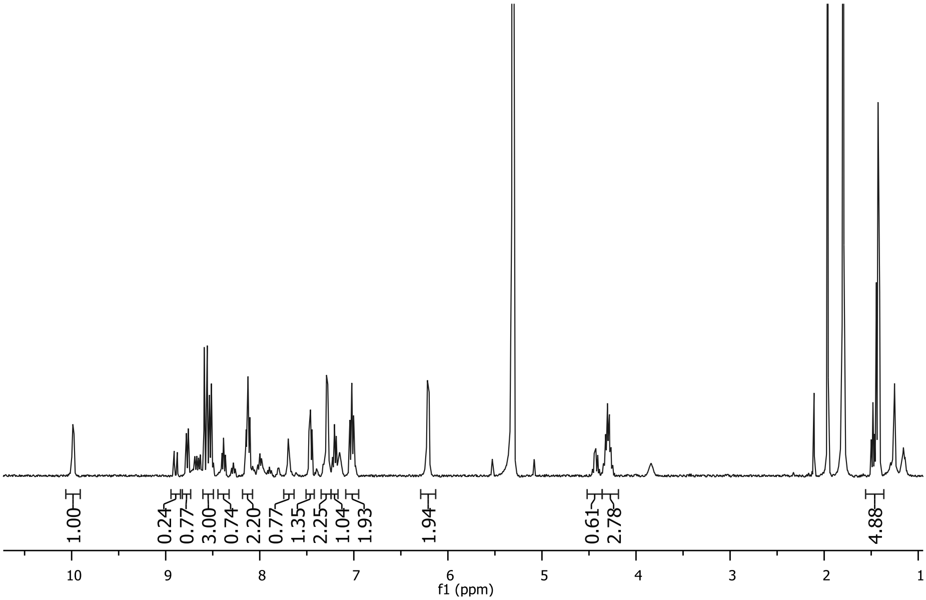

Figure S8. ^{1}H-NMR of the mixture of isomers of **C2**

- **[Ru(L1)(bpm)Cl](PF$_6$) (C3)**

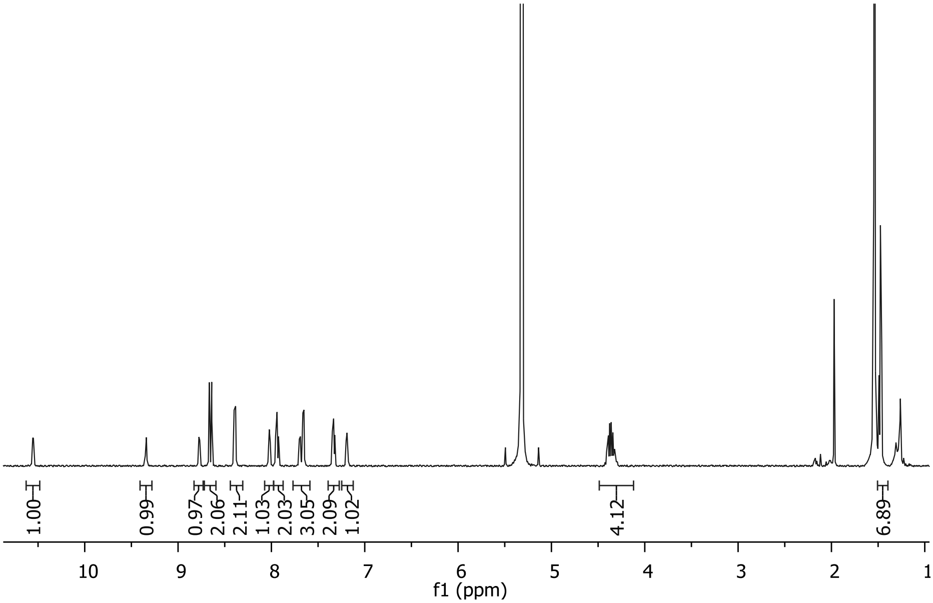

Figure S9. ^{1}H-NMR of **C3**

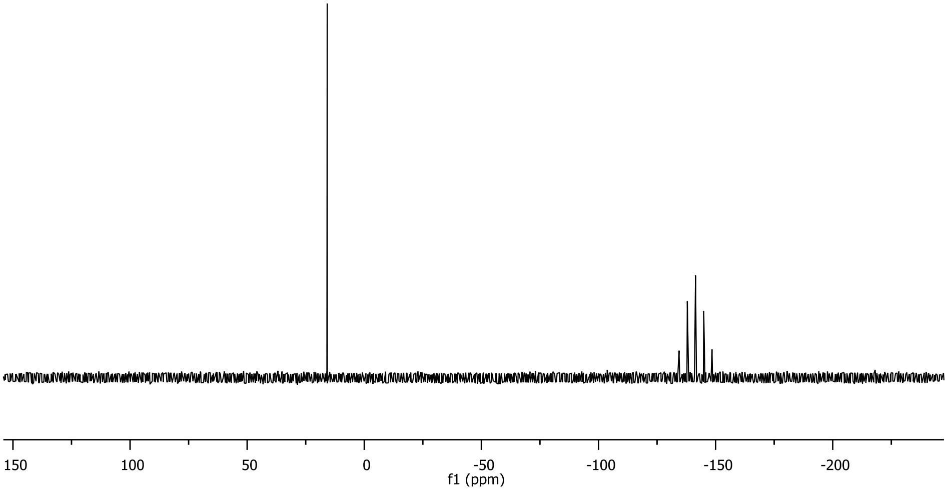

Figure S10. ^{31}P-NMR of **C3**

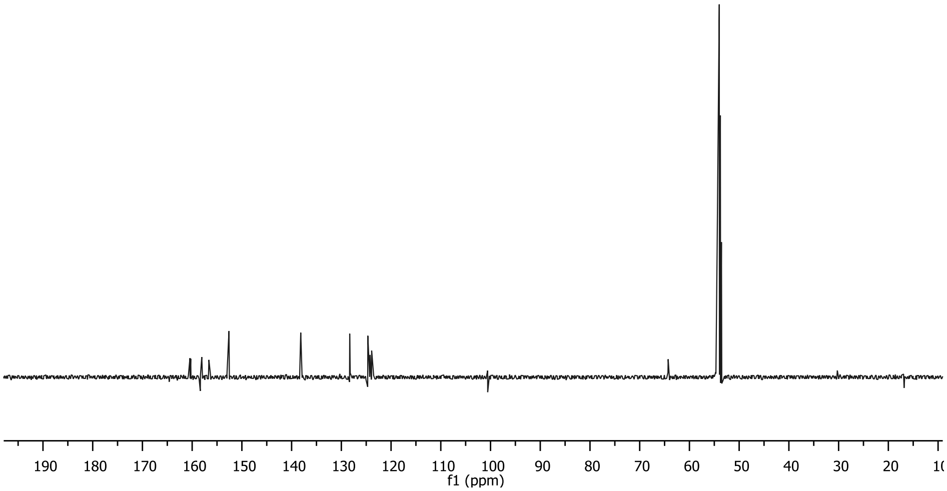

Figure S11. ^{13}C-NMR of **C3**

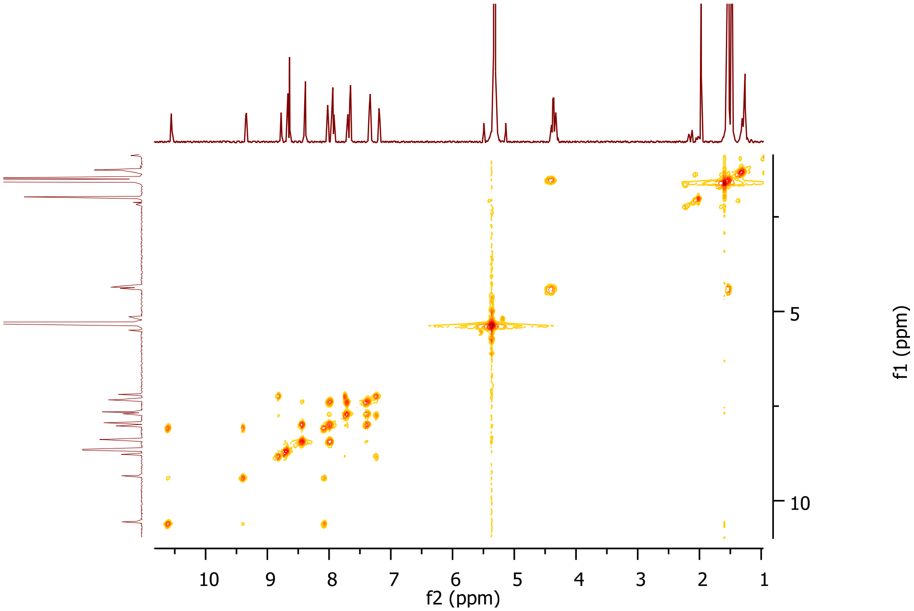

Figure S12. COSY of **C3**

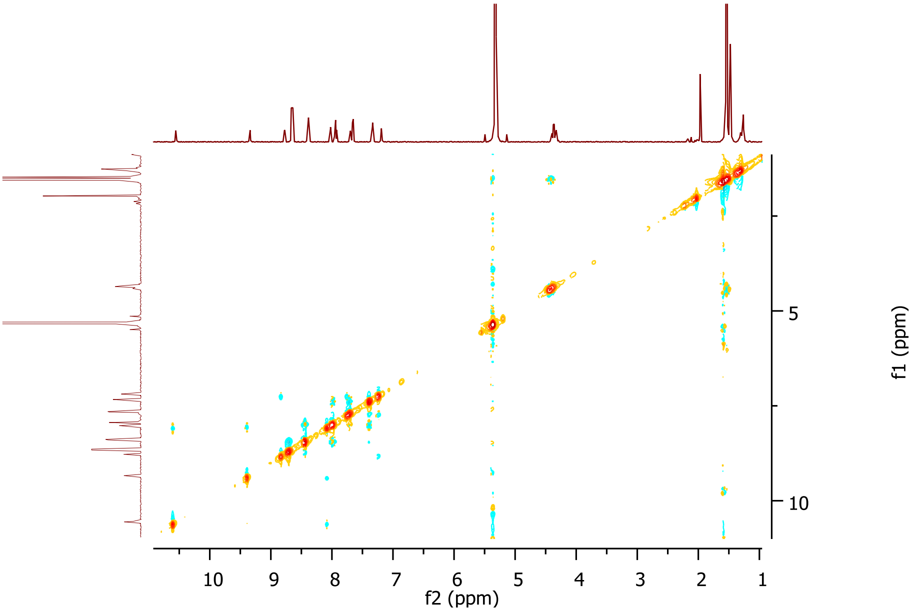

Figure S13. NOESY of **C3**

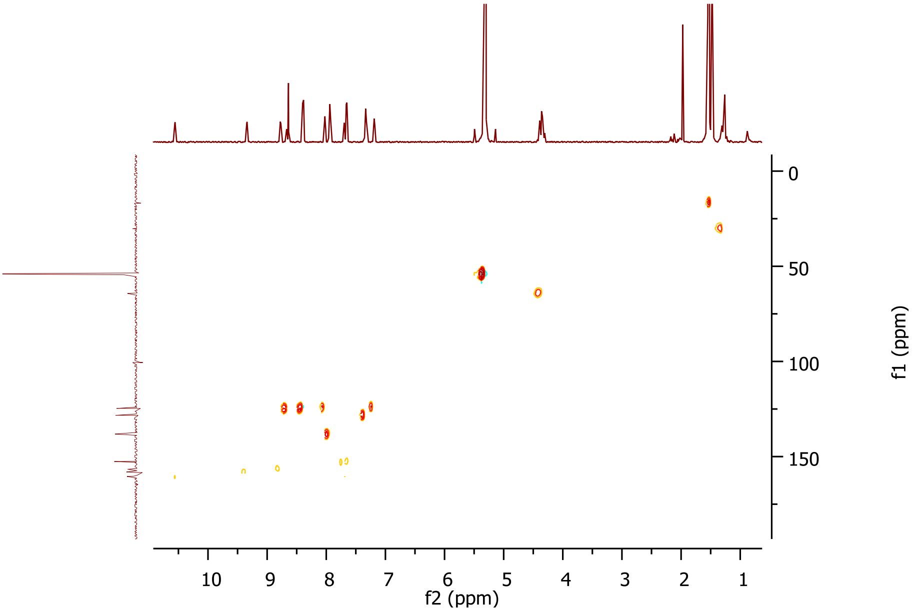

Figure S14. HMQC of **C3**

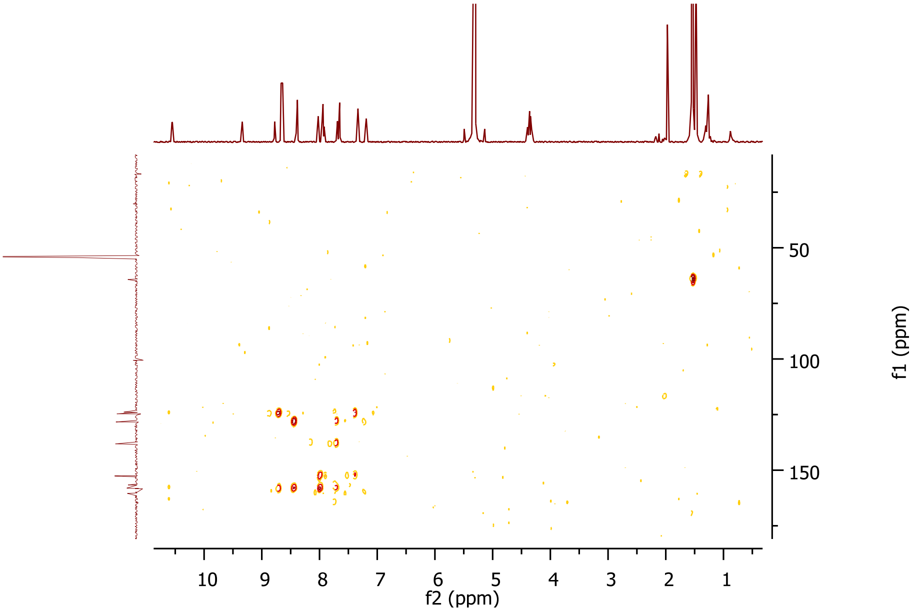

Figure S15. HMBC of **C3**

- **[Ru(L1-POOH)(azpy)Cl]Cl (C4)**

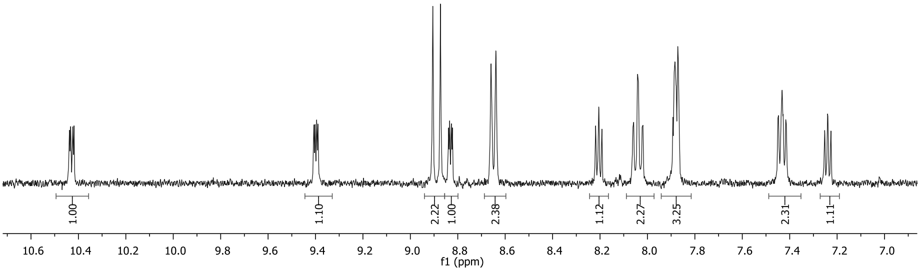

Figure S 16. ^{1}H-NMR of **C4**

- **[Ru(L1-POOH)(bpm)Cl]Cl (C5).**

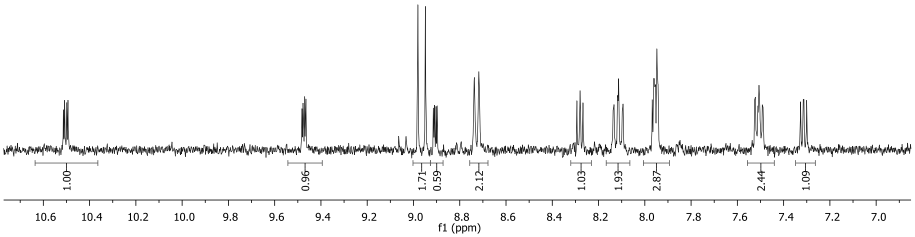

Figure S 17. ^{1}H-NMR of **C5**

Cyclic Voltammetry

- **[Ru(L1)Cl_3] (C1)**

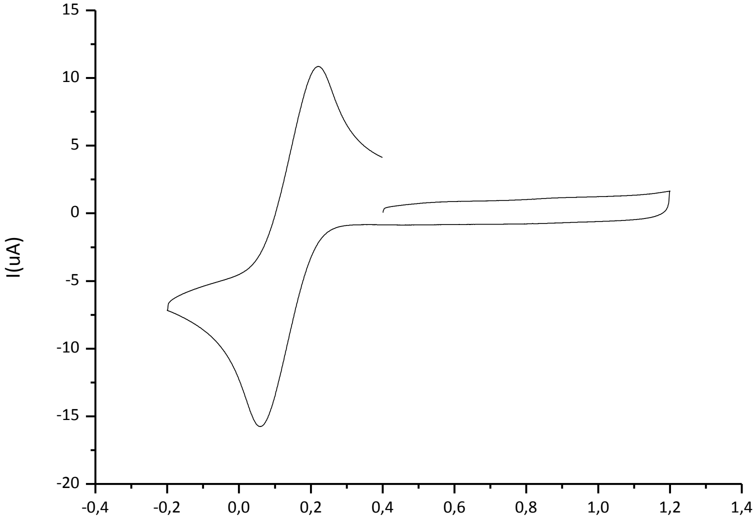

Figure S 18. CV of **C1**

- **[Ru(L1)(azpy)Cl]Cl (C2) and [Ru(L1)(bpm)Cl]Cl (C3)**

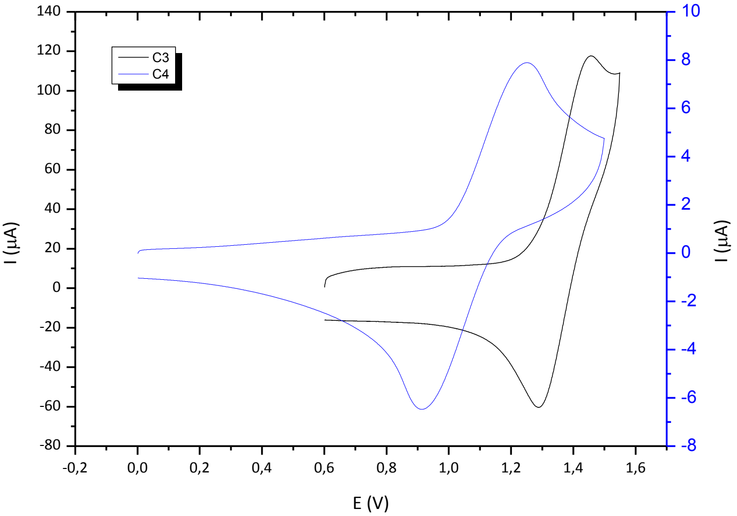

Figure S 19. CV of **C2** and **C3**

Mass spectrometry

- **[Ru(L1)Cl_3] (C1)**

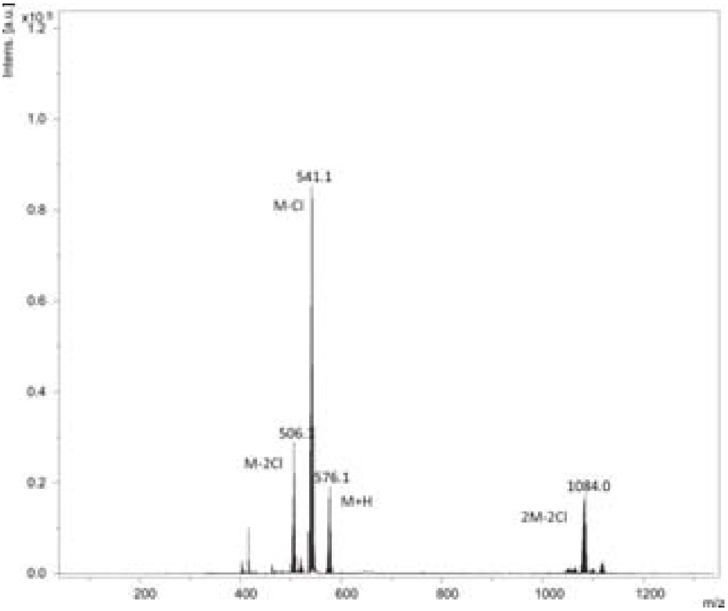

Figure S 20. MS of **C1**

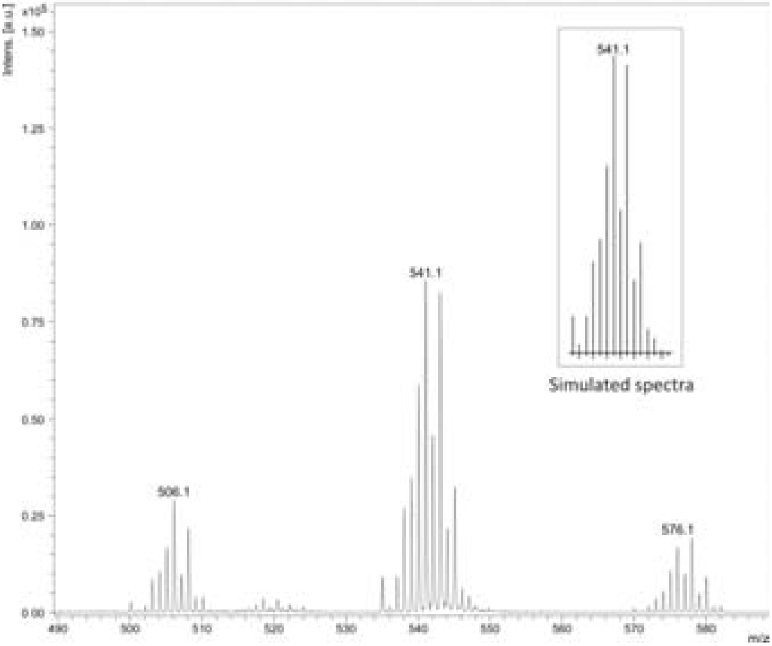

Figure S 21. Zoom of MS of **C1** and simulated spectra.

- **[Ru(L1)(azpy)Cl]Cl (C2)**

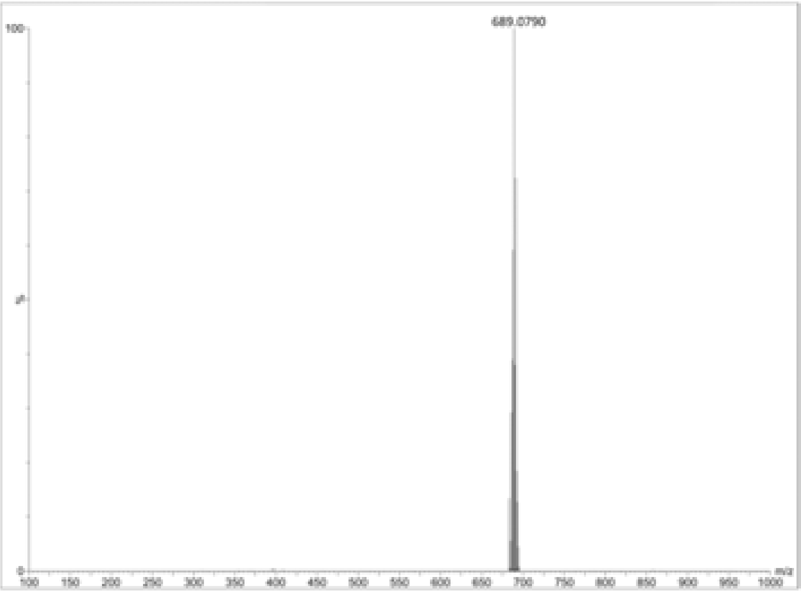

Figure S 22. HRMS of **C2**

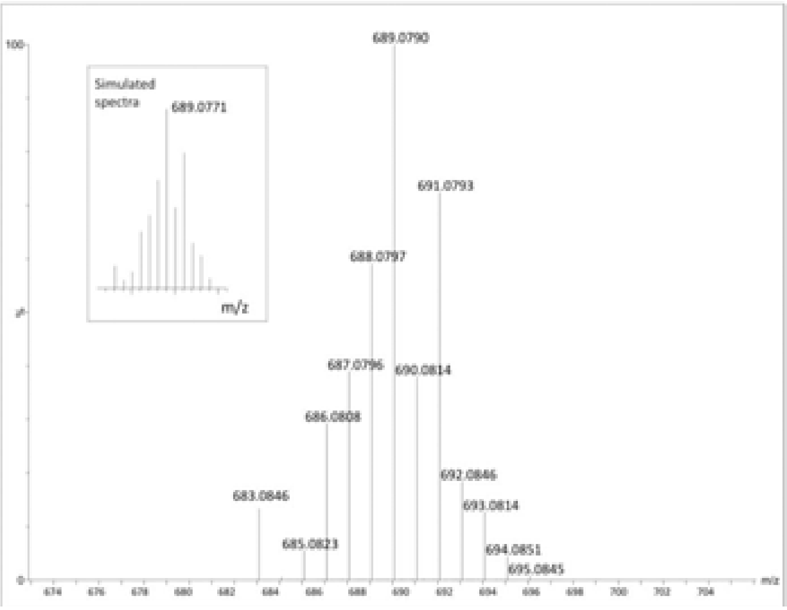

Figure S 23. Zoom of HRMS of **C2**

- **[Ru(L1)(bpm)Cl]Cl (C3)**

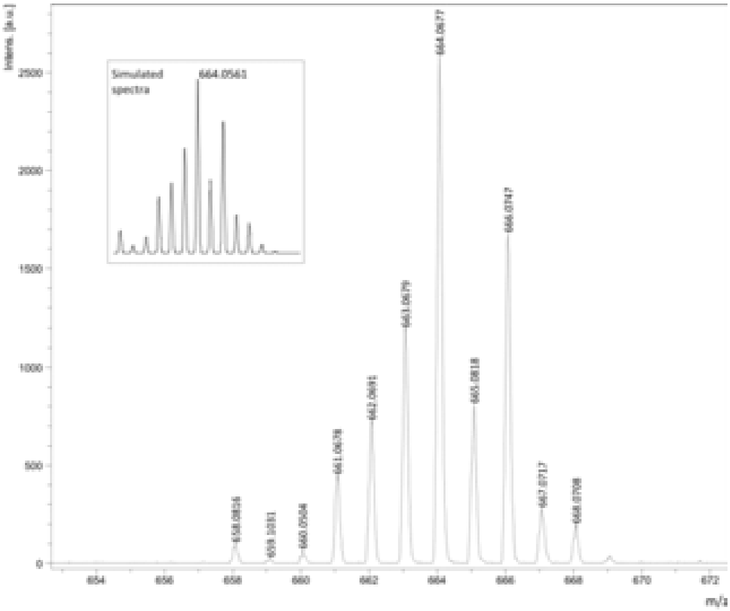

Figure S 24. Zoom of HRMS of **C3**

IR

- **MNP, C5 and NP-C5**

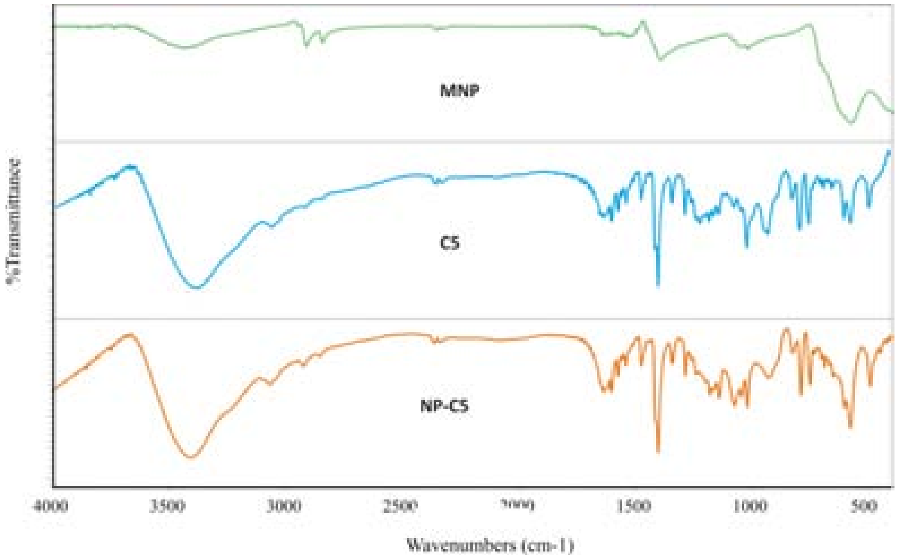

Figure S 25. Comparison of IR of MNP, **C5** and **NP-C5**

Chapter 5

Cavitand-based Ruthenium Complexes: towards Selective Supramolecular Oxidation Catalysts

Ruthenium complexes have also been functionalized with a bulky resorcinarene-based group. These complexes have been designed and synthesized in collaboration with Prof. Pau Ballester (ICIQ) and their activity in epoxidation catalysis has been studied. The resorcinarene cavity shape offers the possibility of being used for supramolecular recognition and, therefore, in regio-selective oxidation catalysis.

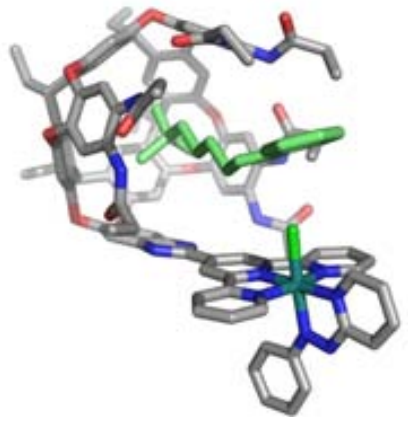

TABLE OF CONTENTS

CHAPTER 5. Cavitand-based Ruthenium Complexes: towards Selective Supramolecular Oxidation Catalysis 137

5.1. Introduction 141

5.1.1. Resorcin-[4]-arene cavitand-based molecular switches 141

5.1.2. Supramolecular catalysis 142

5.2. Results and Discussion 146

5.2.1. Synthesis and characterization of the ligand L1 146

5.2.2. Synthesis and characterization of complexes C3, C4 and C5 149

5.2.3. Catalytic epoxidation of alquenes 152

5.2.4. Experimental section 153

5.3 References 157

5.4. Supporting Information 159

Chapter 5

Cavitand-based Ruthenium Complexes: towards Selective Supramolecular Oxidation Catalysis

5.1. Introduction

5.1.1. Resorcin-[4]-arene cavitand-based molecular switches

One of the most fascinating classes of receptors for molecular recognition studies comprises the resorcin-[4]-arene cavitands bridged by four quinoxaline moieties introduced by Cram and co-workers (Figure 1).[1-3] These cavitands derived from resorcinarenes are macrocyclic structures with one open end that can act as hosts in molecular recognition.[4-6]

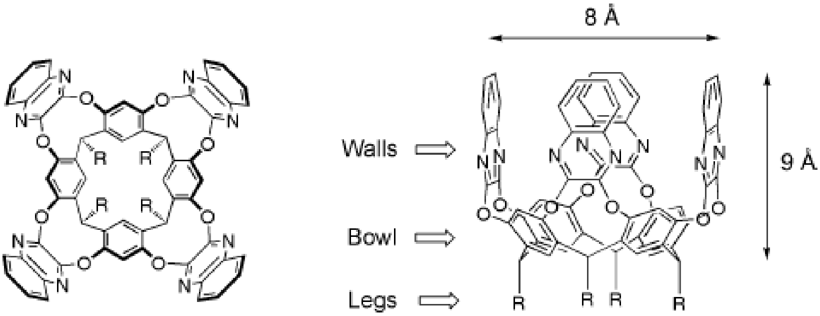

1 R = C_6H_{13}

Figure 1. Top and side view of the original quinoxaline-bridged resorcin-[4]-arene cavitand reported by Cram and co-workers.

A particularly interesting property of these systems is the reversible, temperature-dependent switching between a closed vase conformation (about 7.5 Å wide and 5.6 Å deep)[7] suitable for guest encapsulation,[8-13] and an open kite conformation, with a flat, extended surface of approximately 12.5 Å x 18 Å in size (Figure 2). The vase conformation is prevalent at room temperature and above, whereas the kite conformer is predominant at temperatures ≤ -60 °C. According to Cram and co-workers,[1] the temperature dependence of the vase-kite equilibrium is caused by solvation effects in such a way that, at low temperatures, solvation of the larger solvent-exposed surface favors the kite conformer.

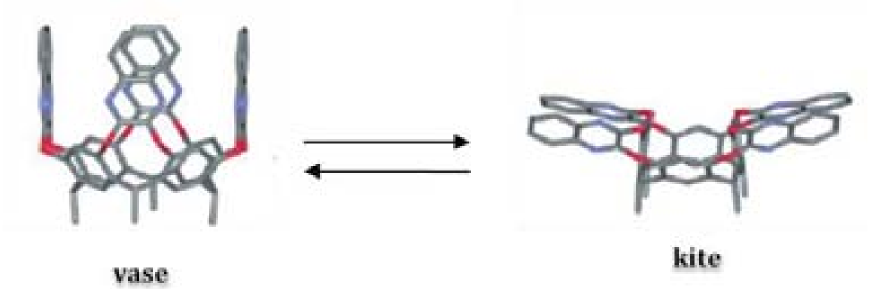

Figure 2. Molecular models of the base and kite conformers of **1**. H and legs are omitted for clarity.

5.1.2. Supramolecular catalysis

Catalysis is a longstanding proposed application of supramolecular chemistry and the production of supramolecular systems capable of mimicking the catalytic ability of natural enzymes is one of the ultimate goals of self-assembly research.[14]

The vase-like conformation of resorcinarene-based cavitands makes them suitable for guest encapsulation. An approach to supramolecular catalysis is based on the functionalization of these cavitands with a metal center capable of undergoing catalytic transformations. In this case, the substrate molecule acts as a guest that interacts with the cavity in such a way that the reacting position is placed near the active site of the catalyst.

As an example of this type of supramolecular catalysis we find the work reported by Rebek *et al*,[15,16] where a resorcin-[4]-arene fused to a salen-type ligand that coordinated to zinc is used. In Figure 3 this Zn-cavitand complex is presented.

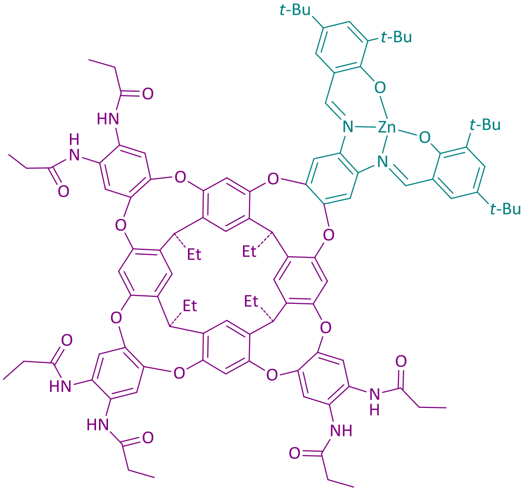

Zn-cavitand

Figure 3. Zn-cavitand formed by a resorcin-[4]-arene (purple) fused with a salen type ligand coordinated to the Zn metal center (green).

The Zn-cavitand complex presents a vase-like conformation, which is stabilized by the hydrogen bonds of the six secondary amides. This structure allows a dynamic exchange in which the guest can enter and depart slowly on the NMR time scale by the folding and unfolding of the cavitand.[17]

The catalytic reaction studied with this complex was the hydrolysis of *para*-nitrophenyl choline carbonate (PNPCC) by a nucleophilic attack of the water present in commercial CH_2Cl_2 buffered with $CF_3CO_2H/EtN(i\text{-}Pr)_2$ (Figure 4). The quaternary amine of this substrate was able to interact with the cavitand by cation-π interactions in such a way that the carbonyl group was activated by the nearby Zn metal center (Figure 4).

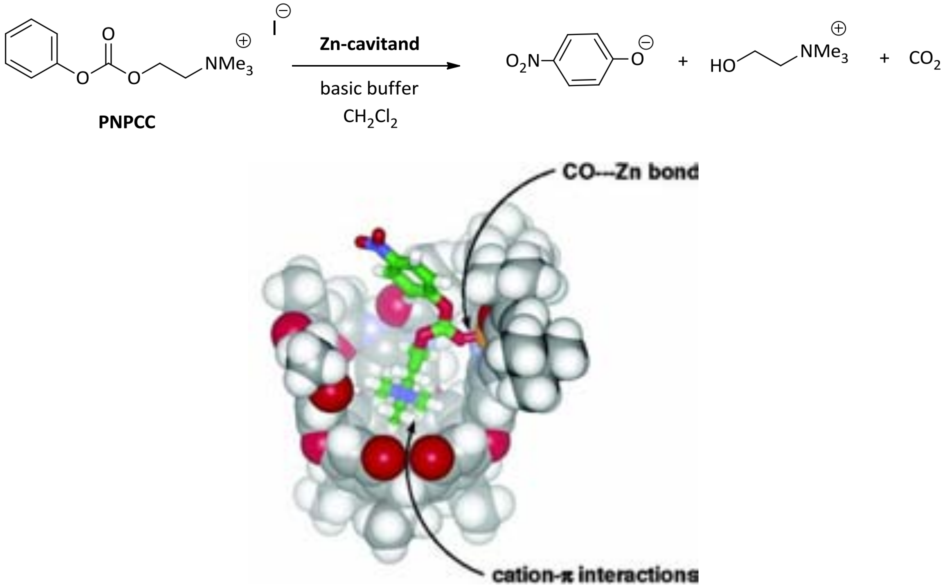
PNPCC
NMe$_3$
I
Zn-cavitand
basic buffer
CH$_2$Cl$_2$
O$_2$N
O
+
HO
NMe$_3$
+
CO$_2$
CO---Zn bond
cation-π interactions

Figure 4. Scheme of the hydrolysis of PNPCC catalyzed by a Zn-cavitand (up); and CaChe minimized structure of the Zn-cavitand interacting with PNPCC (down).

Kinetic studies of this reaction were performed and compared with the analogous complex without cavitand. A significant increase in the reaction rate was observed with the Zn-cavitand complex, being the hydrolytic transformation more than 5 times faster in the presence of cavitand.

Abstract

Herein we envisage the use of our catalytic Ru-OH_2 system in supramolecular catalysis. Following this purpose a collaboration with Prof. Ballester group was initiated at ICIQ. The aim of this project is the functionalization of $[Ru(trpy)(azpy)OH_2)]^{2+}$ (**C1**) and $[Ru(trpy)(bpm)OH_2)]^{2+}$ (**C2**), 2-electron oxidants already described in chapter 3, with a resorcin-[4]-arene cavitand. Following this aim, a tridentate trpy ligand fused with a resorcin-[4]-arene was designed in such a way that, when coordinated to ruthenium, the cavitand is capable to interact with the cationic moiety of a selected substrate, being its double bond adequately disposed in front of the $Ru^{IV}=O$ active site of the catalyst. In Figure 5 this interaction is represented by means of the molecular models of both $[Ru(trpy\text{-}cav)(azpy)(OH_2)]^{2+}$ and an alkene with a terminal cationic secondary amine acting as substrate.

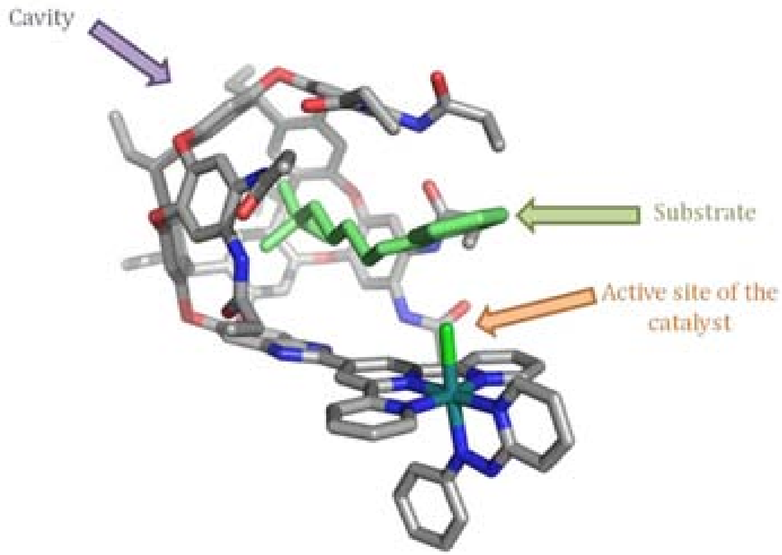

Figure 5. CAChe modelization of the interaction of $[Ru(trpy\text{-}cav)(azpy)(OH_2)]^{2+}$ with a potential substrate.

5.2. Results and Discussion

5.2.1. Synthesis and characterization of the ligand L1

The polypyridyl terpyridine ligand was fused with a resorcin-[4]-arene through the formation of an imidazol ring by a nucleophilic attack of a diamine to an aldehyde (Figure 6).

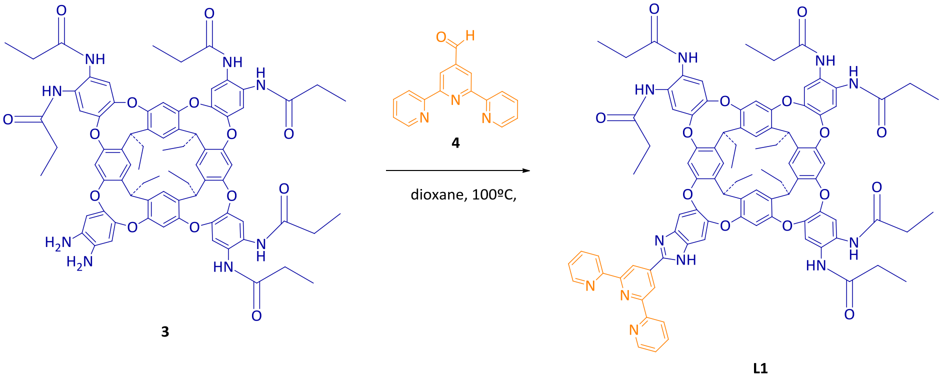

Figure 6. Synthesis of **L1**

The hexaamide-diamine **3** was synthesized following the procedure described by Rebek and Ballester.[18,19] The synthetic pathway is shown in Figure 7, in which starting from a dihydroxibenzene and an aliphatic aldehyde the whole structure is built up. In a first step, the ethyl footed resorcin-[4]-arene (**7**) was formed through a S_EAr. Afterwards, 3 equivalents of 1,2-difluoro-4,5-dinitrobenzene were added to build up 3 of the 4 walls of the cavitand in the presence of a base (**8**), deprotonating the –OH groups and allowing a nucleophilic attack in which fluoride groups were released. Then, an amidation of the nitro groups took place to form the hexaamide dihydroxy compound (**9**). This compound was used to build up the 4th wall of the cavitand by reaction of the OH groups with 1,2-difluoro-4,5-dinitrobenzene. Then, the nitro groups of the obtained hexaamide dinitro species (**10**) were reduced to amine using Ni/Raney as reducing agent to obtain the final hexaamide diamine **3.**

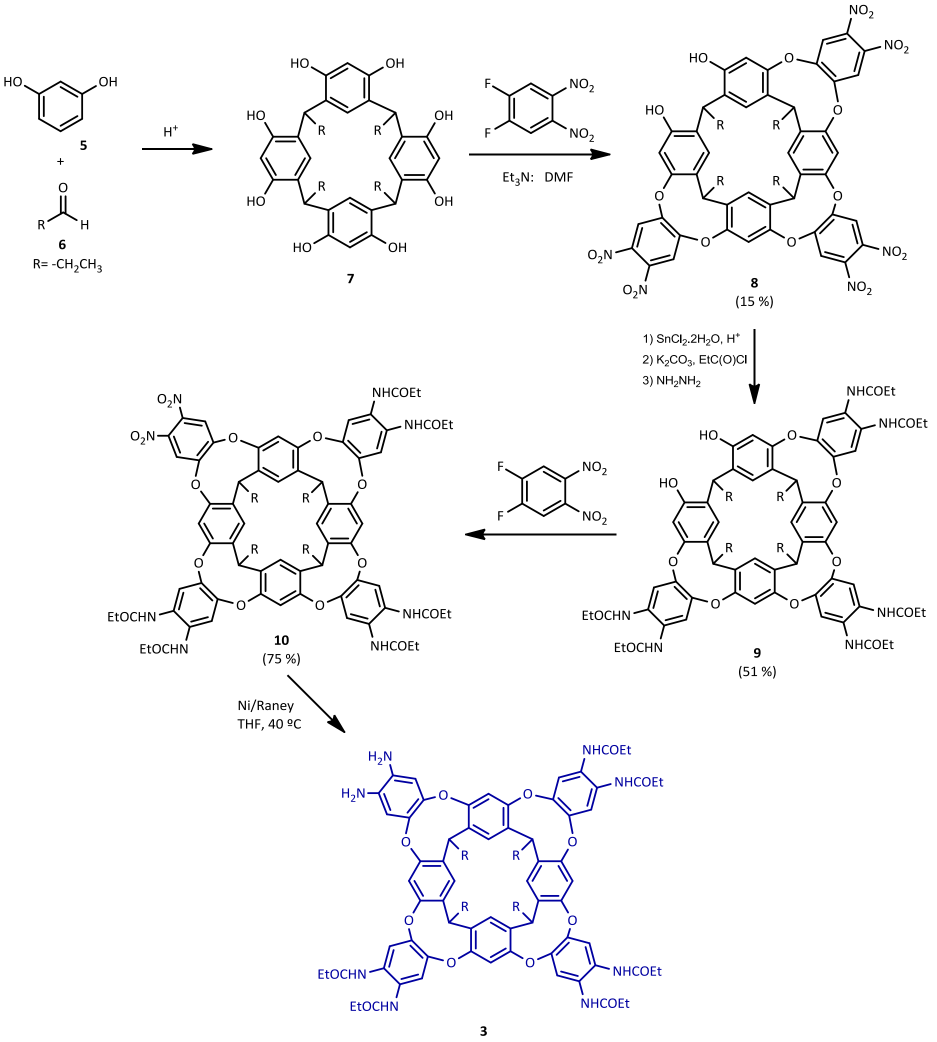

Figure 7. Synthetic pathway for the formation of the hexaamide diamine compound (**3**). R = ethyl group.

The functionalized terpyridine (**4**) used for the synthesis of the final **L1** was synthesized following the procedure decribed by Fallahpour.[20,21] In Figure 8 the followed synthetic pathway is shown, in which citrazinic acid (**11**) is used as starting material. In a first step, a bromination in positions 2 and 6 of the pyridyl ring took place. Afterwards, an esterification of the acid group followed by a reduction to the corresponding alcohol to give compound **14** was developed. Then, the alcohol underwent a Swern oxidation with oxalyl chloride to form the aldehyde **15**. Finally, through a Stille reaction the functionalized terpyridine **4**, capable to react with the hexaamide-diamine cavitand **3** to form **L1**, was obtained.

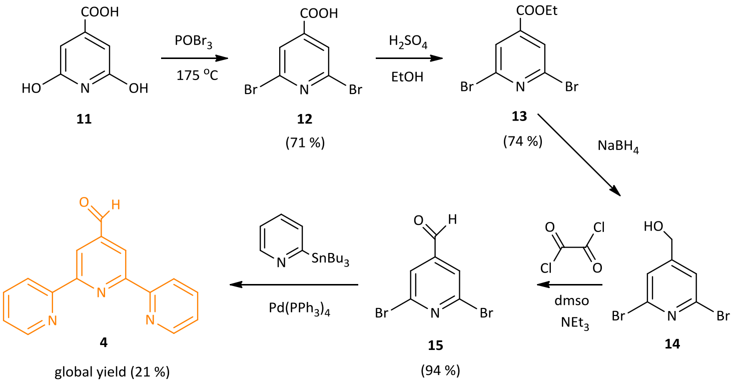
COOH
HO
N
OH
11
POBr3
175 °C
COOH
Br
N
Br
12
(71 %)
H2SO4
EtOH
COOEt
Br
N
Br
13
(74 %)
NaBH4
HO
Br
N
Br
14
O
Cl
Cl
O
dmso
NEt3
O
H
Br
N
Br
15
(94 %)
N
SnBu3
Pd(PPh3)4
O
H
N
N
N
4
global yield (21 %)

Figure 8. Synthetic pathway for the formation of **4**

Suitable crystals for X-Ray diffraction analysis of **L1** were obtained. In Figure 9 the crystal structure of **L1** is shown, where the vase-like shape of this cavitand can be observed, as well as the hydrogen bonds between the six amides of the cavitands' walls that stabilize this conformation.

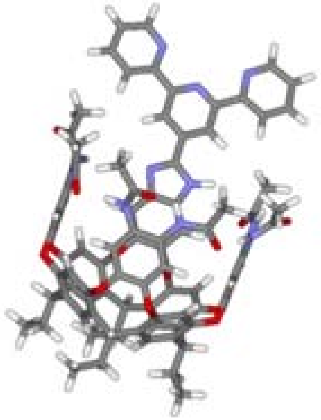

Figure 9. Representation of the X-Ray structure of **L1**.

5.2.2. Synthesis and characterization of complexes C3, C4 and C5.

The synthetic strategy followed for the synthesis of complexes [Ru(trpy-cav)(azpy)(Cl)]$^+$ (**C4**) and [Ru(trpy-cav)(bpm)Cl]$^+$ (**C5**) was based in two steps (Figure 10). In a first step **L1** was coordinated to ruthenium using $RuCl_3$ as metal precursor. Once complex **C3** is formed, the coordination of the bidentate ligand (azpy for complex **C4** and bpm for complex **C5**) took place.

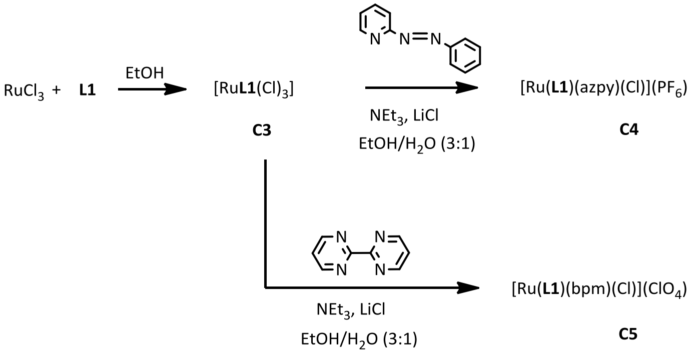

Figure 10. Synthetic pathway followed for the formation of **C3** and **C4**.

C3 could be structurally characterized by X-Ray Diffraction analysis. Monocrystals of this complex were obtained by slow diffusion of *n*-hexane into a dichloromethane solution of the product using the layering technique in a NMR tube at 5 ºC. In Figure 11 the resolved structure is shown. The conformation of the cavitand is an intermediate between the vase- and kite-like shape, being more similar to a vase-like conformation. The distorted octahedral configuration around the ruthenium metal center can also be observed, where the functionalized terpyridine and 3 chloro ligands complete the 6-coordination sphere of Ru.

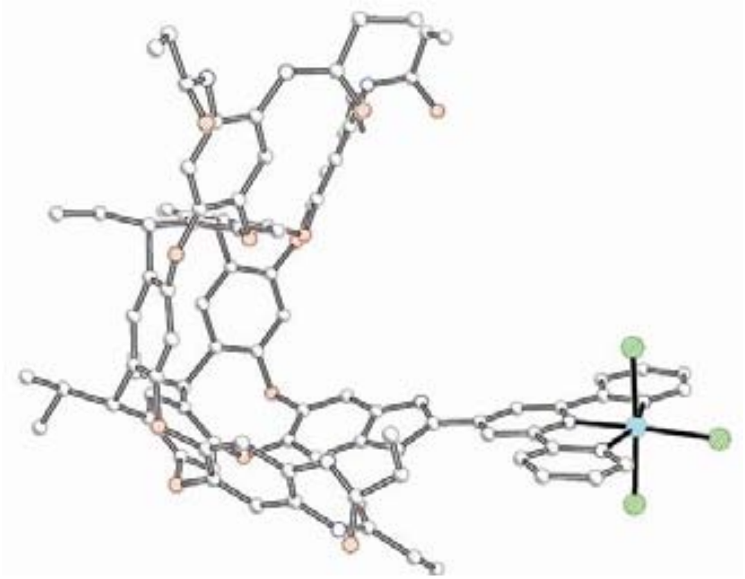

Figure 11. Crystal structure of **C3**

C3 was also characterized by cyclic voltammetry, where a reversible wave at $E_{1/2}$ of 0.12 V was observed, and by mass spectrometry, where the mass of M-Cl (*m/z* of 1765.5) was detected.

Two chloro ligands of **C3** were substituted in the next step by the bidentate azpy and bpm ligands to give the corresponding **C4** and **C5** complexes in moderate to good yields.

C4 was analyzed by the usual spectroscopic and spectrometric techniques. NMR analysis were performed in $CDCl_3$ with the addition of tetramethylamonium chloride. This salt was added in order to fix the cavitand in a vase-like conformation, avoiding the broadening of the signals provoked by the interconversion of both possible conformations. Decisive signals of the ^{1}H-NMR spectra could be identified and are highlighted in Figure 12. Between 10.1 and 11.0 ppm broad signals of protons corresponding to the six amides were observed; the ethyl groups, constituting the "legs" of the cavity appeared at 5.5 ppm (4H) and the pyridylic H of azpy *cis* to the chloro ligand appeared at 10.0 ppm (1H). The integration of these signals is in concordance with the presence of just one isomer where the pyridine of azpy is disposed in *cis* to the chloro ligand.

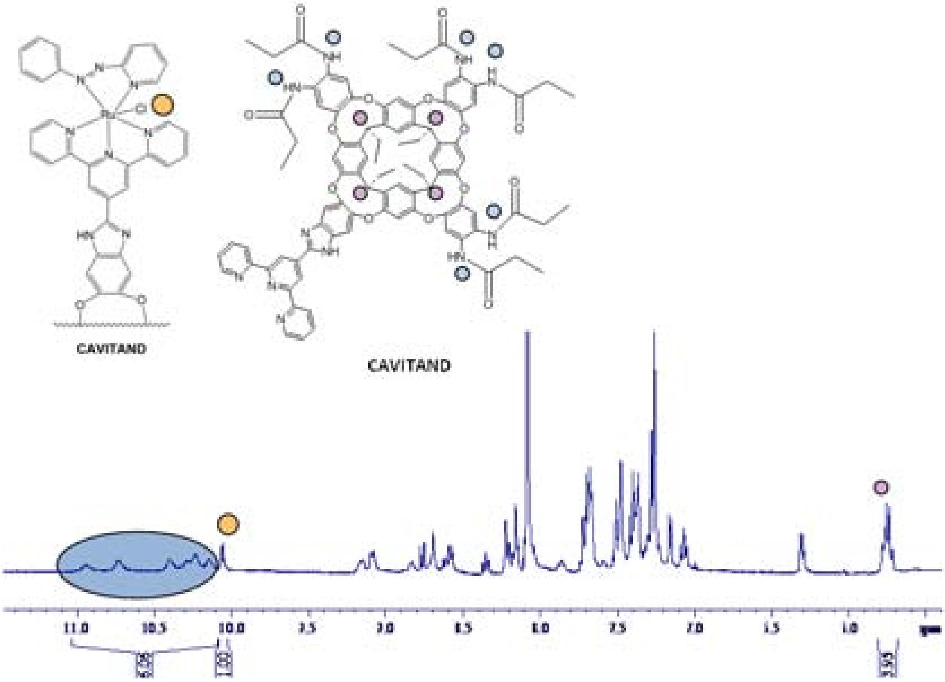

Figure 12. ^{1}H-NMR of **C4** and assignment of selected resonances.

The complex [Ru(trpy-cav)(bpm)Cl]$^+$ (**C5**) could be analyzed by mass spectrometry, where M-ClO$_4$ with a value of *m/z* of 1888.3 was detected (Figure 13). Several attempts for the obtention of a good ^{1}H-NMR spectra were made using different deuterated solvents, such as chloroform, dichloromethane, dmso and methanol, with and without the addition of a tetramethylamonium salt. However, broad bands difficult to assign were always obtained.

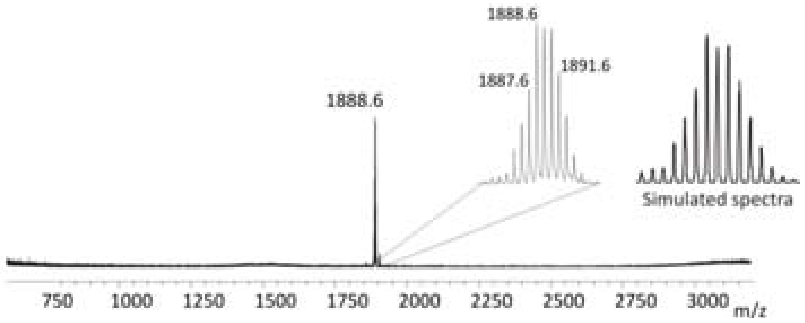

Figure 13. Experimental and simulated mass spectra of **C5**.

5.2.3. Catalytic epoxidation of alquenes.

The catalytic activity of **C5** was tested for the epoxidation of *cis*-β-methylstyrene in dichloromethane, using iodobenzene diacetate as oxidant (Figure 14). The catalysis was followed by ^{1}H-NMR using dodecane (10 μl) as internal standard. After 30 h 3.6 μmol of D_2O were added. The conversion, yield and selectivity were calculated after 17 h of the addition of D_2O, resulting in 77 % yield and complete conversion. This process took place stereoselectively, beign the *cis* isomer the only one observed.

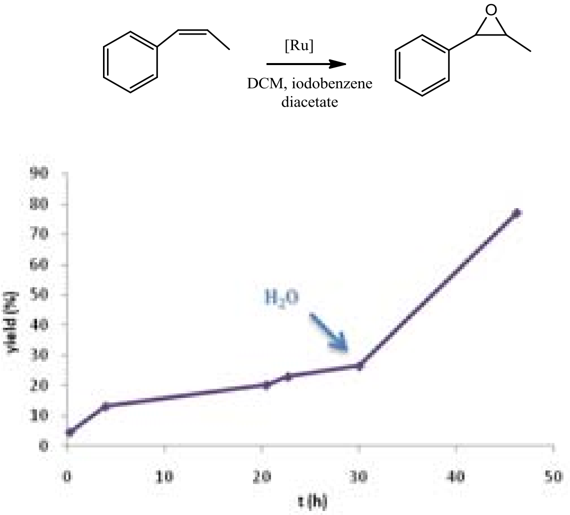

Figure 14. Epoxidation of *cis*-β-mehtylstyrene to the corresponding *cis*-epoxide with **C5.** Conditions: [Ru] = 2.5 mM, [substrate] = 250 mM, $[PhI(OAc)_2]$ = 500 mM $[D_2O]$ = 500 mM (added after 30 h of reaction), CD_2Cl_2 (0.4 mL). Conversions and yields are evaluated by ^{1}H-NMR analysis with dodecane as internal standard.

These results are comparable to the ones obtained for the analogous complex **C2** (68 % yield and 100% conversion, Chapter 3). Thus, the active site of the catalyst remained unaltered after being modified with a cavitand moiety. Further experiments are being developed using a substrate capable to interact with the cavitand. Aditionally, the capacity of the supramolecular system to regioselectively oxidize substrates containing two differently placed double bonds is being also evaluated.

5.2.4. Experimental section

Instrumentation and Measurements. The NMR spectroscopy experiments were performed on a BrukerAvance 500 Ultrashield NMR spectrometer. Samples were run in CD_2Cl_2 and d_3-MeOH. Cyclic Voltammetry (CV) experiments were performed on an IJ-Cambria HI-660 potentiostat using a three-electrode cell. Typical CV experiments were carried out at a scan rate of 100 mV/s. A glassy carbon electrode (2 mm diameter) was used as working electrode, platinum wire as auxiliary electrode, and a SSCE as a reference electrode. Working electrodes were polished with 0.05 micron Alumina paste and washed with distilled water and acetone before each measurement. The complexes were dissolved in CH_2Cl_2 containing the necessary amount of n-Bu_4NPF_6 (TBAH) as supporting electrolyte to yield a 0.1 M ionic strength solution. $E_{1/2}$ values reported in this work were estimated from CV experiments as the average of the oxidative and reductive peak potentials $(E_{p,a} + E_{p,c})/2$. Mass spectrometry analysis were performed in a mass spectrometer with matrix assisted laser desorption ionization (MALDI-TOF, Bruker Autoflex).

X-Ray Structure Determination. Suitable crystals of **C3** were grown up by slow diffusion of n-hexane into a solution of complex in dichloromethane using layering technique in an NMR tube at 5 ^{o}C. Data collection was performed on a Bruker Nonius FR 591 system equipped with a multilayer Montel 200 mirror monochromator Mo Kα (λ = 0.71073 Å) radiation and an Apex II CCD detector. The molecular structure was resolved by direct methods and refined of F^2 by full matrix least squares techniques using SHELX TL package with anisotropic thermal parameters.

Preparations. Compounds **3**,[18] **4**,[20,21] **7**,[19] **8-10**[18] and **12-15**[20,21] were prepared following reported procedures.

Synthesis of L1

A solution of Ni/Raney in THF was added to 100 mg (0.072 mmol) of **10** under hydrogen atmosphere. The reaction was stirred at 40^{o}C overnight. Then, the mixture was filtered through celite, the solent was evaporated and the remaining solid was washed with thf and dried under vacuum in the dark to obtain a white solid (**3**). **3** was used without further purification in the next step, due to its unstability. A solution of the obtained **3** and 16.72 mg of terpyridine **4** in less than 1 ml of dioxane was placed in a 20 mL capped tube. The tube was flushed with air, capped and heated at 100^{o}C for 4 h. The reaction mixture was then concentrated and the residue was purified by column chromatography using silica as stationary phase and CH_2Cl_2:MeOH (15:1) as mobile phase. Yield = 35 %. **^{1}H NMR** (400 MHz, CD_2Cl_2) δ 9.02 (s, 2H, CH_{trpy}), 8.71 (m, 4H, CH_{trpy}), 7.94 (t, 2H, CH_{trpy}), 7.75-7.21 (aromatic CH_{cav}), 7.43 (m, 2H, CH_{trpy}), 5.62 (m, 4H, allylic CH_{cav}), 2.34 (m, 20H, $CH2_{cav}$), 1.01 (m, 30H, $CH3_{cav}$). **MALDI$^+$ MS**: $[M+H]^+$, Calc for C94H87N11O14: 1594.64, Found: 1594.6.

Synthesis of $[Ru(L1)Cl_3]$ (C3):

To a solution of 16 mg (0,0627 mmol) of $RuCl_3{\cdot}3H_2O$ in absolute ethanol (5 ml) an absolute ethanol solution (10 ml) of 100 mg (0,0627 mmol) of **L1** was added dropwise. The reaction mixture was heated to reflux for 4h. The brown solid obtained was filtered and washed with cold ethanol until the filtrate was colorless. 78 mg of **C5** were obtained as a brown solid (yield = 69 %). **CV**: $E_{1/2}$ **=** 120 mV vs. SSCE. **MALDI$^+$ MS**: $[M\text{-}Cl]^+$, 1765.5.

Synthesis of $[Ru(L1)(azpy)(Cl)][PF_6]$ (C4):

To a suspension of 70 mg (0.039 mmol) of **1**, 28 μL (0.195 mmol) of triethylamine and 17 mg (0.390 mmol) of LiCl in 5 ml of ethanol:water (4:1) 10 mg (0.059 mmol) of azpy were added. The solution was heated to reflux for 1 h, while a deep red color solution generated. The solution was filtered hot and 4 mL of saturated aqueous solution of NH_4PF_6 along with water were added until the precipitation of a red solid. This solid was filtered and purified by column chromatography of alumina using a mixture of dichloromethane/acetone (9:1) as eluent. First a yellow band (azpy ligand) is eluted, then solvent polarity was increased (CH_2Cl_2: acetone : MeOH = 10:85:5) to elute a pink band. (Yield = 55 mg, 68 %). **MALDI$^+$ HRMS**: $[M\text{-}ClO_4]^+$, Calc for $C105H96ClN14O14Ru^+$: 1913.5957, Found: 1913.6208.

Synthesis of $[Ru(L1)(bpm)(Cl)][ClO_4]$ (C5):

Complex **C4** was synthesized following the same procedure as of **C3**, but using bpm as bidentate ligand instead of azpy. $NaClO_4$ was used as source of counter anion.

Yield = 52 %. **MALDI⁺ MS**: [M-ClO_4]$^+$, Calc for C102H93ClN15O14Ru$^+$: 1888.58, Found: 1888.6.

Catalytic epoxidation.

General procedure for the epoxidation of cis-β-methylstyrene using a relation of cat:subst:ox:H_2O of 1:100:200:200. All the experiments were developed under Ar atmosphere. 64.4 mg (200 μmol) of iodobenzene diacetate were placed in and NMR tube. 0.4 mL of CD2Cl2, 13 μl (100 μmol) of cis-β-methylstyrene, 10 μl of dodecane (43.6 μmol) and 1 μmol of the Ru catalyst were added. After 30 h of reaction, 3.6 μl (200 μmol) of D_2O were added. The data were colleted by either manual integration of the signals or with the "multi_integ3" macro of TOPSPIN.

Acknowledgements: The synthesis of **L1** was developed by Dr. Mª Angeles Samentero and Dr. Eddy Martin of Prof. Ballester group. The synthesis of **C5** was performed by Dr. Sukanta Mandal in our research group.

5.3 References

(1) Moran, J. R.; Karbach, S.; Cram, D. J. *Journal of the American Chemical Society* **1982**, *104*, 5826-5828.

(2) Moran, J. R.; Ericson, J. L.; Dalcanale, E.; Bryant, J. A.; Knobler, C. B.; Cram, D. J. *Journal of the American Chemical Society* **1991**, *113*, 5707-5714.

(3) Cram, D. J.; Choi, H. J.; Bryant, J. A.; Knobler, C. B. *Journal of the American Chemical Society* **1992**, *114*, 7748-7765.

(4) Cram, D. J. *Science (Washington, D. C., 1883-)* **1983**, *219*, 1177-83.

(5) Dalcanale, E.; Soncini, P.; Bacchilega, G.; Ugozzoli, F. *J. Chem. Soc., Chem. Commun.* **1989**, 500-2.

(6) Soncini, P.; Bonsignore, S.; Dalcanale, E.; Ugozzoli, F. *J. Org. Chem.* **1992**, *57*, 4608-12.

(7) Hof, F.; Craig, S. L.; Nuckolls, C.; Rebek, J. J. *Angewandte Chemie International Edition* **2002**, *41*, 1488-1508.

(8) Soncini, P.; Bonsignore, S.; Dalcanale, E.; Ugozzoli, F. *The Journal of Organic Chemistry* **1992**, *57*, 4608-4612.

(9) Heinz, T.; Rudkevich, D. M.; Rebek, J. *Nature* **1998**, *394*, 764-766.

(10) Heinz, T.; Rudkevich, D. M.; Rebek, J. J. *Angewandte Chemie International Edition* **1999**, *38*, 1136-1139.

(11) Körner, S. K.; Tucci, F. C.; Rudkevich, D. M.; Heinz, T.; Rebek, J. J. *Chemistry – A European Journal* **2000**, *6*, 187-195.

(12) Chen, J.; Rebek, J. *Organic Letters* **2002**, *4*, 327-329.

(13) Hof, F.; Rebek, J. *Proceedings of the National Academy of Sciences* **2002**, *99*, 4775-4777.

(14) van, L. P. W. N.; Editor *Supramolecular Catalysis*; Wiley-VCH Verlag GmbH & Co. KGaA, 2008.

(15) Richeter, S. b.; Rebek *Journal of the American Chemical Society* **2004**, *126*, 16280-16281.

(16) Zelder, F. H.; Rebek, J., Jr. *Chem. Commun. (Cambridge, U. K.)* **2006**, 753-754.

(17) Rudkevich, D. M.; Hilmersson, G.; Rebek, J., Jr. *J. Am. Chem. Soc.* **1997**, *119*, 9911-9912.

(18) Purse, B. W.; Ballester, P.; Rebek, J., Jr. *J. Am. Chem. Soc.* **2003**, *125*, 14682-14683.

(19) Purse, B. W.; Shivanyuk, A.; Rebek, J. *Chem. Commun. (Cambridge, U. K.)* **2002**, 2612-2613.

(20) Fallahpour, R.-A. *Synthesis* **2000**, 1138-1142.

(21) Fallahpour, R.-A. *Synthesis* **2000**, 1665-1667.

5.5. Supporting Information

- **L1**

NMR: Figure S 1-Figure S 2

- **[Ru(L1)Cl$_3$] (C3)**

Mass spectrometry: Figure S 4

- **[Ru(L1)(azpy)Cl](PF$_6$) (C4)**

NMR: Figure S 3

Mass spectrometry: Figure S 5

- **[Ru(L1)(bpm)Cl](PF$_6$) (C5)**

Mass spectrometry: Figure S 6

NMR characterization

- **L1**

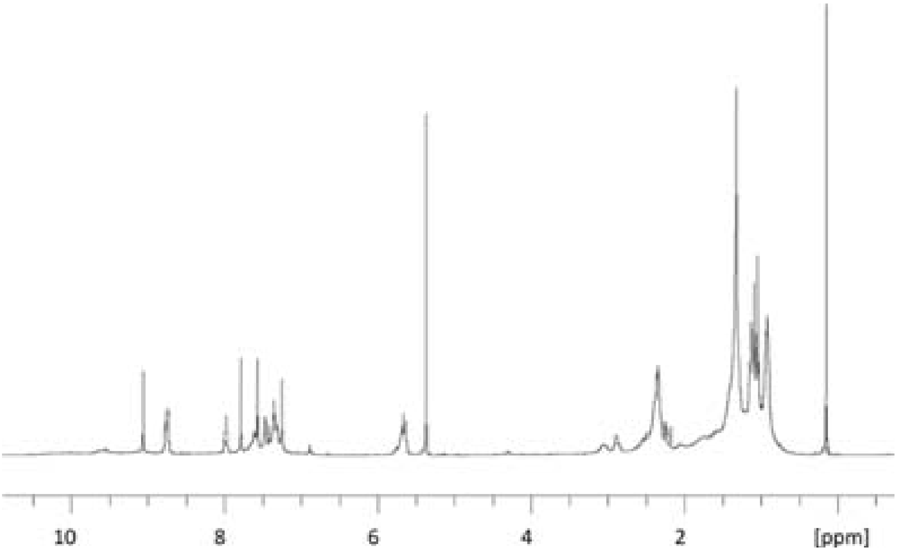

Figure S 1. ^{1}H-NMR of **L1**

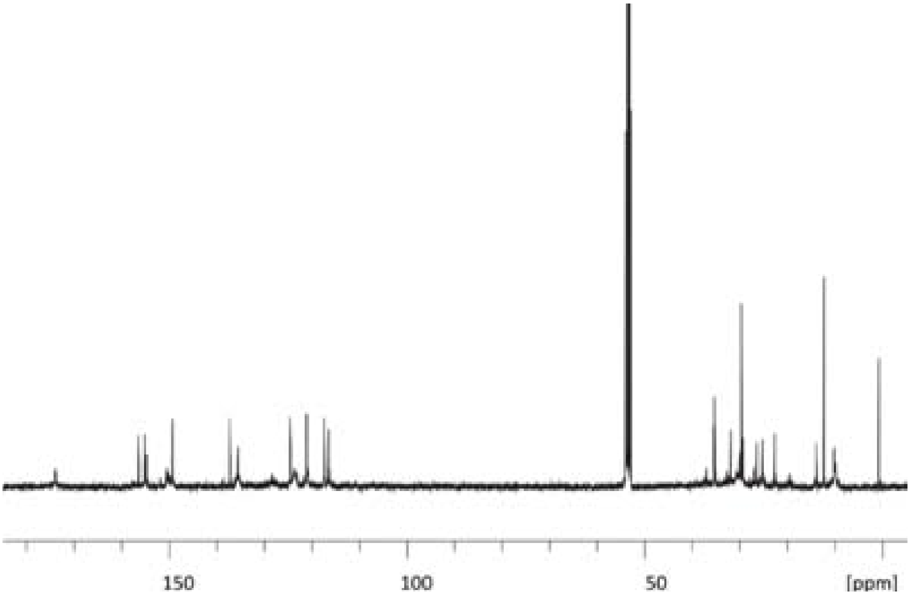

Figure S 2. ^{13}C-NMR of **L1**

- **[Ru(L1)(azpy)Cl](PF_6) (C4)**

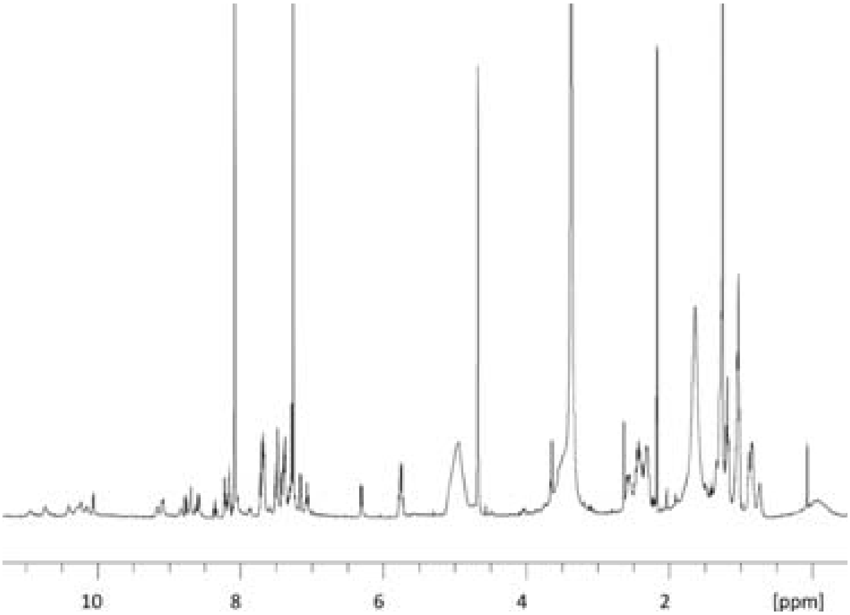

Figure S 3. ^{1}H-NMR of **C4**

Mass spectrometry

- **[Ru(L1)Cl_3] (C3)**

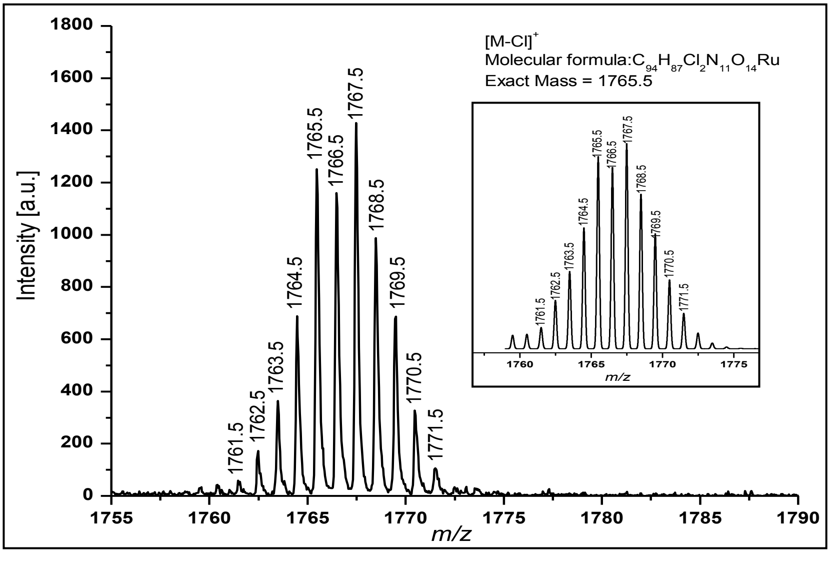

Figure S 4. MS of **C3**

- **[Ru(L1)(azpy)Cl](PF_6) (C4)**

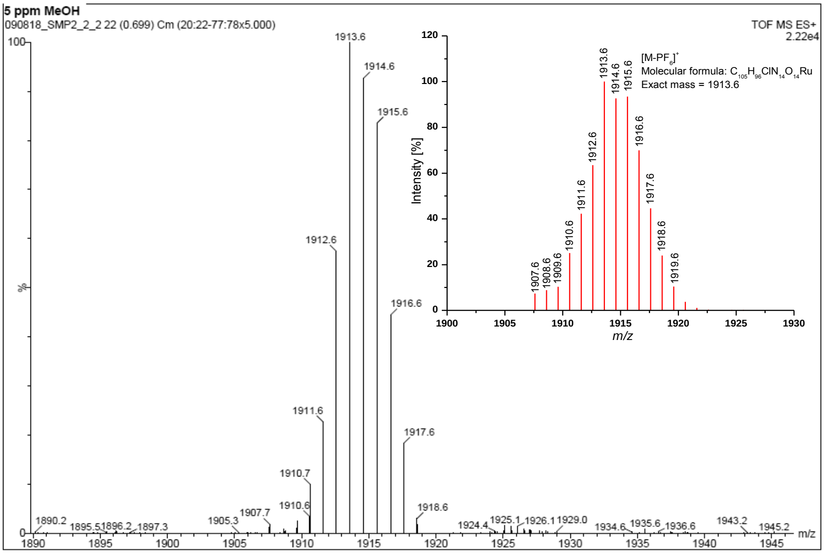

Figure S 5. MS of **C4**

- **[Ru(L1)(bpm)Cl](PF_6) (C5)**

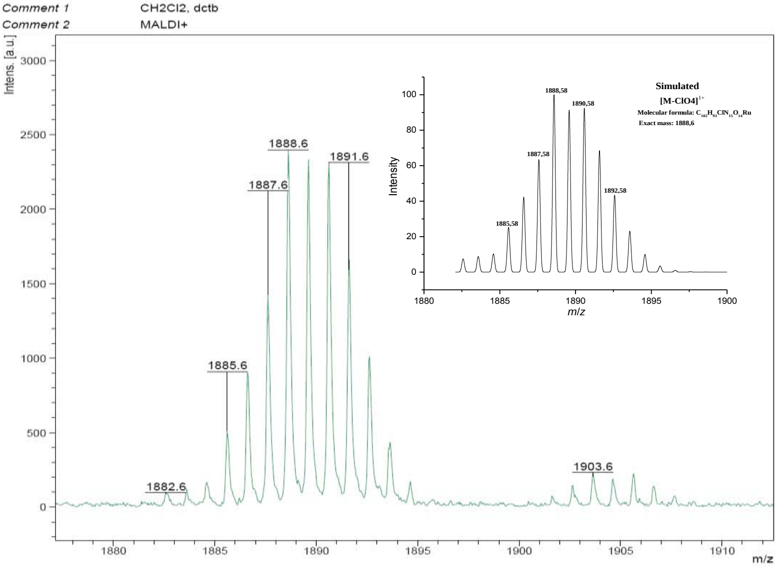

Figure S 6. MS of **C5**

Chapter 6

New Ruthenium Complexes with Enantiomerically pure Bis(pinene) fused Tridentate Ligands

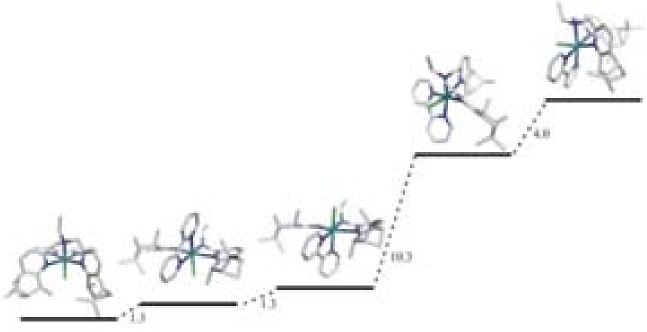

Chirality was introduced into the catalytic system through the coordination of a new pineno-fused bpea ligand. This ligand was synthesized and characterized and its coordination chemistry to ruthenium studied, paying special attention to the influence of the steric hindrance promoted by the ligand in the degree of the resulting isomeric mixture. A light-driven isomerization reaction together with DFT calculations and catalytic results are presented.

TABLE OF CONTENTS

CHAPTER 6. New Ru Complexes with Enantiomerically Pure bis(pinene)-fused Tridentate Ligands 163

6.1. Introduction 167

6.1.1. Chiral ligands 167

6.1.2. Ru-catalyzed asymmetric epoxidation 169

6.1.3. Ru bpea-based chiral complexes 173

6.2. Results and Discussion 177

6.2.1. Synthesis of and characterization of (-)-L3. 177

6.2.2. Synthesis of [Ru((-)-L3)(bpy)Cl]$^+$ (C3). 180

6.2.3. Spectroscopic and Electrochemical Characterization of [Ru((-)-L3)(bpy)Cl]$^+$ (C3). 182

6.2.4. DFT calculations. 184

6.2.5. Isomerization of C3c to C3a. 188

6.2.6. Catalytic epoxidation of alkenes 192

6.2.7. Experimental section 193

6.3. References 202

6.4. Supporting Information 206

Chapter 6

New Ru Complexes with Enantiomerically Pure bis(pinene)-fused Tridentate Ligands.

6.1. Introduction

6.1.1. Chiral ligands

Most asymmetric catalysts reported so far are metal complexes with chiral organic ligands. The nature of the chiral ligand plays a key role in the reactivity and selectivity of the catalytic reaction. However, despite the wide variety of enantiopure ligands reported, just a few of them can create effective asymmetric environments and can be applied to a broad range of reactions and substrates.[1,2] Figure 1 shows some of these "privileged" families. Thus, the design of new chiral ligands that spread those families is still an important challenge.

Among the different ligand classes summarized in Figure 1, phosphines emerged first as useful compounds for asymmetric catalytic reactions. Though being described since the 1960s, it was not until the 1980s, when Noyori's BINAP synthesis was reported and began a real expansion of chiral phosphine ligand applications (Figure 1). The axial chirality in this biaryl ligand results from a restricted rotation around the single C-C bond. The highly skewed position of the naphthyl rings has been suggested as the determining factor in its effectiveness in asymmetric catalytic reactions.[3] More recently, bisoxazolinic ligands have emerged as paradigmatic compounds in the development of nitrogen donor ligand based homogeneous asymmetric catalysis (Figure 1).[4-6] Their wide applicability can be explained by a chelating coordination to the metal center, a generally not complicated synthesis and the availability of the two possible enantiomers.

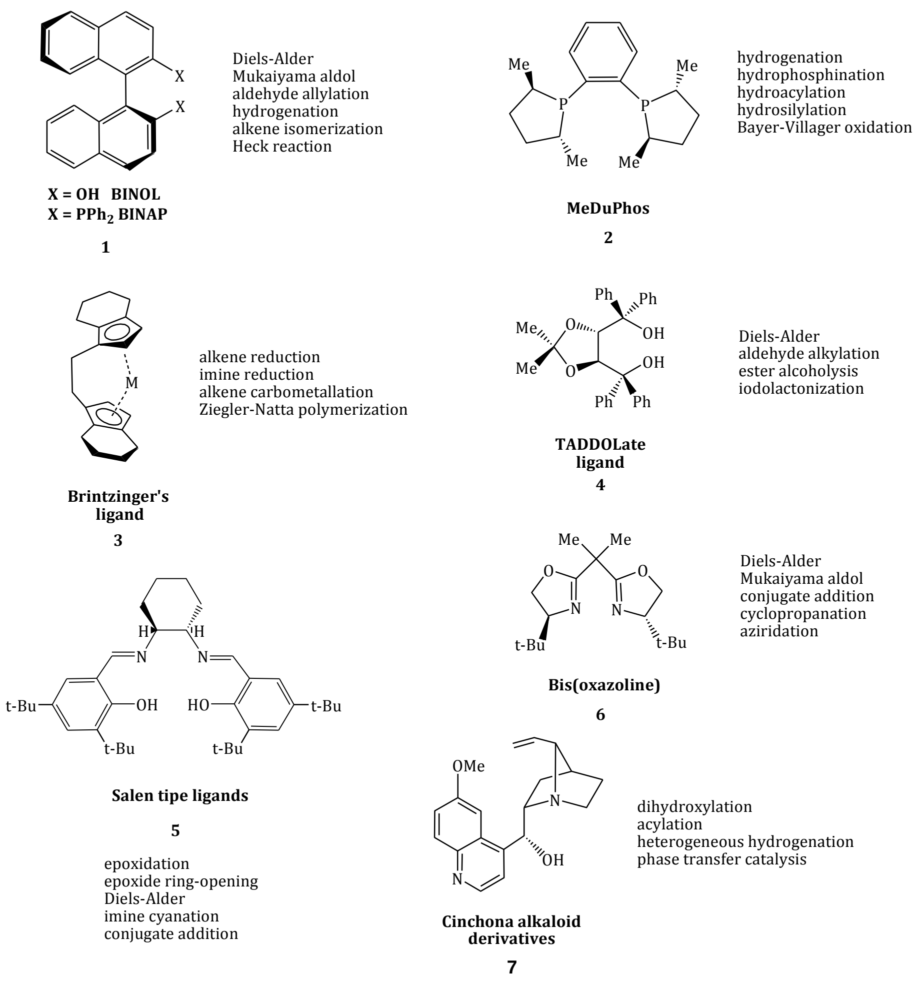
X
X
Diels-Alder
Mukaiyama aldol
aldehyde allylation
hydrogenation
alkene isomerization
Heck reaction
X = OH BINOL
X = PPh2 BINAP
1
Me
Me
P
P
Me
Me
hydrogenation
hydrophosphination
hydroacylation
hydrosilylation
Bayer-Villager oxidation
MeDuPhos
2
M
alkene reduction
imine reduction
alkene carbometallation
Ziegler-Natta polymerization
Brintzinger's ligand
3
Ph
Ph
Me
O
OH
Me
O
OH
Ph
Ph
Diels-Alder
aldehyde alkylation
ester alcoholysis
iodolactonization
TADDOLate ligand
4
H
H
N
N
t-Bu
OH
HO
t-Bu
t-Bu
t-Bu
Salen tipe ligands
5
epoxidation
epoxide ring-opening
Diels-Alder
imine cyanation
conjugate addition
Me
Me
O
O
N
N
t-Bu
t-Bu
Diels-Alder
Mukaiyama aldol
conjugate addition
cyclopropanation
aziridation
Bis(oxazoline)
6
OMe
N
OH
N
dihydroxylation
acylation
heterogeneous hydrogenation
phase transfer catalysis
Cinchona alkaloid derivatives
7

Figure 1. "Privileged" chiral ligand families

Apart from the presented families, polypyridylic ligands with appended chiral substituents are also viewed as promising chiral ligands.[7] However, despite their rich coordination chemistry, chiral polypyridylic ligands have not gathered much attention until the last decade, when Hayoz introduced a chiral α-pinene moiety into a pyridine ring.[8,9]

Since then, a variety of pineno-annellated ligands have been described[10-13] (some examples are shown in Figure 2). [4,5]- and [5,6]-pineno-fused ligands are easily accessible in their enantiomerically pure forms starting from the commercially available (-)-α-pinene or (-)-myrtenal monoterpenes, respectively.

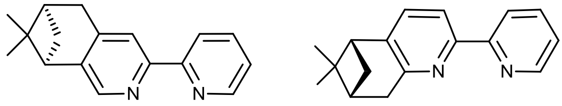

[4,5]-pinene-bpy [5,6]-pinene-bpy

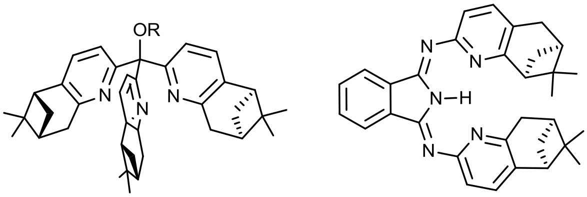

(-)-[5,6]-pinene-tpmOR (-)-[5,6]-pinene-Hbid

Figure 2. Examples of reported polypyridylic chiral ligands

These chiral polypyridylic pineno-fused ligands have found application in a wide range of asymmetric transformations such as Pd(0)-catalyzed allylic substitution,[14] Ni/Cr-catalyzed Nozaki-Kishi coupling,[15,16] Cu-catalyzed cyclopropanation[17] and Ru and Mn-catalyzed epoxidation.[18-21]

6.1.2. Ru-catalyzed asymmetric epoxidation

In the past 30 years, asymmetric catalysis has become one of the most important areas of research and major breakthroughs have been achieved.[22] Such a statement is undoubtedly confirmed by the award of the 2001 Nobel Prize in Chemistry to W. S. Knowles,[23] R. Noyori,[24] and K. B. Sharpless[25] for their work on asymmetric hydrogenation and oxidation reactions.

In the field of epoxidation catalysis, the chiral products obtained are considered as versatile building blocks for the synthesis of numerous natural products and biological active substances.[15,16] Among the various possibilities for their preparation, asymmetric catalysis constitutes an elegant and efficient tool for the synthesis of enantiomerically pure epoxides. Transition metal complexes based on titanium[22,26-29] and manganese[22,30,31] have been widely and successfully used as catalysts for the enantioselective epoxidation of olefins. Ru complexes, well known as useful catalysts for oxidation reactions, have been also employed in the above mentioned transformations.[32] Ru-porphyrin,[33-35] Ru-bisamide,[36,37] Ru/Schiff base,[38] [Ru(salen)],[39] Ru-sulfoxide[40] and Ru-bis(oxazoline)[36,41] complexes, [Ru(PPz)(bpy)] (PPz = 2,6-bis[(4S,7R)-7,8,8-trimethyl-4,5,6,7-tetrahydro-4,7-methanoindazol-2-yl]pyridine)[42] and [Ru(pydyc)(T*)] (pydyc = pyridinedicarboxilate anion, T* = chiral tridentate ligand)[18,43-45], are relevant examples of asymmetric epoxidation catalysts (Figure 3).

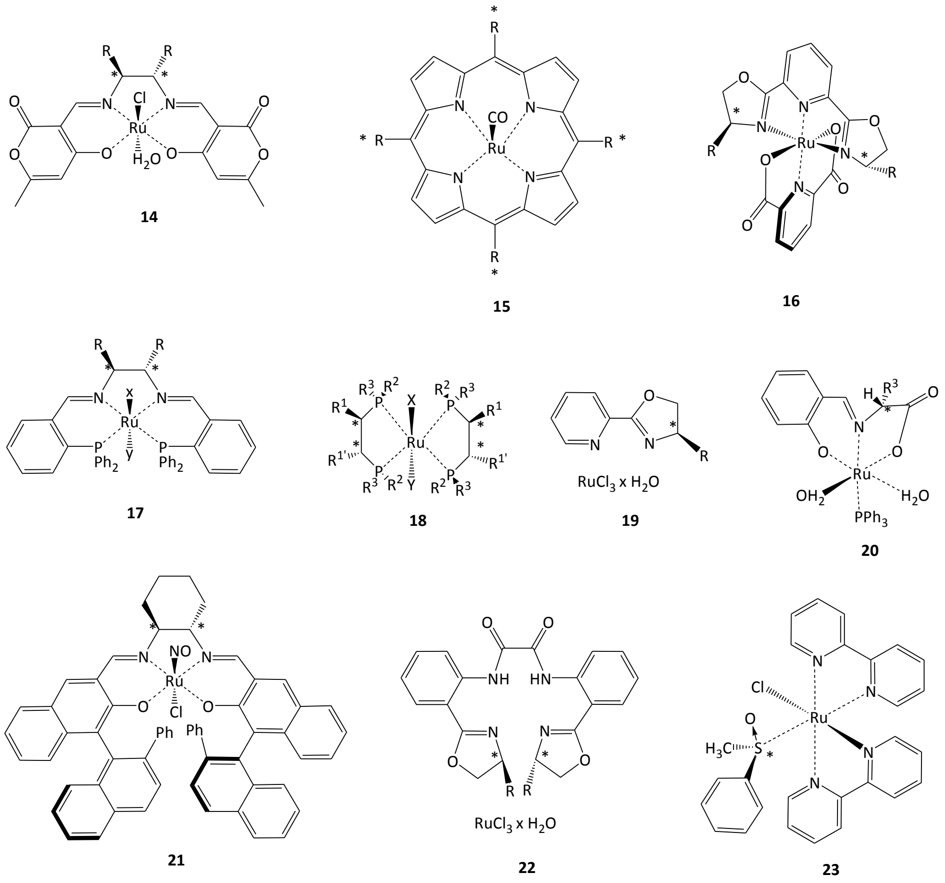

Figure 3. Most relevant active Ru catalysts for the asymmetric epoxidation of olefins.

Among them, the [Ru(pydyc)(T*)] complexes merits particular attention. Nishiyama's complex [Ru-(pyridinebisoxazoline)(pyridine-dicarboxylate)][36,41] (**16** in Figure 3) can be considered as the starting point of these promising catalytic systems, being able to epoxidize *trans*-stilbene with approximately 70% ee (Scheme 1). However, the reported method had important drawbacks (unfortunately, frequent features in Ru-catalyzed asymmetric epoxidation) such as low reactivity (96 h were needed for full conversion) and the limited scope of the catalyst (only *trans*-stilbene was epoxidized).

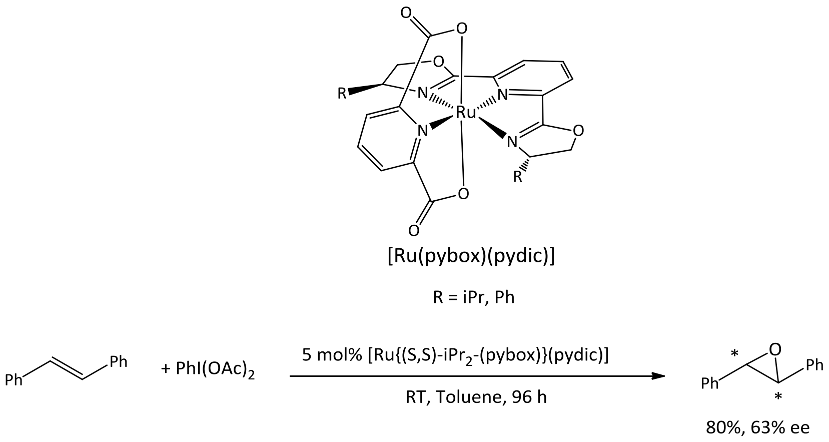
[Ru(pybox)(pydic)]
R = iPr, Ph
+ PhI(OAc)$_2$
5 mol% [Ru{(S,S)-iPr$_2$-(pybox)}(pydic)]
RT, Toluene, 96 h
80%, 63% ee

Scheme 1. Nishiyama's system for the asymmetric epoxidation of *trans*-stilbene

Taking Nishiyama's system as starting point, Beller *et al*. started, few years ago, a thorough study in order to overcome the above-mentioned shortcomings and apply this kind of complexes in a more general sense.[18,43-45] For this purpose systematic variations in the electronic and steric properties of the ligands were developed (Figure 4). Through this variations, a large number of different N,N,N-tridentate pybox and pyboxazine ligands were synthesized and a collection of 35 new ruthenium(II) complexes were fully characterized.

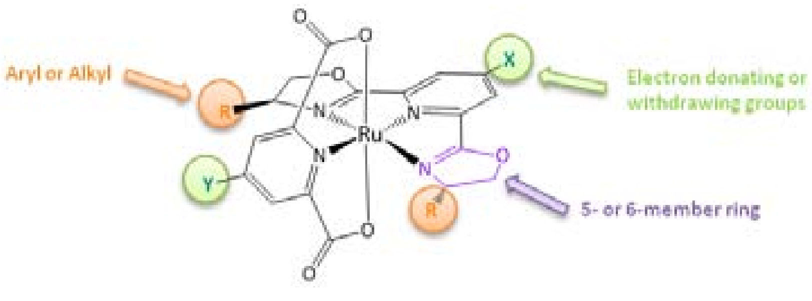
Aryl or Alkyl
Electron donating or
withdrawing groups
5- or 6-member ring

Figure 4. Ligand modularity of Beller's chiral epoxidation catalysts.

This interesting toolbox allowed the authors to develop a methodology for ruthenium-catalyzed asymmetric epoxidation of olefins using hydrogen peroxide as co-oxidant. High yields and chemoselectivities were obtained for the first time with six different classes of olefins and enantioselectivities up to 84% were achieved.

6.1.3. Ru bpea-based chiral complexes

Bpea (**L1**) is a N-donor ligand with a well known coordinative chemistry to ruthenium (Figure 5, left).[46-49] This polypyridylic ligand can become chiral by appending a pinene moiety to the pyridyl rings to give (-)-**L2** (Figure 5, right). The flexibility of **L1** and (-)-**L2** offers rich coordination chemistry, being both facial and meridional coordination possible. For this reason, various isomers can be potentially formed, having each of them a different environment around the metal center and, thus, a potentially different asymmetric induction capacity in catalysis.

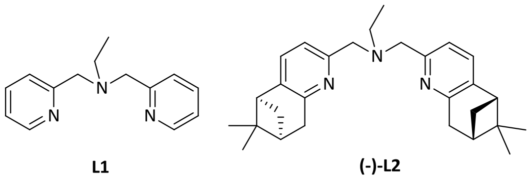

L1
bpea

(-)-L2
pinbpea

Figure 5. Drawing of the bpea type of ligands.

When (-)-**L2** is coordinated to ruthenium and combined with the bidentate 2-2'-bipyridine ligand to form the corresponding [Ru((-)-**L2**)(bpy)Cl]$^+$ complex (**C2**) five different isomers can be formed. In particular, three isomers with a facial configuration (*fac*) and two isomers with a meridional configuration (*mer*) can be obtained.

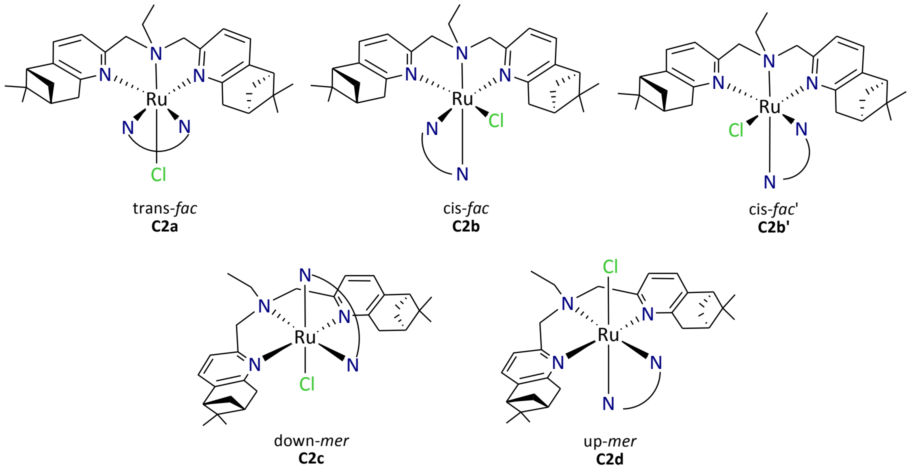

trans-*fac* **C2a**

cis-*fac* **C2b**

cis-*fac*' **C2b'**

down-*mer* **C2c**

up-*mer* **C2d**

Figure 6. Possible isomers of [Ru(**L2**)(bpy)Cl]$^+$ (**C2**).

The drawing of the different isomers as well as the notation used for each of them is shown in Figure 6. The letters a-d following the name of the complex (**C2**) are used to specify the isomer. In the three facial isomers (trans-*fac*, cis-*fac* and cis-*fac*') the notation *cis* and *trans* refers to the relative position of the chloro ligand with regard to the aliphatic N of (-)-**L2**. Two different isomers with a *cis* disposition are presented due to the presence of the non-equivalent chiral moieties of (-)-**L2**. If (-)-**L2** is coordinated in a meridional fashion the three N atoms describe a plane that will guide us in their isomeric notation. If we maintain the ethyl group of (-)-**L2** pointing up of this plane we can focus on the position of the chloro and assign the isomers as down-*mer* (**C2c**) and up-*mer* (**C2d**).

The steric hindrance and the electronic interactions between the ligands coordinated to the metal centre play a key role in the degree of the isomeric mixture obtained. For instance, in the formation of **C2** a mixture of trans-*fac*, cis-*fac* and traces of up-*mer* are obtained,[50] while in the synthesis of the analogous non-chiral complex [Ru(**L1**)(bpy)Cl]$^+$ (**C1**) just the trans-*fac* isomer is formed.[47,48] In the latter case, the hydrogen bonds between the H alpha to the pyridylic nitrogens of **L1** and the chloro ligand dramatically stabilize a trans-*fac* conformation. On the contrary, when the pinene moiety is introduced these protons are substituted and, in consequence, the mentioned hydrogen bond interactions disappear leading to a mixture of isomers. Therefore, this is a clear example of how the understanding of both steric and electronic interactions around the metal ion can allow us to design synthesis where a major isomer is favoured or even to generate only one isomer.[3,9,51,52]The latter would be extremely useful because it would allow us to prepare the catalyst in situ by just mixing the metal precursor and the chiral ligand.

Abstract

Herein we propose a modification of (-)-**L2** maintaining its electronic properties but increasing the steric hindrance in order to destabilize both cis-*fac* isomers and, in consequence, reduce and simplify the isomeric mixture that can be potentially formed. With this purpose the new chiral (-)-**L3** ligand was designed (Figure 7, left). Moreover, with this modification a new chiral center placed closer to the ruthenium ion and the catalytically active site is introduced, thus potentially modifying the enantioselective induction promoted by the complex.

Following this purpose a new pyridyl-pinene aldehyde, where a methyl group was inserted in the pinene moiety in α position to the pyridine was designed ((-)-**24**, Figure 7, right). This building block can easily lead to the formation of (-)-**L3** and presents the opportunity to be used as intermediate for the synthesis of a variety of chiral nitrogenated compounds through simple Schiff-base chemistry.

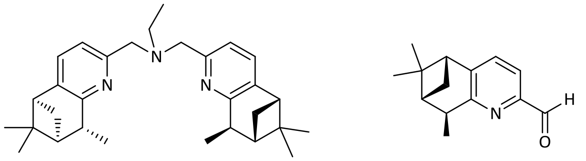
(-)-L3
Me-pinbpea

(-)-24

Figure 7. Drawings of (-)-**L3** and the aldehyde building block (-)-**24**

The coordination chemistry of (-)-**L3** was studied through the formation of [Ru((-)-**L3**)(bpy)Cl]$^+$ and, by comparison with the one reported for [Ru(**L1**)(bpy)Cl]$^+$ and [Ru((-)-**L2**)(bpy)Cl]$^+$, the effect of the introduced modification could be discussed.

6.2. Results and Discussion

6.2.1. Synthesis of and characterization of (-)-L3.

The synthetic pathway followed for the synthesis of the alkylated aldehyde (-)-**24** was based on the work developed by Bernhard and coworkers in 2004, where a furan-derivative (-)-**28** was used as intermediate (Scheme 2).[53]

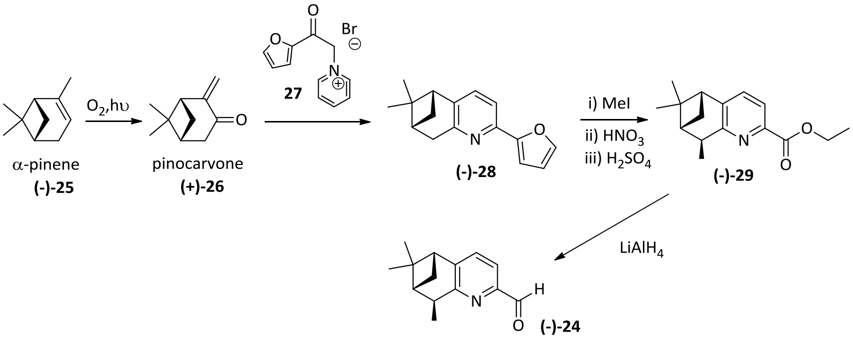
O
Br
⊖
N
⊕
27
O
O_2,hυ
O
O
i) MeI
ii) HNO_3
iii) H_2SO_4
N
N
O
O
α-pinene
(-)-25
pinocarvone
(+)-26
(-)-28
(-)-29
LiAlH$_4$
N
H
O
(-)-24

Scheme 2. Strategy followed for the synthesis of aldehyde (-)-**24**.

The methylation of (-)-**28** took place in a diastereoselective manner following the procedure described by von Zelewsky and Kočovsky using LDA and methyl iodide.[54,55] Once the aldehyde (-)-**24** was obtained it can further react in order to reach the chiral methylated (-)-**L3** ligand. The complete synthetic pathway followed for the obtention of (-)-**L3** is shown in Scheme 3.

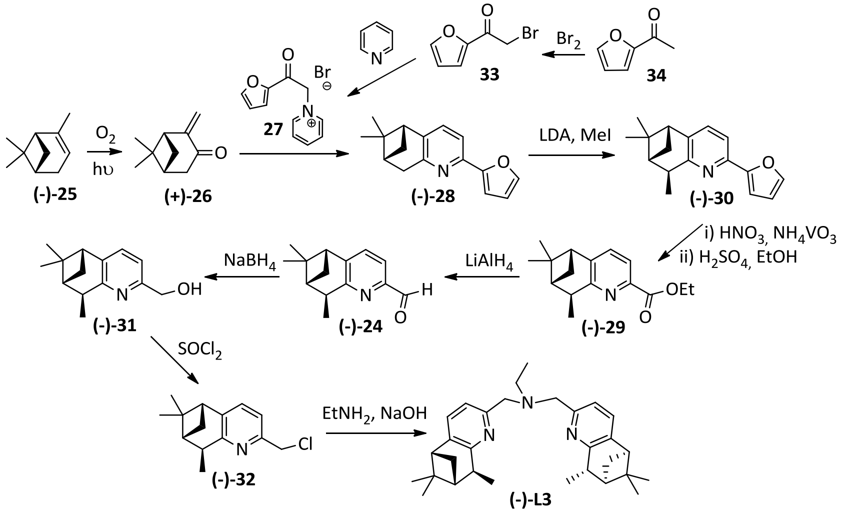

Scheme 3. Synthetic procedure of (-)-**L3**

The commercially available monoterpene (-)-α-pinene, (-)-**25**, with an optical purity of 97% was used as starting material. Through a photochemical reaction with singlet O_2 pinocarvone (+)-**26** was obtained. After a Kröhnke pyridine synthesis[56] based on the condensation of eneone (+)-**26** with α-pyridinium methyl ketone salt **27**, compound (-)-**28** with a furan substituent and an annulated pinene moiety in the 5- and 6- positions of the pyridyl ring was formed.

Then, the methylation of (-)-**28** at the methylene group adjacent to the pyridine ring took place using LDA and methyl iodide. The methyl group approaches on the less sterically hindered side of the pinene moiety giving a stereoselective methylation process. However, the furan moiety is also susceptible to an electrophilic attack. On account of this a mixture of products was obtained: a compound with a methyl group in the pinene moiety and a compound methylated in both the pinene and furan ring. However, the formation of this byproduct was not problematic taking into account that the next step consisted on the oxidative degradation of the furan substituent.

With fuming nitric acid and ammonium metavanadate a carboxylic acid was formed in situ and after esterification with sulfuric acid in ethanol compound (-)-**29** was obtained in 60 % yield. Reduction of the obtained ester (-)-**29** with $LiAlH_4$ resulted mainly in the formation of the desired Me-pinene-aldehyde (-)-**24** and some amount of Me-pinene-alcohol (-)-**31** as byproduct**.** The two products could be separated by column chromatography on silica gel. Taking into account the potential use of the aldehyde (-)-**24** in the synthesis of different chiral ligands some efforts were directed towards the optimization of its synthesis. Therefore, the use of DIBAL as reducing agent was tested (1.2 eq DIBAL, anhydrous THF, -78 ºC, 1 h). However, no aldehyde was formed remaining the initial compound unreacted.

In the next step, the isolated (-)-**24** was reduced with $NaBH_4$ to obtain, almost quantitatively, alcohol (-)-**31**. By slow addition of $SOCl_2$ hydrochloride to (-)-**31,** (-)-**32** was synthesized. Finally, a double nucleophilic attack of ethylamine, deprotonated under basic conditions, over hydrochloride (-)-**32** led to the formation of the desired methylated chiral bpea ligand (-)-**L3** (54 % yield).

(-)-**L3** was characterized by ^1H (Figure 9) and ^{13}C-NMR, mass spectrometry, elemental analysis and optical polarimetry (See the Supporting Information Section). (-)-**L3** presents C_2 symmetry, being the two pyridine-pinene moieties equivalent. The 16 signals observed in ^1H-NMR were unequivocally assigned to the corresponding protons after the analysis of the homo- and hetero-nuclei bidimensional spectra. In the aromatic region two doublets characteristic of an AB system of the pyridyl ring were observed. The allylic H14 close to a N atom appeared shifted to nearly 4 ppm. The relation of integrals between the aromatic signals and the ethyl group (H15 and H16) confirmed the presence of two pyridyl-pinene moieties bonded to the central nitrogen atom. The aliphatic protons of the pinene group could be assigned in the region between 0 and 3.5 ppm (Figure 8).

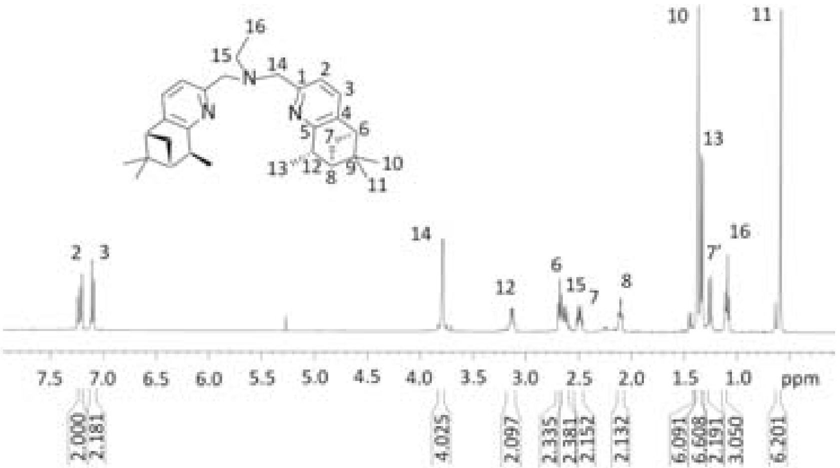

Figure 8. ^{1}H-NMR spectra and resonance assignment of (-)-**L3**.

6.2.2. Synthesis of [Ru((-)-L3)(bpy)Cl]$^+$ (C3).

C3 was synthesized using [Ru(bpy)(MeOH)Cl$_3$]^{57} as metal precursor**.** To a solution of this Ru(III) complex in absolute ethanol (-)-**L3** and triethylamine were added (Scheme 1).

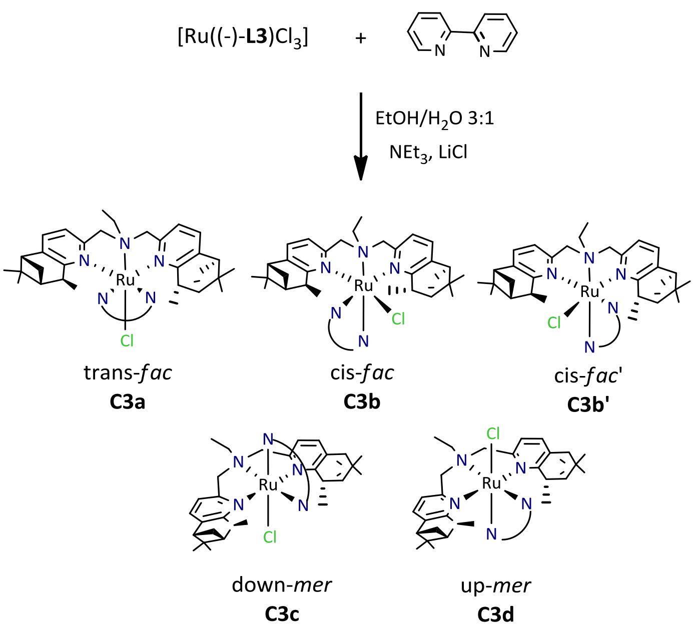
[Ru((-)-L3)Cl3]
+
N
N
EtOH/H2O 3:1
NEt3, LiCl
Ru
N
Cl
trans-fac
C3a
cis-fac
C3b
cis-fac'
C3b'
down-mer
C3c
up-mer
C3d

Scheme 1. Synthetic procedure and potential isomereric products of **C3**.

After heating to reflux for 24 h, the crude solution was analyzed by ^{1}H-NMR in order to elucidate the number of stereoisomers formed. The same notation used for **C2** and presented in Scheme 1 will be used for the different isomers of **C3**. Compound **C3a** was formed as the major isomer and small amounts of **C3c,** with a relation 6.25:1 were observed. Some minor signals of unknown products, probably corresponding to other **C3** isomers, were also observed. In Figure 9 the ^{1}H-NMR of the reaction crude is plotted together with the ^{1}H-NMR of the isolated isomers **C3a** and **C3c**.

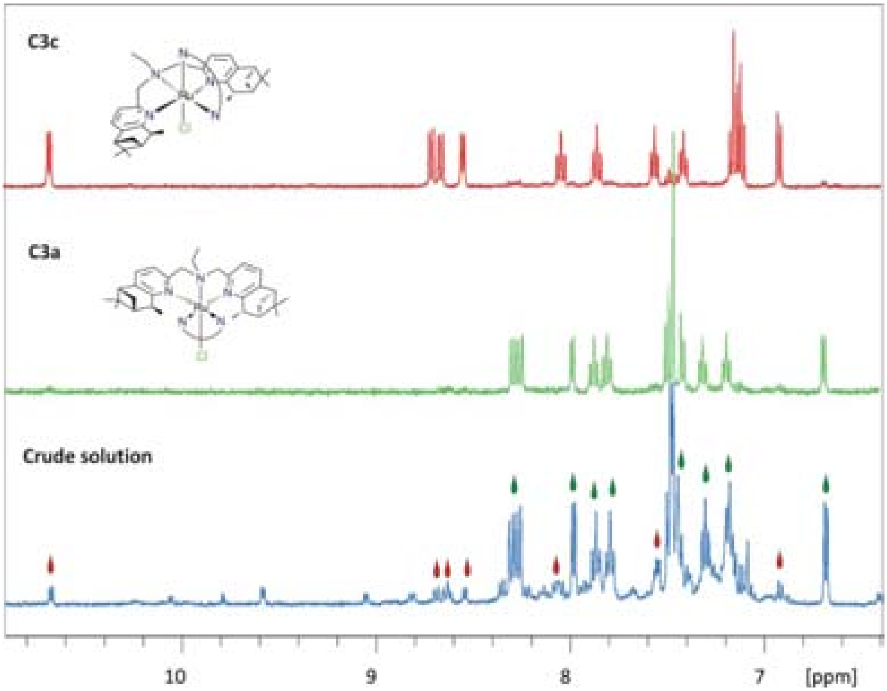

Figure 9. ^{1}H-NMR spectra of the reaction crude (blue), trans-*fac* **C3a** (green) and down-*mer* **C3c** (red)

Isolation of the different isomers was achieved by column chromatography in alumina followed by semi-preparative chromatography. The alumina column was eluted with dichloromethane/methanol 10 : 0.2 obtaining pure **C3a** and a mixture of **C3a** and **C3c. C3c** was then isolated as a pure isomer by an alumina semipreparative TLC, eluted with the same mixture of solvents.

6.2.3. Spectroscopic and Electrochemical Characterization of [Ru((-)-L3)(bpy)Cl]$^+$ (C3).

C3a was analyzed by mass spectrometry (MALDI-MS) where M-Cl was detected. Both molecular weight and isotopic pattern matched with the simulated spectra (See Figure S31 of the Supporting Information).

The redox properties of **C3a** were investigated by means of cyclic voltammetry (CV). This complex presents a quasi-reversible wave at $E_{1/2}$ of 830 mV ($\Delta E_{1/2}$ = 130 mV), what is in agreement with the presence of a negatively charged chloro ligand coordinated to the ruthenium center (Figure S32, Supporting Information).

The analysis of mono- and bidimensional NMR spectra of the isolated compounds allowed us to determine which isomers were formed. The chemical shift of CH_2-N is very indicative of the presence of a facial or a meridional disposition of (-)-**L3**, appearing around 6 ppm in the latter case and more than one ppm shifted to higher fields in the case of the former facial coordination.[58,59] When we analyze the spectra of **C3a** we can observe that these signals appear at around 4 ppm (Figure 10). Moreover, no H shifted to high ppm appears, indicating the presence of a facial conformation where the chloro ligand is not in the plane defined by the bidentate bpy ligand. In order to distinguish between the three facial isomers, analysis of the spatial interactions reflected in NOESY experiments was decisive. Two interactions, a first one between H8 of bpy and H15 (methyl group inserted in (-)-**L3**) and a second one between H1 of bpy and H20 (methyl of the pinene moiety) pointed towards the presence of the trans-*fac* isomer. Moreover, no interaction between the ethyl group of (-)-**L3** and bpy was observed, discarding the presence of a cis-*fac* conformation.

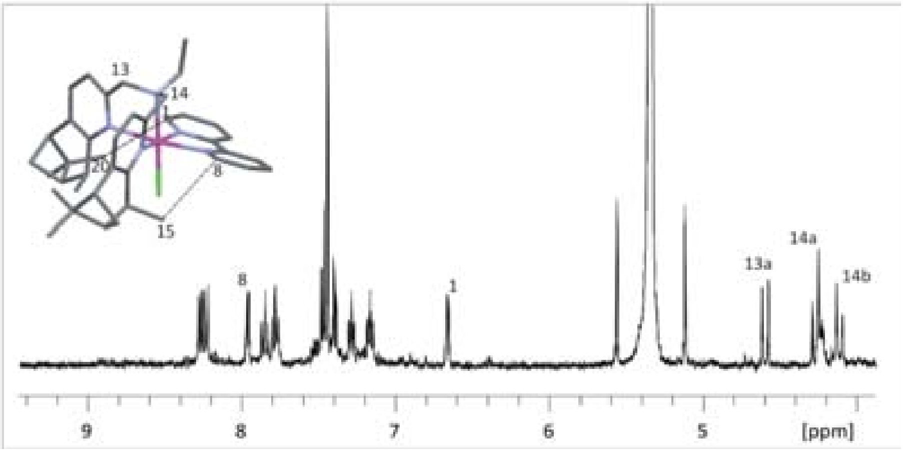

Figure 10. ^{1}H-NMR spectra of **C3a** and assignment of selected resonances.

In the case of the down-*mer* isomer **C3c** three observations can be pointed out. First, the chemical shift of CH_2-N at around 6 ppm suggests a meridional conformation. Secondly, a deshielded doublet shifted to low fields (H1 on Figure 11) reveals the effect of the chloro on the bipyridine that typically occurs just in a meridional isomer.[58] Finally, a NOE interaction between 26a (CH_2 of the ethyl group of (-)-**L3**) and H8 of the bipyridine clearly supports the presence of a down-*mer* isomer.

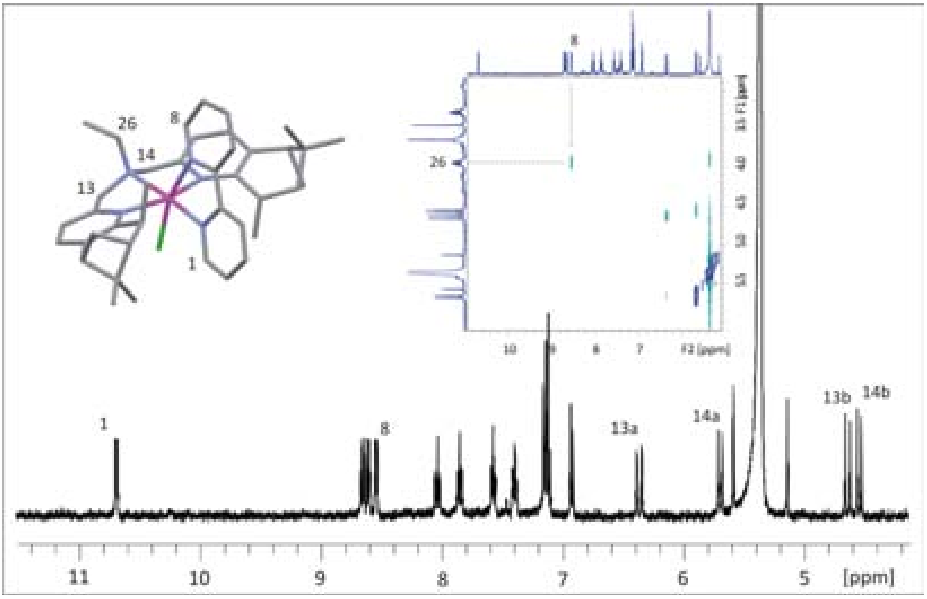

Figure 11. ^{1}H-NMR spectra and NOESY correlation of **C3c**. Assignment of selected resonances and correlation peaks.

6.2.4. DFT calculations.

The isomeric mixture obtained in the synthesis of this type of complexes is strongly influenced by the electronic properties and steric hindrance imposed by the ligands. While the synthesis of **C3** lead to the formation of one isomer as major product, when **C2** was synthesized a mixture of trans-*fac*, both cis-*fac* and traces of the meridional isomers was reported.[50]

Intuitively one can predict that the insertion of a methyl group in the pinene moiety, as it happens from (-)-**L2** to (-)-**L3,** would destabilize a cis-*fac* conformation due to steric hindrance between the new methyl groups and the pyridylic bpea moieties. In order to better understand the influence of the ligand in the final isomeric mixture we envisaged the computational study of these new Ru complexes.

In Figure 13 the optimized structures of the different isomers are shown and in Table 1 the bond distances between the ruthenium metal center and the N and Cl atoms forming its first coordination sphere are presented.

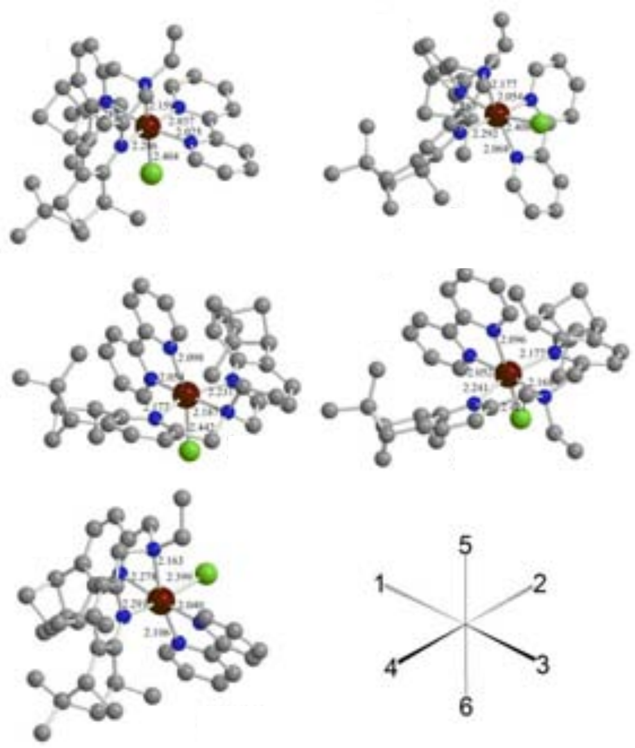

Figure 13. BPW91 optimized structures of **C3a-C3d** isomers

Table 1. Selected bond distances (Å) for BPW91 optimized geometries of **C3a-C3d** isomers.

	Ru-1	**Ru-2**	**Ru-3**	**Ru-4**	**Ru-5**	**Ru-6**
C3a	2.288	2.037	2.025	2.286	2.159	2.404
C3b	2.263	2.054	2.408	2.292	2.177	2.068
C3b’	2.278	2.399	2.040	2.291	2.163	2.106
C3c	2.054	2.231	2.187	2.177	2.098	2.442
C3d	2.052	2.177	2.168	2.241	2.096	2.421

In Figure 13 the stability diagram of the different isomers of **C3** is plotted. In order to facilitate the discussion of these results, the stability diagrams of **C1** and **C2**, previously described by our group, have been also added to this figure.

In the case of complex **C3** non-negligible differences in energy between isomers are observed. Isomer **C3a** presents the most stable configuration. Other possible facial isomers (**C3b**, **C3b'**) are higher in energy (ΔE = 12.9 and 16.9 kcal·mol-1, respectively). Both meridional isomers are quite near but slightly higher in energy compared with **C3a**.

The computational results are in concordance with the experimental results, in the sense that the facial isomer **C3a** has the lowest energy and, thus, is the major product obtained.

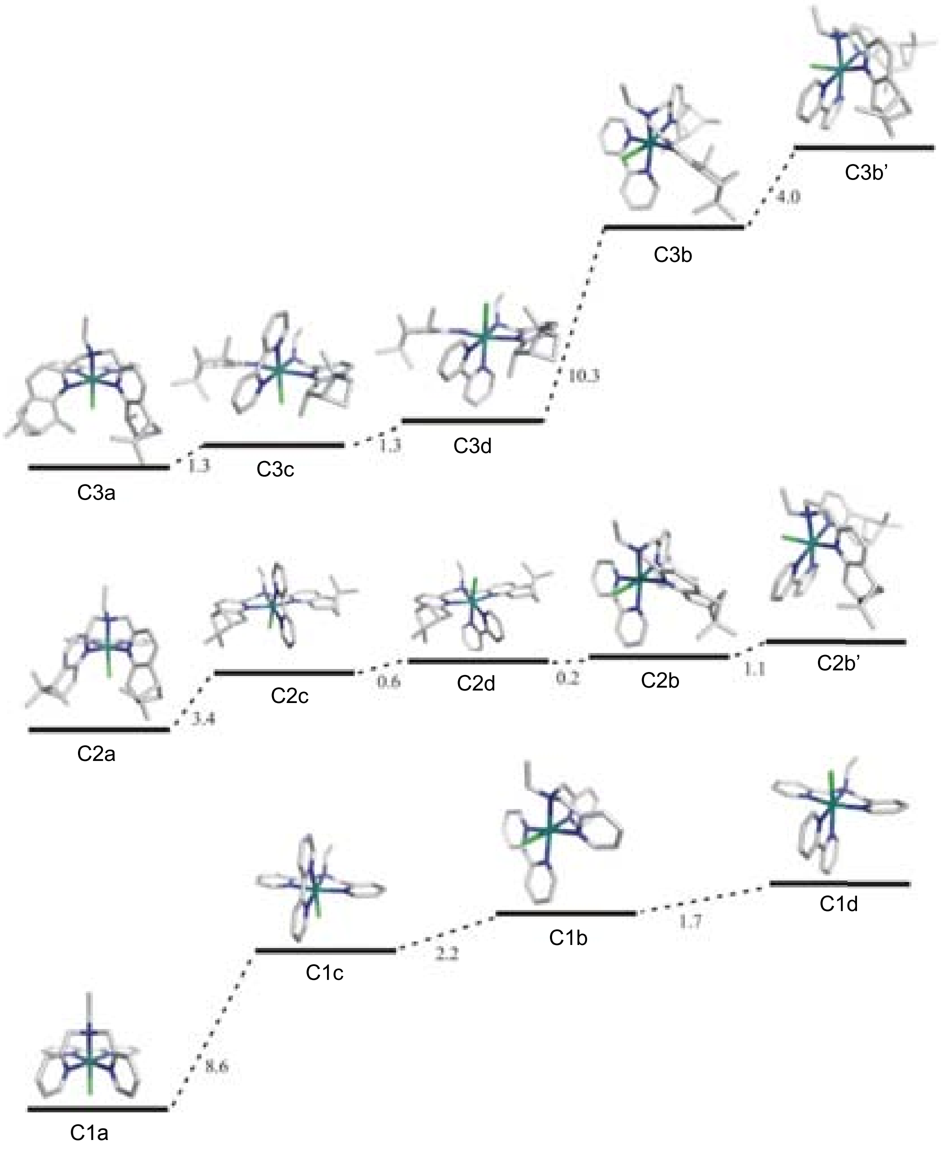
C3b'
4.0
C3b
10.3
C3a
1.3
C3c
1.3
C3d
C2b'
C2a
3.4
C2c
0.6
C2d
0.2
C2b
1.1
C1d
1.7
C1b
2.2
C1c
8.6
C1a

Figure 12. Energy diagram of **C1** (bottom), **C2** (middle) and **C3** (top).

When the stability diagrams of **C1**, **C2** and **C3** are compared important differences can be pointed out. In all cases a trans-*fac* conformation is favoured but the difference in energy with the other isomers is sensibly different in each case. For

C1 a trans-*fac* conformation is dramatically favored. The formation of H bonds between the protons of the pyridyl rings of **L1** and the chloro ligand has a strong influence on this stabilization. When these H bonds are not present (as in the case of **C2** and **C3**) the stabilization of this isomer with regard to the others is not that large. However, despite the disappearance of the H-bonding, a trans-*fac* conformation is still the thermodynamically favored in the **C2** and **C3** families, thus revealing the existence of other factors sustaining this ligand disposition (such as for instance the minor steric hindrance between bpy and (-)-**L2**/(-)-**L3** and the lower strain of the bpea ligand in its *fac* disposition.

In the case of **C2** all five isomers are quite close in energy. This result can be understood by taking into account that no electronic interactions stabilizing a particular isomer are present and considering that the steric hindrance among the different ligands is similar for all the potential isomers.

On the contrary, in **C3** the steric hindrance imposed by the new (-)-**L3** ligand derives in a strong destabilization of a cis-*fac* conformation (**C3b** and **C3b'**). In account of this, the energy of the different isomers is no longer so similar as in the case of **C2** and, in consequence, the probabilities of obtaining a high isomeric mixture decrease, as observed in the here on presented experimental results.

6.2.5. Isomerization of C3c to C3a.

In the presence of light **C3c** is not stable and isomerizes towards the trans-*fac* isomer **C3a**. This evolution could be followed by ^{1}H-NMR by registration of the spectra of a solution of initially pure **C3c** along the isomerization time (Figure 13). After 24 h the down-*mer* isomer **C3c** was no longer present in solution and pure **C3a** could be observed.

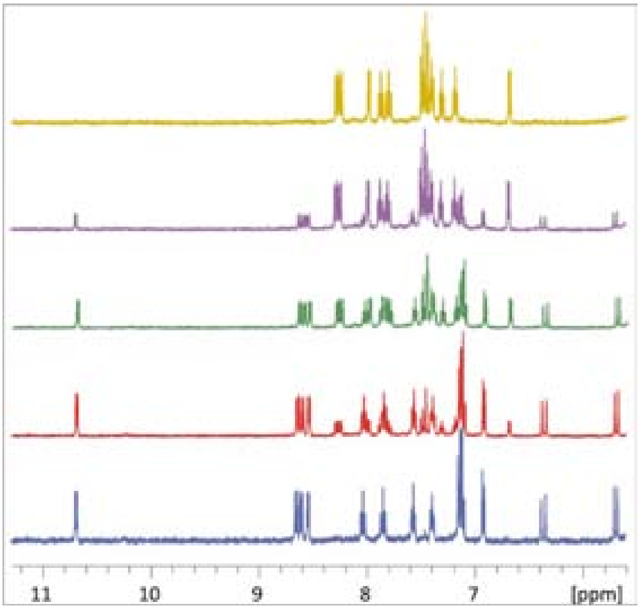

Figure 13. ^{1}H-NMR spectra of a) pure **C3c**; **C3c** in presence of ambient light after b) 3h, c) 7 h, d) 18h, e) 24h.

The kinetics of isomerization could be also followed by UV-Vis spectroscopy. In Figure 15 the different spectra registered every hour of an initially pure **C3c** solution is presented. A decrease in absorbance at 395, 480 and 500 nm together with the appearance of a new band at 530 nm was observed. It's worth mentioning that the same solution stored in absence of light for 24 h presents no modification of the electronic spectra.

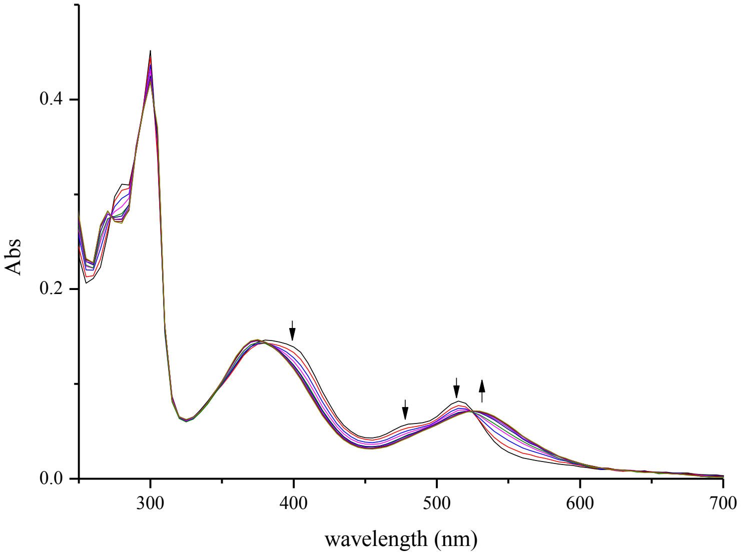

Figure 15. UV-Vis monitoring of the **C3c** to **C3a** isomerization process.

The isomerization of a meridional bpea isomer to a facial isomer was already described by our group for the [Ru(Cl_2)(bpea)(DMSO)] complex.[59] In this case, a dissociative mechanism was proposed, in which a chloro ligand was removed in a first step.

Computational calculations were envisaged also here in order to study the possible isomerization mechanisms from an energetic point of view. Two possible dissociative mechanisms were proposed; a first one based on the dissociation of one pyridine of (-)-**L3** ((a), Figure 16) and a second one based on the removal of the chloro ligand ((b), Figure 16). The energies of the different calculated species involved in both mechanisms are represented in the following diagram.

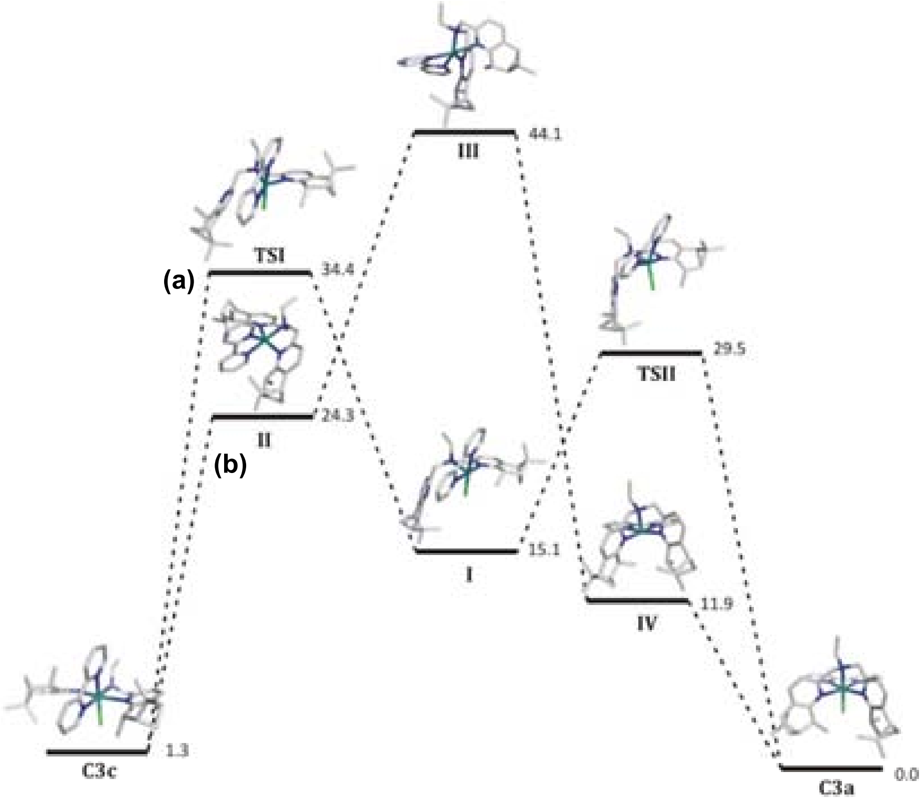

Figure 16. Relative energy diagram for the BPW91 optimized **C3c→C3a** isomerization

Following pathway **(a)**, one pyridyl ring of **(-)-L3** is firstly decoordinated to reach the **TSI** transition state by means of 34.4 Kcal/mol. However, the first step of pathway **(b)**, where the chloro ligand is firstly removed, leads to the formation of pentacoordinated species **III** through an energetically demanding reorganization process (44.1 Kcal/mol). Afterwards, further ligand reorganization allows gathering species **V** where **(-)-L3** is already coordinated in a facial manner. Therefore, the highly demanding reorganization needed in pathway **(b)** after Cl dissociation disfavors this mechanism against the pyridylic decoordination **(a)**.

In general, the decoordination of an “arm” of a quelating ligand is disfavored with regard to the decoordination of a monodentate ligand.[59] Moreover, Ru(II) is more strongly bonded to the N than to the Cl atoms, what can be inferred by comparing their Ru-X (X = N or Cl) bond distances presented in Table 1 (the Ru-Cl bond is larger than the Ru-N bond for both **C3a** and **C3c** complexes). However, in this case, the steric hindrance exerted by the pinene moieties difficult the reorganization of the pentacoordinated species (up to 44.1 Kcal/mol) fact that hampers the viability of this mechanism. However, the decoordination of one pyridyl ring, gives rise to a much more flexible intermediate, less sterically hindered and easier to reorganize to its facial form. These steric and electronic arguments would also explain why, in the case of the previously reported $[Ru(Cl_2)(bpea)(DMSO)]$ complex where no bulky ligands are used, the proposed *mer* to *fac* isomerization mechanism was based on the initial removal of a chloro ligand.[59]

6.2.6. Catalytic epoxidation of alkenes.

Preliminar catalytic experiments testing the activity of **C3a** towards the epoxidation of styrene, *cis*-β-methylstyrene and *trans*-β-methylstyrene were developed. A [cat] of 2.5 mM in 2.5 mL of t-amylalcohol, iodobenzene diacetate as oxidant and a relation of cat:subst:ox:H_2O of 1:100:200:200 was used.

T-amylalcohol was chosen as solvent after testing the activity of **C3a** in 1,2-dichloroehtane, acetonitrile, dichloromethane, chloroform and t-amylacohol, giving with the latter solvent the best results and obtaining low yields with the others, either with or without the addition of water (yield <10%). In all cases, no enantioselectivity was observed. For the epoxidation of *cis*-β-methylstyrene, the corresponding *cis*-epoxide was obtained stereoselectively (select. *cis*/*trans* = 96 %, yield *cis*-epox = 56 %, conversion = 100%, after 24 h of reaction).

Several attempts in order to improve the selectivity of the system were developed by modifying the reaction temperature. Thus, the reaction was tested at 40 °C, 25 °C and 0 °C. The results obtained are shown in Table 2.

Table 2. Catalytic epoxidation of alkenes with complex **C3a**.[a]

Substrate	T (°C)	Conversion (%)	Yield (%)	Select. (%)
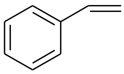	40	100	64	64
	25	100	58	58
	0	94	70	74
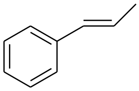	40	100	70	70
	25	100	57	57
	0	100	89	89

[a]Conditions: [Ru] = 2.5 mM, [substrate] = 250 mM, [$PhI(OAc)_2$] = 500 mM, [D_2O] = 500 mM, t-amylalcohol (2.5 mL). Conversions and yields are evaluated by GC-FID analysis with dodecane as internal standard

It can be observed that by decreasing the temperature longer reaction times are needed to reach complete conversion. The best results were obtained at 0 °C with the epoxidation of *trans*-β-methylstyrene, obtaining selectivity in epoxide of 89 %.

Further work is in progress to optimize reaction conditions for this system in order to improve enantioselectivities. Furthermore, the catalytic activity of **C3c** will be evaluated.

6.2.7. Experimental section

Instrumentation and Measurements. The NMR spectroscopy experiments were performed on a BrukerAvance 400 and 500 Ultrashield NMR spectrometer. Samples were run in CD_2Cl_2 and d_3-MeOH. Cyclic Voltammetry (CV) experiments were performed on an IJ-Cambria HI-660 potentiostat using a three-electrode cell. Typical CV experiments were carried out at a scan rate of 100 mV/s. A glassy carbon electrode (2 mm diameter) was used as working electrode, platinum wire as auxiliary electrode, and a SSCE as a reference electrode. Working electrodes were polished with 0.05 micron Alumina paste and washed with distilled water and acetone before each measurement. The complexes were dissolved in CH_2Cl_2 containing the necessary amount of n-Bu_4NPF_6 (TBAH) as supporting electrolyte to yield a 0.1 M ionic strength solution. $E_{1/2}$ values reported in this work were estimated from CV experiments as the average of the oxidative and reductive peak potentials $(E_{p,a} + E_{p,c})/2$. UV-Vis spectroscopy was performed on a Cary 50 (Varian) UV-Vis spectrophotometer in 1 cm quartz cuvettes. Mass spectrometry analysis were performed in a mass spectrometer with matrix assisted laser desorption ionization (MALDI-TOF, Bruker Autoflex). Elemental analysis was performed in EA-1108, CHNS-O elemental analyzer from Fisons Instruments (Universidad de Santiago). $[\alpha]_D$ was measured in a Jasco P-1030 polarimeter with symmetric angular oscillation for the sodium D line and photomultiplier tube detector. Angular range: ± 90ºC. Catalytic experiments were analyzed in an Agilent 6890N gas chromatograph coupled to a mass selective detector with ionization by electronic impact and in an Agilent 6890N with a FID detector using an HP-5 and β-Dex 225 column.

Computational Details.

The density functional theory (DFT) calculations have been carried out with the hybrid B3PW91 density functional,[60,61] as implemented in the Gaussian 03 package.[62] The Ru atoms have been represented with the quasi relativistic effective core pseudo-potentials (RECP) of the Stuttgart group and the associated basis sets augmented with a f polarization function ($\alpha = 1.235$).[63,64] The remaining atoms (C, N, P, Cl, and H) have been represented with 6-31G(d,p) basis sets.[65,66] The B3PW91 geometry optimizations were performed without any symmetry constraints, and the nature of minima was checked by analytical frequency calculations. The energies given throughout the paper are electronic energies without ZPE corrections (inclusion of the ZPE corrections does not significantly modify the results) or Gibbs free energy values computed at 298 K and 1 atm. Solvent effects including contributions of non electrostatic terms have been estimated in single point calculations on the gas phase optimized structures, based on the polarizable continuous solvation model PCM using ethanol as a solvent.[67,68]

Preparations.

Compounds **(+)-26**,[53] **27**, [53] **(-)-28**, [53] **33**[53] and [Ru(bpy)(MeOH)Cl_3][57] were prepared following the procedures described in the literature.

Me-pinene-furan (-)-30.

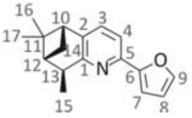

A solution of n-BuLi (26 mL, 1.6 M in hexanes, 42.21 mmol) was added dropwise over a solution of diisopropylamine (6.5 mL, 46.4 mmol) in dry THF (120 mL) at -40 ^{o}C. The solution of the formed LDA was brought to 0 ºC in an ice bath, stirred for 30 min and cooled again to -40 ^{o}C. A solution of the pyridine-pinene derivative (-)-**28** (4.5 g, 18.8 mmol) in THF (120 mL) was added slowly during 1 h. The resulting red solution was stirred at -40 ^{o}C during 2 h. Then, methyl iodide (2.6 mL, 42.21 mmol) was added dropwise during 1h and the mixture stirred overnight at room temperature. Water (310 mL) was added and the product was extracted with dichloromethane, washed with brine and dried with magnesium sulfate. The product was purified by column chromatography on silica gel using a mixture of hexane/ethyl acetate (95:5) as eluent. Compound (-)-**30** was obtained as a mixture 1:0.3 of Me-pinene-furan and Me-pinene-Me-furan. This product was used without further purification in the next step. Yield: 74 % (3.5 g, 13.8 mmol). **^{1}H-NMR** (400 MHz, $CDCl_3$) δ = 7.49 (d, *J* = 1.5 Hz, 1H, H9), 7.37 (d, *J* = 7.8 Hz, 1H, H3), 7.20 (d, *J* = 8.0 Hz, 1H, H4), 6.87 (d, *J* = 3.4 Hz, 1H, H7), 6.5 (dd, *J* = 3.2, 1.6 Hz, 1H, H8), 3.23 (m, 1H, H13), 2.75 (t, *J* = 4.8 Hz, 1H, H10), 2.56 (m, 1H, H14), 2.16 (m, 1H, H12), 1.42 (m, 6H, H15, H16), 1.29 (d, *J* = 9.4, 1H, H14'), 0.67 (s, 3H, H17). **^{13}C-NMR** ($CDCl_3$) δ = 160.8 (C, C2), 160.6 (C, C1), 154.4 (C, C6), 142.5 (CH, C9), 140.3 (C, C5), 133.1 (CH, C3), 115.4 (CH, C4), 111.8 (CH, C8), 107.2 (CH, C7), 47.1 (CH, C10), 46.8 (CH, C12), 41.4 (C, C11), 38.8 (CH, C13), 28.6 (CH2, C14), 26.3 (CH3, C16), 20.9 (CH3, C17), 18.3 (CH3, C15)); $[\alpha]_D$ -7.2 (*c* 1.5 CH_2Cl_2); ESI-MS (*m/z*) 254.1 $[M+H]^+$, 276.1 $[M+Na]^+$

Me-pinene-COOEt (-)-29.

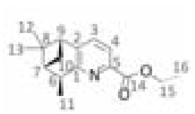

(-)**30** (23 g, 90.0 mmol) and ammonium metavanadate (1.5 g, 13.0 mmol) were dissolved in 400 mL of water. The mixture was heated to 65 ºC and 190 mL of fuming nitric acid were added slowly. The evolved gases were trapped by connecting the reflux condenser to a solution of water and a mixture of NaOH 5 M (aq.) and H_2O_2 2-3 %. The solution is heated to reflux for 5 h. After distilling the solvent under vacuum 175 mL of ethanol and 64 mL of sulfuric acid 96% were added. The resulting solution was heated to reflux overnight. 800 mL of water were added and the solution was neutralized with a saturated aqueous solution of sodium carbonate. The black solid was filtered and extracted through a Soxhlet with hexane. The solvent was evaporated to obtain 14 g of (-)-**29** as a yellow oil. Yield: 60 % (14 g, 54 mmol). **^{1}H-NMR** (400 MHz, $CDCl_3$) δ = 7.82 (d, *J* = 7.9 Hz, 1H, H4), 7.29 (d, *J* = 7.9 Hz, 1H, H3), 4.46 (m, 2H, H15), 3.32 (m, 1H, H6), 2.83 (t, *J* = 5.6 Hz, 1H, H9), 2.58 (m, 1H, H10), 2.18 (m, 1H, H7), 1.44 (m, 9H, H12, H11, H16), 1.30 (d, *J* = 9.1 Hz, 1H, H10'), 0.63 (s, 3H, H13). **^{13}C-NMR** ($CDCl_3$) δ = 165.7 (C, C4), 157.6 (C, C1), 146.2 (C, C5), 145.5 (C, C2), 133.4 (CH, C3), 122.5 (CH, C4), 61.6 (CH2, C15), 46.8 (CH, C9), 40.0 (CH, C7), 39.4 (C, C8), 36.7 (CH, C6), 31.5 (CH2, C10), 25.9 (CH3, C12), 21.3 (CH3, C13), 18.1 (CH3, C11), 14.4 (CH, C16)); $[\alpha]_D$ (*c* CH_2Cl_2); ESI-MS (*m/z*) X $[M+H]^+$

Me-pinene-ald (-)-24.

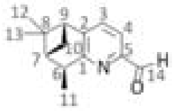

(-)-**29** (13.7 g, 52.8 mmol) was dissolved in 200 mL of anhydrous THF and the solution was cooled to -78 ºC. 63.4 mL of $LiAlH_4$ 1M in hexanes were added during a period of 20 min with a syringe pump. The resulting solution was stirred for 1 h at the same temperature. 27 mL of glacial acetic acid were added and the solution was left at room temperature. 400 mL of hexane were added and the solution was poured over 400 mL of water. The solution was neutralized with a saturated solution of sodium bicarbonate, extracted with hexane, washed with water and dried with magnesium sulfate. After collection and evaporation of the organic phases a mixture of aldehyde (-)-**24** and alcohol (-)-**31** was obtained. This mixture was purified by column chromatography on silica gel. Using dichloromethane as mobile phase 6.8 g of (-)-**24** were eluted. Increasing the polarity to pure acetone 3.5 g of (-)-**31** were obtained. Yield: 60 % (6.8 g; 31.6 mmol). **^{1}H-NMR** (400 MHz, $CDCl_3$) δ = 10.04 (s, 1H, H14), 7.68 (d, *J* = 7.5 Hz, 1H, H4), 7.34 (d, *J* = 7.5 Hz, 1H, H3), 3.27 (m, 1H, H6), 2.86 (t, *J* = 5.3 Hz, 1H, H9), 2.60 (m, 1H, H10), 2.20 (m, 1H, H7), 1.44 (m, 6H, H11, H12), 1.31 (d, 10.0 Hz, 1H, H10'), 0.64 (s, 3H, H13). **^{13}C-NMR** ($CDCl_3$) δ = 193.6 (COH, H14), 161.8 (C, C1), 150.8 (C, C2), 147.4 (C, C5), 133.3 (CH, C3), 119.5 (CH, C4), 47.6 (CH, C9), 46.5 (CH, C7), 41.4 (C, C8), 38.7 (CH, C6), 28.2 (CH2, C10), 26.2 (CH3, C12), 20.8 (CH3, C13), 18.1 (CH3, C11) ; $[\alpha]_D$ -19.4 (*c* 0.98 CH_2Cl_2); ESI-MS (*m/z*) 216.1 $[M+H]^+$, 238.1 $[M+Na]^+$

Me-pinene-OH (-)-31.

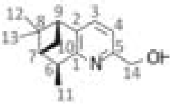

(-)-**24** (3 g, 13.9 mmol) was dissolved in 34 mL of dry methanol. 1 g (26.5 mmol) of sodium borhydrate was added slowly, the solution was left at room temperature and the stirring was continued for 4 h. After evaporation of the solvent 34 mL of dichloromethane and 26 mL of water were added. The product was extracted with dichloromethane, washed with water and dried with magnesium sulfate. After evaporation 2.8 g of pure (-)-**31** as a yellow solid were obtained. Yield: 92 % (2.8 g, 12.9 mmol). **^{1}H-NMR** (400 MHz, $CDCl_3$) δ = 7.17 (d, *J* = 7.5 Hz, 1H, H3), 6.87 (d, *J* = 7.5 Hz, 1H, H4), 4.70 (b s, 2H, H14), 4.00 (b s, 1H, OH), 3.17 (m, 1H, H6), 2.75 (t, *J* = 5.4 Hz, 1H, H9), 2.55 (m, 1H, H10), 2.15 (m, 1H, H7), 1.43 (s, 3H, H12), 1.38 (d, *J* = 7.2 Hz, 3H, H11), 1.30 (d, *J* = 9.8 Hz, 1H, H10'), 0.63 (s, 3H, H13). **^{13}C-NMR** ($CDCl_3$) δ = 159.6 (C, C1), 155.3 (C, C2), 140.4 (C, C5), 133.4 (CH,C3), 117.0 (CH, C4), 63.8 (CH2, C14), 46.9 (CH, C9), 46.8 (CH, C7), 41.3 (C, C8), 38.6 (CH, C6), 28.7 (CH2, C10), 26.3 (CH3, C12), 20.8 (CH3, C13), 18.1 (CH3, C11) ; $[\alpha]_D$ -22.9 (*c* 1.2 CH_2Cl_2); ESI-MS (*m/z*) 218.1 $[M+H]^+$, 240.1 $[M+Na]^+$

Me-pinene-Cl (-)-32.

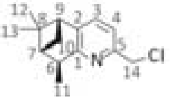

(-)-**31** (5.15 g, 23.7 mmol) was dissolved in 55 mL of dry dichloromethane. A solution of 5 mL (71 mmol) of SOCl$_2$ in 44 mL of dry dichloromethane was added dropwise. The solution was kept stirring overnight. The solvent was carefully evaporated. Dichloromethane and 666 mL of an aqueous solution of sodium hydroxide 0.4 M were added. The product was extracted with dichloromethane, washed with water and dried with magnesium sulfate. After evaporation Me-pinene-Cl (-)-**32** was obtained as a yellow oil. Yield: 88 % (4.9 g, 21 mmol). **^{1}H-NMR** (400 MHz, CDCl$_3$) δ = 7.23 (d, *J* = 7.5 Hz, 1H, H3), 7.16 (d, *J* = 7.4 Hz, 1H, H4), 4.68 (s, 2H, H14), 3.20 (m, 1H, H6), 3.78 (t, *J* = 5.7 Hz, 1H, H9), 2.57 (m, 1H, H10), 2.17 (m, 1H, H7), 1.44 (s, 3H, H12), 1.40 (d, *J* = 7.1 Hz, 3H, H11), 1.32 (d, *J* = 9.7 Hz, 1H, H10'), 0.65 (s, 3H, H13). **^{13}C-NMR** (CDCl$_3$) δ = 160.4 (C, C1), 153.1 (C, C2), 141.6 (C, C5), 134.1 (CH, C3), 119.9 (CH, C4), 47.0 (CH, C9), 46.7 (CH, C7), 46.6 (CH2, C14), 41.3 (C, C8), 38.5 (CH, C6), 28.5 (CH2, C10), 26.2 (CH3, C12), 20.8 (CH3, C13), 18.3 (CH3, C11) ; $[\alpha]_D$ -16.4 (*c* 1.3 CH$_2$Cl$_2$); ESI-MS (*m/z*) 236.1 [M+H]$^+$

Me-pinbpea ((-)-L3).

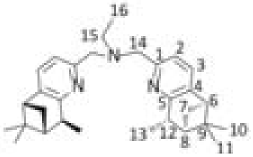

(-)-**32** (2.29 mg, 9.7 mmol) was dissolved in 10 mL of a mixture acetonitrile/water 1:1 and 172 μl (4.8 mmol) of ethylamine 70 % (aq.) were added. The solution was heated to 60 ºC for 5 min. 850 μl (10.7 mmol) of an aqueous solution of NaOH 10 M were added slowly. The solution was heated at 60 ºC for 1 h. The product was extracted with chloroform and dried with magnesium sulfate. The crude was purified by column chromatography of neutral alumina. Using a mixture dichloromethane/acetone 9:1 Me-pinbpea was eluted. Yield: 54 % (1.17 g, 2.6 mmol). **^{1}H-NMR** (400 MHz, CDCl$_3$) δ = 7.23 (d, *J* = 7.7 Hz, 2H, H2), 7.12 (d, *J* = 7.7 Hz, 2H, H3), 3.80 (s, 4H, H14), 3.15 (m, 2H, H12), 2.70 (t, *J* = 5.6 Hz, 2H, H6), 2.65 (q, *J* = 7.1 Hz, 2H, H15), 2.51 (m, 2H, H7), 2.12 (m, 2H, H8), 1.39 (s, 6H, H10), 1.35 (d, *J* = 7.1 Hz, 6H, H13), 1.28 (d, *J* = 9.6 Hz, 2H, H7'), 1.11 (t, *J* = 7.1 Hz, 3H, H16), 0.61 (s, 6H, H11). **^{13}C-NMR** (400 MHz, CDCl$_3$, 25 ºC) δ = 159.8 (C, C5), 157.1 (C, C1), 139.4 (C, C4), 133.1 (CH, C3), 119.3 (CH, C2), 59.9 (CH2, C14), 48.2 (CH2, C15), 47.0 (2CH, C6, C8), 41.3 (C, C9), 38.7 (CH, C12), 28.7 (CH2, C7), 26.3 (CH3, C10), 20.9 (CH3, C11), 18.5 (CH3, C13), 12.3 (CH3, C16); $[\alpha]_D$ -18.2 (*c* 1.4 CH_2Cl_2); **ESI$^+$ HRMS**: $[M+H]^+$ (*m/z*), Calc. for C30H43N2: 444.3373; Found: 444.3398.

trans-*fac*-[Ru((-)-L3)(bpy)Cl]Cl (C3a) and down-*mer*-[Ru((-)-L3)(bpy)Cl]Cl (C3c).

To a solution of 53 mg (0.134 mmol) of $[Ru(bpy)(MeOH)Cl_3]$ and 28 μl (0.20 mmol) of triethylamine in 20 mL of dry ethanol, 56 mg (0.134 mmol) of (-)-L3 were added. The mixture was heated to reflux during 24 h. To the resulting red solution 50 mL of dry diethyl ether were added. The red solution was filtrated and separated from a green solid. The solution was evaporated and the obtained solid was purified by column chromatography of alumina. Starting with dichloromethane the polarity of the mobile phase was increased with methanol. With a relation of 100:2 DCM/MeOH a red band was eluted. The first fractions of this band, which had a darker color and contained a mixture of **C3a** and **C3c** (11 mg), were separated. The next fractions contained pure **C3a** (37 mg; yield 36 %). **C3c** was isolated by purification of the mixture of **C3a** and **C3c** with an alumina semipreparative TLC using DCM/MeOH (100:2) as mobile phase, obtaining 5 mg of pure **C3c** (yield 5%).

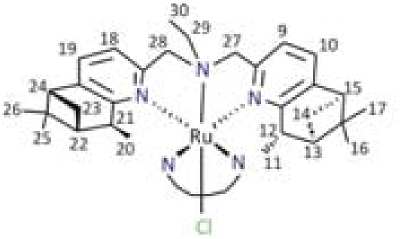

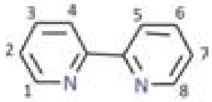

C3a: **^{1}H NMR** (500 MHz, CD_2Cl_2) δ 8.28 (d, *J* = 8.0 Hz, 1H, H4), 8.25 (d, *J* = 7.8 Hz, 1H, H5), 7.98 (d, *J* = 5.5 Hz, 1H, H1), 7.87 (t, *J* = 7.3 Hz, 1H, H3), 7.80 (t, *J* = 7.3 Hz, 1H, H6), 7.50-7.40 (4H, H9, H10, H18, H19), 7.30 (t, *J* = 6.4 Hz, 1H, H2), 7.18 (t, *J* = 6.2 Hz, 1H, H7), 6.68 (d, *J* = 5.2 Hz, 1H, H8), 5.34 (H21), 4.59 (d, *J* = 15.6 Hz, 1H, 28a), 4.26 (2H, H27a, H12), 4.14 (d, *J* = 15.7 Hz, 1H, H27b), 3.78 (d, *J* = 15.7 Hz, 1H, H28b), 2.95 (dt, *J* = 10.3, 5.4 Hz, 2H, H15, H24), 2.67 – 2.58 (m, 1H, 29a), 2.58 – 2.51 (m, 1H, H14a), 2.48 (dd, *J* = 13.7, 7.0 Hz, 1H, H29b), 2.23-2.15 (m, 4H, H13, H22, H14b, H23b), 1.76 – 1.68 (m, 3H, H30), 1.47 (s, 3H, H26), 1.44 (s, 3H, H16), 1.37 – 1.26 (m, 6H, H11, H20), 0.87 (s, 3H, H25), 0.59 (s, 3H, H16). **CV**: 0.83 V vs. SSCE, ΔE = 130 mV. **ESI$^+$ HRMS**: [M-2Cl]$^{2+}$ (*m/z*; *z* = 2), Calc. for C40H49N5Ru: 347.6532 found: 347.6518.

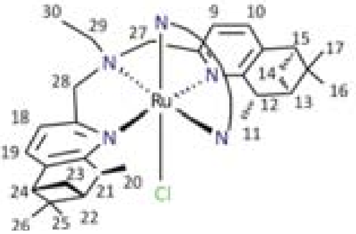

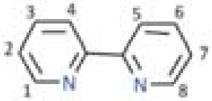

C3c: ^{1}H NMR (500 MHz, CD$_2$Cl$_2$) δ 10.63 (d, *J* = 5.0 Hz, 1H, H1), 8.65 (d, *J* = 7.9 Hz, 1H, H4), 8.61 (d, *J* = 6.9 Hz, 1H, H5), 8.50 (d, *J* = 5.7 Hz, 1H, H8), 8.02 – 7.95 (m, 1H, H3), 7.80 (dd, *J* = 11.3, 4.3 Hz, 1H, H6), 7.51 (ddd, *J* = 7.4, 6.0, 1.4 Hz, 1H, H2), 7.38 – 7.32 (m, 1H, H7), 7.08 – 6.87 (m, 4H, H9 H10, H18, H19), 6.31 (d, *J* = 16.6 Hz, 1H, H28a), 5.63 (d, *J* = 13.3 Hz, 1H, H27a), 4.60 (d, *J* = 16.7 Hz, 1H, H28b), 4.52 (d, *J* = 13.4 Hz, 1H, H27b), 3.89 (dq, *J* = 13.3, 6.6 Hz, 1H, H29a), 3.24 (dq, *J* = 14.5, 7.3 Hz, 1H, H29b), 2.53 (dd, *J* = 6.4, 5.5 Hz, 1H, H15), 2.49 (dd, *J* = 6.4, 5.5 Hz 1H, H24), 1.24 (m, 1H, H21), 1.15 – 1.05 (m, 3H, H30), 0.75 (d, *J* = 6.9 Hz, 3H, H20), 0.65 – 0.58 (m, 1H, H12), -0.17 (d, *J* = 7.0 Hz, 3H, H11).

Catalytic epoxidation.

To a solution of 2.5 μmol of Ru catalyst in 0.4 mL of *tert*-amylalcohol in a glass tube, 33 μl (250 μmol) of cis-β-methylstyrene, 20 μl of dodecane, 165 mg (500 μmol) of iodobenzene diacetate and 0.6 mL more of *tert*-amylalcohol were added. Aliquot for analysis of t_0 was taken and 9 μl (500 μmol) of H_2O were added. Aliquots taken for the analysis by GC-FID and/or GC-MS were filtered through celite and diethyl ether was added in order to elute the organic compounds.

Acknowledgements:
DFT calculations were performed by Dr. Albert Poater, “Ramón y Cajal” researcher of “Institut Català de Recerca de l’Aigua (ICRA).

6.3. References.

(1) Yoon, T. P.; Jacobsen, E. N. *Science* **2003**, *299*, 1691-1693.

(2) Pfaltz, A.; Drury, W. J., III *Proc. Natl. Acad. Sci. U. S. A.* **2004**, *101*, 5723-5726.

(3) Ohta, T.; Takaya, H.; Noyori, R. *Inorg. Chem.* **1988**, *27*, 566-9.

(4) McManus, H. A.; Guiry, P. J. *Chem. Rev. (Washington, DC, U. S.)* **2004**, *104*, 4151-4202.

(5) Johnson, J. S.; Evans, D. A. *Acc. Chem. Res.* **2000**, *33*, 325-335.

(6) Ghosh, A. K.; Mathivanan, P.; Cappiello, J. *Tetrahedron: Asymmetry* **1998**, *9*, 1-45.

(7) Chelucci, G.; Thummel, R. P. *Chem. Rev. (Washington, DC, U. S.)* **2002**, *102*, 3129-3170.

(8) Hayoz, P.; Von, Z. A. *Tetrahedron Lett.* **1992**, *33*, 5165-8.

(9) Hayoz, P.; Von, Z. A.; Stoeckli-Evans, H. *J. Am. Chem. Soc.* **1993**, *115*, 5111-14.

(10) Malkov, A. V.; Pernazza, D.; Bell, M.; Bella, M.; Massa, A.; Teply, F.; Meghani, P.; Kocovsky, P. *J. Org. Chem.* **2003**, *68*, 4727-4742.

(11) Malkov, A. V.; Baxendale, I. R.; Bella, M.; Langer, V.; Fawcett, J.; Russell, D. R.; Mansfield, D. J.; Valko, M.; Kocovsky, P. *Organometallics* **2001**, *20*, 673-690.

(12) Loetscher, D.; Rupprecht, S.; Collomb, P.; Belser, P.; Viebrock, H.; von, Z. A.; Burger, P. *Inorg. Chem.* **2001**, *40*, 5675-5681.

(13) Langlotz, B. K.; Wadepohl, H.; Gade, L. H. *Angew. Chem., Int. Ed.* **2008**, *47*, 4670-4674.

(14) Chelucci, G.; Pinna, G. A.; Saba, A.; Valenti, R. *Tetrahedron: Asymmetry* **2000**, *11*, 4027-4036.

(15) Majetich, G. *J. Nat. Prod.* **1995**, *58*, 1795.

(16) Wipf, P. *Angew. Chem., Int. Ed.* **1999**, *38*, 2453-2454.

(17) Kwong, H. L.; Lee, W. S. *Tetrahedron: Asymmetry* **2000**, *11*, 2299-2308.

(18) Tse, M. K.; Klawonn, M.; Bhor, S.; Doebler, C.; Anilkumar, G.; Hugl, H.; Maegerlein, W.; Beller, M. *Org. Lett.* **2005**, *7*, 987-990.

(19) Sala, X.; RodrIguez, A. M.; RodrÃ-guez, M.; Romero, I.; Parella, T.; von Zelewsky, A.; Llobet, A.; Benet-Buchholz, J. *The Journal of Organic Chemistry* **2006**, *71*, 9283-9290.

(20) Rich, J.; Rodriguez, M.; Romero, I.; Vaquer, L.; Sala, X.; Llobet, A.; Corbella, M.; Collomb, M.-N.; Fontrodona, X. *Dalton Trans.* **2009**, 8117-8126.

(21) Gomez, L.; Garcia-Bosch, I.; Company, A.; Sala, X.; Fontrodona, X.; Ribas, X.; Costas, M. *Dalton Trans.* **2007**, 5539-5545.

(22) Ojima, I.; Editor *Catalytic Asymmetric Synthesis, Third Edition*; John Wiley & Sons, Inc., 2010.

(23) Knowles, W. S. *Angew. Chem., Int. Ed.* **2002**, *41*, 1998-2007.

(24) Noyori, R. *Angew. Chem., Int. Ed.* **2002**, *41*, 2008-2022.

(25) Sharpless, K. B. *Angew. Chem., Int. Ed.* **2002**, *41*, 2024-2032.

(26) Matsumoto, K.; Sawada, Y.; Katsuki, T. *Pure Appl. Chem.* **2008**, *80*, 1071-1077.

(27) Katsuki, T. *Kagaku to Kyoiku* **2001**, *49*, 643-646.

(28) Sharpless, K. B. *CHEMTECH* **1985**, *15*, 692-700.

(29) Knight, J. G. *Adv. Synth. Catal.* **2001**, *343*, 141.

(30) Katsuki, T. *Adv. Synth. Catal.* **2002**, *344*, 131-147.

(31) Borner, A. *Angew. Chem., Int. Ed.* **2000**, *39*, 4385-4386.

(32) Murahashi, S.-I.; Editor *Ruthenium in Organic Synthesis*; Wiely-VCH Verlag GmbH & Co. KGaA, 2004.

(33) Zhang, R.; Yu, W.-Y.; Lai, T.-S.; Che, C.-M. *Chem. Commun. (Cambridge)* **1999**, 409-410.

(34) Fierman, M.; Nelson, A.; Khan, S. I.; Barfield, M.; O'Leary, D. J. *Org. Lett.* **2000**, *2*, 2077-2080.

(35) Lai, T.-S.; Zhang, R.; Cheung, K.-K.; Che, C.-M.; Kwong, H.-L. *Chem. Commun. (Cambridge)* **1998**, 1583-1584.

(36) End, N.; Pfaltz, A. *Chem. Commun. (Cambridge)* **1998**, 589-590.

(37) End, N.; Macko, L.; Zehnder, M.; Pfaltz, A. *Chem.--Eur. J.* **1998**, *4*, 818-824.

(38) Kureshy, R. I.; Khan, N. H.; Abdi, S. H. R. *J. Mol. Catal. A: Chem.* **1995**, *96*, 117-22.

(39) Nakata, K.; Takeda, T.; Mihara, J.; Hamada, T.; Irie, R.; Katsuki, T. *Chem.--Eur. J.* **2001**, *7*, 3776-3782.

(40) Pezet, F.; Ait-Haddou, H.; Daran, J.-C.; Sasaki, I.; Balavoine, G. G. A. *Chem. Commun. (Cambridge, U. K.)* **2002**, 510-511.

(41) Nishiyama, H.; Shimada, T.; Itoh, H.; Sugiyama, H.; Motoyama, Y. *Chem. Commun. (Cambridge)* **1997**, 1863-1864.

(42) Fung, W.-H.; Yu, W.-Y.; Che, C.-M. *J. Org. Chem.* **1998**, *63*, 7715-7726.

(43) Tse, M. K.; Bhor, S.; Klawonn, M.; Anilkumar, G.; Jiao, H.; Spannenberg, A.; Doebler, C.; Maegerlein, W.; Hugl, H.; Beller, M. *Chem.--Eur. J.* **2006**, *12*, 1875-1888.

(44) Tse, M. K.; Bhor, S.; Klawonn, M.; Anilkumar, G.; Jiao, H.; Doebler, C.; Spannenberg, A.; Maegerlein, W.; Hugl, H.; Beller, M. *Chem.--Eur. J.* **2006**, *12*, 1855-1874.

(45) Bhor, S.; Tse, M. K.; Klawonn, M.; Doebler, C.; Maegerlein, W.; Beller, M. *Adv. Synth. Catal.* **2004**, *346*, 263-267.

(46) Mola, J.; Rodriguez, M.; Romero, I.; Llobet, A.; Parella, T.; Poater, A.; Duran, M.; Sola, M.; Benet-Buchholz, J. *Inorg. Chem.* **2006**, *45*, 10520-10529.

(47) Rodriguez, M.; Romero, I.; Llobet, A.; Deronzier, A.; Biner, M.; Parella, T.; Stoeckli-Evans, H. *Inorg. Chem.* **2001**, *40*, 4150-4156.

(48) Romero, I.; Rodriguez, M.; Llobet, A.; Collomb-Dunand-Sauthier, M.-N.; Deronzier, A.; Parella, T.; Stoeckli-Evans, H. *Dalton* **2000**, 1689-1694.

(49) Serrano, I.; Rodriguez, M.; Romero, I.; Llobet, A.; Parella, T.; Campelo, J. M.; Luna, D.; Marinas, J. M.; Benet-Buchholz, J. *Inorg. Chem.* **2006**, *45*, 2644-2651.

(50) Sala, X.; Poater, A.; Zelewsky, A. v.; Parella, T.; Fontrodona, X.; Romero, I.; Sola, M.; RodrIguez, M.; Llobet, A. *Inorganic Chemistry* **2008**, *47*, 8016-8024.

(51) Muerner, H.; von, Z. A.; Stoeckli-Evans, H. *Inorg. Chem.* **1996**, *35*, 3931-3935.

(52) Yang, L.; Von, Z. A.; Stoeckli-Evans, H. *Chem. Commun. (Cambridge, U. K.)* **2005**, 4155-4157.

(53) Sauers, A. L.; Ho, D. M.; Bernhard, S. *The Journal of Organic Chemistry* **2004**, *69*, 8910-8915.

(54) Loetscher, D.; Rupprecht, S.; Collomb, P.; Belser, P.; Viebrock, H.; von Zelewsky, A.; Burger, P. *Inorganic Chemistry* **2001**, *40*, 5675-5681.

(55) Malkov, A. V.; Bell, M.; Castelluzzo, F.; Kocovski, P. *Organic Letters* **2005**, *7*, 3219-3222.

(56) Kröhnke, F. *Synthesis* **1976**, 1-24.

(57) Eskelinen, E.; Da Costa, P.; Haukka, M. *Journal of Electroanalytical Chemistry* **2005**, *579*, 257-265.

(58) Mola, J.; Rodriguez, M.; Romero, I.; Llobet, A.; Parella, T.; Poater, A.; Duran, M.; Sola , M.; Benet-Buchholz, J. *Inorganic Chemistry* **2006**, *45*, 10520-10529.

(59) Mola, J.; Romero, I.; Rodriguez, M.; Bozoglian, F.; Poater, A.; Sola , M.; Parella, T.; Benet-Buchholz, J.; Fontrodona, X.; Llobet, A. *Inorganic Chemistry* **2007**, *46*, 10707-10716.

(60) Becke, A. D. *Chem. Phys.* **1993**, *98*, 5648-5652.

(61) Perdew, J. P. W., Y. *Phys. Rev. B* **1992**, *45*, 13244-13249.

(62) F., M. J.; Trucks, G. W.; Schlegel, H. B.; Scuseria, G. E.; Robb, M. A.; Cheeseman, J. R.; Montgomery, J. A., Jr.; Vreven, T.; Kudin, K. N.; Burant. J. C.; Millam, J. M.; Iyengar, S. S.; Tomasi, J.; Barone, V.; Mennucci, B.; Cossi, M.; Scalmani, G.; Rega, N.; Petersson, G. A.;

Nakatsuji, H.; Hada, M.; Ehara, M.; Toyota, K.; Fukuda, R.; Hasegawa, J.; Ishida, M.; Nakajima, T.; Honda, Y.; Kitao, O.; Nakai, H.; Klene, M.; Li, X.; Knox, J. E.; Hratchian, H. P.; Cross, J. B.; Bakken, V.; Adamo, C.; Jaramillo, J.; Gomperts, R.; Stratmann, R. E.; Yazyev, O.; Austin, A. J.; Cammi, R.; Pomelli, C.; Ochterski, J. W.; Ayala, P. Y.; Morokuma, K.; Voth, G. A.; Salvador, P.; Dannenberg, J. J.; Zakrzewski, V. G.; Dapprich, S.; Daniels, A. D.; Strain, M. C.; Farkas, Ö.; Malick, D. K.; Rabuck, A. D.; Raghavachari, K.; Foresman, J. B.; Ortiz, J. V.; Cui, Q.; Baboul, A. G.; Clifford, S.; Cioslowski, J.; Stefanov, B. B.; Liu, G.; Liashenko, A.; Piskorz, P.; Komaromi, I.; Martin, R. L.; Fox, D. J.; Keith, T.; Al-Laham, M. A.; Peng, C. Y.; Nanayakkara, A.; Challacombe, M.; Gill, P. M. W.; Johnson, B.; Chen, W.; Wong, M. W.; Gonzalez, C.; Pople, J. A.; Gaussian, I., Ed.; Wallingford CT: 2004.

(63) Andrae, D. H., U.; Dolg, M.; Stoll, H.; Preuss, H. *Theor. Chim. Acta* **1990**, *77*, 123-141.

(64) Bergner, A. D., M.; Kuchle, W.; Stoll, H.; Preuss, H. *Mol. Phys.* **1993**, *80*, 1431-1444.

(65) Hariharan, P. C. P., J. A. *Theor. Chim. Acta* **1973**, *28*, 213-222.

(66) Hehre, W. J. D., R.; Pople, J. A. *J. Chem. Phys.* **1972**, *56*, 2257-2261.

(67) Barone, V. C., M. *J. Phys. Chem. A* **1998**, *102*, 1995-2001.

(68) Tomasi, J. P., M. *Chem. Rev.* **1994**, *94*, 2027-2094.

6.4. Supporting Information

- **(-)-30**

NMR: Figure S 1 - Figure S 2

- **(-)-29**

NMR: Figure S 3 **-** Figure S 4

- **(-)-24**

NMR: Figure S 5 **-** Figure S 10

- **(-)-31**

NMR: Figure S 11 **-** Figure S 12

- **(-)-32**

NMR: Figure S 13 - Figure S 14

- **(-)-L3**

NMR: Figure S 15 - Figure S 20

- *trans-fac*-**[Ru(L3)(bpy)Cl]Cl (C3a)**

NMR: Figure S 21 - Figure S 25

Mass spectrometry: Figure S 31

Cyclic Voltammetry: Figure S 32

- *down*-mer**-[Ru(L3)(bpy)Cl]Cl (C3c)**

NMR: Figure S 26 - Figure S 30

NMR characterization

- **(-)-30**

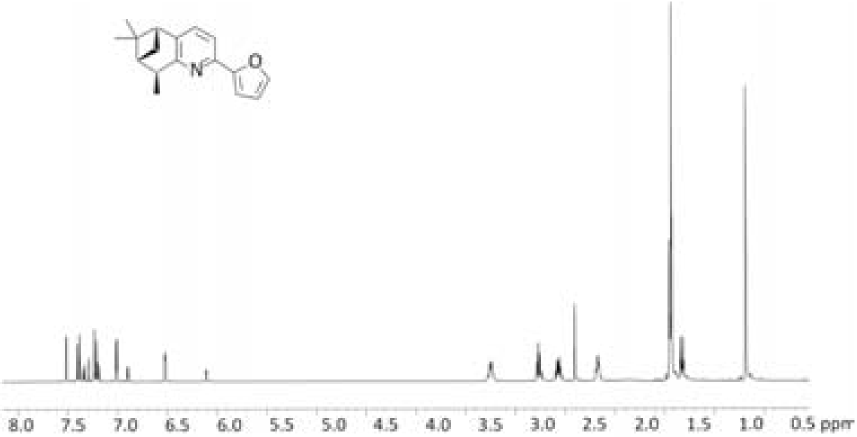

Figure S 1. ^{1}H-NMR of (-)-**30**

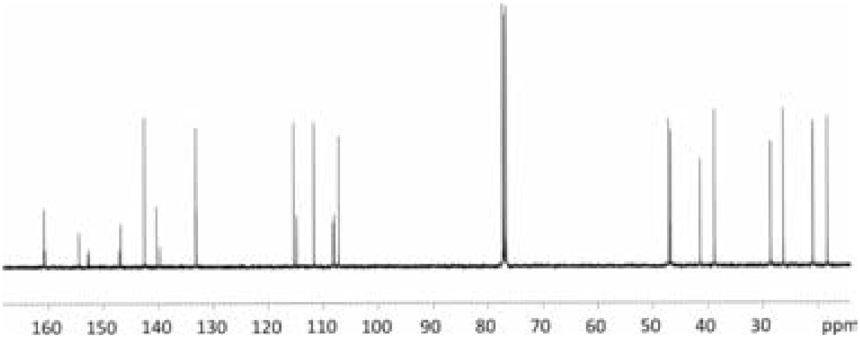

Figure S 2. ^{13}C-NMR of (-)-**30**

- **(-)-29**

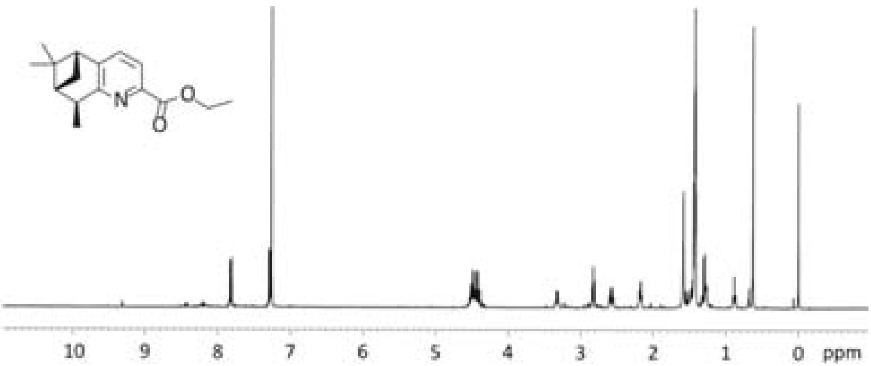

Figure S 3. ^{1}H-NMR of (-)-**29**

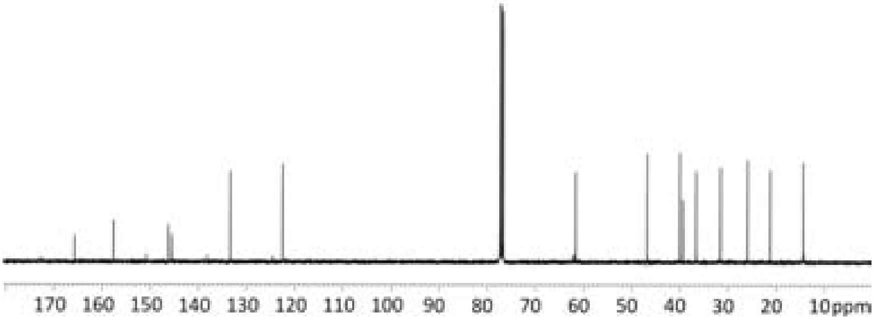

Figure S 4. ^{13}C-NMR of (-)-**29**

- **(-)-24**

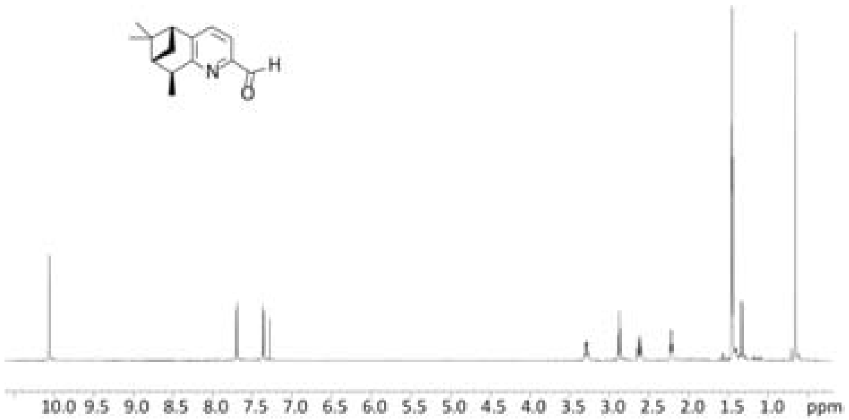

Figure S 5. ^{1}H-NMR of (-)-**24**

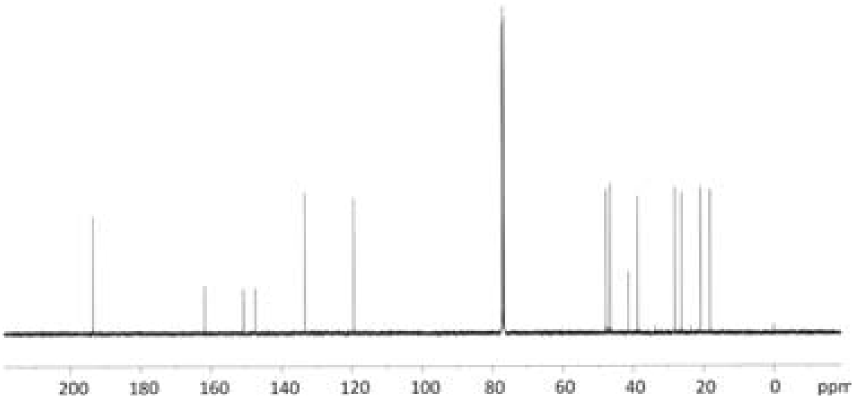

Figure S 6. ^{13}C-NMR of (-)-**24**

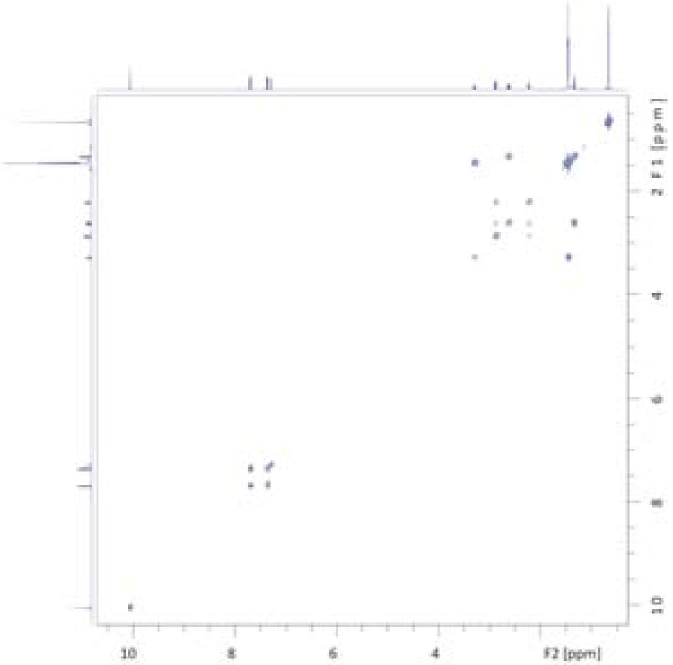

Figure S 7. COSY of (-)-**24**

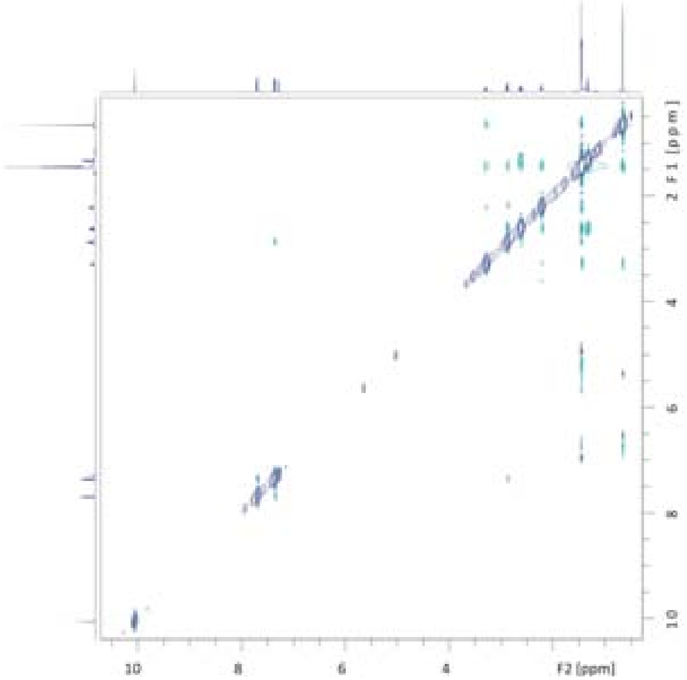

Figure S 8. NOESY of (-)-**24**

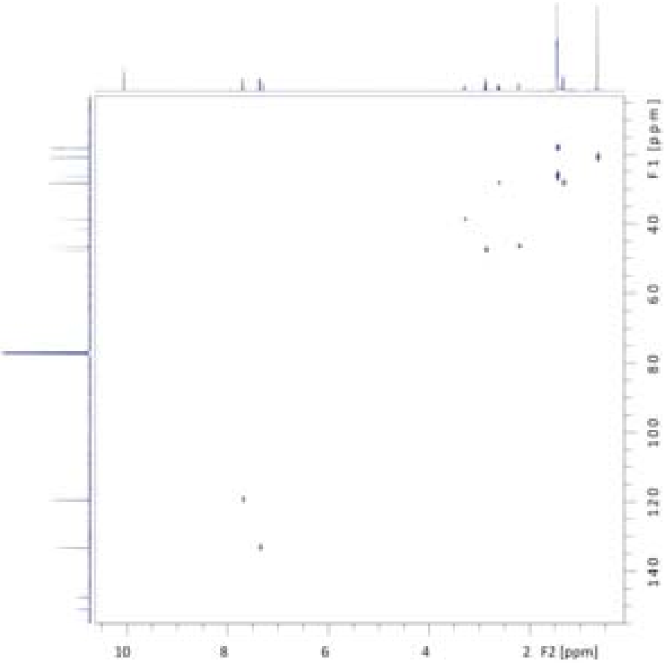

Figure S 9. HMQC of (-)-24

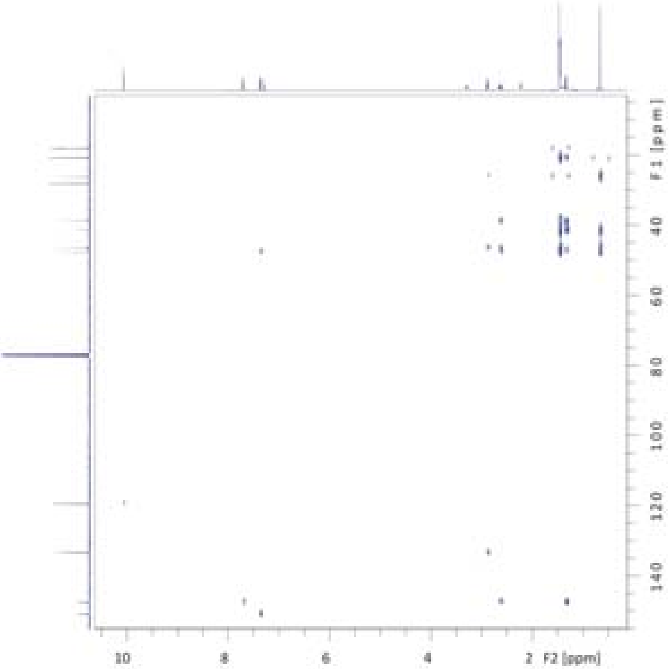

Figure S 10. HMBC of (-)-24

- **(-)-31**

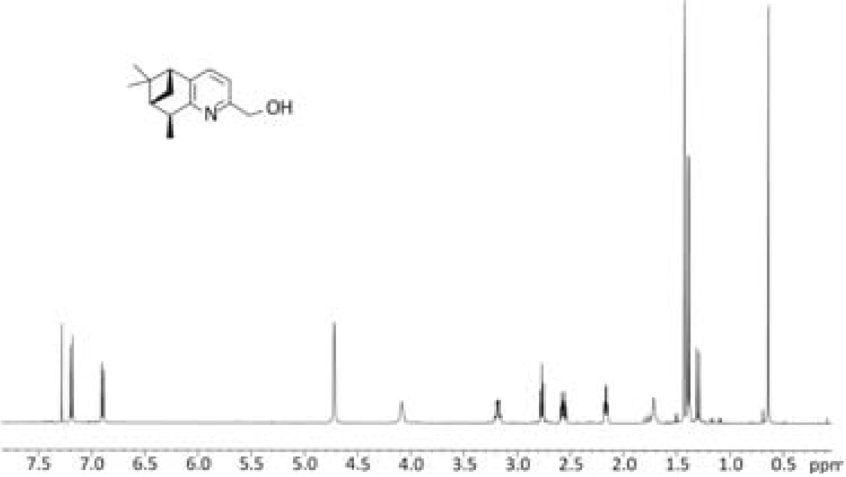

Figure S 11. ^{1}H-NMR of (-)-**31**

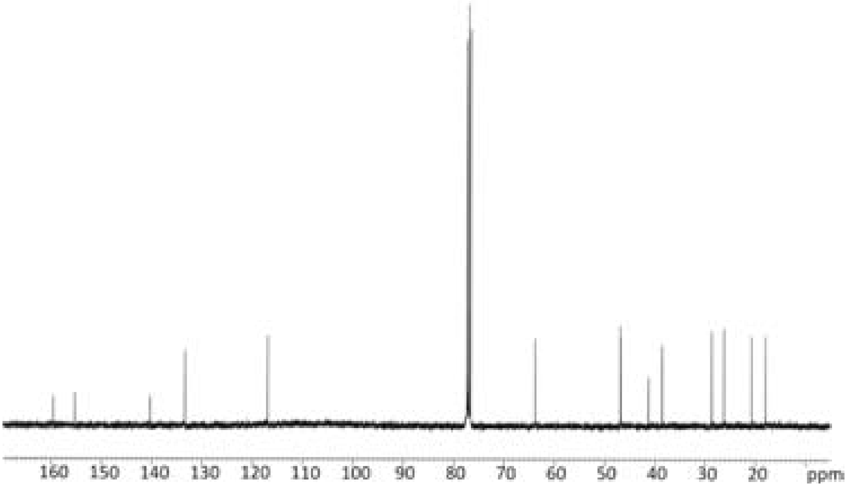

Figure S 12. ^{13}C-NMR of (-)-**31**

- **(-)-32**

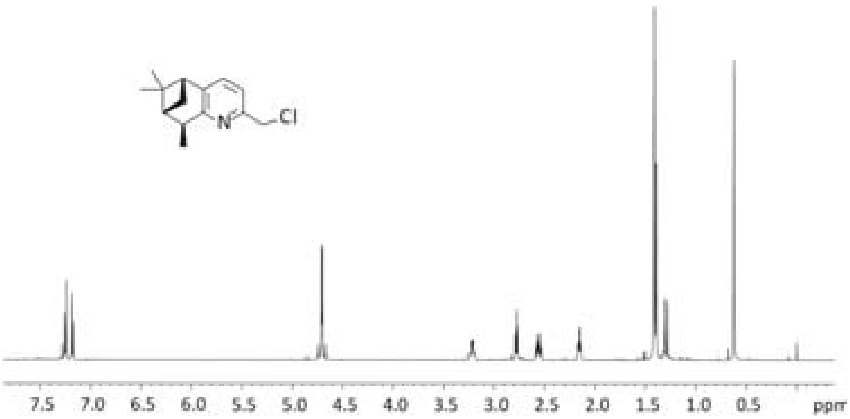

Figure S 13. ^{1}H-NMR of (-)-**32**

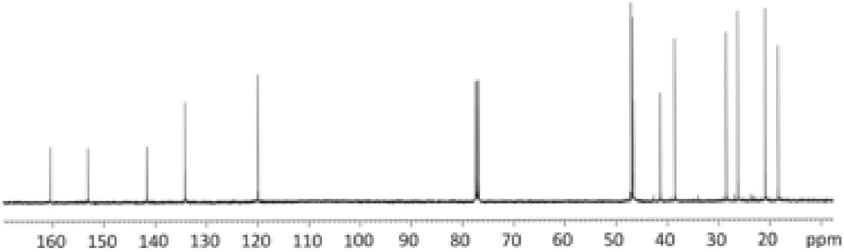

Figure S 14. ^{13}C-NMR of (-)-**32**

- **(-)-L3**

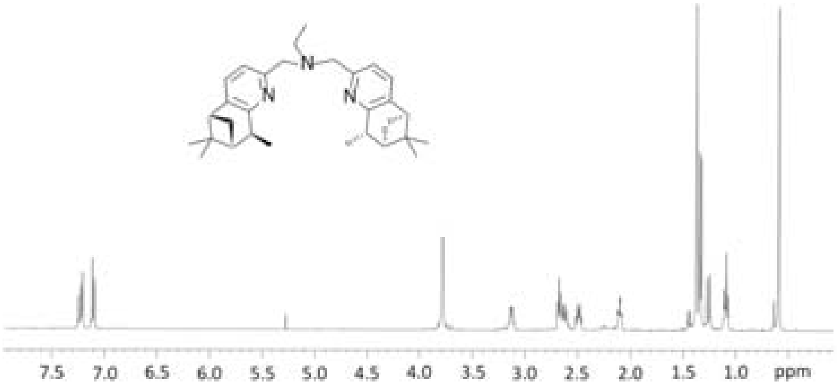

Figure S 15. ^{1}H-NMR of (-)-**L3**

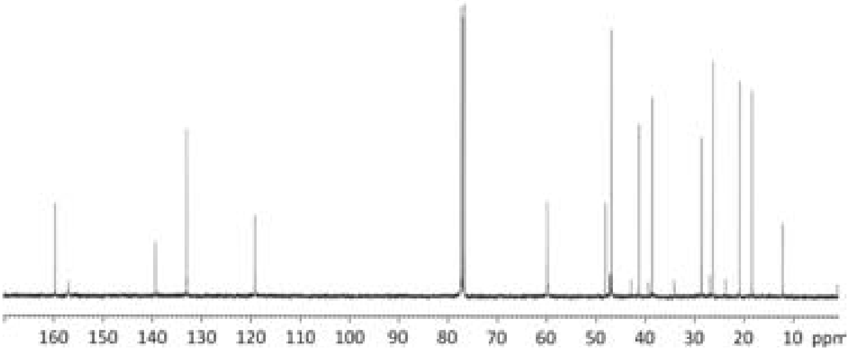

Figure S 16. ^{13}C-NMR of (-)-**L3**

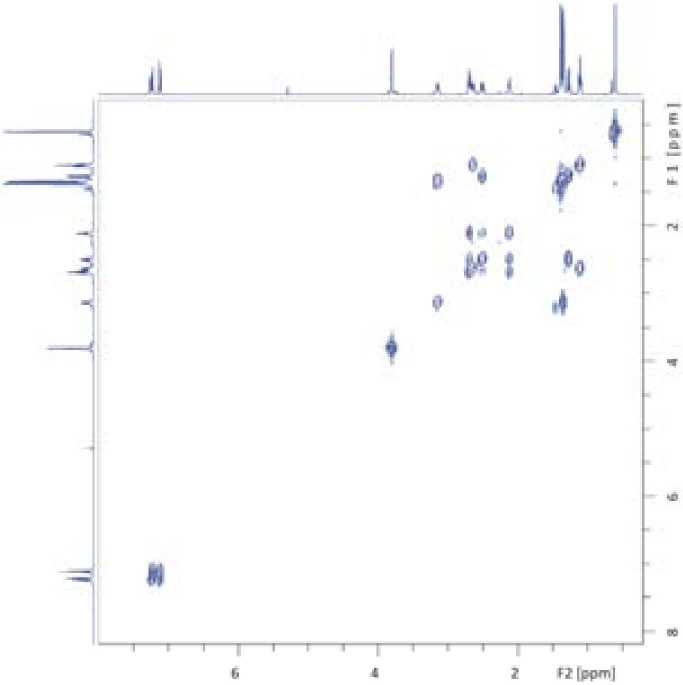

Figure S 17. COSY of (-)-**L3**

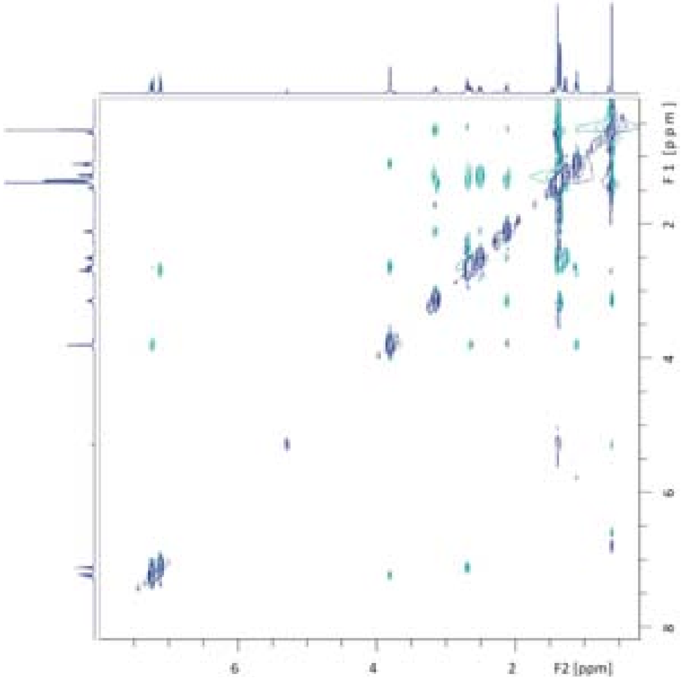

Figure S 18. NOESY of (-)-**L3**

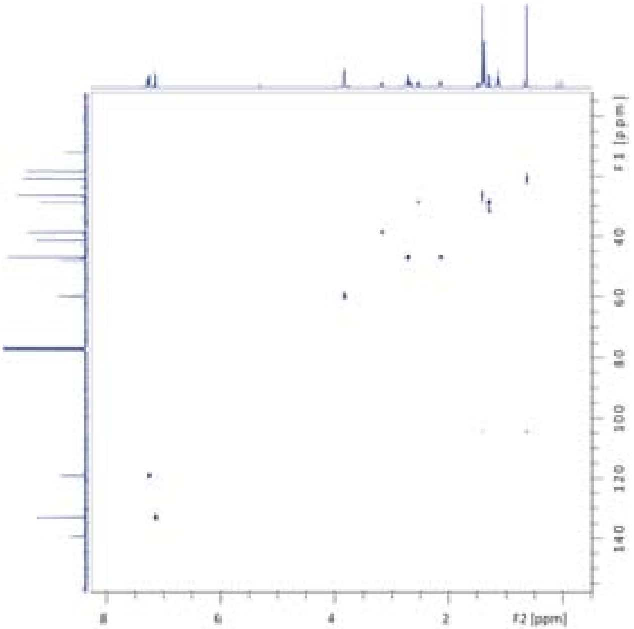

Figure S 19. HMQC of (-)-**L3**

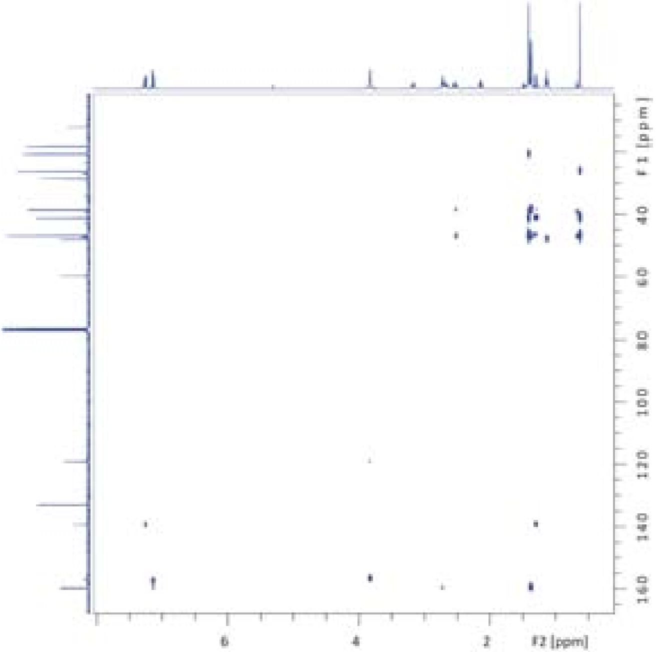

Figure S 20. HMBC of (-)-**L3**

- *trans*-*fac*-**[Ru(L3)(bpy)Cl]Cl (C3a)**

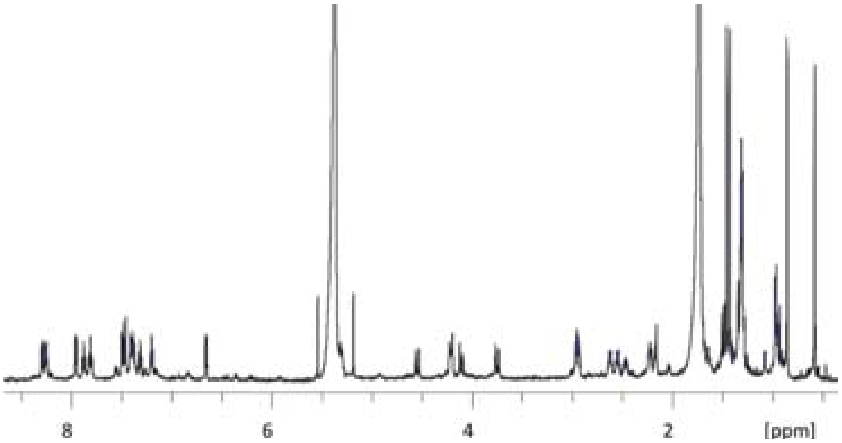

Figure S 21. ^{1}H-NMR of **C3a**

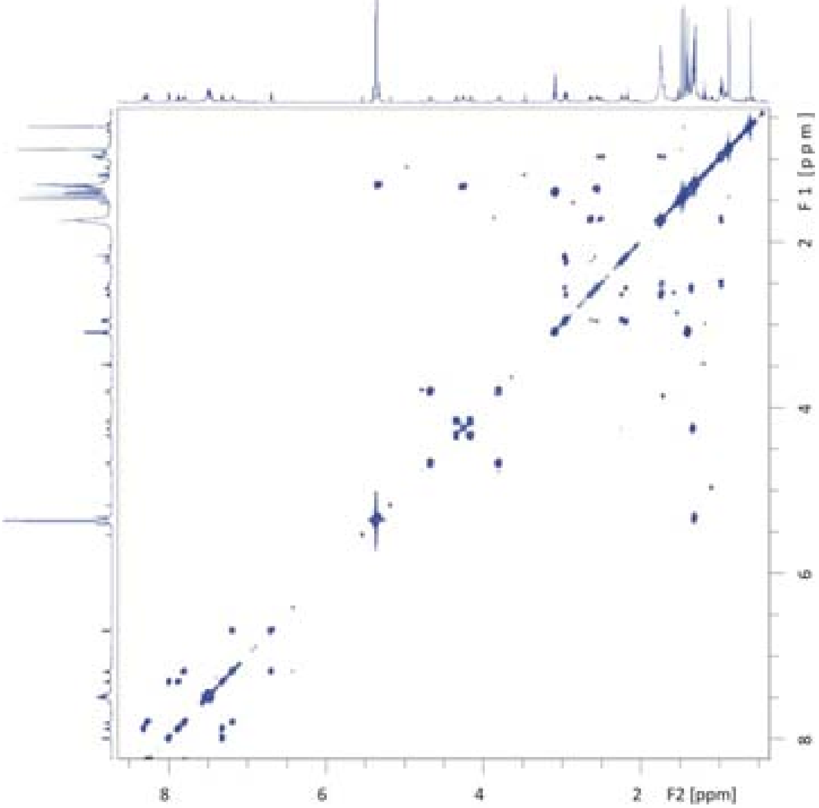

Figure S 22. COSY of **C3a**

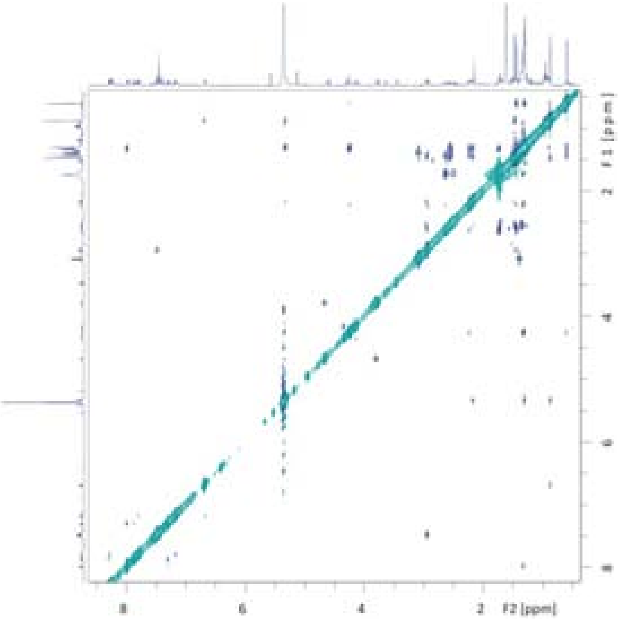

Figure S 23. NOESY of **C3a**

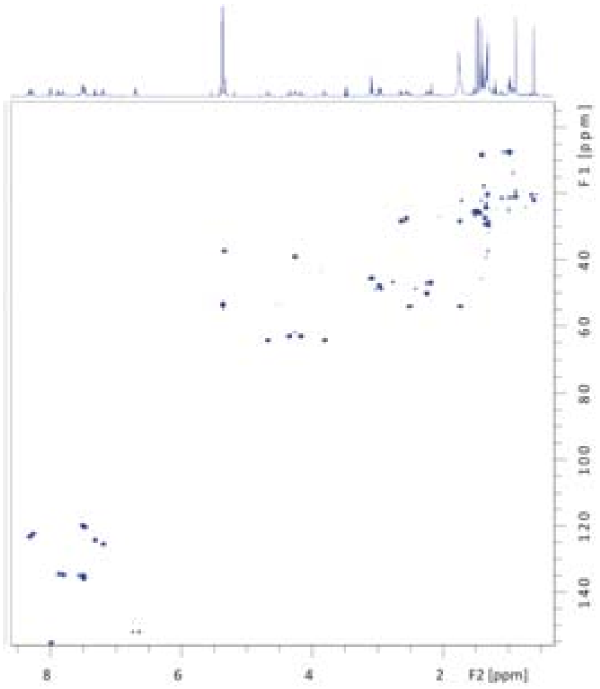

Figure S 24. HMQC of **C3a**

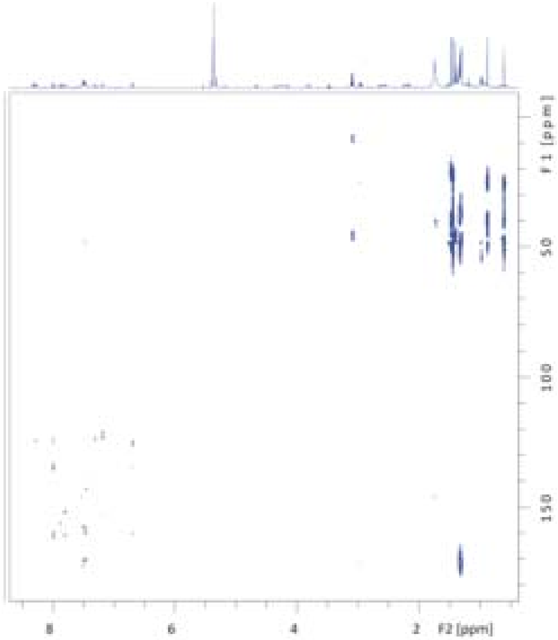

Figure S 25. HMBC of **C3a**

- *down*-mer-**[Ru(L3)(bpy)Cl]Cl (C3c)**

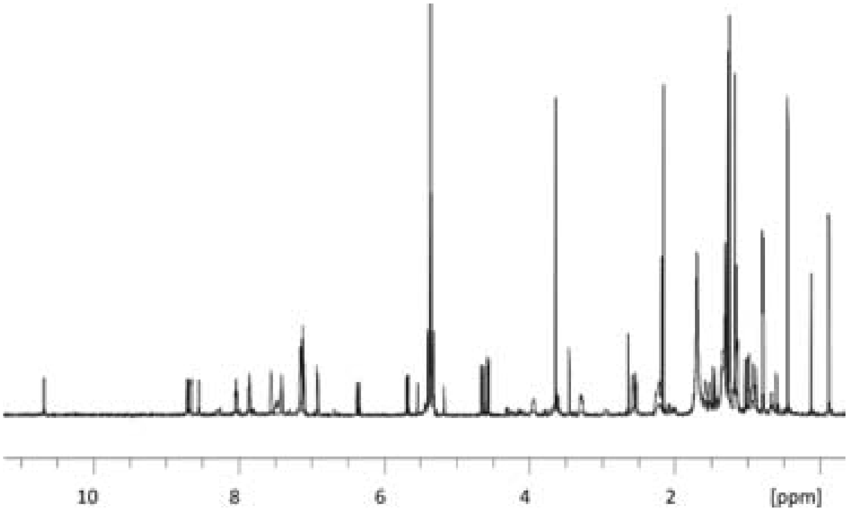

Figure S 26. ^{1}H-NMR of **C3c**

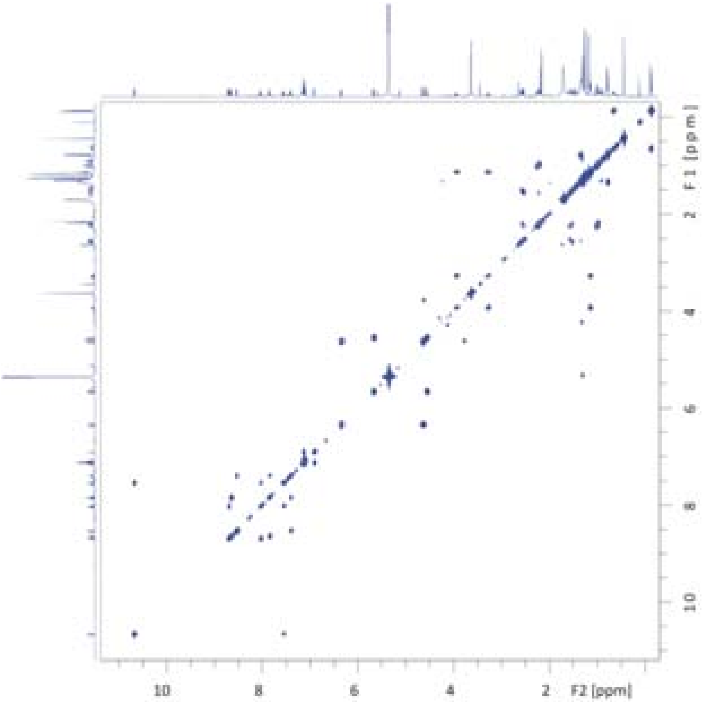

Figure S 27. COSY of **C3c**

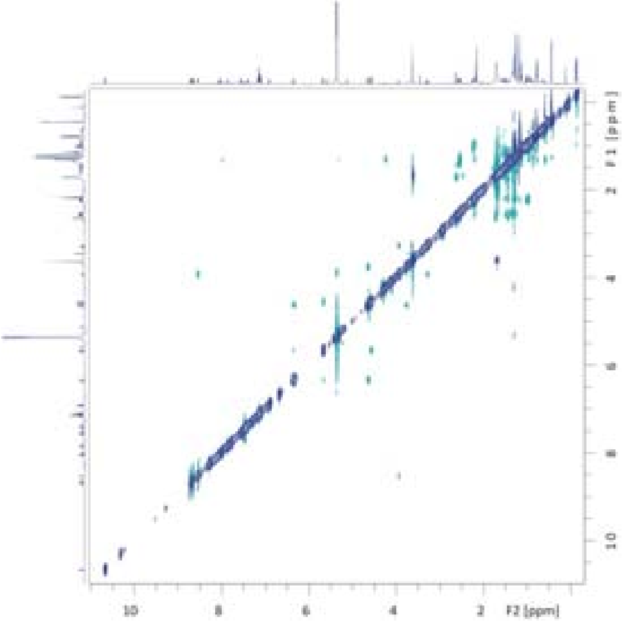

Figure S 28. NOESY of **C3c**

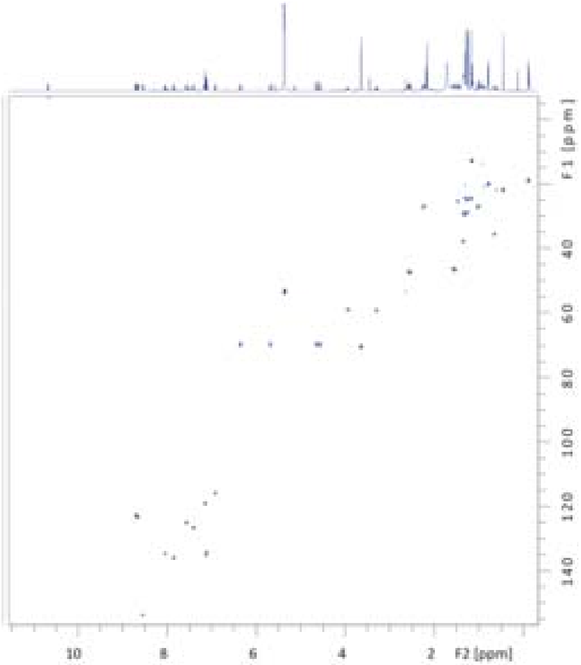

Figure S 29. HMQC of **C3c**

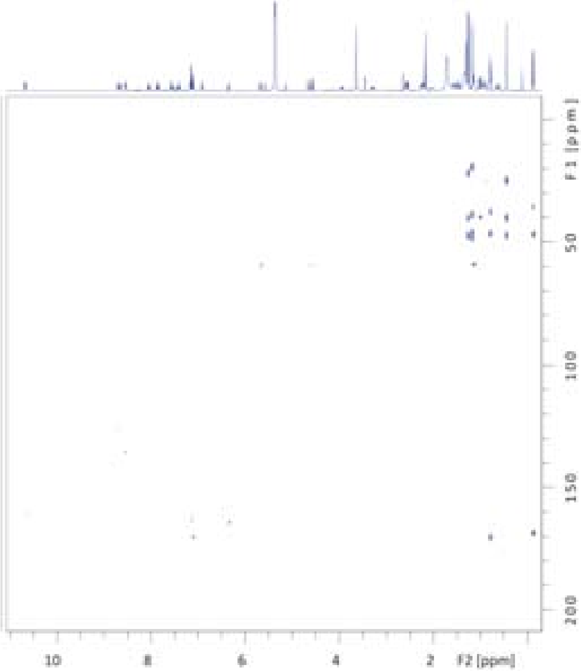

Figure S 30. HMBC of **C3c**

Mass spectrometry

- ***trans-fac*-[Ru(L3)(bpy)Cl]Cl (C3a)**

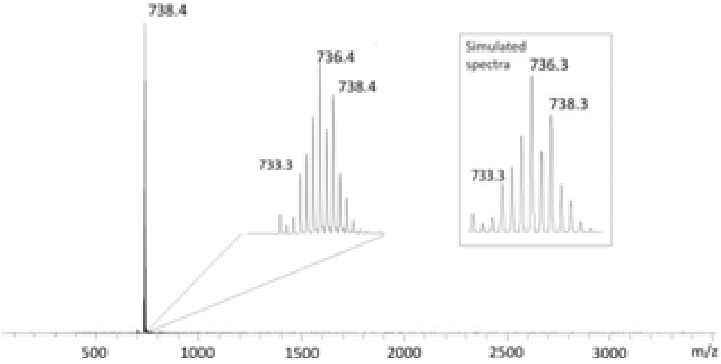

Figure S 31. MS of **C3a**

Cyclic Voltammetry

- ***trans-fac*-[Ru(L3)(bpy)Cl]Cl (C3a)**

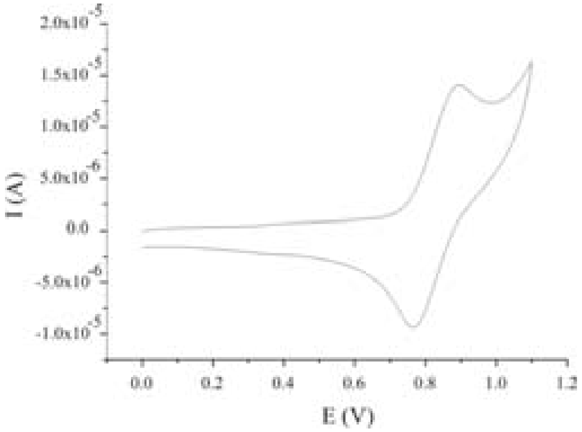

Figure S 32. CV of **C3a**

Chapter 7

Summary and Conclusions

Chapter 7

Summary and Conclusions

- A family of Ru-OH_2 complexes, bearing ligands with different electronic properties, has been synthesized. These complexes have been classified in 3 groups (Group I: complexes with π-acceptor ligands; Group II: complexes with σ-donor ligands; and Group III: complexes with π-acceptor and σ-donor ligands).

- The influence of the electronic properties of the ligands in the redox potentials of the complexes has been studied and rationalized.

- Taking as reference the complex $[Ru(trpy)(bpy)(OH_2)]^{2+}$, the presence of σ-donor ligands, such as picolinate and bid, promotes a decrease in the redox potentials. On the contrary, the use of π-acceptor ligands increases de redox potentials.

- The electronic properties of the ligands change the redox potentials of the couple II/III and III/IV in different degree. In consequence, the electronic properties of the ligands have a great influence in $\Delta E_{1/2}$.

- When π-acceptor ligands, such as azpy and bpm, are used the resulting $[Ru(trpy)(azpy)(OH_2)]^{2+}$ (**C1**) and $[Ru(trpy)(bpm)(OH_2)]^{2+}$ (**C2**) complexes acquire interesting electronic properties, being Ru(III) unstable and favoring a direct 2-electron process.

- The reactivity of the synthesized complexes has been studied for the oxidation of C-H bonds and the epoxidation of alkenes.

- For the oxidation of both xanthene and fluorene, complexes **C1** and **C2** (Group I) are significantly more effective than those with σ-donor ligands, such as **C8** (Group II).
- The formation of dimeric species was not observed for the oxidation of xanthene and, in the case of fluorene, just traces of these species were detected.

- This observation would be in concordance with a) a faster radical trapping by $Ru^{IV}=O$ in comparison with the rate of reaction between two radical species; or b) a direct oxene insertion favored by the overlap of the Ru(IV/III) and Ru(III/II) redox couples.

- The family of $Ru^{IV}=O$ complexes was active in the epoxidation of alkenes, being significantly better catalysts those complexes with π-acceptor (Group I) or σ-donor (Group II) ligands.

- In the epoxidation of *cis*-β-methylstyrene, just the *cis* epoxide was obtained; *i.e.* a stereoselective process takes place.

- This stereoselectivity can be explained either by a direct 2-electron process trough an oxene insertion, or by a faster formation of the epoxide ring to the detriment of a C-C bond rotation of radicalary species.

- Two-electron complexes, **C1** and **C2**, were functionalized with a phosphonate group that allowed the immobilization of these Ru complexes on the surface of magnetic nanoparticles (NPs).

- The new ruthenium complexes were completely characterized by structural, electrochemical, spectroscopic and spectrometric techniques.

- The heterogeneous system was very well solubilized in methanol and the effective immobilization of the Ru complex was confirmed by UV-Vis and elemental analysis.

- The resulting Ru-NP presented no aggregation when analyzed by TEM microscopy.

- The heterogeneous system was effective in the epoxidation of a wide variety of organic substrates.

- For the epoxidation of *cis*-β-methylstyrene, just the *cis*-epoxide was obtained, maintaining the steroeselective properties of the analogous homogeneous system.

- The heterogeneous system was able to undergo up to 770 catalytic cycles.

- Homogeneous and heterogeneous systems presented similar behavior, reaching the latter the paradigm of the "quasi-homogeneous" systems.

- Recycling experiments were developed, where the catalyst was recovered by application of an external magnetic field, without significant loss of activity within 5 recycling cycles.

- New ruthenium complexes functionalized with a resorcin[4]arene cavitand were designed and synthesized.

- These complexes were characterized by structural, electrochemical, spectroscopic and spectrometric techniques.

- The resulting complexes were active in the stereoselective epoxidation of *cis*-β-methylstyrene.

- A new chiral pineno-fused bpea ligand (**L1**) was designed and synthesized.

- Its coordination chemistry to ruthenium was studied and the isomeric mixture obtained in the formation of $[Ru(\mathbf{L1})(bpy)Cl]^+$ (**C3**) was analyzed and compared with similar reported complexes.

- The steric hindrance added in the chiral ligand had a clear effect in the isomeric mixture obtained, being just one isomer formed as a major product (trans-*fac*, **C3a**).

- DFT calculations of the relative energies of the different isomers were in concordance with the isomeric distribution obtained.

- The light-driven isomerization process of **C3c** to **C3a** was studied by UV-Vis.

- DFT calculations of this isomerization process were also developed and a dissociation of a pyridyl ring of **L1** is proposed as potential mechanism.

- **C3** was active in the epoxidation of organic substrates and stereoselectively oxidized cis-β-methylstyrene to the corresponding *cis*-epoxide.